New injectable scaffolds for cell and drug delivery

Lloyd G. Hamilton

Thesis submitted to the University of Nottingham

for the degree of Doctor of Philosophy

September 2008

Acknowledgements

I wish to express my gratitude professor Kevin M. Shakesheff, for his faith, patience and guidance in the completion of this work. I also wish to acknowledge and thank Regentec for funding and the support of Dr. R France and R. Quirk for their guidance and assistance from the start of this project. I would further wish to extend my thanks and admiration to colleagues and staff at the School of Pharmacy for their assistance and indulgence to engage in discussions around various aspects of my work. My appreciation and thanks to Lisa White for assistance and training on the micro-computed tomography equipment; Daniel Howard, Mieke Heyde, Alex Huber, David Chau and Teresa Burton.

To my long suffering wife and family, I am eternally grateful for their patience and understanding in the pursuit of my quest.

The work in this thesis has contributed to the following patent applications.

Patent Number: GB0800289 A composition comprising polymer particles and a carrier, wherein the polymer particles are arranged such that they can join together to form a scaffold of polymer particles, and wherein the composition is administrable to a human or non-human animal.

Patent Number: WO2008041001 Production of porous particles useful for producing a tissue scaffold or medical implant.

Abstract

An injectable scaffold system for the delivery of cells and growth factors was developed in this project to enhance healing of bone fractures. The project was focused to meet the clinical need for an off-the-shelf synthetic biodegradable bone graft material. The concept required the injection of a paste to fill defects then rapidly solidify to a mechanically supportive macroporous structure. The injectable paste was developed from a two-component biodegradable microparticle scaffold based on poly(lactic-co-glycolic acid) (PLGA) and comprised of a versatile temperature insensitive (type 1) carrier and an adhesive (type 2) component made temperature sensitive with the addition of poly(ethylene glycol) (PEG) as a plasticizer. The plasticized adhesive type 2 component achieved wet compressive strengths up to 18 MPa at 37 °C after 24 hours. The sintering strategy utilised the changes in viscoelastic and mechanical properties that occur in the glass transition region of amorphous polymers. The specific mechanism devised in this thesis exploited the biocompatibility and diffusivity of PEG to increase polymer glass transition temperature in the wet sintering process.

The solidification speed was demonstrated by rheological assessment of storage modulus and wet compressive strengths up to 2 MPa after 15 minutes at 37 °C. Restricting particle size distribution to narrow 100 µm bands controlled porosity between 35-65%. The interconnectivity of the macroporous structures was

demonstrated by the invasion of 3T3 cells seeded on the outer surface of the scaffold and evaluated by microcomputed tomography. The innocuous nature of the solidification process was demonstrated by the survival and proliferation of *in situ* seeded primary human fibroblasts, osteoblasts and murine C2C12 cells. The multifunctional type 1 component acted as a porous spacer, protein delivery vehicle and cell carrier when modified with polyethylenimin. The potential use of the scaffold as a controlled delivery system for recombinant human bone morphogenetic protein-2 (rhBMP-2) was demonstrated by the sustained differentiation of murine C2C12 myoblast to osteogenic alkaline phosphatase positive cells over 28 days.

In this thesis a novel sintering mechanism has been developed that facilitates control of pore size and porosity of injectable scaffolds. The benign nature of the process facilitates the potential use of this injectable system as a delivery vehicle for cell and growth factor therapy.

Chapter 1

List of Figures

1.1 List of abbreviations

%	per cent
±	plus or minus
µg	microgram
µL	microlitre
µm	micrometer
µM	micromolar
˚C	degree Celcius
2D	two-dimensional
3D	three-dimensional
ANOVA	one-way analysis of variance
bFGF	basic fibroblast growth factor
BMP	bone morphogenetic protein
BSA	bovine serum albumin
CAS	chemical abstracts service
cc	centilitre
cm^2	square centimetre
cm^3	centimetre cubed
em	emission
ex	excitation
Da	Dalton
DCM	dichloromethane
DMEM	Dulbecco's modified eagle's medium
DMSO	dimethylsulfoxide
DNA	deoxyribonucleic acid
D-PLA	D-Poly(lactic acid)
DSC	Differential Scanning Calorimetry
FCS	foetal calf serum
FDA	Food & Drug Administration

FGF	fibroblast growth factor
FITC-BSA	fluorescein isothiocyanate bovine serum albumin
GAG	glycosaminoglycan
G’	storage modulus
G’’	loss modulus
G*	complex shear modulus
g	gram
GPa	Giga Pascal
HBSS	Hank’s balanced salt solution
HPLC	High pressure liquid chromatography
Hz	Hertz
IUPAC	international union of pure and applied chemists
J/g	joules per gram
kDa	kilo Dalton
kV	kilo Volt
L	litre
L-PLA	L-Poly(lactic acid)
MDSC	Modulated Differential Scanning Calorimetry
mg	Miligram
mL	millilitre
mm	millimetre
mM	milli molar
Micro CT	micro-computed tomography
MPa	Mega Pascal
N	Newtons
NaCl	sodium chloride
ng	nanogram
oz	ounce
p	probability
Pa	Pascal
$P_{DL}LA$	Poly(D,L-lactic acid)

PEG	Poly(ethylene glycol)
PGA	poly(glycolic acid)
PBS	Phosphate buffered saline
PDGF	platelet derived growth factor
PEI	Polyethyleneimine
pH	measure of acidity/alkalinity
PLA	poly(lactic acid)
P_LLA	poly(L-lactic acid)
PLGA	poly(lactide-co-glycolide)
PTFE	polytetrafluoroethylene
PVA	Poly(vinyl alcohol)
rhBMP-2	recombinant bone morphogenetic protein-2
s^{-1}	reciprocal second
SEM	scanning electron microscopy
TCP	Tricalcium phosphate
Tg	glass transition temperature
UV	ultra violet
VEGF	vascular endothelial growth factor),
$^{v}/_{v}$	volume per unit volume
W/g	heat flow Watts per gram
W/O	Water in oil
W/O/W	Water in oil in water
$^{w}/_{w}$	weight per weight
x3	three times

1 Introduction

Tissue engineering and regenerative medicine share a common goal for the restoration or replacement of function lost through trauma and disease [1]. The aim of tissue engineering is to generate new tissues from cells seeded onto scaffolds [3, 4]. Examples of early engineered tissues using naturally derived scaffolds include keratinocyte sheets to treat skin burns and cloned endothelial cells reforming a capillary network *in vitro* [5, 6]. Both examples demonstrated the strategy for tissue growth from a combination of cells, inducing factors and scaffolds. Scaffolds are at the core of the tissue engineering approach and interaction with cells, matrix and growth factors determine the effectiveness of repair[7, 8].

The elderly have an increasing share of fracture complications and in recognition of the growing socioeconomic cost, the World Health Organization declared the years 2000-2010 the bone and joint decade. The number of reconstructive bone and joint surgical procedures in the period 2002-2003 in England alone was 636, 000 [9]. When bone damage is larger than self-reconstruction can repair (critical size defect) alternative fillers or grafts are required. Graft materials are classified by source as autograft, allograft, xenograft and synthetic materials. There is a need for synthetic off the shelf solutions that are widely compatible between patients [10]. Due to cost, the complexity of scale up and cell death, few new materials have translated into clinical practise [1, 11].

Tissue engineered solutions needs to be effective, safe, clinically expeditious, generic, inexpensive and compatible with existing procedures [12]. The classical tissue engineered approach is the in *vitro* expansion of cells and seeding of scaffolds outside the body; however, for connective tissues with microstructure that reflects their native mechanical environment, endogenous repair is advantageous to regenerate the tissue [13]. In this thesis an injectable scaffold is developed for endogenous repair of bone tissue. The injectable scaffold is innocuous but effective in the delivery of cells and growth factor to improve tissue regeneration and repair.

1.1 Bone

Bone is composed of extracellular matrix, which is mineralized to varying extents conferring rigidity and strength whilst maintaining elasticity [14]. Bone is remodelled throughout life in response to loading, retaining form and function. Reduced bone loading results in decreased mineral density and muscle atrophy in fracture patients and astronauts subjected to prolonged low gravity conditions [15]. Bone structure and composition therefore vary with age, site, health and level of activity (Figure 1-1). Collagen type I is the dominant protein component of organic bone matrix and the template for mineralisation [16, 17]. In bone cells, tropocollagen is produced as three polypeptide chains linked by cysteine disulfide links. Outside cells, the cysteine links are cleaved leaving the tri-polypeptide held together by hydrogen bonding.

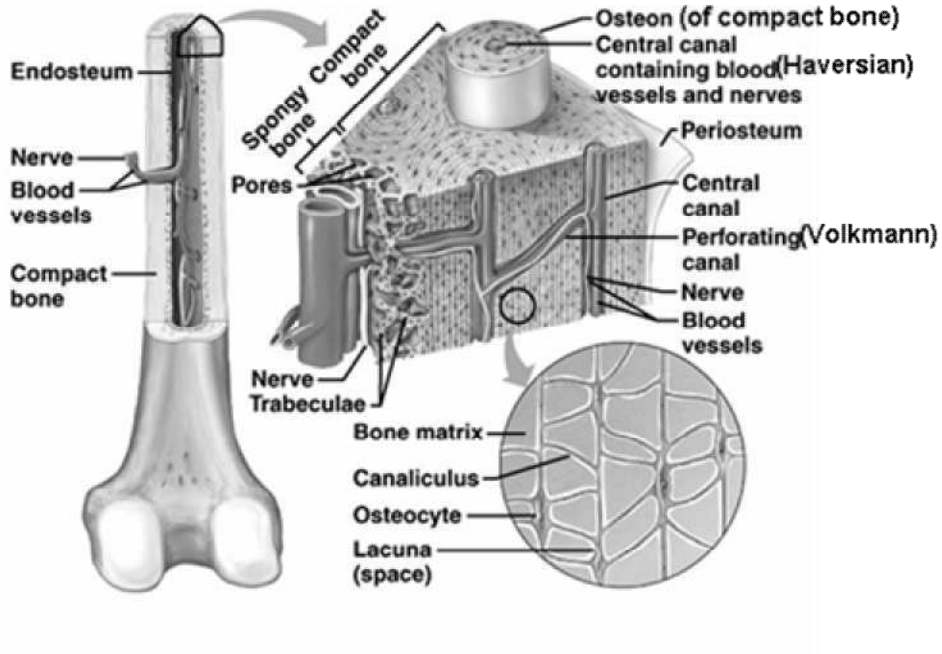

Figure 1-1 A schematic of long bone showing the periosteum, osteon, compact and trabecular bone organization (biology.bangor.ac.uk/.../module/BSX1016/muscskel) Bangor University.

Tri-polypeptides self-assemble in a staggered alignment; head to tail, forming micro fibrils stabilised by intermolecular cross-links between tri-valent pyrodinolines and pyrroles with gap regions. During mineralization, hydroxyapatite crystals are deposited into the gap regions of collagen fibres adding mechanical rigidity and load bearing capacity [18]. The hydroxyapatite crystals contain impurities, such as carbonate, citrate, magnesium and fluoride making it more soluble than geologic apatite for bone to be remodelled [19]

The organisation of collagen matrix gives rise to two patterns of mineral deposition known as woven (random) and lamellar (ordered) bone. Woven bone is a temporary matrix deposited rapidly by osteoblasts during embryonic skeletal development, early fracture healing, longitudinal bone growth and osteosarcoma formation [19]. After fracture, a bony callus is rapidly formed providing a temporary functional scaffold structure to partially restore mechanical stiffness properties. This allows functional loading to stimulate remodelling and replacement of woven with lamellar bone. Osteoblasts deposit collagen fibres in parallel aligned lamellae sheets, layer by layer, 3-20 μm thick with highly ordered and extensive mineralisation for bone strength [20]. The 20-30 concentric lamellar sheets known as osteons are observed in the Haversian system of cortical bone and are mechanically strong to withstand torsion loading [21].

Cortical and cancellous bones are structurally and functionally distinct. In humans cortical bone is 3-12% porous due to the Haversian and Volkmann's canals that

contain blood vessels and nervous tissue [19]. The Haversian canals, 200-300 μm in diameter are bordered by the cement line that links one osteon to another. Osteons are permeated with embedded osteocytes in lacunae chambers linked by canaliculi (Figure 1-1). Cortical bone is oriented to the surface surrounding cancellous bone in a tubular arrangement that varies in thickness. Adult cancellous bones are formed by lamellar sheets in a porous (50-90%) network of trabeculae rods and plates interconnected by pores up to 1 mm in size [22]. Trabeculae are preferentially aligned giving anisotropy to the structure and elastic support to resist compression [17].

Property	Cortical bone	Cancellous bone
Compressive strength (MPa)	100-230	2-12
Flexural, tensile strength (MPa)	50-150	10-20
Strain to failure (%)	1-3	5-7
Young's modulus (GPa)	7-30	0.05-0.5

Table 1 Compilation of the mechanical properties of cortical and cancellous bone [23].

Bone strength is the maximum stress resisted before failure and is determined by mineralisation and organisation of structure [24]. Stress is defined as the force applied divided by the area of the load. Strain is a change in dimension as a result of the applied stress. Young's modulus is the stress divided by strain in the linear region where stress is proportional to strain and indicates the stiffness of the material under loading. The size and weight of animals do vary across species, but the average strain and mechanical properties are similar with the femoral bone in rats and humans having the same Young's modulus [17, 25].

1.1.1 Bone Repair and Remodelling

The major bone modifying cells are osteoblasts, osteocytes and bone lining cells derived from mesenchymal stem cells and osteoclasts [26]. Multinucleated osteoclasts 20-100 µm in diameter are derived from fused monocytes and macrophages and have a half-life of 6-10 day [27]. Osteoclasts create ruffled cavities 200µm in diameter and 300 µm long [19]. At the end of osteoclast activity, a cement line is formed by osteoblasts in the cavity as the outer sheath of the Haversian system. The cavity is lined with new bone deposited in concentric lamellae layers, forming the Haversian system with central blood vessels and nerves over 2-4 months. [17]. The cement sheath is permeated by canaliculi connecting new to old bone and is a site of osteopontin concentration [16].

In development and repair, intramembranous bone formation occurs in an environment where no pre-existing bone matrix is present. Invading undifferentiated mesenchymal stem cells proliferate then differentiate via pre-osteoblasts to osteoblasts which synthesise, then secrete collagen fibrils in a random array. During collagen assembly some osteoblasts lag behind, becoming embedded in matrix that is, mineralised by deposition to woven bone. Matrix embedded osteoblasts, differentiate to smaller osteocytes and shrink from 7-1 µm in height at the end of bone formation and connect to adjacent osteocytes via fluid filled canaliculi [28].

Osteocytes are embedded in a lacunae chamber and have a reduced size and few synthetic organelles. They are connected to other osteocytes and bone lining cells by the canaliculi. Bone-lining cells are derived from surface osteoblasts after bone formation and have an elongated appearance up to 12 µm diameter with a 1 µm thick nucleus [29]. They communicate with other lining cells and osteocytes through gap junctions and may be reactivated to active osteoblasts 20-40 µm in diameter [28]. Bone lining cells are believed to act as mechanical sensors, being connected to the surface and the osteocytic extracellular fluid filled lacuo-canalicular network. Distortions and deformations of the bone matrix are detected as fluid flow that stimulates remodelling [30].

1.1.2 Fracture Environment

Fracture disrupts marrow architecture and periosteum blood vessels inducing an inflammatory cascade producing pain, swelling, cytokine release, heat and blood clot (haematoma) formation [31]. Inflammation is initially localised to a tissue by arteriole dilation and the temperature generated can reach 41 °C [32]. Haematoma produces an internal soft callus enclosing the fracture areas [33]. Haematoma removal attenuates repair and its transplantation stimulates new bone formation [34]. If the nutrient supply becomes impaired, osteocytes nearest the fracture site die, creating a necrotic zone and osteoprogenitor cells differentiate to chondrocytes and produce cartilage to stabilise the fracture. The cartilage is mineralised during endochondrial ossification by invading osteoblasts concurrent with angiogenesis.

1.1.3 Self-Repair Mechanisms

The mechanisms of bone repair are dependent on the biophysical environment [35]. In normal bone, the blood supply is split between the medullary, osseous and periosteal supply (Figure 1-2) and the mechanism of repair can be specific to each region [34]. New blood vessels formed during repair persist until the medullary supply is regenerated. The fibrous periosteum membrane that surrounds compact bone is rich in undifferentiated cells and blood vessels (Figure 1-1). When fractured, recruitment of macrophage and periosteal fibroblasts simultaneously remove damaged tissue by resorption and fibroblast growth factor (FGF) stimulates osteoclastic action initiating bone remodelling [36, 37].

Repair by endochondral callus bone formation is mediated by the inner periosteal layer and marrow tissue forming an internal callus, which is mineralized first to woven, then replaced by lamellar bone. Intramembranous ossification of the periosteum forms a hard callus around the injury, providing mechanical stability [34]. In the central necrotic zone, osteoclasts initiate bone resorption. In areas of rigid stability primary contact bone repair occurs exclusively by Haversian system osteoblasts that synthesise lamellar bone [35]. Gap repair in the interfragmentory spaces >100 µm wide is by direct bone synthesis from mesenchymal and marrow derived tissue [38].

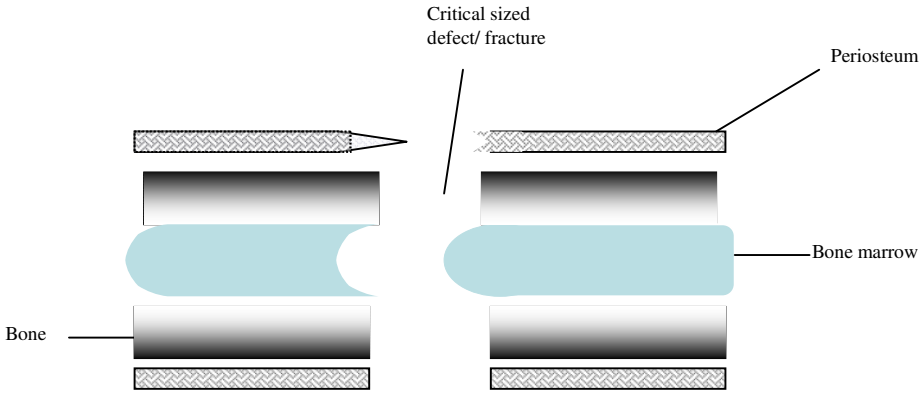

Figure 1-2 Schematic representation of bone fracture showing the composite layers of bone that correlate with blood supply (adapted from [2])

1.2 Intervention Strategies of Fracture Repair

Impaired healing occurs in 5-10% of fractures [39]. Critical size defects require intervention to stabilise the fracture fragments and promote healing. Historically external splints have been used for up to 2 months with inherently stable fractures and for correcting bending deformities [9]. Such immobilisation avoids twisting and shortening, but mechanical disuse results in trophic damage with pain, swelling, patchy bone loss, and depletion of bone forming cells [40].

Materials used in repair can be divided into metals, polymers, ceramics and natural substrates [41]. Independent of the type of material used to fill non-union gaps is the concern of provoking inflammation at the biomaterial-host-tissue interface [31]. A variety of factors influence tissue response from implant design, to its localisation, physiochemical properties, mechanical loading, surface texture and the general health of the patient [15]. Surgery utilises compression between fracture surfaces to immobilise, align and stimulate repair. The trade off for optimal healing is the loss of strength as implants can remain in place for up to two years [42]. Deformable splints with variable degrees of immobilisation enable fracture detection and healing through mechano-biological stimulation and transmission of strain. Osteoblasts in *vitro* respond to dynamic oscillatory fluid flow by up regulating osteopontin and increasing proliferation in culture [43, 44]. The natural movement of tissues induce shear stress and strain at the tissue-biomaterial interface promoting mechanical interaction. Submicron wear particles generated by friction from artificial prostheses can

stimulate an immune cascade leading to high macrophage activity, bone resorption and loosening of the implant. The time to reaction is modulated by the surrounding tissue and in bone this may occur after a delay of up to 3 months leading to increased osteocyte resorption [45]. Implants having a higher Young's modulus than the tissue, concentrate stress at the tissue-implant interface when movement occurs, resulting in inflammation, fibrotic encapsulation and a conclusion of poor biocompatibility [15].

1.2.1 Autografts

Large segmental bone injuries caused by trauma and disease do not heal spontaneously [46]. The implantation of cancellous bone grafts into wounds was demonstrated to induce bone formation [47, 48]. Vascularised autografts are now a standard treatment, having live cells with inherent osteogenecity, osteoinductivity and osteoconductivity [49]. Autografts utilising expanded bone marrow aspirate cells, is an option for elective surgery where time is not an issue, unlike trauma cases. The survival and maintenance of bone marrow stem cells (BMSC) is dependent on microenvironment [50]. BMSC can populate injured tissue through implantation in scaffolds for articular cartilage and bone defects escaping alloantigen recognition [47, 51]. The major procedural drawbacks for autografts are: limited availability of tissue in young and old patients, coupled with potential donor site morbidity, infection, variable fusion rates and the creation of secondary defects with, long-term pain [52]. In paediatric and geriatric patients, autografts are ineffective when the defect size exceeds the volume of healthy graft available to bridge it [53]. Calcium phosphate cements have been utilised to reduce donor site morbidity, alleviating some issues [54].

1.2.2 Allografts

Allograft transplants are clinically common because of on-shelf availability following harvesting from cadaver donors [55]. Protein removal reduces the risk of disease transmission and avoids immunogenic reaction but has reduced osteoinductive and osteoconductive performance [9]. Allogenic transplants suffer high (25-35 %) levels of complications and re-fracture rates within 3 years [53]. The levels reach 60 % within 10 years and were associated with osteoclastic resorption, increased micro fracture and decreased bone mineral density within cortical and cancellous bone [56]. Allografts are subject to infection and immune responses after implantation as large defects have limited osteoinductivity, suffer poor vascularisation and mass transport [57, 58]. Sterilisation of allograft with ethylene oxide and gamma irradiation reduces strength and the osteoinductive properties of the material [59]. Both autografts and allografts suffer limited availability [60]. Hence, the need for alternative synthetic bone grafts to be developed.

1.3 Regulators of Bone Activity

In principle, autologous bone grafts contain the essential elements of matrix, cells and growth factors required for repair and vascularisation [57]. More than 40 proteins have been identified that can induce endochondral bone formation in a variety of animals [61]. Transforming growth factor-β (TGF-β) and insulin growth factor (IGF) regulate differentiated bone cell proliferation, metabolism, motility and extracellular matrix tissue formation [34]. IGF is believed to extend the effect of TGF-β and bone morphogenetic proteins (BMPs) [62]. Bone growth factors have a localised action on angiogenesis through basal fibroblast growth factor and vascular endothelial growth

factor (VEGF) [63]. Platelet derived growth factor (PDGF) was shown to stimulate fracture healing, up regulate VEGF and mesenchymal cell proliferation in an osteoporotic geriatric rat model [64]. The rate of new bone formation is believed to be proportional to the number of active osteoblasts and osteoclast [39].

The other principal regulators of bone mineralisation and remodelling are osteocalcin, bone sialoprotein, osteopontin, osteonectin, sulphated and acid mucopolysaccharides. Osteocalcin has a high specific affinity for hydroxyapatite (HA) suppressing bone formation [65]. Bone sialoprotein is multifunctional, promoting osteoblasts adhesion, differentiation, osteoclast resorption, remodelling, and facilitating carbonate hydroxyapatite nucleation [17, 21]. Osteopontin, involved in early cell attachment to extracellular matrix slows giant cell formation and inhibits hydroxyapatite crystal growth in solution but initiates it when attached to a solid surface through its negative charged density [50, 66, 67].

1.3.1 Bone Morphogenetic Proteins

Bone morphogenetic proteins are effective across species from Drosophila melanogaster flies to humans, controlling embryogenesis, homeostasis, postnatal morphogenesis and repair [68-70]. To date at least 20 BMP isoforms have been identified that can stimulate chemotaxis, proliferation of mesenchymal stem cells and promote differentiation to either chondrocytes or osteoblasts [39]. The fate of differentiated mesenchymal stem cells depends on the degree of vascularisation present, with bone development requiring high oxygenation and short diffusion distances. Low oxygen tension promotes cartilage formation [71].

Both rhBMP-2 and rhBMP-7 on collagen type I sponge are FDA approved for limited clinical use in open fractures to increase the likelihood of union in spinal fusion and tibial fracture procedures [72]. BMP-2 and -7 are synchronous but spatially and functionally distinct; they are used singly, in pharmacological rather than physiological doses. BMP-7 was the first to be cloned; but work by [73] suggests BMP-2, -6 and -9 to have the most potent osteogenic activity. Mice deficient in BMP-2 are nonviable at the embryonic pre-limb patterning stage, whereas mice deficient in BMP-7 die after birth because of poor kidney development [74]. The response to BMPs was demonstrated to depend on cell type and differentiation status [73]. BMP-2 stimulates mouse mesenchymal progenitor (C3H16T1/2) cells, preosteoblastic C2C12 myoblasts and committed osteoblastic TE85 cells to produce osteoblast differentiation markers alkaline phosphatase, osteocalcin and matrix mineralization (Figure 1-3). The activity of BMP-7 was poor in mesenchymal progenitor cells and a third of that for BMP-2 in preosteoblastic C2C12 myoblast cells. Both BMP-2 and -7 stimulated alkaline phosphatase activity in committed osteoblasts (TE85). Several growth factors inhibit myogenic differentiation of C2C12 but do not induce osteoblastic differentiation. Osteoblastic differentiation of C2C12 in culture was maintained by continuous daily refreshment of low concentrations of rhBMP-2 [75]. C2C12 cells induced by BMP have up regulated core binding factor-1(Cbfa1) and can mimic part of the process of ectopic bone formation [76]. Mice not expressing the Cbfa1 gene fail to develop a mineralized skeleton [77].

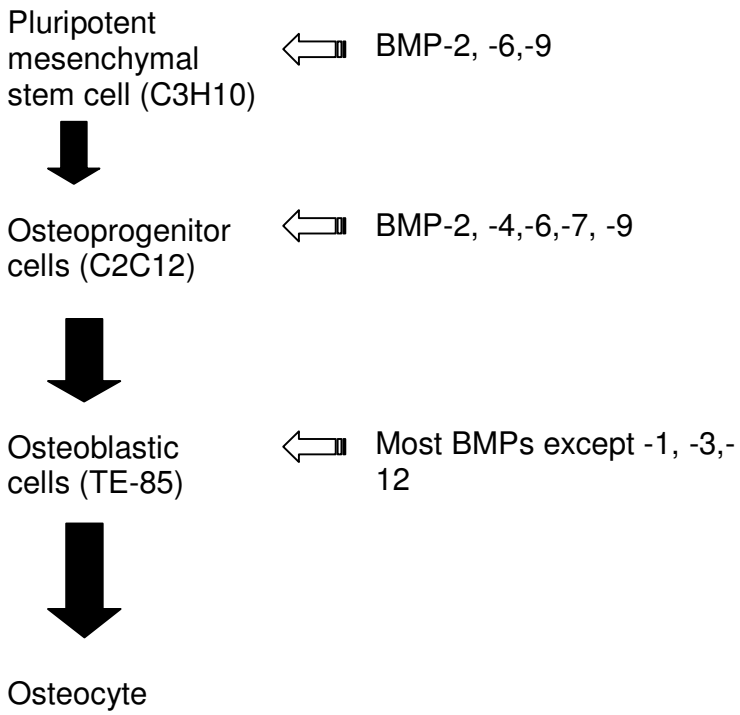

Figure 1-3 Hierarchical description of BMP activity on cells from mesenchymal progenitor to terminal differentiation state (adopted from [73]).

1.3.2 BMP Signal Transduction

Integrins mediate cell adhesion to extracellular matrix and biomaterial surfaces regulating, motility, shape and differentiation [78]. Integrins form non-covalent αβ-heterodimers and 24 combinations were identified [79]. The integrins and growth factor receptors expressed, vary by cell type with stage of differentiation [77]. BMP-signal transduction occurs *via* interaction with a heterodimeric complex of (type I and II) transmembrane serine/ threonine kinase receptors (Figure1-4). Type II receptors are activated by BMP binding and activate type I receptors by transphosphorylation. The activated kinase receptor phosphorylates Smad proteins 1, 5 and 8. Two of these receptor-regulated Smads form a heterotrimeric complex with Smad 4, which is translocated into the nucleus to modulate target genes [73]. Smads are the main signal transducers of serine-threonine receptors and regulators of TGF-β family gene transcription. These receptor regulated Smads stimulate gene expression by binding to the regulatory sequence in the target promoter resulting in chromatin unfolding [80]. BMPs also stimulate the production of inhibitory molecules to regulate the signalling cascade. In the nucleus Smad 6 and 7, negatively regulate the cascade through gene repression. Noggin, a BMP-2,-4 and-7 antagonist, is induced as part of the negative feedback loop to block BMP binding to receptors in the extracellular space [39, 74, 76].

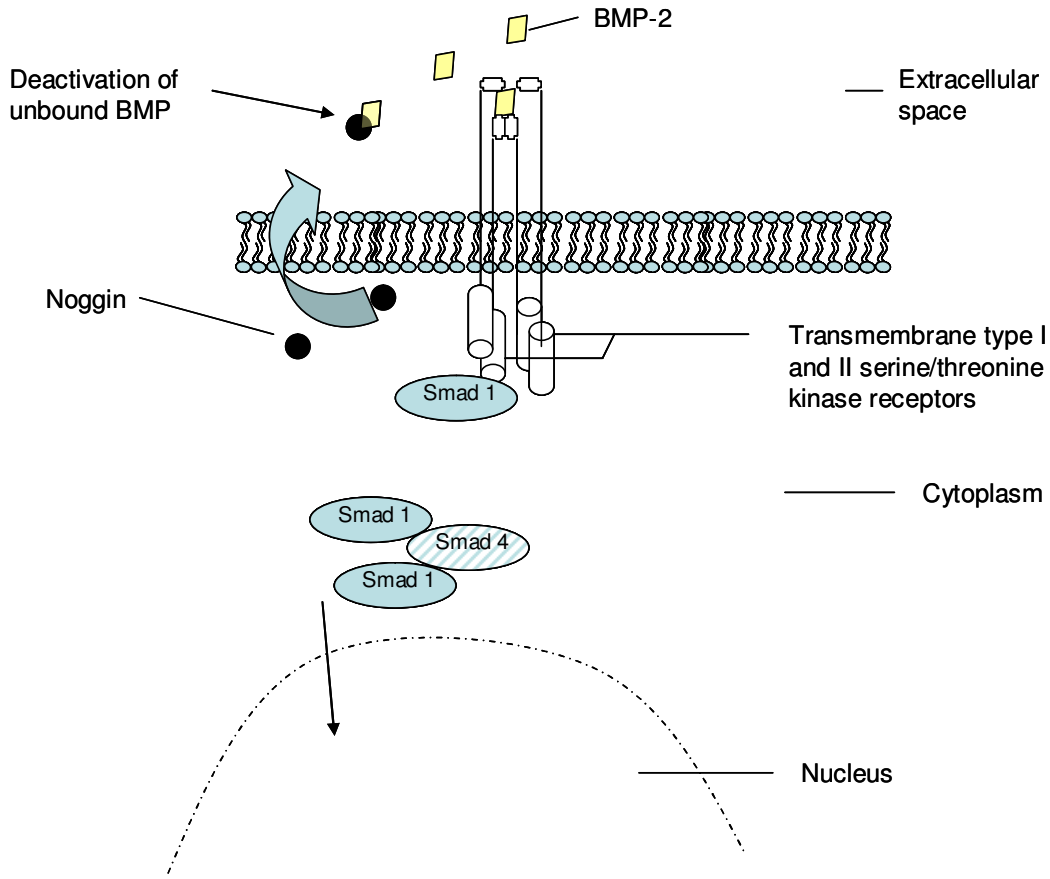

Figure 1-4 Schematic representation of a BMP signaling transduction pathway with representative regulators. BMP signals are mediated by type I and II receptor complexes and downstream Smad molecules that are translocated into the nucleus to regulate gene transcription (adapted from [74]. Noggin is an antagonist that binds with BMP-2, 4, and 7 to block signaling.

1.3.3 Clinical use of BMPs

In primates and humans, BMP-2 induced greater mineralized tissue and matrix than equivalent BMP-7 [61]. Induction of endochondral bone formation has been demonstrated with rhBMP-2 implants preventing collapse of poly(propylene) fumarate/tricalcium phosphate scaffolds in load bearing rat femur [9]. In Europe, the maximum dose of rhBMP-7 is 2 units [81]. Each unit containing 3.5mg rhBMP-7 and 1g collagen type I administered in 3-5ml sterile saline [39]. BMPs promote osteoclast activation and expansion before osteoblast formation; therefore, large doses can stimulate resorption before significant bone formation. The upper limit for rhBMP-2 is 12 mg on absorbable collagen sponge, which is more than is present in 1000 humans and 18% of patients treated developed antibodies to bovine collagen [57, 82]. Regardless of this, BMP induction shows effectiveness similar to autografts [83].

BMPs on collagen sponges may suffer a combination of inactivation, physical displacement and high rates of diffusion from the implant site causing local ectopic bone formation and inflammation [61]. Humans require a BMP dose forty times higher than rodents [84]. Large rhBMP-2 doses can induce monocyte adhesion and contribute to atherosclerosis, swelling and heterotopic ossification [53, 85, 86]. As soluble factors, BMPs have a short half-life of minutes up to 4 hours and are systemically cleared by the kidneys [81, 87]. The in *vitro* effects of recombinant and human BMP can be detected at femto- and nanomolar concentrations and may indicate a flaw in the single morphogen approach. Improved efficacy of low dose

human BMP-7 with recombinant TGF-β was demonstrated in primates [68]. Multiple growth factor combinations may be more effective than single factor release but variation in site by site requirement and interactions occurring between specific signaling pathways triggered by each growth factor adds complexity *in vivo* [88].

In orthopedic procedures risk factors retarding healing include age, poor nutrition, diabetes, rheumatoid arthritis, and osteoporosis [89]. Smoking was a predictor of poor surgical outcome accounting for 75% of post-operative infections [71, 90]. In circumstances of non-union the number of cells responding to BMP may be limited, predominantly in the elderly [39]. Efficacy varies with patients, but in aged and more clinically complex cases rhBMP-2 is less effective than rhBMP-7 [57]. In impaired patients, rhBMP-7 was superior to autologous bone grafts but more expensive even with shortened surgery time, reduced pain, morbidity and faster recovery [91]. Due to high cost rhBMP-2 and -7 are used when all other treatment options are exhausted.

1.3.4 BMP Carriers

Transplanted bovine bone pastes into rats were demonstrated to induce new bone and marrow cavity formation only in the implantation area and never beyond it [48, 92]. BMPs were found combined with extracellular matrix and transformed attached responding mesenchymal cells [93]. Purified BMP protein was shown to have reduced potency when isolated from the matrix; hence, the need for a carrier and correct local placement to prevent ectopic bone formation in adjacent muscle, nerve and blood vessels [16]. To trigger the cascade of tissue induction and morphogenesis

in large animals, sustained delivery of osteogenic BMP is required [93]. Associating BMP with a carrier restricts degradation, distribution and solubility, to sustain and enhance gene expression [81]. Heparin adsorption was demonstrated to extend 20-fold, the half-life of rhBMP-2 and more recently a specific binding peptide sustained delivery [76, 87].

Established BMP carriers include collagen, guanidine-extracted demineralized bone matrix, hydroxyapatite and degradable poly(α-hydroxyacid) polymers [39]. Collagen sponge compared with a buffer delivery system in a rabbit ulna model retained ten times more of the initial rhBMP-2 dose after surgery for twice as long [53]. Collagen I depending on processing has an isoelectric point at neutral to slightly acidic pH and electrostatically binds rhBMP-2 in the pH range 4.5-6.5, due to a positive net charge below pH 9 [53].

The ideal qualities of a morphogen delivery vehicle include adequate porosity for blood vessel invasion; spatial and temporal control of diffusion; mould to defect shape, provide immediate structural support; minimal immunological response and undergo resorption coupled to an advancing osteogenic front [94]. To date current systems based on collagen, biomaterials and hydroxyapatite have advantages but fail to provide all the requirements of an ideal delivery system.

Recombinant BMP-2 has been effective in reducing secondary surgical intervention in comparison to treatment without growth factors. However, the activity of recombinant BMP-2 from bacteria is 10% of purified human BMP-2 [46] [9]. Competing scaffold growth factor release profile, i.e. burst versus slow release, remains an issue for maintaining a localized effect, but a poly(lactide-co- glycolide) scaffold delivering VEGF with plasmid DNA, coding for BMP-2, regenerated bone in mice over 15 weeks [88].

1.4 Scaffolds

The scaffold is a temporary framework used for access and support in the erection and repair of large structures. Bioabsorbable engineered scaffolds are temporary replacement structures that preserve tissue dimension, provide anchorage and guidance to cells in regeneration and repair [45, 95]. Scaffolds are produced from inorganic, synthetic and naturally derived materials for use as alternatives to autografts and allografts [96]. In orthopaedics, bone regeneration is compromised by foreign body reactions and physical blocking due to incomplete degradation of the scaffold [81]. Successful scaffold architecture and design should stimulate diffusion, dictate spatial distribution and tissue ingrowth; hence, pore size and porosity are crucial parameters.

Ideal bone graft materials incorporate features of a morphogen delivery vehicle with responding cells [97, 98]. Cell diameter dictates scaffold pore size with 5 µm for neovascularisation, 5-15 µm for fibroblast ingrowth, 40-100 µm for osteoid ingrowth, 100-350 µm for bone regeneration and > 500 µm recommended for rapid

vascularisation and survival of transplanted cells [99, 100]. Surgeons want reliable off-the-shelf graft materials for use in all patients [57]. Inorganic, synthetic and composite graft materials to date have improved functionality and reduced antigenicity; but the challenge remains to raise performance to be equal to or better than autologous grafts [101].

Engineered solutions use metal splints, screws, plates and cages, restoring functionality with little biological regeneration and interferes with normal growth patterns, requiring follow up procedures to adjust and remove [45]. Titanium is the most widely used material for orthopaedic reconstruction and its osteoconductivity and integration are gained through calcium phosphate coating and surface architecture [102]. Warnke repaired a mandibular discontinuity in a patient by seeding a custom made ceramic scaffold with allograft bone marrow cells and rhBMP-7 into a bovine derived bone mineral scaffold contained within a titanium mesh [103]. The scaffold initially worked well restoring function, but developed a fracture in the titanium mesh. Large tissue engineered bone constructs can fail and be limited by insufficient vasculature and nutrient supply [37].Treating bone fractures with synthetic tissue engineered bioactive constructs and the patients' own cells can potentially improve healing, reduce cost and the need for retrieval [104].

1.4.1 Scaffold Integration in Bone Healing

Bone-bonding is defined as a "physiochemical process of continuity between an implant and bone matrix" [105]. At fracture sites, bone formation requires recruitment and migration of potentially osteogenic cells through the clot to reach the damaged interface to initiate healing. Osteogenic cells that differentiate before reaching the target surface stop migrating and produce bone matrix that appear as bony spicules advancing towards the fracture site [105]. Mechanical stimuli vary the remodelling rates that control the adaptive response of bone. Scaffold that transmit strain, stimulate guided bone repair by creeping osteoid formation at 2-10μm/day in the direction of dominant stress and at 0.3-1 μm/day for general bone remodelling [20]. Strain stimulates both osteoblastic and osteoclastic activities in bone modelling and remodelling [106]. Mechanotransduction of cyclic mechanical compression has been demonstrated to positively influence repair; up regulating proteoglycan and collagen I production in a chondrogenic model [107]. Strain in young bone can cause diffuse cracks, but linear microcracks are formed in older bone [108]. Microcrack formation stimulates bone development but can cause implants to loosen.

The cement line is the first extracellular interfacial matrix formed by osteogenic cells during new bone synthesis. It is a calcified interfacial bone matrix formed at stable interfaces to tie surfaces together and anchor new to existing bone [105]. Cement lines are formed during normal bone remodelling (section 1.1.1) and are highly conserved features across species marking the boundary between one Haversian system and the surrounding interstitial bone. Osteoclast resorption is an acidic two

phase process of inorganic matrix dissolution and enzyme degradation to create a recipient ruffled concave surface approximately 1µm deep, of demineralised collagen [16].

The carbonated hydroxyapatite matrix of the cement line is deposited within these invaginated surface contusions forming an interlocked, interdigitated anchorage [17]. Osteoblast attachment is followed by secretion and adsorption of bone sialoprotein and osteopontin onto the prepared surface, initiating mineralization followed by calcified crystal growth forming the cement line (Figure 1-5). Collagen is deposited on the cement line becoming encrusted in it to form anchorage points for new mineralised bone. The cement line is formed by direct contact osteogenesis on surfaces with micron scale topography and submicron indentations as discrete nanocrystalline deposits of calcium phosphate [109].

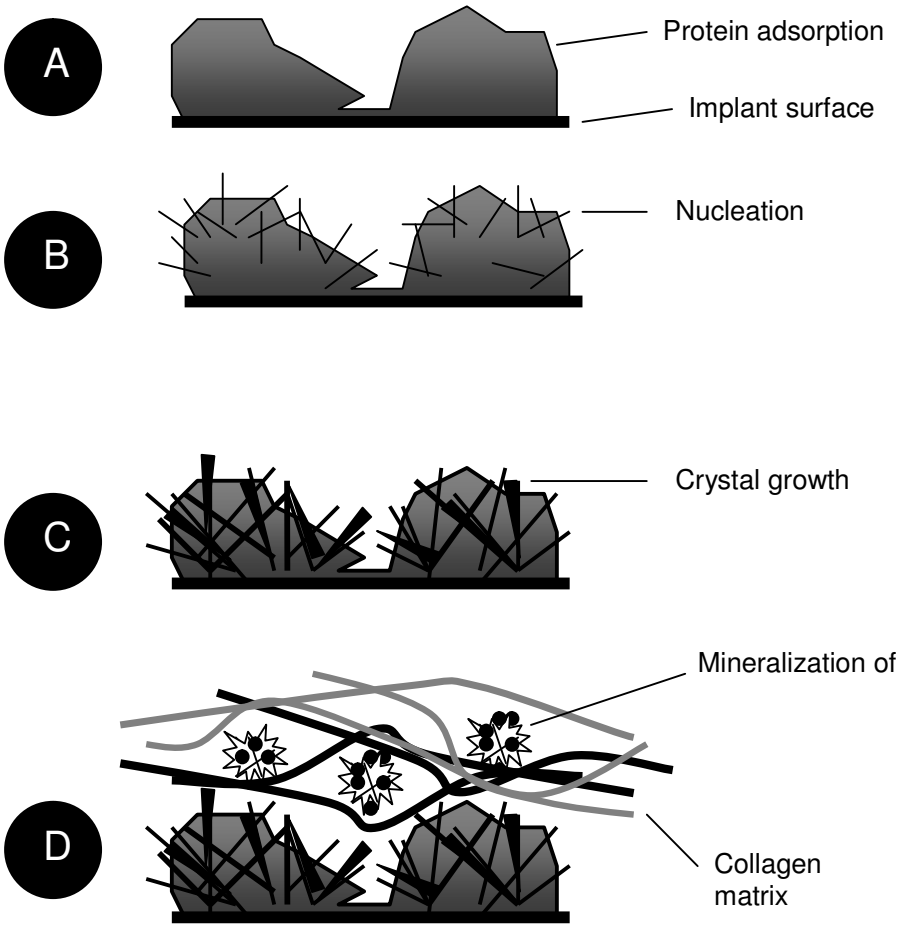

Figure 1-5 Illustration of surface deposition of calcified bone matrix on new and remodelled surfaces. The first step (a) involves adsorption of protein responsible for (b) mineral nucleation and (c) crystal growth that is followed by (d) extracellular matrix deposition and mineralization to bone (adapted from [27]).

Intramembranous bone formation has been observed on inorganic calcified implant surfaces and synthetic poly(α-hydroxy acid) based polymers [10, 105, 110, 111]. Implant surfaces that are unstable or lack topological features and pores, including hydroxyapatite have no cement line formation and poor osteoblast adhesion [112]. The cement line has adhesive bone-bonding and biomechanical function to absorb energy and provide resistance to fatigue damage and crack growth. At the interface of materials, direct scaffold contact with bone cement line results in structural continuity and stability [109]. Hence as scaffolds degrade, the support function can be adopted by the developing bone structure [113].

Acid etched titanium implants produce surface features on which a coating of nanometre sized calcium phosphate crystals provide the interdigitation for cement line formation, bone-bonding (Figure 1-6) and bone growth by apposition [109]. There is no evidence to suggest that the mechanism of bone-bonding with artificial materials is any different to that which occurs normally [105, 114].

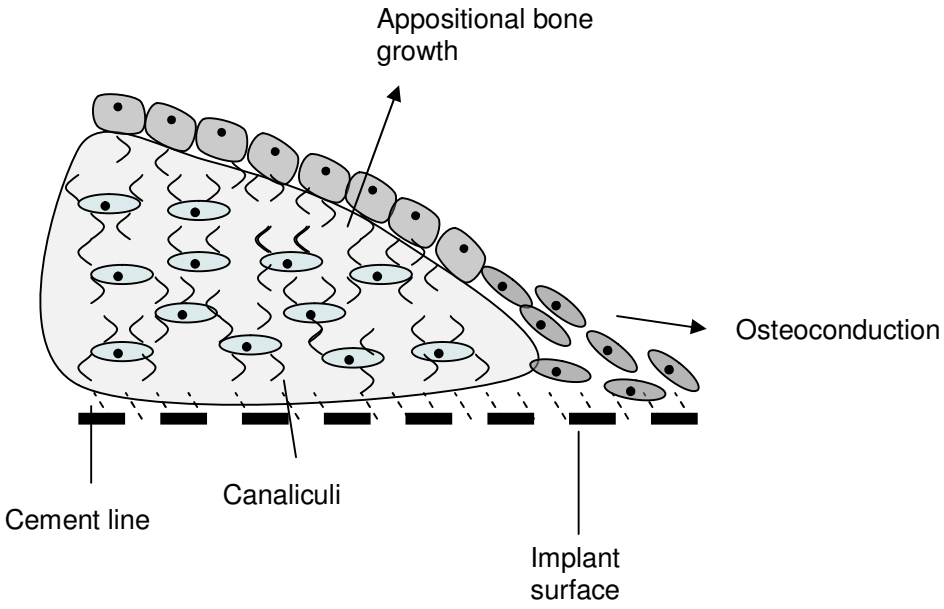

Figure 1-6 Illustration of appositional bone growth and colonization of an osteogenic surface by osteoconduction (adapted from [105]).

1.4.2 Angiogenesis and Scaffolds

The formation of new blood vessels is a key process in tissue generation and is stimulated by sustained supply of VEGF, PDGF and FGF [34]. VEGF stimulates osteoblasts and osteoclasts survival, proliferation and migration of endothelial cells that assemble, forming tubular structures [115]. Increased differentiation in *vitro* was observed by co-transplanting endothelial cells in direct contact with bone mesenchymal stem cells (BMSC), compared to BMSC alone [116]. Both endothelial and smooth muscle cells produce BMP-2 when in direct contact with osteoblastic cells, stimulating production of differentiation markers such as alkaline phosphatase and osteocalcin [117, 118]. The intimate contact of endothelial with osteogenic cells promotes direct exchange of BMP-2 that was less effectively reproduced by supplementing media with 100ng/ml rhBMP-2 [115]. Endothelial cell transplantation on polymeric scaffolds had improved angiogenesis, forming vessels that fused with host vasculature. Production of BMP-2 by endothelial cells was increased under hypoxic conditions that could occur after transplantation [117].

1.4.3 Scaffold Formats

Scaffolds can be classified as preformed structures, gels and particulates (microspheres, fibres) [119]. Preformed fabrication techniques include supercritical foaming; Rapid Prototyping, electrospinning and sintering [114]. A variety of natural materials have been used as hydrogels including agar, fibrin, gelatine, and collagen that form stable networks. Hydrogels can fill defects and deliver mesenchymal stem cells facilitating their migration across gaps. However, they do not have the

mechanical properties required for bone function [120]. As tissue engineered scaffolds hydrogels are problematic suffering poor diffusion properties for nutrient and oxygen supply which potentially restricts scaffold size [121, 122]. Combinations of high and low molecular weight alginate gels achieved mechanical rigidity with rapid bone tissue invasion by the selective diffusion of polymer fragments after chain scission [123].

Wound closure is a priority action by contractile fibroblast to initiate repair through scar tissue formation [124]. Porous particulate scaffolds can fill critical-sized defects (Figure 1-7) providing a 3D template of the void that is, readily accessed by cells regenerating extracellular matrix [2, 125]. Poly(lactide-co- glycolide) (PLGA) microspheres cultured with adipose tissue-derived stem cells were demonstrated to-self aggregate *in vivo* after injection and provide appropriate rigidity to function as porous scaffolds for muscle development in nude mice [126]. Particulate scaffolds with crenulated morphology at the interface may, improve interlocking between the implant and surrounding fractured tissue walls to participate in bone bonding with direct deposition of new bone by osteoconductive invasion from adjacent tissue into the interconnected spaces (Figure 1-7) [55] [105].

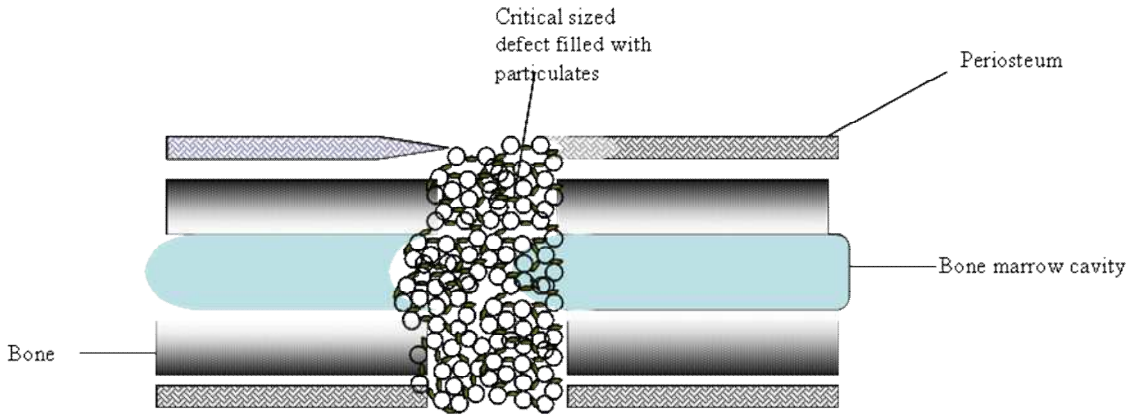

Figure 1-7 Representation of a bone fracture filled with particulate scaffold that define the space and bridge the gap to connect wound surfaces (adapted from [2]).

1.5 Particulates in Tissue Engineering

Bone has high tensile and flexural strength with energy dissipation through the ability to distort [22]. Bone has a hierarchical structure and previous work has established that it is not feasible to implant an exact replica of trabecular architecture as it represents an end state unsupported by vascularisation [20]. The preservation and regeneration of form and function are aims of tissue engineering that are achievable with particulate materials when controlling parameters such as particle size, interconnectivity, surface area, architecture and mechanical properties close to native bone [127]. Commercially available injectable calcium phosphate cements are biocompatible bone graft substitutes that can custom fit irregular bone defects then harden *in situ* [71]. The cement adheres to soft tissue in the absence of blood and is used for filling cancellous bone [128]. However, cement mixtures extruded beyond the defect damage surrounding tissue and subtle differences in processing can alter performance unduly [129]. Cements at 50-60% porosity are brittle with slow degradation profiles in excess of 5 years [130].

Materials designed to fill bone voids must meet changing mechanical and biological requirements by providing initial stabilisation, facilitating integration and new bone-ingrowth with full degradation on completion of defect remodelling [131, 132]. Polyester implants possess mechanical strength that can be tailored to meet initial requirements then progressively transfer load to surrounding tissues if the speed of degradation is synchronous with integration and new tissue growth [119, 133].

Scaffolds that utilise an open-cell repeated architecture have properties similar to bone and cells may penetrate deeper into them to facilitate endogenous repair [12].

1.5.1 Particulate Design Requirements

Lickorish et al surmised that for bone, no one material possesses all the physicochemical properties needed for success *in situ*; hence, there is a need for adaptation and harnessing the advantages of multiple materials as composites [55]. Particulates may be regarded as modular components of a system that can be administered by injection. Particulate scaffolds have reduced density in comparison to monolith materials with increased surface area for physicochemical interaction [127]. Particle shape is a key determinant of packing density that controls porosity and rough, porous surfaces aid cell spreading and bone integration [134].[135, 136].High porosity increases the surface area available for protein adsorption, ion exchange and bone ingrowth in comparison to solid walled materials [137].

1.5.2 Particulate Scaffolds with Gels

Fracture disrupts blood supply and results in fibrin clot formation, which adheres to most surfaces and facilitates rapid osteogenic cell migration [21]. Combinations of particulates in fibrin glue lacked porosity and had restricted cell penetration in common with other gelled systems [122]. Fibrin and poly(ethylene glycol) based hydrogels with FGF-1 in poly(D,L-lactic acid) and TGF-β1 loaded PLGA microspheres had retarded release rates that varied with viscosity [138, 139]. This property of retarded diffusion has been used to protect cartilage cells in an FDA approved injectable alginate wound dressing. Angiogenesis was stimulated from a

slow release delivery system of VEGF linked to a fibrin-conjugated network [118, 140, 141]. Bone was produced in nude mice after an injection of goat mesenchymal progenitor cells and ceramic particles were bound together by extracellular matrix after *in vitro* culture [142].

1.5.3 Polymer Ceramic Composites

Preformed ceramic HA and β-Tricalcium phosphate based scaffolds difficult to shape in theatre to fit defect shapes and may encounter micro-motion that can cause implant loosening [143]. This loosening can result in considerable tissue disruption; bleeding, inflammation, coagulation and foreign body response with formation of a fibrous capsule. Composite calcium phosphate and polymer microparticle based systems rely on initial cell-polymer attachment and subsequent non-toxic polymer degradation to form macropores and improve cell ingrowth [144, 145]. Polymer ceramic composites have shown varying abilities to stimulate tissue growth and give adequate degradation profile due to a buffering effect [114, 146]. Systems incorporating enzymes to hasten degradation have been proposed, but such matrices do not possess structural stability [147]. In addition, the compressive strength of a dry poly(L-lactide-co-D,L-lactide)-tricalcium phosphate scaffold was reduced from 3.1 to 1.5 MPa in water [119].

1.5.4 Polymer Scaffolds

Biodegradable polymers are reliably reproduced in high volumes and used in a variety of fabricated formats in clinical procedures, having features of good biocompatibility and reliable degradation characteristics [148]. Synthetic polymers mimic biological matrix in facilitating cell attachment [149]. Scaffold surfaces favouring strong adhesion and spreading promote osteoblast proliferation and mineralisation [78, 150]. Demineralised bone matrix, a recognised osteoregenerative material, produced faster healing when combined with PLGA [151, 152]. Controlled growth factor release has been demonstrated by surface immobilization and encapsulation into polymer devices that stabilised the protein and prevented proteolysis [153], [154]. Protein loss, during fabrication, encapsulation and elevated heat sintering, remain as issues [155, 156].

1.5.5 Particulate Sintering

The process of sintering enables a single unit to be manufactured from composites and pure particulate materials [157]. The strength of particulate scaffolds is a result of material composition, intergranular friction and geometric locking due to topological surface irregularities [158]. Particulates used in drug delivery systems are now seen as a means of achieving higher control of parameters such as pore size, surface area and interconnectivity [127]. The method of manufacture influences the parameters of shape, compressibility and apparent density. Only the high points of irregular particles touch forming struts that define the edges of interconnecting (open) pores [119]. A network of struts produce a low-density solid with voids connected to each

other through open faces to accommodate mass transfer. Aggregation involves particle adhesion resulting in higher resistance to compression and tensile stress [159]. Adhesion between particles is a result of intermolecular forces affected by material hardness, elastic modulus and temperature of glass transition (Tg), [160]. Adhesion is augmented by increasing the duration of contact or raising the temperature of the particles.

Compacted, aggregates can be shaped to generate large porous supportive structures that mimic cancellous bone. For sintering to proceed surface molecules must have sufficient mobility to move to new positions which is temperature and solvent dependent. Molecular motion is a consequence of thermal softening that is, time and temperature dependent [161]. Packed powders will bond when heated in excess of approximately half their absolute melting temperature in response to atomic motion [162]. This temperature can be reduced by the addition of plasticizers and heat can be localised by laser to produce complex shapes with interconnected pores [163]. Sintering involves the mobilization of surface molecules by mechanisms that may including viscous flow, surface diffusion or evaporation and condensation as illustrated by the partial dissolution of microsphere in solvent/non-solvent sintering using ethanol and acetone [162, 164-166]. Surface area is reduced and strength increased (Figure 1-8) [167]. Surface diffusion produces neck growth between particles without shrinkage [168]. Recent work shows glassy state materials to have orders of magnitude more mobility at the surface than in the bulk below Tg [169].

Therefore, at low temperatures, viscoelastic sintering with reduced densification can occur [170].

Glass transition varies interchangeably with time and temperature and is accompanied by changes in thermal conductivity and ductility [160, 171]. Those particles in cohesive contact with each other form a skeleton capable of mechanotransduction, compression and resisting shear. After sintering, voids become pores, adding structure, ductility and transmission [20].

In liquid sintering, a fluid phase coexists with a particulate solid at the sintering temperature and enhances particle bonding with faster atomic diffusion and densification during curing [162]. Sintering is quicker in liquid rather than solid phase and the cohesive internal force generated through liquid capillary action on the particulate solid gives rapid compact densification without the need for a large external pressure [162]. An interconnected pore network is formed by the liquid phase.

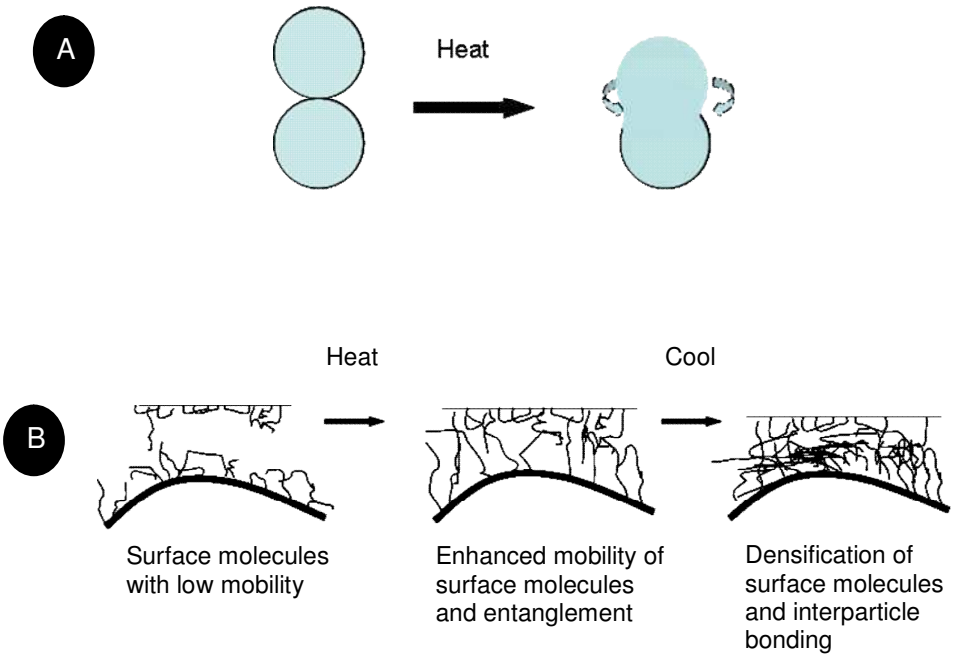

Figure 1-8 Illustration of the particulate heat sintering process to show (A) mass flow and coalescence through neck formation between particles and (B) diffusion bonding through heat induced molecular mobility, entanglement, collapse and densification at the interface of particles (adapted from [160, 162]).

1.6 Review of Lactide Based Polymers in Scaffold Design

Poly(lactide) is a thermoplastic, biodegradable, aliphatic polyester derived from lactic acid which is chiral in nature and exists as D and L optical isomers [172]. L- lactic acid is naturally occurring as a metabolite in the body. Poly(D,L-lactide) is an amorphous synthetic blend of the isomers made from the cyclic dimers. Condensation reaction of cyclic lactide with glycolide dimers produces poly(lactide-co- glycolide) (PLGA) copolymers that can be varied by composition with respect to component ratio, molecular weight, crystallinity; feed rate during polymerization and post formed processing to alter properties of strength, degradation rate and solubility [173, 174].

Crystalline polymers undergo a melt phase transition that is absent in amorphous polymers [175]. The International Union of Pure and Applied Chemists defined Tg as a second order phase transition, as there is no latent heat involved. Glass transition is a time dependent change fixed by heating rate and marks the onset of segmental mobility [168]. Amorphous non-cross linked thermoplastic polymers passing through the glass transition region with increasing temperature change from brittle solids to viscoelastic liquids. The properties that make PLGA copolymers suitable for use include thermoplasticity, biocompatibility, controlled degradation and proven non toxicity [176]. Lactide polymers and copolymers are thermoplastic and can be fabricated by a myriad of techniques into structures from nano to centimetre scale

with custom mechanical properties to fit roles as diverse as drug delivery and orthopaedic fixation devices [177, 178]. Material use *in vivo* shows an absence of infections and transient inflammation, dependent on copolymer blend and site drainage [59, 179].

1.6.1 PLGA Interaction with Cells

PLGA 75:25 was demonstrated to have a higher rate of osteoblast adhesion in comparison to tissue culture polystyrene despite being more hydrophobic [113]. Comparison with polystyrene showed the polymer to stimulate higher levels mineralisation, support deposition of a mineralised cement line, extracellular matrix production and extended the cell growth period [78, 113]. The initial rate of adherence was significantly higher for PLGA in comparison to PLA for the first 12 hours with greater osteocalcin production indicating osteoblastic maturation [148]. Initial osteoblast attachment was higher for PLGA 50:50 than PLGA 85:15 but was reversed by day 15 [180]. In conjunction with this, PLGA 50:50 was demonstrated to be osteoconductive to osteoblast and fibroblast cells that migrated through the structure using cytoplasmic extensions [113] [181]. Acellular scaffolds regenerated bone slower than *in vitro* seeded constructs in the absence of growth factors [111].

Comparison of primary human osteoblastic cell growth on a variety of poly(α-hydroxy esters) used in skeletal engineering, found full expression of key osteogenic markers, mineralization and maturation of cells [180, 182]. Foamed, porogen leached and sintered PLGA copolymers have been shown to stimulate bone and cartilage

repair [183-186]. Bone sialoprotein expression was limited and associated with the mineralisation process. In combination with BMP-7, PLGA scaffold closed a 15 mm segmental defect in a rabbit bone model [153].

1.6.2 PLGA Degradation

The popularity of polyesters is attributable to FDA approval status for selective application, history of use, known degradation profile *via* ester linkages (Figure 1-9), and relatively low toxicity potential of metabolites [153, 187]. Degradation *in vivo/vitro* begins with random bulk (acid/ alkali) hydrolysis of the backbone ester linkages with pH reduction, erosion of mechanical strength without direct enzymatic cleavage and progressive fragment mobility [179, 188]. Particles up to 10 µm can be phagocytosed, stimulating an immune response [110, 189]. Enzymes can enhance the initial *in vivo* attack producing lactic acid that is metabolised. PLGA copolymer degradation rates are dependent on composition ratio as higher hydrophilic glycolide content results in faster degradation [190].

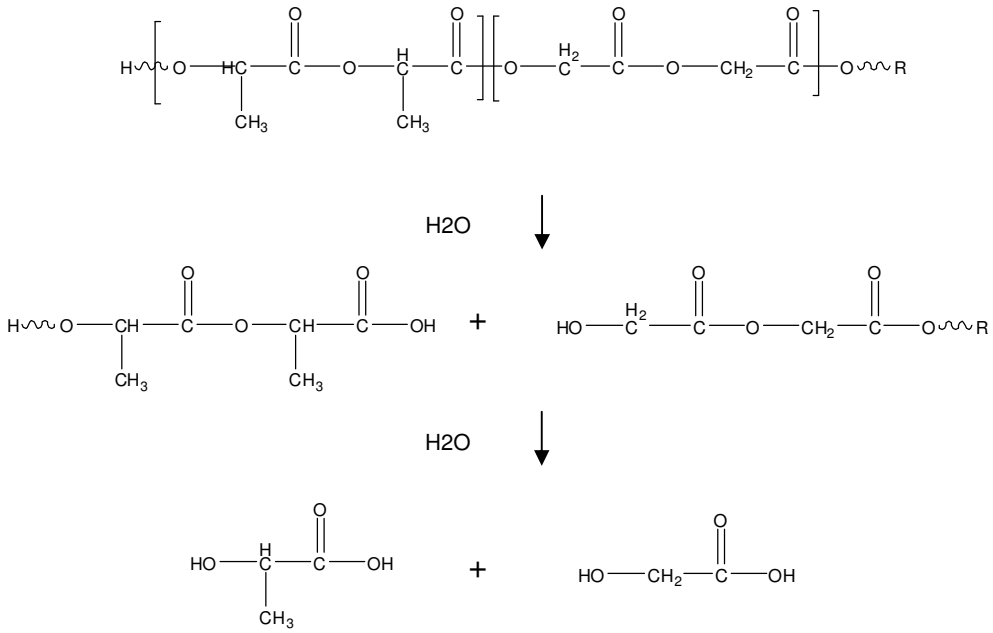

Figure 1-9 Schematic showing the degradation of poly(DL-lactide-co-glycolide) by hydrolysis to its constituent materials lactic and glycolic acids that can be further degraded within the body.

PLGA 50:50 has the fastest degradation rate and copolymer lifetime is progressively longer with diminished glycolide content; in addition, thick films degraded faster than corresponding thin films of the same composition [191]. Fast degradation due to acid stimulated autocatalysis is associated with low porosity and long diffusion path lengths [113] [192]. Tissue necrosis occurs when clearance of breakdown products and nutrient exchange becomes inadequate [34, 144, 193]. Calcium phosphate addition to PLGA polymers reduced degradation rate and enhanced mechanical strength [194]. Poly(glycolic acid) degrades quickly with the potential for toxic acid accumulation as glycolic acid can dimerize to glycolide and activate the complement inflammatory pathway [195] [190].

The polymer mass initially lost in degradation changes slowly until hydrolysed chains are small enough to diffuse out of the polymer matrix. Degradation of PLGA microspheres in mice to glycolic acid, lactic acid and lactoyllactic acid stimulated increased production of glycosaminoglycans and type II collagen [196, 197]. Localised pH shifts from 7.4-6.8 inhibit alkaline phosphatase activity by > 90% and stimulated osteoclastic bone reabsorption [198]. Studies with macroporous scaffolds show bone formation was not demineralised by the acidic degradation products in porous PLGA systems [10, 111].

1.6.3 Polyester Plasticization

Polymer blending is a method used for developing new properties from existing materials. To broaden polyester applications the physical properties of flexibility and impact resistance are improved by the addition of plasticizers [199]. Plasticizers are at least partially miscible with the polymer and reduce the temperature at which glass transition occurs by disrupting the packing of amorphous polymers [200]. PLGA monomers and oligomers, themselves, are effective plasticizers but accelerate degradation; hence, choice is limited by the requirements of the application [192, 201, 202]. In the Tg region strength, volume, Young's modulus and viscoelasticity change significantly [203]. The mechanical properties of amorphous thermoplastic materials can therefore be tuned by adjustment of the Tg to a desired temperature [204].

1.6.4 PEG

PEG acts as a hydrogen bond acceptor and its properties are temperature and molecular weight dependent [205, 206]. High molecular weight PEG is FDA approved for internal use and polymers 3,350-10000 Da are utilized as mild laxatives [37, 207]. Ingested PEG 400 is used as an intestinal permeability marker in humans and excreted unchanged [208]. Intravenous injections of 60% solutions of PEG 400 into primates were nontoxic and PEG 200 at 10% has been used in the microencapsulation of L929 mouse fibroblast cells [209, 210]. Short chained PEG has a low capacity to crystallize and high mobility [211]. PEG polymers below 400

Da can be sequentially oxidised by alcohol and aldehyde dehydrogenase to toxic diacid and hydroxy acid products and excreted in urine [212]. Reaction rates decrease with increasing PEG molecular weight [213].

In melt blends with polyesters PEG forms a physical solution without chemical reaction [214]. Excess plasticizer can separate, crystallize and promote polymer crack formation under stress [201, 202, 215, 216]. At constant PEG loading PLGA strength is increased with lactide content [200]. PEG addition exceeding 10% $^{w}/_{w}$ to PLGA significantly reduced tensile strength, and increased ductility [133]. Plasticizer separation and migration to the surface results in spinodal decomposition (Figure 1-10) and is accelerated by humidity and storage at temperatures close to and exceeding the blend Tg [216].

Low molecular weight PEG has improved miscibility and increased plasticization efficiency [214]. Polymer blends below glass transition undergo molecular relaxation towards thermodynamic equilibrium [217]. This ageing process lowers the free volume for molecular motion as a function of time. The further restrictions of molecular motion in aged polymers prevent the absorption of impact energy and the material becomes more brittle [218].

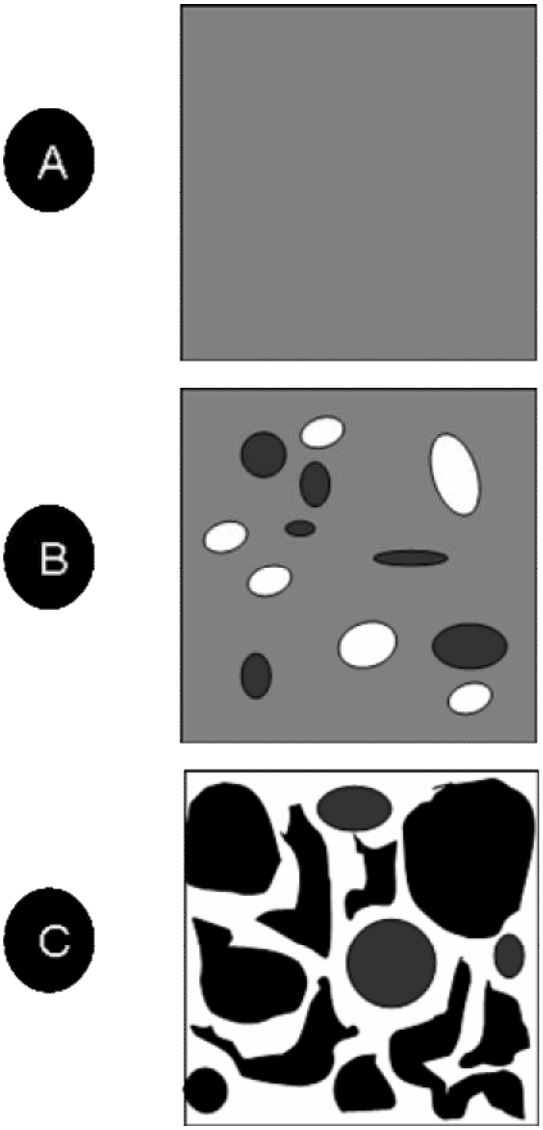

Figure 1-10 Illustration of (A) thermodynamically unstable annealed polymer blend that undergoes spontaneous separation, starting with small fluctuations in composition (B) to produce a dispersed droplet structure and spinodal demixing through to (C) coalescence of the segregated phases.

PEG leached from PLGA left the polymer surface pitted [133]. PLGA wet strength is inversely related to glycolide content [204]. Wet PLGA-PEG copolymers at pH 7.4 swell by a factor greater than 3.5 times and are progressively softened; losing significant strength after a week; whereas wet PLGA polymers show increased modulus [219, 220]. PEG *via* physical and covalent coating can modify polymer biocompatibility [221, 222].

1.7 Structuring Mechanisms of Injectable Scaffolds

Injectable scaffolds administered by arthroscopic and open surgical procedures can be moulded to fit defects then undergo *in situ* polymerization or cross linking to develop mechanical integrity and interconnected porosity within clinically relevant timescales for cell survival [223, 224] . All components of the injectable system introduced individually and collectively must be non-toxic and the solidification mechanisms have minimal impact on the homeostatic balance within the wound and surrounding tissue.

Curing *via* chemical initiators activated by UV and visible light wavelengths include camphorquinone and benzoyl peroxide [189]. Chemical cross-linking is a versatile strategy as shown by poly(propylene fumarate) that cross links *via* thermal and photochemical reactions with compressive strengths comparable to cortical bone [225]. These cross linkable polymers must avoid dilution of the initiator and cross linker ratios in order to control the density of the final polymer network structure

[143, 226]. The toxicity of reactive agents in addition to collateral reactions require temporary cell encapsulation in e.g. gelatine to improve viability [227].

Thermal gelation has been used for a number of synthetic and naturally derived polymers such as poly N-isopropylacrylamide, gelatin and agarose [228]. Polymers undergo reversible solubility changes involving chain entanglement and collapse in response to temperature changes [229]. The sol-gel transition temperature can be tuned by altering copolymer composition and polymer molecular weight [230, 231]. Poly-D,L-lactic acid-polyethylene glycol copolymer had to be heated to become injectable and was used to deliver rhBMP-2 in mice with bone formation [232, 233].

Work at Nottingham University demonstrated the injectable delivery of solid biotinylated PLA-PEG microspheres mixed with cells [234]. The system relied on the specific interaction of avidin with biotin transforming an injectable dispersion into an elastic solid with high storage modulus. The crosslinked structure, formed *in situ* with cells, had controllable pore size up to 100µm in diameter and was capable of delivering growth factors. The system achieved full structural integrity within seconds to perform the tertiary function of retaining the existing tissue shape to promote cell ingrowth.

1.8 Porosity and Pore Size of Scaffolds

Scaffolds are a balance of competing parameters with mechanical strength inversely related to the scaffold pore size [235] [236]. As the size of particulate scaffold components are scaled up, porosity and flux are increased, but fewer struts hold the construct together for a given volume. Pore size distribution, architecture, and interconnectivity influences nutrient permeability, cell migration and polymer degradation characteristics [58, 237]. The need for porosity to support bone regeneration was demonstrated by comparing solid with porous HA implants delivering BMP-2 in a rat ectopic model. Bone was formed only on the porous implant [112, 238]. Low porosity and reduced pore size (< 40 µm) induced hypoxia, cell aggregation and differentiation to chondrocytes [20, 236].

Increasing scaffold porosity alone is insufficient; the balance between mechanical strength and sufficient initial void volume for cells must be met [132, 239]. High porosity (>80 %) *in vivo* and large pore size produce improved bone ingrowth but compromised scaffold strength [240]. PLGA scaffold collapse due to extracellular matrix contractile forces from fibroblasts and osteoblasts was observed [240] [49, 143, 241].

The clinical requirement for porosity vary by fracture site with spinal fusion 80% porosity and hip revision 60% porosity[7]. The 100 µm minimum pore size was proposed following *in vivo* work in dog femoral bone with calcium aluminate

cylindrical pellets of 46% porosity [242]. In contrast titanium plates with 50-125 µm pore sizes, implanted in non load-bearing rabbit femoral had bone ingrowth in all voids [236]. Scaffolds with pore diameters of 10-100 µm have been used as haemostatic devices [111]. Optimal pore size for tissue regeneration was believed to be in the 100-500µm range with bone ingrowth biased towards larger pores [243] [244]. Rose *et al* showed a minimal diameter of 80µm was required for cell migration in ceramic scaffolds, but Jones and Hench suggested pore diameters >100µm to be secondary to interconnectivity affecting the type of tissue and rate of formation as early fibrous tissue invasion can choke pores[132, 245]. Work with HA based scaffolds with BMP-2 showed pore diameters of 95-120 µm to initially favour chondrogenesis and pores > 350 µm osteogenesis [246]. Recently, 350-800 µm diameter pores were shown to have a limited impact on bone regeneration *in vivo* with poor growth factor retention [247]. Pore dimensions and diffusion path lengths play a crucial role in solute transport and the occurrence of autocatalysis in PLGA microparticle based scaffolds [192]. Material and biological requirements play a key role in determining minimum pore size and interconnectivity.

In vitro culture and cell colonization of constructs can indicate porosity requirements quite different to that required *in vivo* and was most notable in load bearing conditions where HA with pore diameter < 200 µm was not regarded as suitable for *in vitro* cell seeding due to limited cell penetration and growth of cell sheaths that choked pores, further restricting diffusion [111, 248].

1.8.1 The Compromise of Structure and Morphology

Dense ceramics and polymers have high strength and stiffness to match cortical and cancellous bone; but porosity causes a reduction in strength [249]. The designed mechanical properties of a scaffold are dependent on geometry, material composition, compilation and must be based on measurable bone mechanical properties such as stiffness (Young's Modulus) and strain encountered [101]. Young's modulus is a structure-insensitive property barely influenced by small in-homogeneities in micro- and macro- construction [250]. The mechanical properties of cancellous bone vary with orientation and the morphology of bone present with the upper limits of porosity and pore size dependent on mechanical and structural constraints specific to the tissue sites [22] [251]. Scaffolds must satisfy local mechanical properties specific to the implant site, in order to optimise integration with surrounding tissue [15, 251].

1.8.2 Living Constructs

Cell survival in large (4-8 cm diameter) scaffolds for segmental bone defects remain an issue as initial surface growth at the implant boundary can limit nutrient and oxygen transport to the interior in osteogenic scaffolds [49]. Asymmetric cell loading to the periphery of scaffolds produced greater ingrowth in comparison to evenly seeded structures [252]. To increase the potential for vascularisation and cell penetration a polarised hierarchical distribution design with large pores oriented to the exterior in a heat sintered PLGA scaffolds has been proposed [49]. In mice, defects showed faster cell differentiation and bone deposition to occur with PLGA implants than without and seeded scaffolds in critical-sized defects produced faster

bone regeneration than acellular constructs [111, 253]. However, this method potentially requires two invasive procedures; the first to recover bone fragments for expansion and seeding of the scaffold and the second to implant the construct. Ex-*vivo* cultivation is expensive with potential to introduce infections [243].

There is a clinical need to ensure even cell growth throughout tissue engineered scaffolds, avoiding dead void volumes. Strategies devised to facilitate this include *in vitro* use of rotational bio cultures to perfuse media throughout preformed scaffolds, plasma polymerised surface chemical gradients, entrapment of chemotropic growth factors acting to stimulate inward cell migration and pre-vascularised implants generated in the body [254-258].

1.9 Injectable Scaffolds

The emergence of arthroscopic techniques in tissue repair, provide alternative procedures to open surgery and implant removal. Minimally invasive techniques preserve the integrity of blood supply in soft tissues, decrease complications and reduce recovery time [90]. Injectable bulking agents have been delivered endoscopically to treat clinical conditions of reflux and incontinence [118]. The reduced invasiveness of procedures and low associated morbidity minimise scar tissue formation, patient discomfort and make this an outpatient procedure. Injectable poly(lactide) nanoparticles have been widely used in parenteral drug delivery and molecular self-assembly systems that reside at the injection site until biodegraded [259, 260]. Injection of polymeric micro and nanoparticles form porous networks of fluid permeated diffusion channels and improved localised targeted drug efficacy over conventional applications with reductions in side effects, drug costs and

frequency of administration [84, 261]. Injectable solid rhBMP-2 formats would have low systemic exposure and provide an alternative to open surgical procedure [70, 81, 262]. Simultaneously delivery of cells with growth factor may therefore be advantageous in stimulating healing.

1.10 Aim:

If Tg controls amorphous material transition from soft to hard matter then reduction of polymer Tg may improve particulate sintering at physiological temperature. This research aims to develop an injectable scaffold system for use in bone regeneration and repair. In this system, micron sized particulate PLGA based polymer will be applied as an injectable cell delivery vehicle that can custom fit defects then harden to a macroporous structure to support and regenerate bone with the option for localised controlled growth factor release.

In detail, the material is injectable as a two component system with a component I that is temperature insensitive. Component II is the cohesive temperature sensitive constituent with a Tg within the normal physiological range of the body. Component I depending on its morphology and composition may functions as a porous spacer, cell carrier and drug delivery vehicle. Component I can be a randomly shaped microparticle or microsphere that can be further modified to be of low or high porosity with surface modifications for enhanced cell attachment and or drug delivery potential. Mixing Component I and II in an appropriate ratio with exposure to body heat results in a crosslinked fully-interconnected porous structure (Figure 1-11).

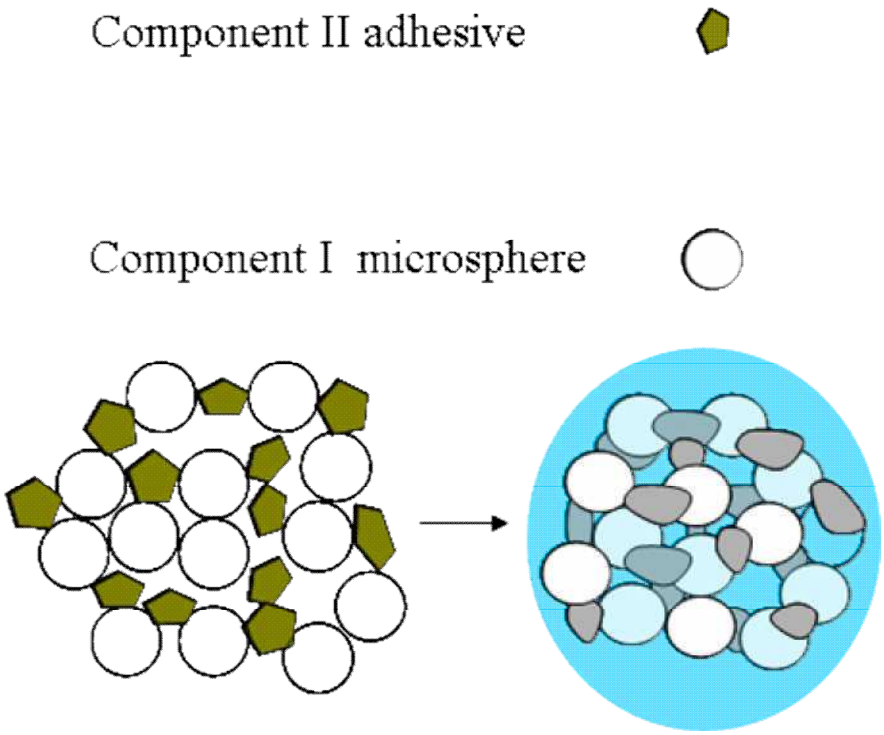

Figure 1-11 Illustration of scaffold components that are sintered to form a porous structure composed of microspheres in combination with adhesive component II. When the temperature is raised above the glass transition temperature of the adhesive component II, it softens and deforms by mass flow resulting in particle coalescence. Component I microspheres have a glass transition temperature higher than the adhesive component and are not deformed at the sintering temperature; this results in limited shrinkage and retained interconnected porosity.

The objectives will be to:

- Optimise temperature sensitivity to be clinically relevant and non-toxic to cells.
- Design in mechanical properties compatible with the structural properties of bone.
- Be injectable and mouldable
- Define and measure what is happening macroscopically to the scaffold around the softening and sintering points.
- Control porosity to improve nutrient diffusion and cell ingrowth into the scaffold.
- Demonstrate cell and therapeutic growth factor delivery

1.11 Conclusion

Improved understanding of fracture complications has enabled the use of degradable synthetic materials to be considered advantageous in tissue engineered solutions. The current challenges and complications in bone repair are infections, low strength of union, incomplete degradation of implants and poor vascularisation leading to re-fracture with slow and painful healing rates in some patients [42]. Tissue engineering as a concept can address these challenges. In this work, cells, growth factor and scaffold are deliverable by a minimally invasive technique to develop an environment suitable for bone growth.

2 Materials and Methods

This chapter describes the materials and methods used for work carried out in this thesis. All general chemicals and reagents were purchased from Sigma-Aldrich (Dorset, UK) unless otherwise stated.

2.1.1.1 Microspheres Preparation by Emulsion and Solvent Evaporation

Poly(vinyl alcohol) (PVA) molecular weight 23,000 and 87-89% hydrolyzed was purchased from Sigma-Aldrich (UK) and poly(DL-lactide-co-glycolide) from Lakeshore Biomaterials, USA (PLGA 50:50, Low I.V. inherent viscosity of 0.57 dL/g and 2kD polydispersity). A 1litre solution of PVA 0.3% $^{w}/_{v}$ in distilled water was made the day before use and stirred overnight in a glass container. The solution was filtered twice: first through a Whatman 540 ashless filter followed by a 0.2 μm pore size filter before use. In a scintillation vial, 6 mL of dichloromethane (HPLC grade) was added to PLGA (1.2 g) and blended. PEG 400 (Fluka, Germany), 0.9 mM, (360 mg) was added to the scintillation vial and vortex mixed at 2750 rpm for 2 minutes. PVA 0.3% solution, 6 mL, was added to the scintillation vial and vortexed for 20-30 seconds at 1500 rpm. The resulting mixture was pipette transferred to a hardening bath containing 800 mL of PVA 0.3% solution and stirred overnight in the fume hood to allow evaporation of DCM. The microspheres were

recovered on a Whatman 540 filter, washed three times with distilled water, vacuum-dried for a minimum of 48 hours and vacuum-sealed prior to storage in a fridge until used.

2.1.1.2 Microsphere Preparation with Polyethylenimine

In a scintillation vial, 4 mL of dichloromethane was added to PLGA (1.2 g) and blended. Dichloromethane 1.5 mL was added to a blend of 1.33 µM polyethylenimine (0.033 g) (Sigma-Aldrich (UK)) with PEG 400, 0.9 mM, (0.36 g) and dispersed by vortex before being added to the scintillation vial with PLGA and mixed at 2750 rpm for 2 minutes. PVA solution, 6 mL, was added to the scintillation vial and vortexed for 20-30 seconds at 1500 rpm. The resulting mixture was pipette transferred to a hardening bath (800mL of PVA 0.3% solution) and stirred overnight in the fume hood to allow evaporation of DCM and microspheres recovered as previously described in section 2.1.1.1.

2.1.2 Salt Leached Porous Particles

PLGA (0.9 g), was placed into a 50 mL centrifuge tube with 2 mL DCM and blended until homogenous. Sieved 212-300 µm sodium chloride (Sigma-Aldrich, UK), (12 g), was added in stages to the centrifuge tube interspersed with vortex mixing to form a sticky ball. Additional sodium chloride (6 g), was placed onto a ceramic tile and the polymer ball blended with it and flattened to a thin flake layer using a rolling pin. The solvent was removed from the flakes by evaporation in a fume hood over 24 hours [133]. After evaporation, the

brittle flakes were broken into pieces approximately 1x1 cm in dimension and placed in 2 L of distilled water with 4 changes in 48 hours to leach the sodium chloride out of the polymer. The leached particles were recovered on a Whatman 540 ashless 125 mm filter and dried overnight at 40 °C. The dried flakes were vitrified in liquid nitrogen; ground and sieved fractions were vacuum sealed and stored in the fridge.

2.1.3 Type II Temperature Sensitive Particles

PEG 200 was supplied by Fluka (UK) and PEG 1000, 2000 and 5000 by Sigma-Aldrich (UK). PLGA and PEG were combined in a range of weight fraction melt-blends as small (2 g) batches.

PLGA	100	99	98	95	85	80	0
PEG 1000	0	1	2	5	15	20	100

Blends were ground into a powder using a standard coffee bean grinder. Melt blend PLGA with PEG powder (approximately 110 mg) was placed in each well x12 of a Teflon mould (5 mm diameter and 10 mm height), used to standardise scaffold dimensions for testing.

2.1.4 Compression Testing

Scaffolds, 9 mm long and 5 mm diameter were cast in a mould and sintered at different combinations of time and temperature, dry and wet. Constrained and unconstrained uniaxial compression tests were conducted with a TA XT plus Texture Analyser from Stable Micro Systems (Surrey, England) fitted with a Peltier controlled environmental chamber. The ramp speed of 0.01 mm/sec was used for all test conditions, dry and wet [17]. Uniaxial compression test measurements were displayed as stress versus strain graphs. For each specimen tested, the maximum force resisted (strength) and Young's modulus were recorded and displayed as mean ± standard deviation. Statistical tests used were analysis of variance and Tukey-Kramer multiple comparison test to determine significance between variables.

2.1.5 Rheology

Rheological measurements were conducted on a Physica RC 301 (Anton Paar, Austria) with parallel plate geometry and environmental hood. Non-destructive oscillatory measurements were conducted under nitrogen gas flow to determine structural change with temperature. Figure 2-1 shows the temperature response profile of an amorphous PLGA material and the Tg detected by the three principal parameters of elastic modulus (G'), loss modulus (G'') and phase angle (δ). The phase angle (δ) plot (Figures 2-2)

provides more information on the structural changes occurring in response to temperature and was used in this thesis. The rubber plateau occurs in the region after the Tg where the material has a deformable structure due to increased molecular mobility but does not flow as polymer network entanglement and interactions form a highly viscoelastic state.

Oscillation measurements were conducted at constant gap and controlled strain (0.1%) with a 25 mm parallel plate. The temperature was ramped from 4-90 °C at a rate of 1 °C / minute. Samples (0.2-0.4 g) were loaded onto the plate at 18 °C and the environmental hood lowered into place. The temperature was lowered to 4 °C under a dry nitrogen stream, prior to starting the experiment. This procedure was necessary to prevent condensation of water on the sample.

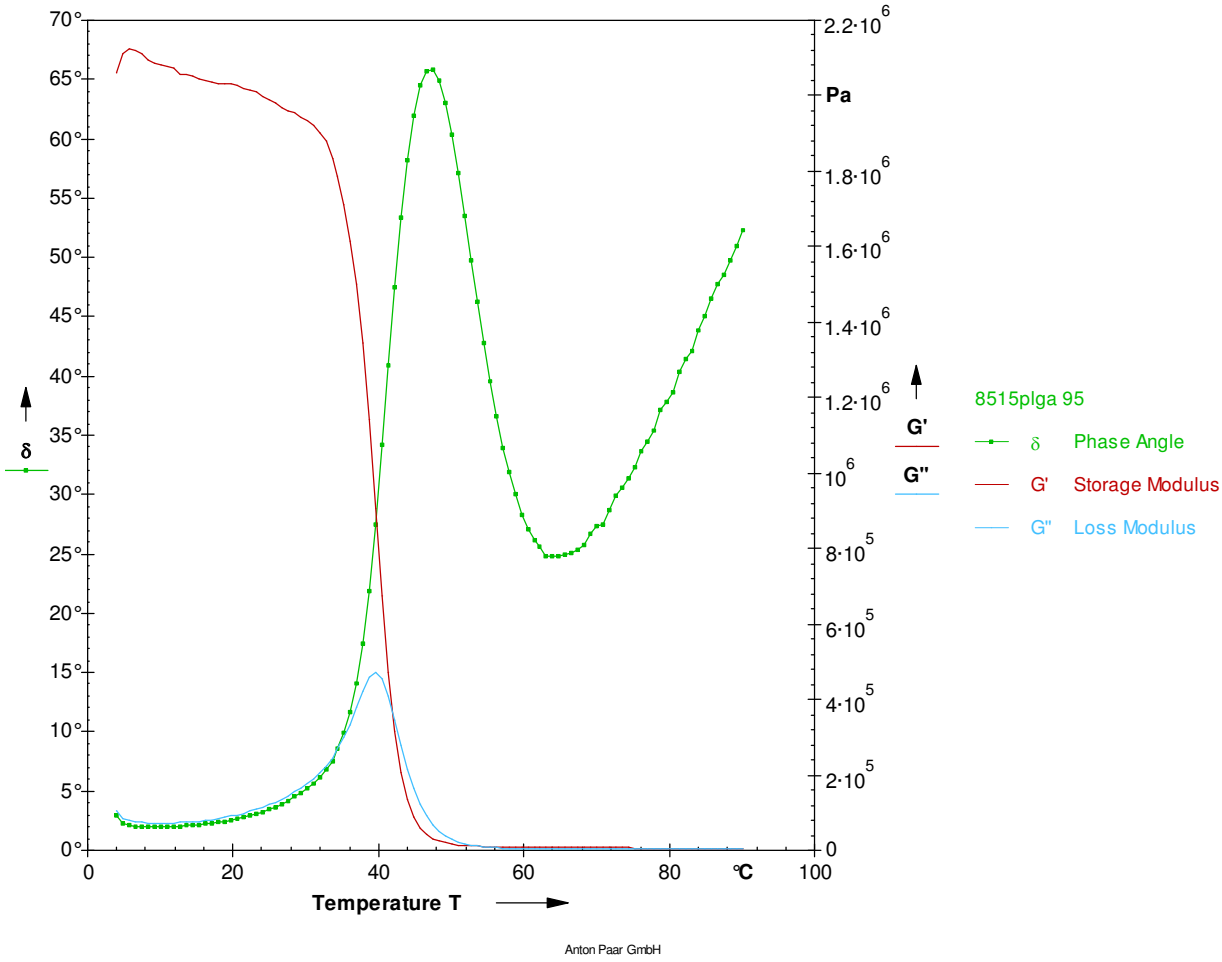

Figure 2-1 Oscillation temperature ramp profile from 4-90 °C of amorphous PLGA 85:15 with 5% PEG content at 0.1% strain. It shows the phase angle (ratio of loss modulus to storage modulus) plot (δ) to provide the most information on structural changes in response to temperature.

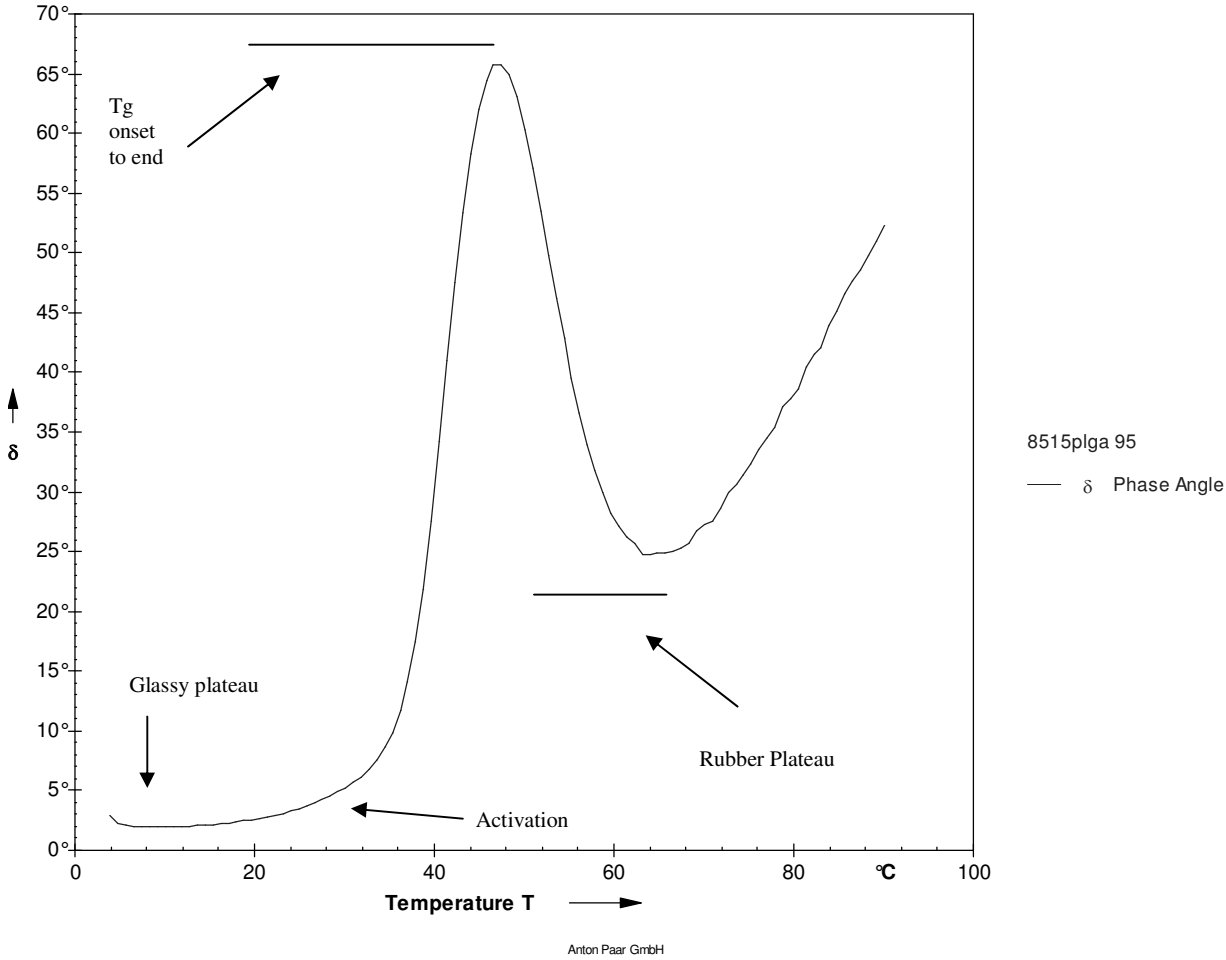

Figure 2-2 Oscillation phase angle profile illustrating changes in the material in response to temperature ramp from 4-90 °C and 0.1% strain. Physical properties such as elastic and viscous moduli change significantly across the glass transition region.

2.2 Differential Scanning Calorimetry (DSC)

Differential scanning calorimetry measures heat flows associated with temperature-induced transitions (Figure 2-3). Standard DSC experiments were conducted to find the temperature and width of transitions. Differential scanning calorimetry measurements were conducted on a 2920 DSC from TA Instruments (UK). Powder polymer samples, 5-10 mg, were placed into aluminium pans and hermitically sealed. The samples were heated at 10 °C per minute under a flow of nitrogen in temperature ramps from –40 °C to 120 °C followed by a 10 °C per minute cooling ramp and subjected to five temperature ramp cycles.

2.2.1 Modulated DSC

It is not possible to achieve optimum sensitivity and resolution in a single standard DSC experiment. Modulated DSC measurements were conducted on samples at a heating rate of 1 °C per minute, from -20 °C to 120 °C, ±0.159 °C amplitude, 60 seconds modulation period and cooled at 10 °C/minute to -20 °C for two repeated cycles.

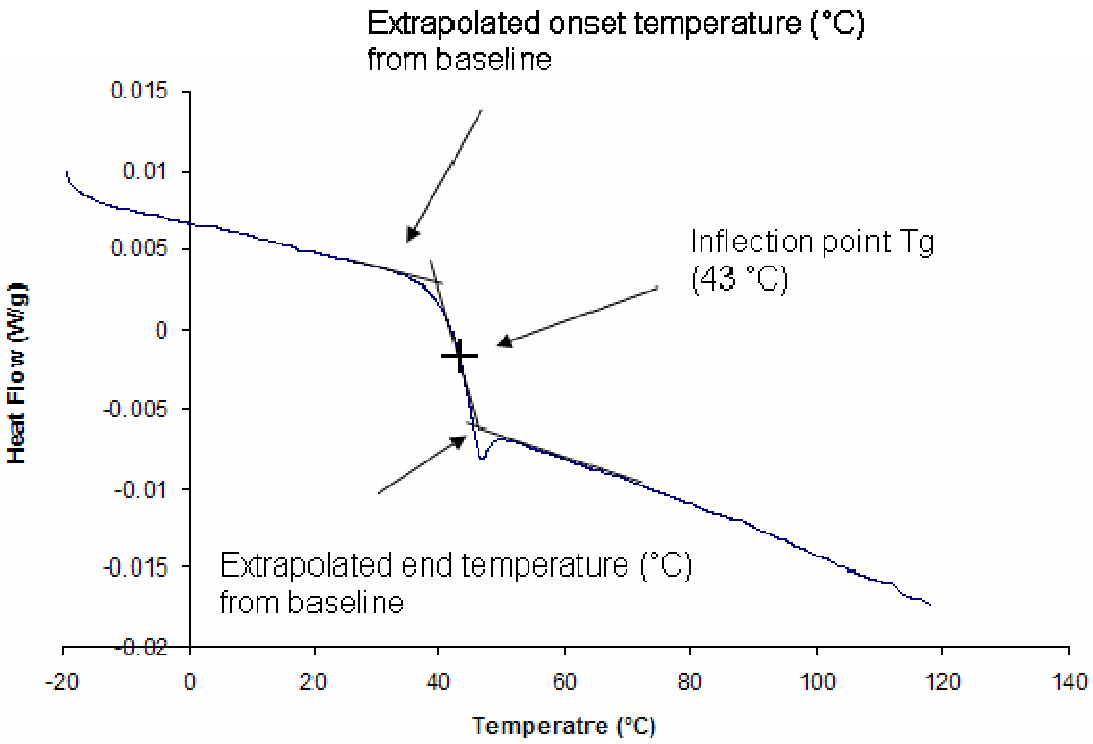

Figure 2-3 A differential scanning calorimetry (DSC) profile of an amorphous polymer with a glass transition phase detected as a sigmoidal shift in heat flow. Typically, a single temperature taken at the inflection point (the midpoint between extrapolated onset and end temperatures) represents the temperature range over which the glass transition takes place.

2.3 Wenger Transition Phase Analyser

The Wenger Transition Phase Analyser is a closed-chamber capillary rheometer designed to detect softening and flow of multi-component solid materials in response to temperature at a constant pressure. The closed system does not allow moisture to escape; hence, its effect can be measured linking thermal transitions to physical compaction strength [263]. Particulate scaffold materials were made up fresh and stored at 5 °C under vacuum before 1.83 g was loaded into the compression chamber. Samples were compacted at 10 °C and 150 Bar pressure for 5 seconds to form solid pellets. The pressure was reduced to 100 Bar and the temperature ramped linearly at 5 °C per minute. The experiment was ended when the material was mobile enough to flow out of the chamber through a rubber seal under pressure. The equipment measures displacement induced by temperature and enables the controlling glass and melt transitions to be detected (Figure 2-4). The controlling Tg onset, is the temperature at which displacement begins when a sufficient amount of the sample has softened. The transition melt is the point at which the material begins to flow. The Transition Phase Analyser enables the correlation between temperature and physical change. The amount of plasticizer and increasing pressure can shift the measured Tg [264].

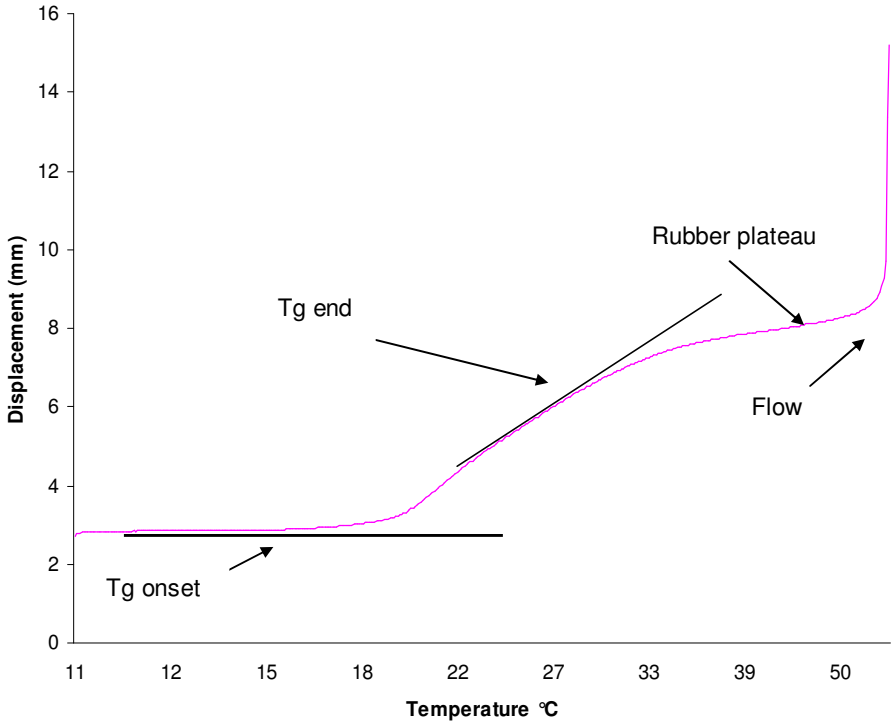

Figure 2-4 Displacement plot showing features of a Transition Phase Analyser curve, relating thermal transitions to physical compaction.

2.4 Cell Culture Methodology

Cells were seeded in Dulbecco's Modified Eagle's Medium (42430-025) from Gibco (Paisley, Scotland), supplemented with 10% ($^{v}/_{v}$) foetal bovine serum (FCS), antibiotic consisted of 100 units/mL penicillin, 25 µg/mL amphotericin B and 0.1 mg/mL streptomycin. Recombinant BMP-2 was purchased from Peprotech Incorporated (New Jersey, USA), BSA Fraction V (A7906) and FITC-BSA (A9771) from Sigma.

2.4.1 Metabolic Assay

The Alamar Blue (Serotec) oxidation-reduction assay was used to determine cell activity. Nonfluorescent resazurin indicator was reduced in cells to resorufin within minutes and correlate with the number viable cells [265]. Dead and dying cells reduce resazurin slowly over two to four days and heat inactivation stops reduction showing enzyme dependence [266, 267]. Alamar blue was diluted to 10% ($^{v}/_{v}$) in phenol free Hank's balanced salt solution (HBSS) buffer, sterile filtered and equilibrated to 37 °C. Scaffolds (x3) were washed in PBS (x3) and transferred into new tissue culture wells. Cells grown on tissue culture plastic were rinsed (x3) in PBS and incubated in a standardized volume (1 mL) of Alamar Blue solution for a maximum of 90 minutes and measured on a MFX Microtiter plate fluorimeter at 530 nm extinction and 590 nm emission with Dynex Revelation 4.21 software.

2.4.2 Hoechst 33258 Quantification of DNA/ Cell Number

Scaffolds and controls without cells were washed (x3) in phosphate buffered saline then freeze dried overnight. Dried scaffolds were incubated with 1 mL papain solution (1.06 mg/mL) overnight at 60°C in pH 6.5 papain buffer. Papain buffer (200 mL) was prepared by dissolving 0.1 M dibasic sodium phosphate (1.42 g) , 0.005 M cysteine hydrochloride (0.079 g) and 0.005 M EDTA (0.186 g) in distilled water. Papain digest aliquots (38 µL) were placed in triplicates in a 24-well plate and 0.75 mL Hoechst 33258 ($1.8x\ 10^{-6}$ M) in distilled water added to each well. Fluorescence induced by the DNA and dye complex was measured using a MFX Microtiter plate fluorimeter at 355 nm excitation and 450 nm emission.

2.4.3 *In situ* Cell Seeding

The introduction of a cell suspension to compressed particulates in the barrel of a 1ml syringe (with the nozzle cut off) to trigger wet sintering of a scaffold, was termed *in situ* seeding (Figure 2-5). Blended type 1 and 2 particles, 200 mg, in a 1:3 ratio was loaded and compressed using a plunger from another 1ml syringe (secondary plunger). A suspension of $5x10^5$ cells in 100 µL buffer was introduced into the syringe barrel with a pipette and mixed through the compacted particulate by the pull/push (x4) action of the primary plunger. The syringe was placed upright in a humidified incubator (37 °C, 5% carbon dioxide in air) for 15 minutes to sinter and the moulded scaffold ejected into warmed media and cultured on an orbital rocker plate (88 rpm).

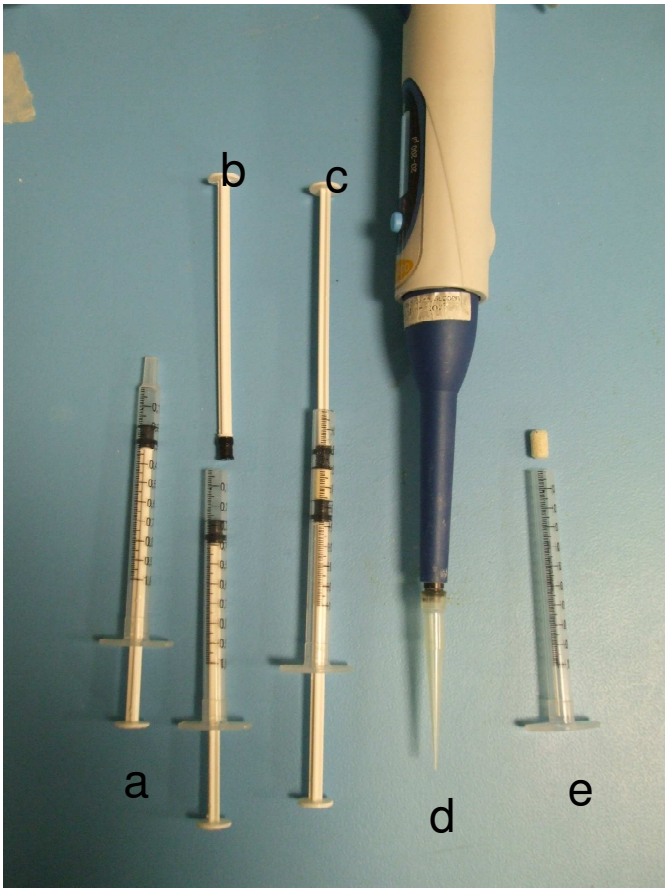

Figure 2-5 The staged process of *in situ* scaffold production with (a) 1 mL syringe from which the nozzle was removed (b): a secondary plunger was provided and used in (c) to compress particulates before introducing (d) the cell suspension dose. After sintering in the upright position the cell seeded scaffold (e) was ejected.

2.4.4 Scanning Electron Microscopy (SEM)

Scaffolds with cells were washed with PBS (x3) to remove media then immersed in glutaraldehyde solution 3% in PBS overnight at 4 ^{o}C. These scaffolds were rinsed (x3) in PBS and covered in 1% osmium tetroxide solution (TAAB Laboratories, UK) for two hours at room temperature. Osmium tetroxide oxidises unsaturated bonds to carboxylic acid and is itself reduced adding density /contrast to cells. Scaffolds were washed in distilled water (3 x 15 minutes) and air dried in a fume hood overnight. At this stage samples could be viewed by micro CT prior to gold coating for SEM. Scaffolds without cells were air dried, mounted on adhesive aluminium stubs and gold coated for 3 minutes in a Blazer SCD 030 sputter at 30 mA (Blazers Union Ltd. Liechtenstein). The samples were viewed with a Jeol 6060LV variable pressure scanning electron microscope (Jeol Ltd. UK) at an accelerating voltage of 15 kV.

2.4.5 Alizarin Red Staining

Cell seeded scaffolds were fixed in cold buffered formalin 10% solution overnight and washed (x3) in distilled water. A 2% ($^{w}/_{v}$) solution of Alizarin red (Sigma, UK) in water was prepared fresh, prior to use and adjusted to pH 4.2 with sodium hydroxide. Samples were stained for 5 minutes then rinsed three times in distilled water.

2.4.6 Alkaline Phosphatase Detection on Tissue Culture Plastic

The Sigma Fast™ p-Nitorphenyl phosphate test kit (Sigma, UK) was used as per the instructions. Briefly, the tablets were dissolved in 20 ml distilled water forming a 1 mg/mL solution and 600 µL was added to the test material for a specified period of time and measured on the KC4 (Bio-Tek Instruments USA) plate reader at 410 nm. Alkaline phosphatase activity was expressed per well or per cell.

2.4.6.1 Alkaline Phosphatase Detection on Scaffolds

Scaffolds were washed in PBS prior to staining for the localization of alkaline phosphatase activity. Scaffolds were immersed in Napthol AS-MS buffer solution (Sigma, UK) containing 1 mg/mL Fast violet B salt (Sigma, UK) up to 25 minutes at room temperature for colour development by precipitation onto the cells due to the action of alkaline phosphatase enzyme. Scaffolds were washed three times in distilled water then viewed.

2.4.7 Micro-computed Tomography of Scaffolds

Micro-computed tomography (micro-ct) is a non-invasive technique combining x-ray with tomographical reconstruction to create 2D consecutive images (slices) of the internal structure of porous materials. From the 2D slices 3D images of scaffolds can be reconstructed to show internal structure. Scaffolds, with and without cells were examined with a Micro-CT 40 instrument from Scanco Medical, Bassersdorf, Switzerland; to determine

porosity and pore size distribution. The visualisation of cells required densification or use of a contrast agent such as osmium tetroxide [268, 269] detailed in section 2.4.4. Scaffolds were scanned at the same power setting of 55 kV and 145 mA current. Scaffold 2D images were threshold to distinguish polymeric structures from pores. Parameters such as volume, porosity and pore size were determined from the threshold images.

2.4.8 Statistical Analysis

All the results were expressed as the mean ± standard deviation. The statistical package used was GraphPad InStat® 3.05 (GraphPad Software Inc., San Diego). Statistical analysis was performed on a minimum number of samples ($n = 3$) and comparison between groups was performed using a one-way analysis of variance (ANOVA) with Tukey-Kramer multiple comparisons post-test. Statistical significance was set at $p < 0.05$ (*), very significant $p < 0.01$ (**) and highly significant $p < 0.001$ (***).

3 Plasticization of PLGA Particles

3.1 Introduction

Minimally invasive surgical techniques with injectable matrices can readily fill a defect void to mimic its shape [270]. To prevent collapse of the filled volume the injectable material must harden to become self supporting against the local mechanical environment. In order to develop mechanical integrity, injectable materials must polymerise or crosslink *in situ* requiring the components and process to be non-toxic to the surrounding tissue [271]. If solidification can be achieved at body temperature with minimal cell disruption, then the low invasiveness of the procedure retains tissue integrity and function whilst filling the architecture of the defect [272]. The structural rigidity developed by the scaffold facilitates healing by bridging the void to provide continuity with migratory access to cells if porous and a boundary for the regenerating tissue [2, 225].

The work in this chapter builds on the literature reports of PEG as a plasticizer for PLGA. The Tg of blends with PLGA and PEG was tailored to undergo a phase transition, post injection; as it is warmed to body temperature. The aim of the work in this chapter was to produce a particulate PLGA formulation optimised to sinter within the body. The amorphous state is unstable to thermal and mechanical stress [203, 273]. Retaining the amorphous state is essential to control the physiomechanical properties of the material. DSC and rheology are established

independent material characterisation techniques that are complementary for measuring thermal and structural changes.

3.2 Methods

3.2.1 Manufacturing Particles

PLGA with PEG melt-blends were prepared as described in chapter 2, section 2.1.4. Particles were reduced in size to pass through a 500 µm sieve then dried and stored under vacuum until used.

3.2.2 Differential Scanning Calorimetry (DSC) Evaluation

Standard DSC heating rate of 10 °C/minute has a high level of sensitivity and low rate of resolution. The polymers PLGA 50:50 Low IV and 85:15 High IV were supplied by Alkermes Inc. Blends of PLGA with PEG were stored in vacuum sealed glass vials in the fridge. The weighed samples (5-10 mg) were sealed into hermitic aluminium pans and measurements were conducted on a TA2920 DSC (TA Instruments, UK) at 10 °C/min ramp from -40 to 120 °C. Modulated DSC was conducted on PLGA with PEG blends to improve resolution at heat only amplitude of ± 0.159 °C over a modulation period of 60 seconds and 1 °C/minute heating rate to determine Tg and the impact of composition on thermal transitions.

3.2.3 Rheological Evaluation

Oscillation temperature ramp measurements were conducted as described in chapter 2, section 2.1.5.

3.2.4 Wenger Transition Analyzer

The transition analyzer measures the ability of a material to resist physical compaction as a function of increasing temperature. Blends of 50:50 PLGA with PEG 1000 were compared to determine the impact of varying PEG content on compression strength. The second series of experiments combined the temperature sensitive 50:50 PLGA with PEG 1000 microparticle blend with microspheres or porous salt leached particles at a ratio of 3:1 whilst maintaining the weight load of 1.83 g. Experiments were conducted using the procedure detailed in chapter 2, section 2.3.

3.3 Results and Discussion

3.3.1 Rheological Evaluation of PLGA Blends with PEG of Varying Molecular Weights

The oscillation temperature ramp profile detects thermally induced phase changes occurring between 4-90 °C. PEG 200 and 400 were fluid with viscous behaviour under the test conditions used. For clarity PEG 200 was not included in Figure 3-1 as it was overlaid by the PEG 400 profile. PEG 600 and 1000 were of a paste or soft wax consistency at 4 °C.

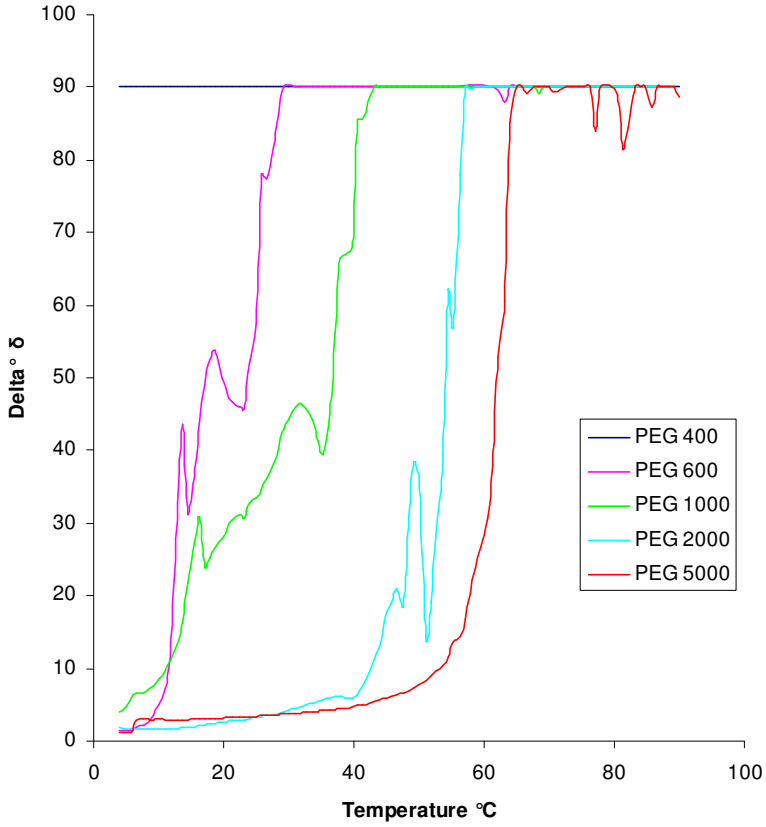

Figure 3-1 Comparison of oscillation temperature ramp profile of PEG using controlled strain (0.1%) from 4-90 °C. The graph compares PEG 400, 600, 1000, 2000 and 5000 used to modify the Tg of PLGA.

PEG 600 and 1000 lose structure over a narrow temperature range and Figure 3-1 shows the materials to have a staggered increase in Delta values. PEG 2000 and 5000 had a low delta plateau at temperatures below 40 °C followed by a rapid increase in values. The oscillation profile clearly distinguishes between those materials (PEG 400, 600 and 1000) that melt below 37 °C and higher molecular weight material that do not. The staggered rise in Delta value may be due to the polydisperse nature of the melting phases of PEG materials that are often blended to achieve an average molecular weight [212, 274].

3.3.2 DSC Evaluation

The DSC trace of PLGA 50:50 in Figure 3-2 show the glass transition in the heating curve and solidification from the cooling cycle. The first cycle in Figure 3-2 detected transitions in the material influenced by processing, and storage conditions referred to as thermal history. This was observed as the separation of the first from the 4 successive repeat cycles. The energy required to traverse the phase transition on the first heating cycle was 2.67 J/g with 0.44 J/g for the second and subsequent heating cycles. For amorphous materials ageing effects occur in the glass transition region [217]. Thermal history of a sample can be eliminated by heating 30 °C above the Tg and maintaining temperature for 5 minutes.

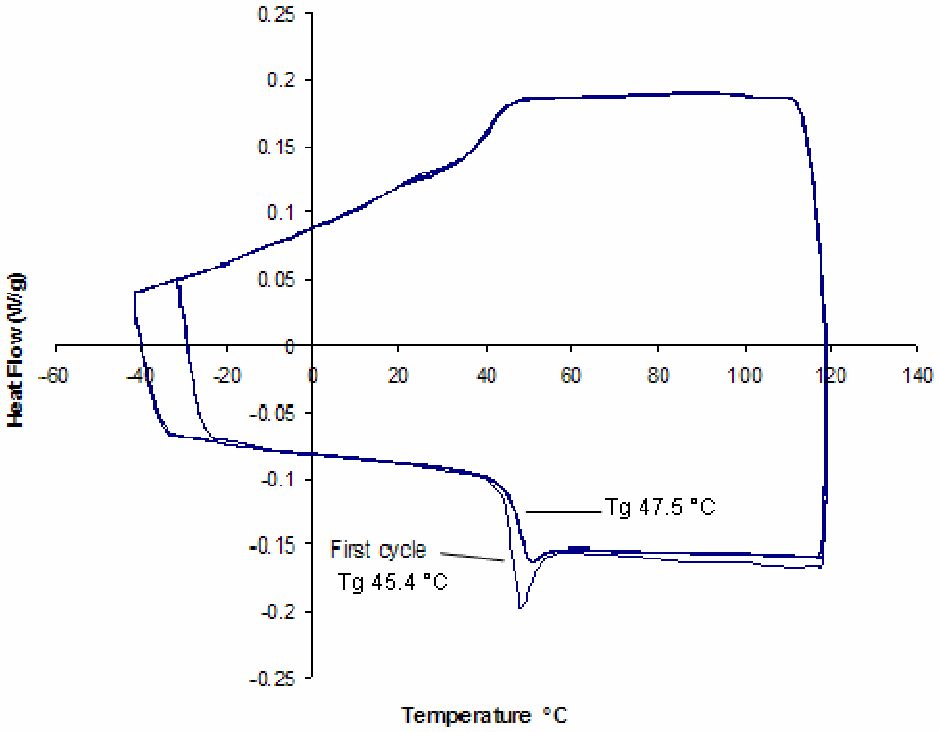

Figure 3-2 DSC trace of 50:50 PLGA (36 kDa) ramped at 10 °C/ minute through five cycles from -40 to 120 °C. The plot shows the Tg region to shift with the elimination of the ageing effects after the first cycle. Tg values for the first and fifth cycles are shown.

The heating protocol used in these experiments eliminated the ageing effect and the overlay of subsequent cycles shows the DSC characterization did not damage or alter the polymer. The age induced shift in the Tg was to a lower temperature value, but required greater energy input to pass through the transition.

The result for PEG 1000 run on the same protocol (Figure 3-3a) shows that there was no glass transition present in this material, only a broad melting peak with the midpoint at 40.48 ±15 °C. The large crystallization peak in the cooling cycle began below 20 °C. The first heat ramp cycle was displaced to a higher temperature in comparison to successive cycles that overlap to show repeatability. The PEG 1000 cooling cycle profile detected solidification beginning at 19 °C and showing less uniformity than the melting curve. These results may indicate the disperse molecular weights of components or the presence of competing PEG crystal forms in the cooling exotherm. Enthalpy relaxation involves molecular rearrangement to a more stable configuration and a reduction in free volume with time [218]. Ageing enhances crystallization of PEG with higher rigidity resulting in a shift to higher temperature and energy being required for the melt transition [201, 273].

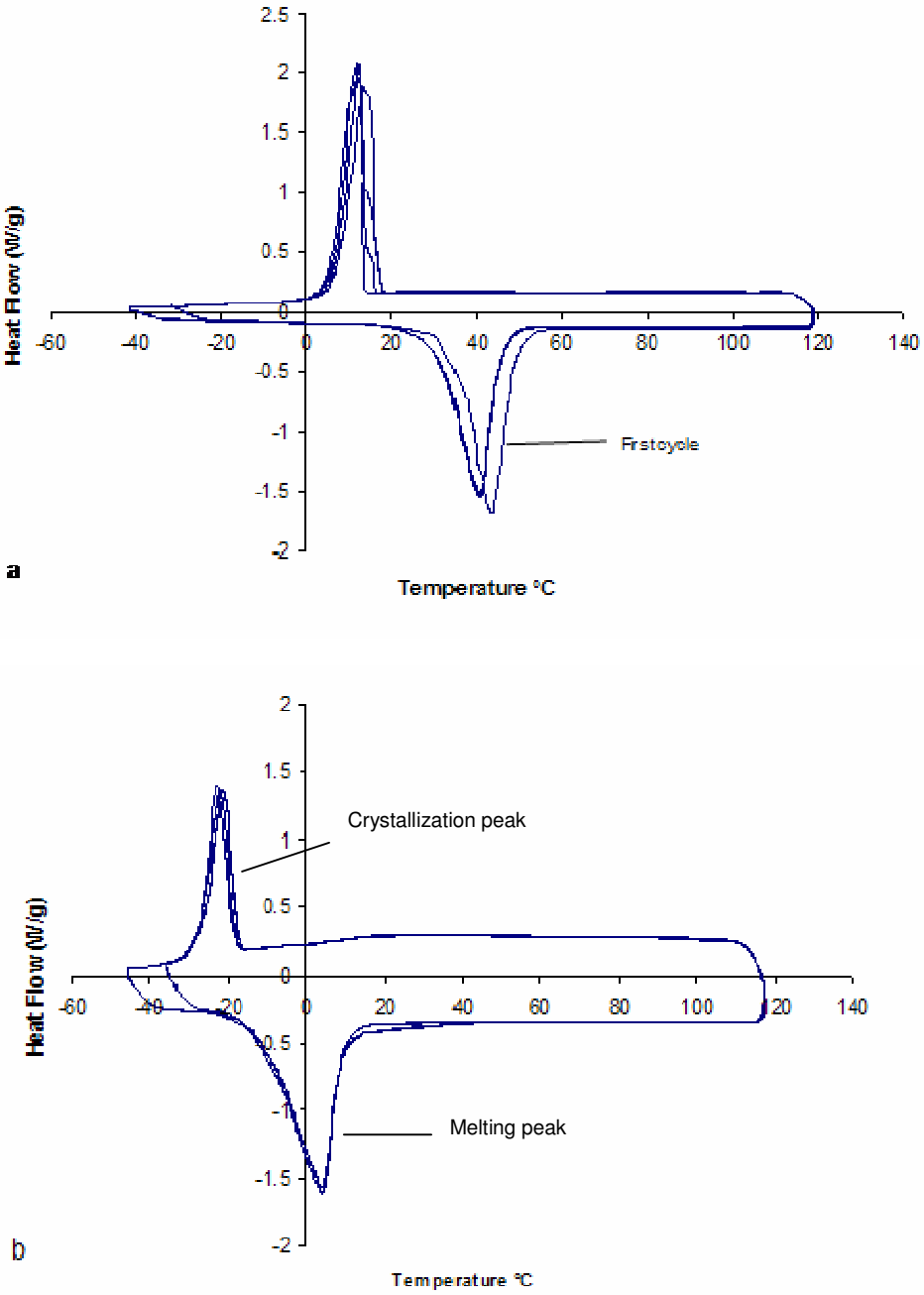

Figure 3-3 DSC trace showing melt and crystallization peaks of (a) PEG 1000 and (b) PEG 400 ramped at 10 °C/ minute through five cycles from -40 to 120 °C.

The DSC profile for PEG 400 (Figure 3-3b) has similar features of melt and crystallization peaks to PEG 1000, but displaced to lower temperatures. The crystallization peak for PEG 400 was displaced below -5 °C and the melting peak began at -20 °C. The transitions for PEG 400 were overlaid for each cycle and were below the proposed conditions for use in the body (37 °C). There was no age induced effect present in the PEG 400 DSC profile as crystallization occurs below storage conditions. Additional structures were therefore present in PEG 1000 and eliminated by the heating protocol. Comparison of Figures 3-2, PLGA and 3-3a, b shows the dominance of the PEG transitions from the scaling of the heat flow. PEG 1000 melt transitions occur at a lower temperature than the Tg of PLGA and the re-crystallization transition was close to fridge (0-5 °C) storage conditions indicating that sample ageing was likely to occur.

In Figure 3-4, the 99% PLGA with 1% PEG 1000 blend and Figure 3-5 98% PLGA with 2% PEG 1000 showed a progressive displacement of the Tg to lower temperatures with increased PEG content. In melt blends with polyesters PEG forms a physical solution without chemical reaction [214]. The 95% PLGA blend with 5% PEG (Figure 3-6) shows a separation of the first from successive cycles. For the 95% blend the transition was displaced to below body temperature. The age induced displacement of the first run was present in all blended materials. Similar effects have been reported for PLA [275].

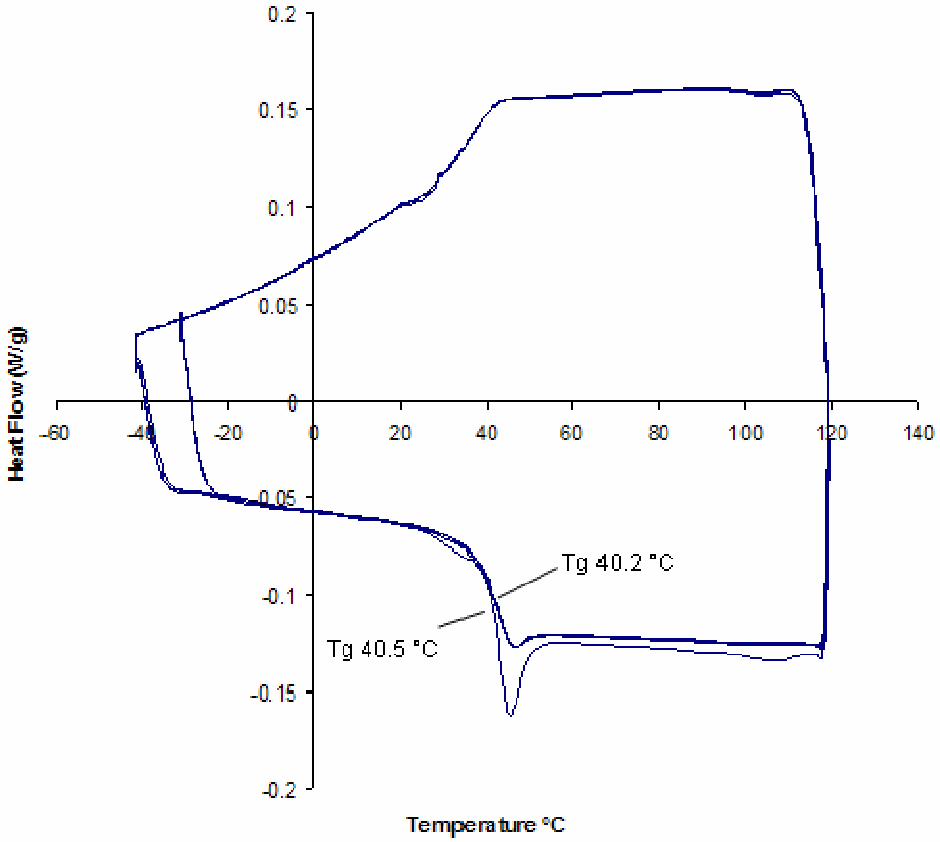

Figure 3-4 DSC trace of 50:50 PLGA (36KDa) with 1% PEG 1000 ramped at 10 °C/ minute through five cycles from -40 to 120 °C . The graph shows the separation of the first from subsequent cycles that overlay each other. The Tg values for the first and fifth cycles are shown.

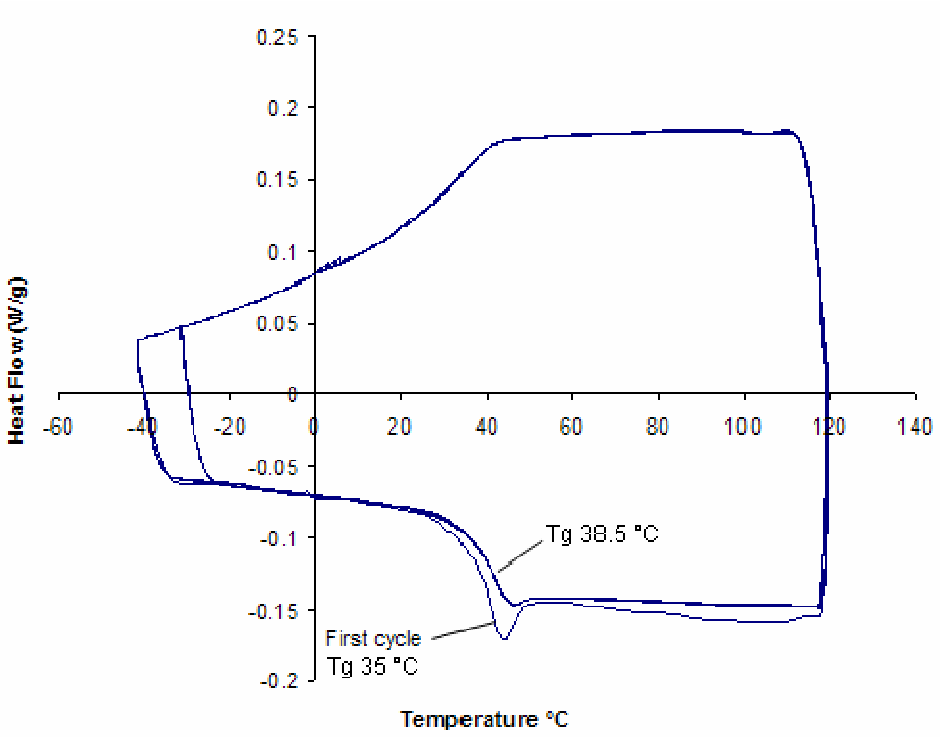

Figure 3-5 DSC trace of 50:50 PLGA with 2% PEG 1000 ramped at 10 °C/ minute through five cycles from -40 to 120 °C. The graph shows the separation of the first Tg from subsequent repeat cycles that overlay each other. The Tg for cycle 1 and 5 are shown.

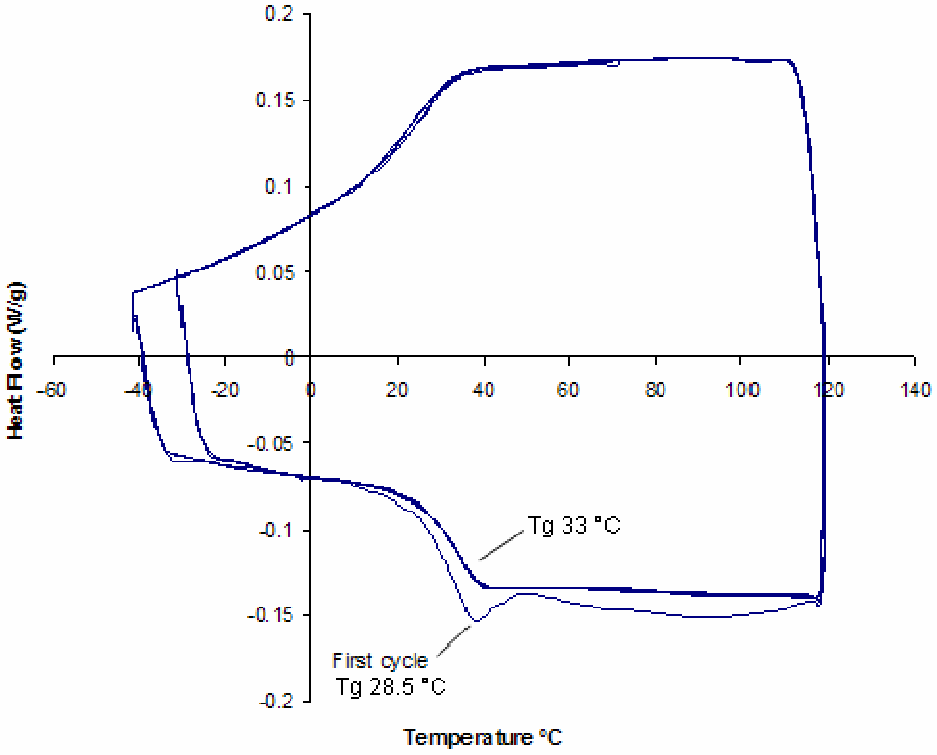

Figure 3-6 DSC trace of 50:50 PLGA with 5% PEG 1000 blend ramped at 10 °C/ minute through five cycles from -40 to 120 °C. The graph shows the Tg for cycle 1 and 5.

The DSC trace of 85% PLGA with 15% PEG blend (Figure 3-7) shows separation of each of the successive temperature ramp cycles, resolved in the Tg region. These phase transitions were not eliminated after the first or successive temperature ramp cycles, but diminished. The gradual erosion of this phase transition may indicate the increasing effect of PEG. The first cycle transition peak also shows a shoulder at 32 °C that was not repeated in the successive cycles. The DSC plot for the 80% blend showed a definite shoulder and separation of the successive ramp cycles in Figure 3-8. The separation occurred not just in the peak transition, but also throughout the heating ramp indicating that high PEG content introduces variability in the thermal transitions and phase separation. Uneven mixing of PEG at 20 % $^{w}/_{w}$ with PLA has been recorded, with separation in PLGA at 30 % $^{w}/_{w}$ [133, 201].

At high PEG content ≥ 15% $^{w}/_{w}$, the inability of the heating protocol to overlay successive temperature ramp cycles indicates possible de-mixing and separation of the blend has occurred. The effect of PEG has been previously recorded to become dominant at 10% addition with evidence of rapid demixing at higher levels [200, 273]. Molecular mobility effects in glassy materials have been detected by DSC up to 50 °C below Tg [203].

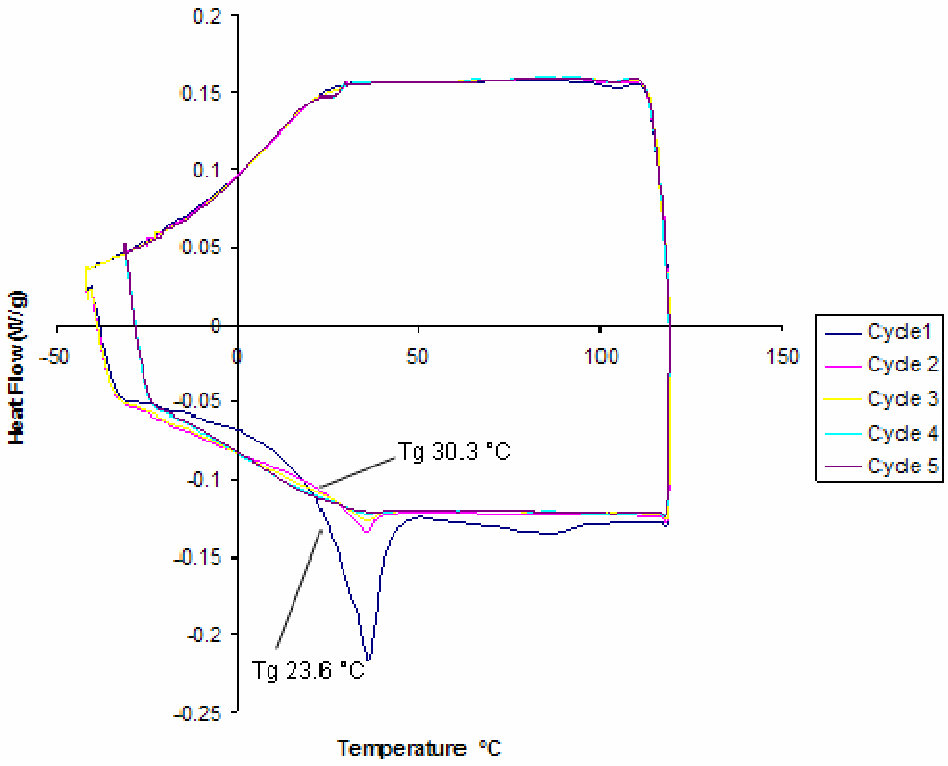

Figure 3-7 DSC profile of 50:50 PLGA with 15% PEG 1000 ramped at 10 °C/ minute through five cycles from -40 to 120 °C. The graph shows a separation of first and successive cycles with a large endothermic transition. The Tg for run 1 and 5 are shown.

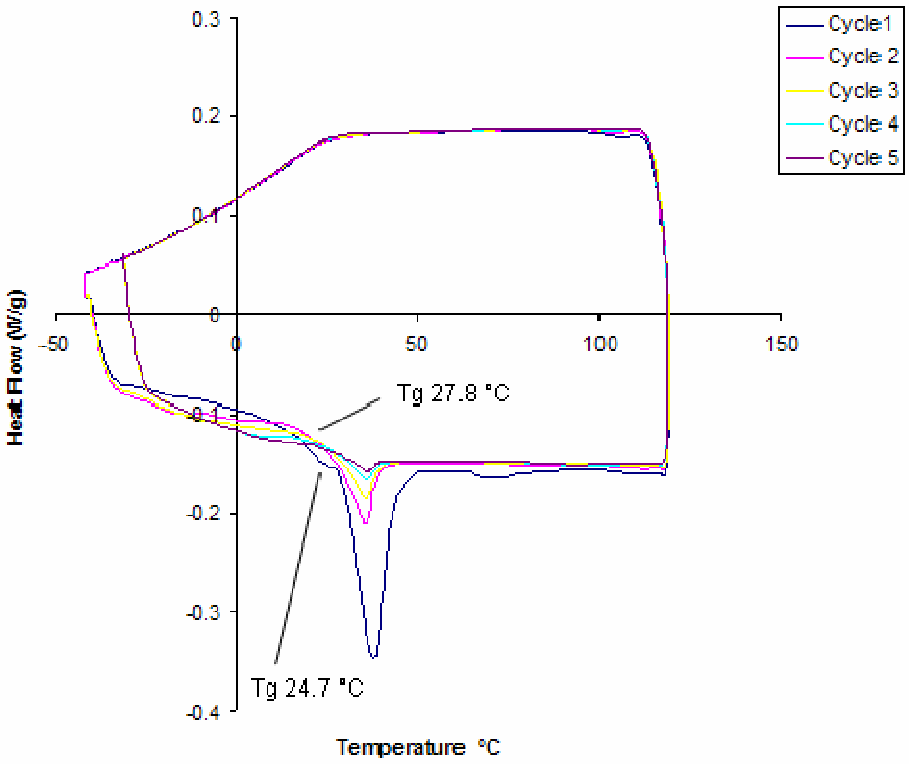

Figure 3-8 DSC five cycle run of 50:50 PLGA 80% with 20% PEG 1000 ramped at 10 °C/ minute from -40 to 120 °C. The graph shows a separation and change in heat flow for each successive heating ramp. The Tg values for run1 and 5 are shown.

Comparison of the first cycle run MDSC data from 50:50 PLGA blends with PEG 1000 in Figure 3-9 show a positive correlation of increasing transition width with increased PEG content of the blends. Thermal sensitivity of PLGA blends with PEG 1000 up to 15 $\%^{w}/_{w}$ was enhanced and broadened; responding to lower trigger temperatures. The increasing PEG 1000 content lowers the transition temperature reaching an optimum at 5% content. The peaks for the 95 and 85% PLGA 50:50 blends coincide on the temperature scale as can be seen in Figure 3-9 differing in the energy required to traverse the transition by 50%. This may have implications in the body with a restricted maximum temperature and limited heating rate; it would take longer to traverse the transition.

For the 50:50 PLGA dominated materials containing up to 5% PEG, the effect of ageing was a decrease in the transition temperature whereas for the blends containing greater than 15% PEG there were two glass transition regions above and below the normal region in Figure 3-9. The 80% PLGA 50:50 blend has a first cycle transition similar to a melting event and is attributable to the dominance of PEG that requires 6 times more energy to go through the thermal melt transition and may indicate separation of the blend. In contrast, the second MDSC heat cycle in Figure 3-10 shows a single broad transition displaced to lower temperatures, requiring less energy.

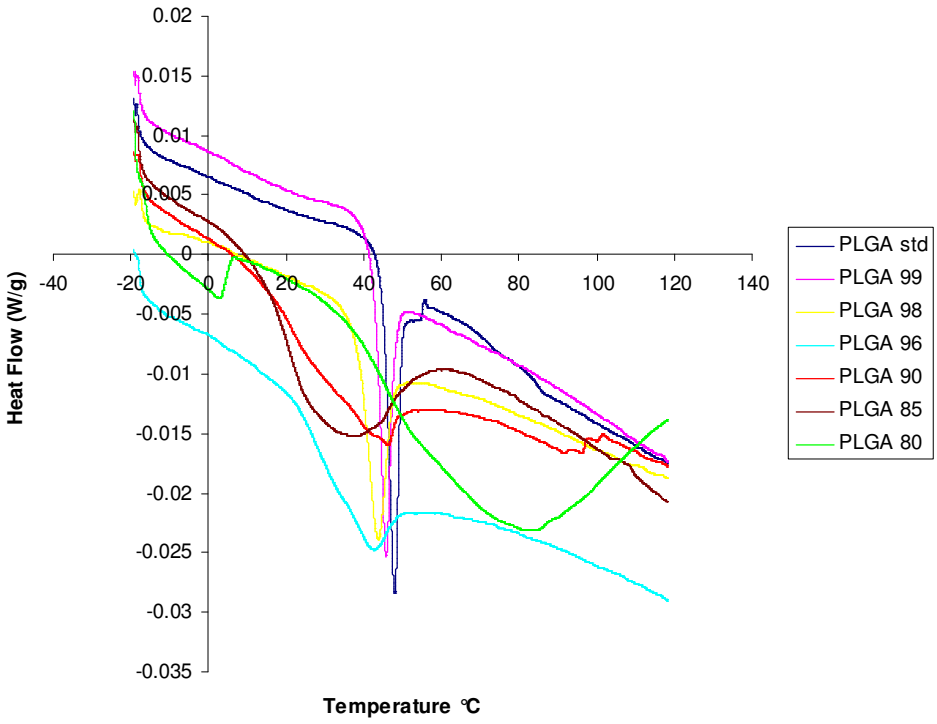

Figure 3-9 MDSC comparison of the first heating cycle of 50:50 PLGA and blends with increasing levels of PEG 1000. MDCS was conducted at 1 °C/minute from -20 to 120 °C, modulated ± 0.16 °C for 60 seconds (n = 3). The width of the transitions increased with PEG addition.

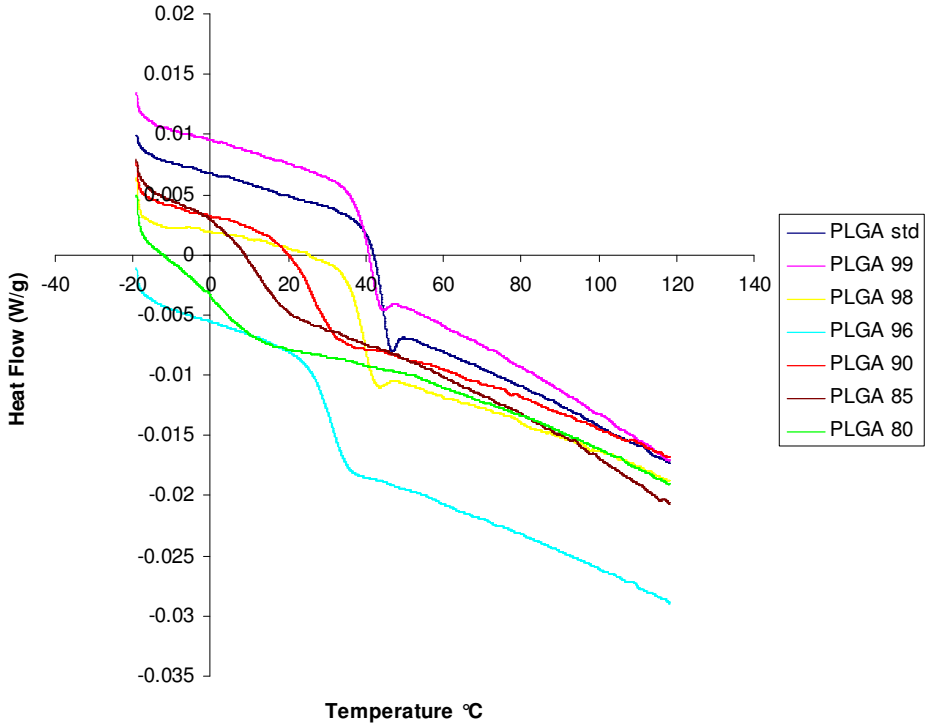

Figure 3-10 Comparison of the second MDSC heating cycles of 50:50 PLGA with increasing levels of PEG 1000 in blends. MDCS was conducted at 1 °C/minute from -20 to 120 °C, modulated ± 0.16 °C for 60 seconds (n = 3). The plot shows a reduction in the temperature at which transitions occur with increased PEG content.

PLGA 85:15 polymer with blends varying in PEG 400 content were evaluated by MDSC and the first cycle results in Figure 3-11 shows that Tg was reduced with increased levels of PEG 400. The width of the transitions was widened with increasing levels of PEG 400 extending Tg onset to lower temperatures. For the PLGA 80 curve with 20% PEG 400 added, there was a second transition present; displaced to below 0 °C. A similar feature was present in the 80% PLGA 50:50 blend with PEG 1000 in Figure 3-9. Comparison of the second heating cycles for 85:15 PLGA 80 Figure 3-12 and 50:50 PLGA Figure 3-11, shows only one transition that began below 0 °C. Comparison of the heat flow energy between the first and second cycles of Figures 3-11 and 3-12 show them to be much reduced. Hence the impact of ageing was to increase the energy required to effect a transition.

Summary of the second cycle Tg values in Figure 3-13 compare PLGA 50:50 and 85:15 blends and shows PEG 400 to be more effective than PEG 1000 in reducing glass transition temperatures despite differences in the molecular weight and composition of the initial materials. The efficiency of Tg reduction by low molecular weight PEG has been previously reported [276]. Miscibility of blends was improved by lower PEG molecular weight and reduced polydispersity [277]. Both PLGA polymers show a similar profile with declining impact on Tg reduction above 5% PEG addition.

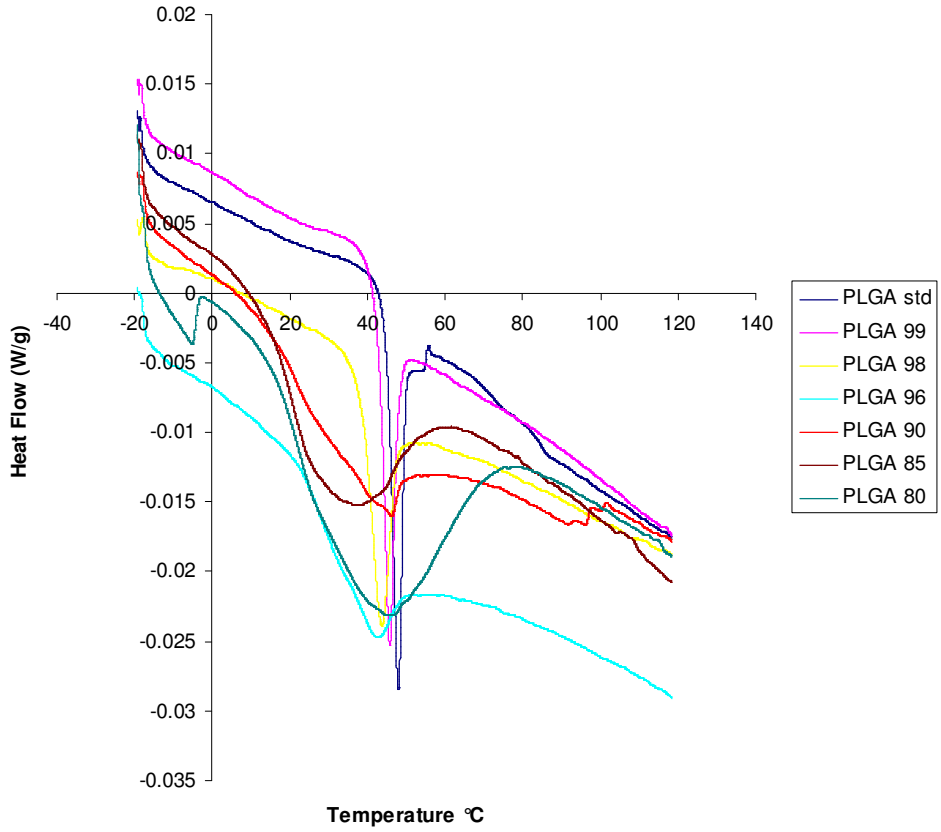

Figure 3-11 First cycle MDSC profiles comparing 85:15 PLGA blends with increasing PEG 400 content. MDCS was conducted at 1 °C/minute from -20 to 120 °C, modulated ± 0.16 °C for 60 seconds (n = 3). The plot shows a reduction in Tg and a widening of the transitions with the increased addition of PEG 400.

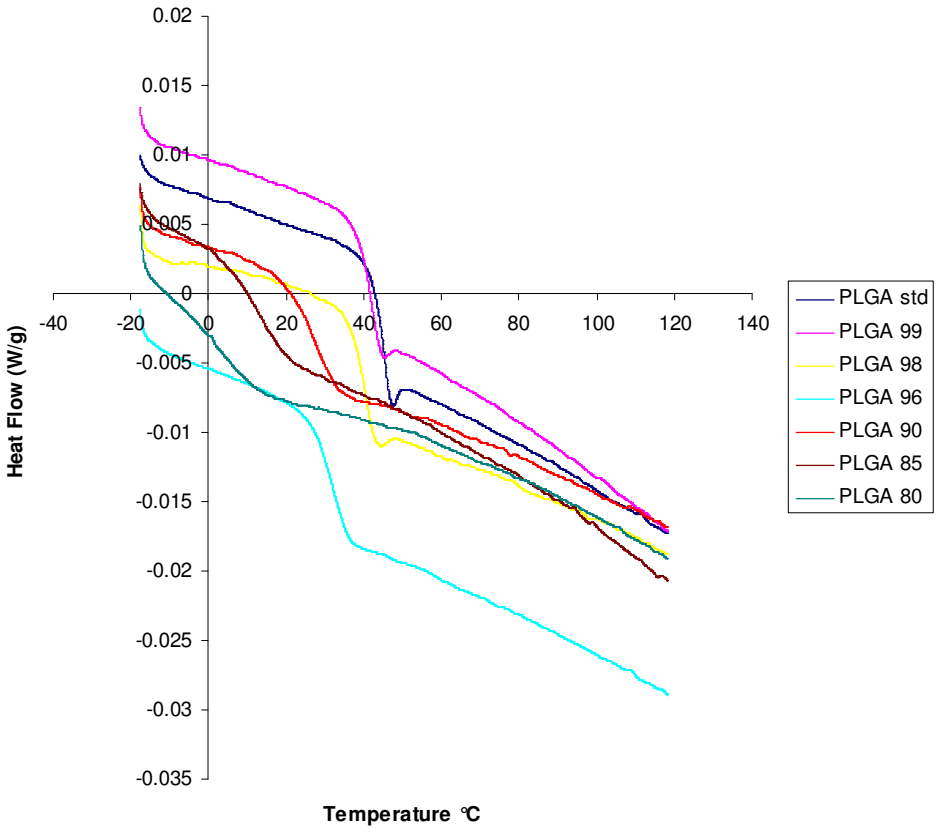

Figure 3-12 Second heating cycle MDSC comparison of 85:15 PLGA with PEG 400 blends. MDCS was conducted at 1 °C/minute from -20 to 120 °C, modulated ± 0.16 °C for 60 seconds (n = 3). The plots show a progressive reduction of Tg with increasing PEG content.

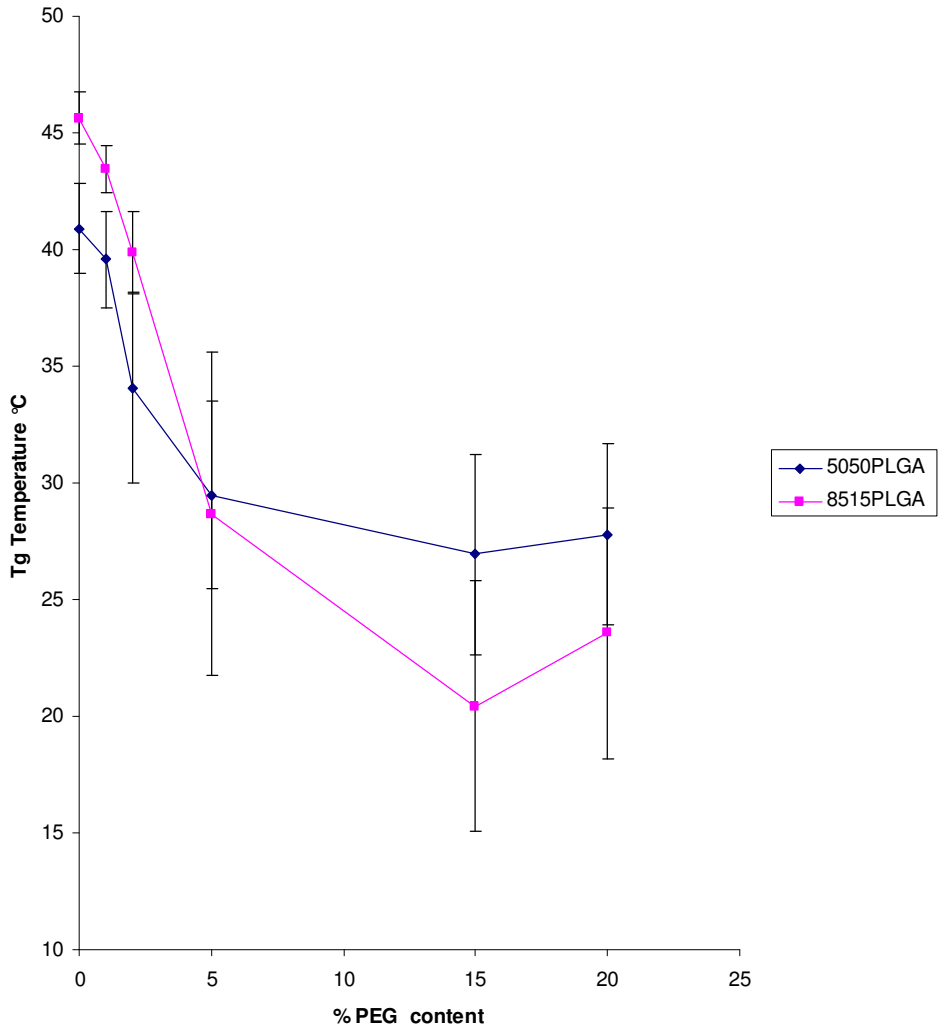

Figure 3-13 Second cycle MDSC derived glass transition temperature summary compares blends of 50:50 PLGA /PEG 1000 with 85:15 PLGA/ PEG 400 (n = 3). The profiles show increasing PEG content to reduce Tg.

3.3.3 Rheological evaluation

The oscillation rheology profiles of 50:50 PLGA blends with PEG 1000 in Figure 3-14 show the onset of phase angle increase to occur at progressively lower temperatures with increased PEG content. The increased phase angle values at low temperature indicate enhanced viscoelastic mobility with PEG addition. Increasing the PEG content of blends to 15 % and above produced a shoulder in the curve displaced to lower temperatures that may indicate thermal demixing and spinodal decomposition within the composite.

The increased viscoelastic mobility of the blends at low temperatures was reconciled with the MDSC observations of widening transitions with higher PEG content. The phase angle increase at lower temperatures with elevated PEG 1000 content show that the material was more readily deformed. Similar changes in phase angle have been observed for plasticized PLA [202]. The temperature range of the rubbery phase after Tg was reduced and displaced to lower temperatures with increased plasticizer content. This may indicate the disruption of polymer molecular packing and chain interaction.

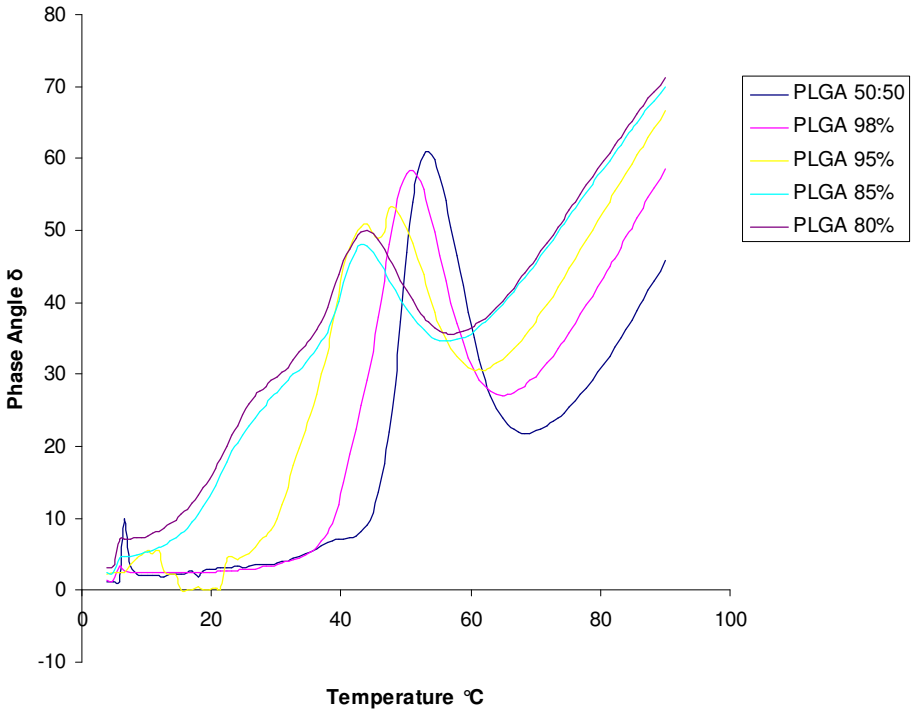

Figure 3-14 Oscillation rheology temperature ramp comparison of 50:50 PLGA and blends with PEG. The temperature ramp from 4-90 °C (n = 3) shows increased low temperature sensitivity with elevated levels of PEG addition.

The rheological profile for PLGA 85:15 blends with PEG (Figure 3-15) show similar trends in Tg reduction and viscoelasticity to that of the 50:50 PLGA in Figure 3-14. Increasing levels of PEG 400 enhanced viscoelastic mobility at low temperatures. PLGA 85:15 blend with 10% PEG 400 had two peaks in the temperature ramp profile that may indicate phase separation at this level of addition. Similar changes in thermal transitions and mechanical properties in response to increased PEG content have been reported [216].

The graphs (Figures 3-14, 15) differ in appearance with the 50:50 PLGA peaks becoming broader with increased PEG content and the 85:15 PLGA profiles remaining narrow, but shifted to a lower temperature. This may be due to a molecular weight effect with 85:15 PLGA 118 kDa and 50:50 PLGA 36 kDa . The impact of increased plasticizer levels on disrupting molecular packing results in a loss of structure. A similar loss in phase angle was reported by [202]. The graph in Figure 3-16 provides a summary of the Tg shift determined by oscillation rheometry and shows PEG 400 to have a greater reducing effect on the glass transition temperature. The Tg values of the blends compared show a plateau effect on increasing PEG content above 5% in Figure 3-16. From the MDSC and rheology results, the 5% blend was regarded as optimum for Tg reduction to within body temperature whilst retaining miscibility and used on both PLGA 50:50 and PLGA 85:15 blends for further studies.

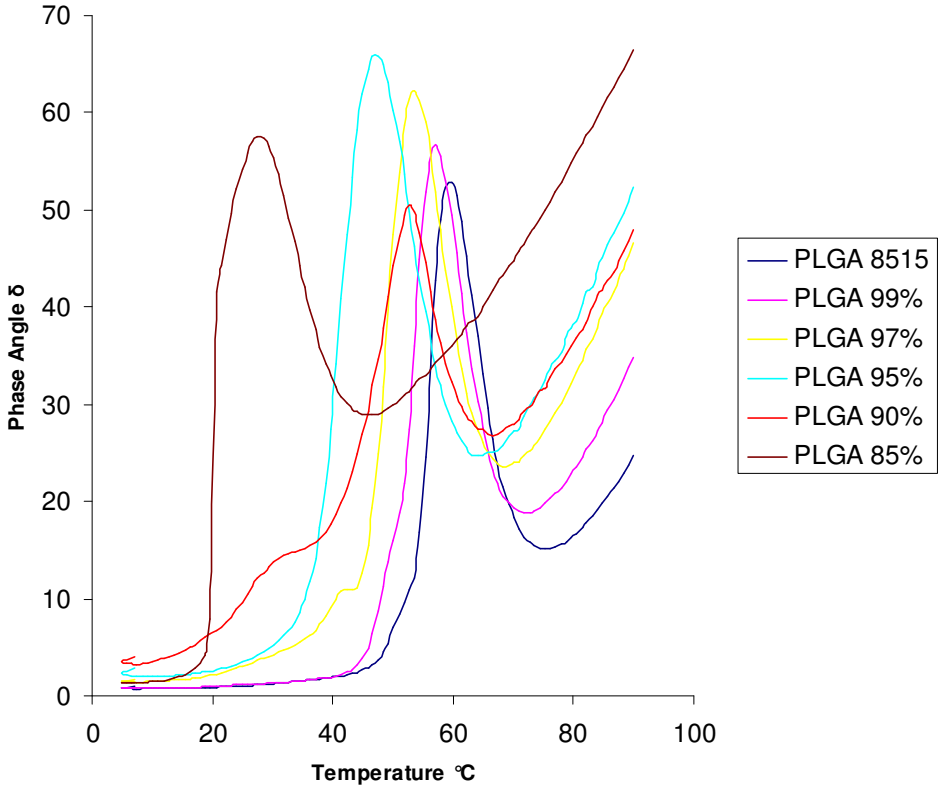

Figure 3-15 Oscillation temperature ramp rheology profile of 85:15 PLGA blended with PEG 400 from 4-90 °C showing increased viscoelastic behavior at lower temperatures with increasing levels of PEG (n = 3).

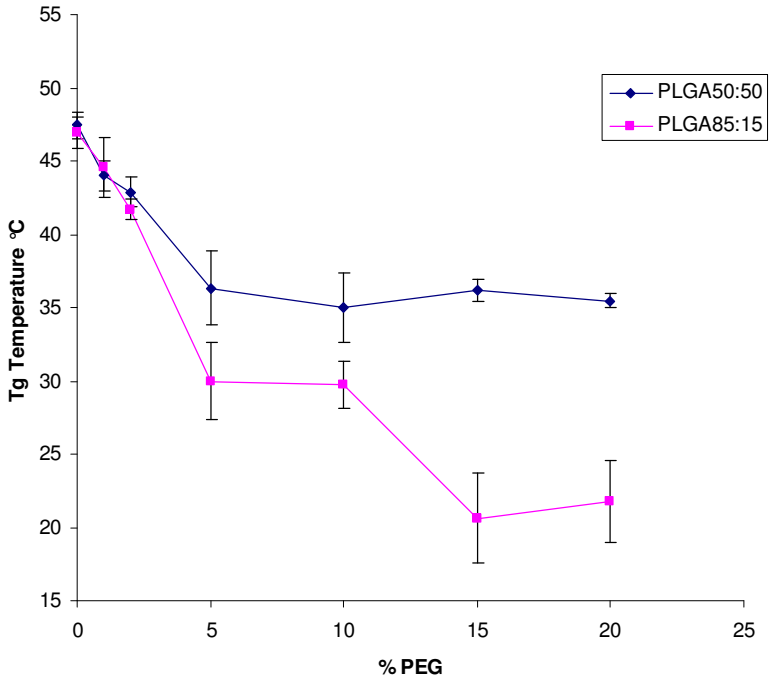

Figure 3-16 Comparison of glass transition temperature determined by oscillaton rheology; comparing the polymers PLGA 50:50 blended with PEG 1000 and PLGA 85:15 blended with PEG 400; showing Tg reduction with increased PEG addition (n = 3). PEG 400 achieved a greater effect on lowering Tg temperature.

3.3.4 Transition Phase Analyzer

Unmodified PLGA particulates under pressure had a stable plateau up to a Tg onset temperature of 18.5 °C in Figure 3-17 and indicates the ability of the material to withstand loading. The rate of deformation slowed to a second (rubber) plateau between 39 and 50 °C, after which the rate of deformation increased with further softening of the polymer in this region. The results for particulate blends of PLGA 50:50 with PEG 1000 in Figure 3-17 showed Tg displacement to begin at lower temperatures with increased PEG content.

As the PEG content of the blends increased the low temperature plateau became shorter to not being detected in the 85% PLGA sample under the run conditions used. Increased PEG content has also reduced the extent of the upper rubber plateau and the temperature at which it occurs. Increased levels of PEG reduced the network structure of the polymer, its ability to bear load and therefore maintain porosity. The glass plateau region for 85% PLGA 50:50 was therefore below the measurable operating temperature of the equipment indicating that the thermal sensitivity for such blends could occur close to fridge storage temperatures of 4 °C. These results were in agreement with the parallel plate oscillation experiments. Similar observations of reduced strength and increased ductility have been reported [133, 200].

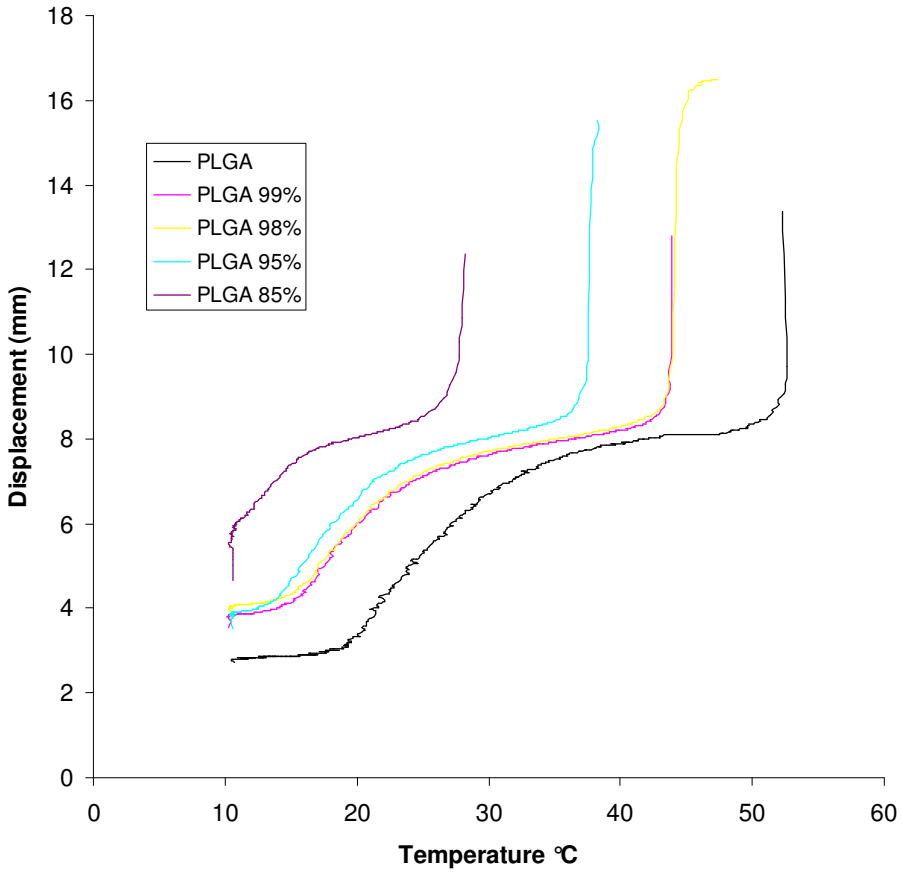

Figure 3-17 Transition phase analyzer 5 °C/min temperature ramp profiles of PLGA 50:50 blends with PEG 1000 under 100 Bar constant load. It shows decreasing structural resistance to deformation under pressure with increased PEG 1000 content.

The relationship between storage temperature and Tg is crucial to preventing premature particle aggregation and ageing. There was good agreement between results obtained with the phase analyzer and MDSC glass transition onset temperature. The glass transition region covers a temperature range conventionally quoted as a midpoint value; however, a more relevant measure for use might be to quote an onset value given our intention to place the material in bone cavities under pressure from the surrounding tissues.

The Transition Phase Analyzer measures the controlling Tg of blended materials under constant load and increasing temperature as structural loss and displacement attributable to increased polymer chain mobility [264, 278]. The magnitude of thermal change as detected by DSC was small in comparison to the physical impact of the change in solid structure under compression. Thermomechanical methods are more sensitive in resolving the strength of transitions than DSC measurements [279].

Figure 3-18 compared 95% PLGA 50:50 particulate blends in combination with PLGA 50:50 microspheres or PLA salt leached particles. The data shows that the inclusion of spheres and particles increased resistance to compression. Plasticized 95% PLGA 50:50 particulates had lower compression resistance than unmodified PLGA with higher displacement at lower temperatures.

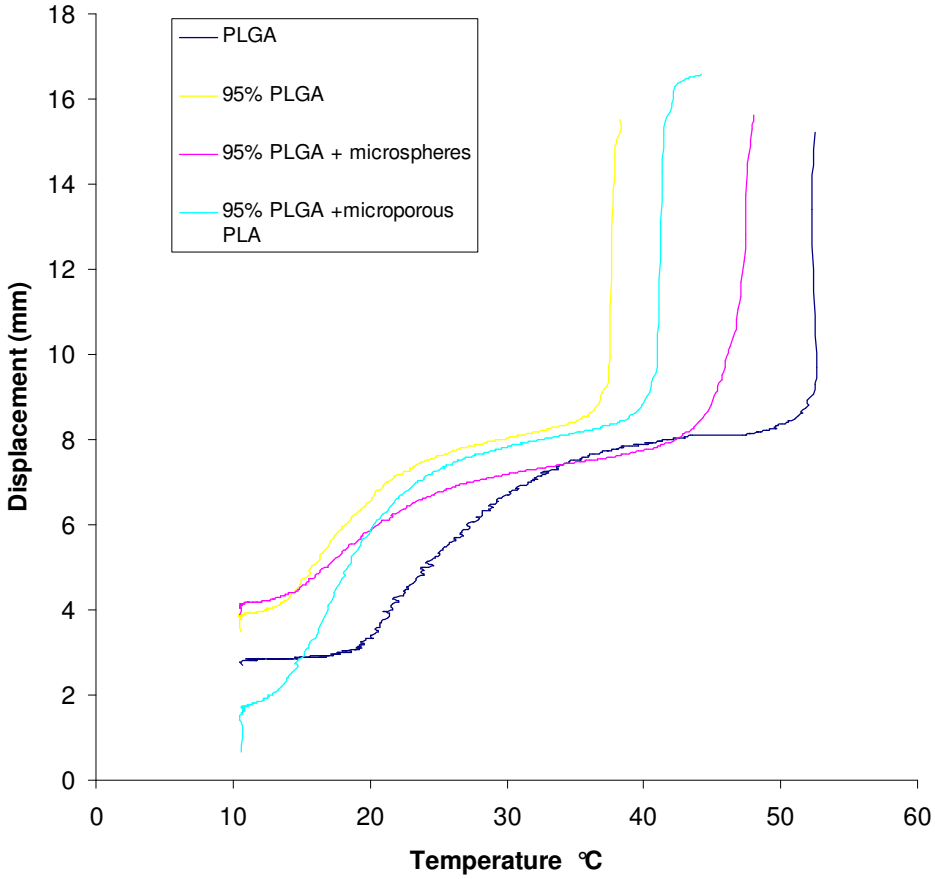

Figure 3-18 Comparison of a 3:1 weight ratio of 50:50 PLGA 95% PEG blend with microsphere and microporous PLA salt leached particles in resisting compression forces in a Transition phase analyzer. The 5 °C/min temperature ramp profiles were conducted with 100 Bar constant load.

Both microspheres and salt leached spacer particles increased the length of the rubber plateau compared to the starting 95% PLGA 50:50 blend. Microspheres showed higher compression resistance that extended above 40 °C. Figure 3-18 shows the rapid compression of salt leached particulates. The lower density of the salt leached material was apparent from the initial loading equilibration point showing a larger volume to be occupied by the same loading weight of particles. The displacement for the 95% PLGA with microsphere combination was 2 mm in comparison to 6.2 mm for the salt leached particulate. This salt leached material had faster compaction under loading in comparison to the other materials under test at lower temperature, indicating high porosity and low strength [204, 280, 281]. To increase the strength of salt leached PLGA particulate scaffolds, compression moulding in the rubber region but below flow was conducted to retain porosity [282].

The 95% PLGA 50:50 blend and microsphere particulate combination had higher strength and resistance to compression than salt leached particles. Compression resistance is a critical feature in supporting the integrity of scaffold filled defects.

3.4 Conclusion

Hot blended PLGA with PEG mixtures produced polymers with reduced Tg and mechanical properties that could be tuned to desired temperatures. The combination of PLGA with PEG blends was shown by DSC to reduce Tg and induce an enthalpic ageing shift that required more energy to pass through the phase transition. The dominant effect of phase separation was detected at 10% and higher PEG addition levels with DSC and oscillation methods. The impact of PEG extends beyond initial glass transition temperature reduction to influence compressive strength, manufacturing consistency and storage stability of the blend. The selection of the 95% PLGA blend for further work represents a compromise between required body temperature sensitivity, reproducibility, strength as measured rheologically and the properties desirable for application of the blended material.

DSC measures the amount of energy needed to effect phase changes in materials. PEG 400 achieved a greater reduction in Tg at moderate addition levels of 5% in comparison to PEG 1000, but the magnitude of enthalpy change in the blends were similar. DSC does not indicate the point at which temperature stimulates flow. Rheology was complementary in linking physiochemical properties with thermal transitions. The oscillation method used, produced results similar to the DSC showing PEG 400 to have a greater reduction of the glass transition temperature.

Within a multi-component system, a major component may become sufficiently melted to flow without other components approaching their melt temperature. The results from the Transition Phase Analyzer showed that minimizing PEG content increased the resistive compressive strength of PLGA blends. The addition of the porous component increased compression resistance with microspheres having a greater impact than salt leached microporous material. Microspheres as spacers formed pores as could be discerned from the starting displacement position. Microspheres in combination with blended temperature responsive 95% PLGA improved scaffold compression resistance strength and may help retain porosity post sintering. The two-component scaffold system has been formulated, based, on a single polymer using different processing routes.

The aim of the work in this chapter was to produce a blend of PLGA and PEG with a glass transition phase response below 37 °C. The Tg of the PEG/PLGA blend was tailored close to body temperature, in order to undergo a phase transition post injection; during the rise to body temperature. The techniques used to detect changes in the physiochemical and mechanical properties of the blended polymers passing through the glass transition indicated a requirement to minimize plasticizer levels to reduce the impact of ageing and phase separation. Optimization of scaffold features including strength, porosity and degradation are determined by application and influence the choice between PLGA 50:50 and 85:15.

4 Evaluation of Sintering Characteristics and Scaffold Strength

4.1 Introduction

Injectable scaffolds for connective tissue repair must undergo a mechanism of structuring to develop mechanical integrity. Scaffold mechanical integrity is necessary to maintain the bone-implant interface and enable load transfer [97]. Mechanical stress and strain provides essential stimulus as part of the normal signal transduction pathway for maintenance, growth and the repair of injury [15, 283]. Mechanical stimuli vary with the remodelling rate of bone [20, 284, 285]. Bone cells respond to static, cyclic and compressive strain with increased remodelling and BMP-2 release [117, 286, 287]. Implants that elastically oscillate reproducing normal mechanical stresses have a reduced foreign body response at the tissue- implant interface [251].

Thermoresponding systems undergo physico-chemical changes at transition temperatures that may depend on molecular weight and adsorption. The determination of setting time to gain mechanical integrity for injectable calcium phosphate cements was evaluated by compressive strength testing of cylinders after various incubation times and by rheological measurement methods [288, 289].

4.1.1 Aims

The aim of the work in this chapter was to evaluate particulate sintering of PLGA 85:15 blends with PEG. To investigate the setting time and compressive strength, measurements were conducted on cylinders sintered under various conditions of temperature, time and environment. The fluids tested included potential carriers for cell transplantation. To determine solidification times and analyze the nature of the sintering mechanisms, oscillation rheology and DSC techniques were used to inform discussion of the sintering mechanism. The objective was to develop a particulate formulation that can be triggered to assemble *in situ* at normal body temperature, forming a self-supporting, porous, biodegradable scaffold with strength comparable to cancellous bone.

4.2 Methods

4.2.1 Viscoelastic Measurements and Tg

Oscillatory temperature ramp measurements were conducted as described in chapter 2, section 2.1.5. The effect of varying PEG molecular weights on PLGA phase transitions were monitored with phase angle.

4.2.2 Scaffold Compressive Strength Evaluation

Scaffolds were sintered in a Teflon mould from compacted melt blended particulates to determine the strength and the impact on mechanical properties. Temperature and sintering duration were varied. Cylindrical scaffolds (5 x 9 mm high) were ejected from the moulds prior to unconstrained compression testing.

Uniaxial compressive strength of the scaffolds formed, was determined at a constant strain rate of 0.01 mm/sec. A Peltier hood attached to the equipment allowed samples to be tested under constant environment of temperature, wet and dry.

4.2.3 Wet Sintering

The fluids tested for wet sintering were distilled water, phosphate buffered saline (PBS), supplemented Dulbecco media (42430) containing 10% serum, 0.9% sodium chloride solution (NaCl) and Hanks balanced salt solution (HBSS). A range of PLGA 85:15 compositions with PEG 400 were evaluated for temperature sensitivity and the strength of association formed.

4.2.4 Constrained and Unconstrained Compression

To determine the impact of confining environments on scaffold strength, constrained compression tests were conducted on 97 and 95% PLGA 85:15 blends with PEG 400. Scaffolds were sintered for one hour in a variety of wet and dry environments; equilibrated for a period of 30 minutes at 37°C and tested immersed in the sintering fluid.

4.2.5 Evaluation of Liquid-scaffold Interaction

To evaluate compositional changes in the particulate components, sintering was conducted for fixed 24 hour time periods and the materials vacuum dried for 5 days. Samples pre and 24 hour post sintering were subjected to oscillation rheology and MDSC evaluation.

4.3 Results and Discussion

4.3.1 Rheological Evaluation of PLGA Blends with PEG

PLGA 50:50 was blended with 5% $^{wt}/_{wt}$ PEG of varying molecular weight to form 95% PLGA 50:50 and the effect on Tg profile compared to the unmodified material. All PEG materials reduced the Tg of PLGA 50:50 to varying extents as shown in Figure 4-1 and increased the viscoelastic mobility of the blended material at lower temperatures. The glass transition temperature values for the series PEG 200 - 5000 varies from -63 to -23 °C [290].

The thermal responsiveness of the blends did not correlate with PEG molecular weight as can be seen in the onset temperature rise in delta value of the PLGA 50:50 blends. The pattern of delta values below 40 °C differed to those above 60 °C. Blends formed with PEG 5000, 2000 and 200 had lower mobility above 60 °C and the results were not correlated with PEG molecular weight. Below 40 °C the highest mobility was achieved with PEG 600 followed by PEG 1000 and 400. The PLGA 50:50 blend with PEG 1000 shows a double peak in the oscillation temperature ramp profile. The peaks coincide with PEG 1000 melting point and Tg end point peak for the PLGA blend at 49 °C (Figure 4-1).

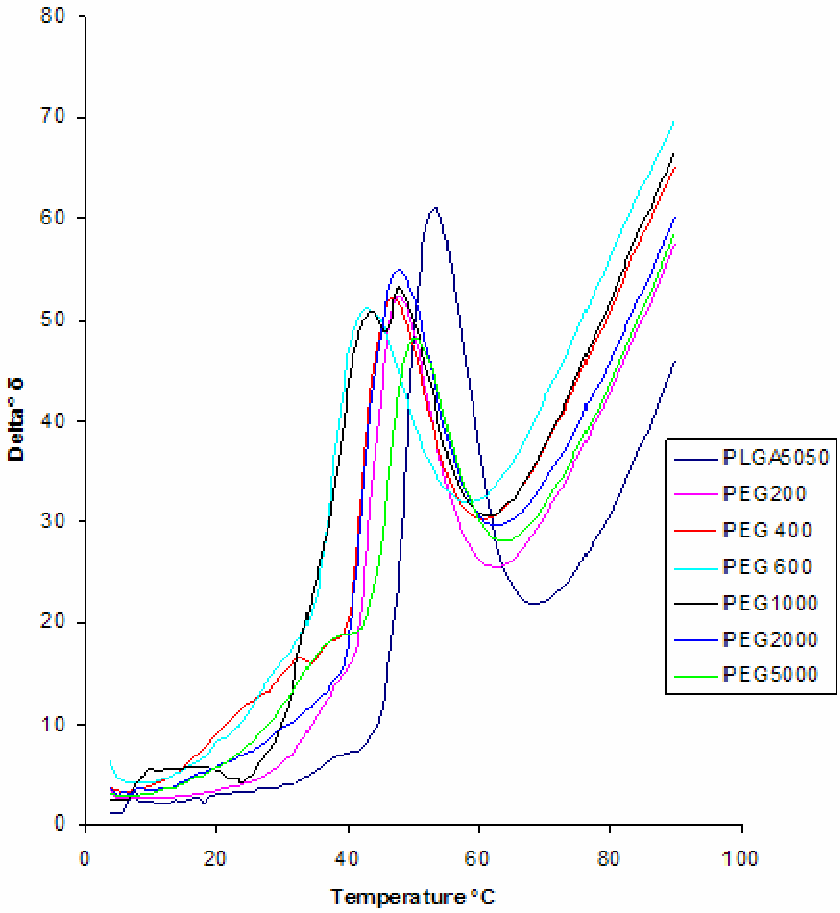

Figure 4-1 Oscillation temperature ramp comparison of PLGA 50:50 and 5% weight fraction blends of PEG, varying in molecular weight, to determine the shift in viscoelastic properties (phase angle). Oscillation temperature ramp profiles were conducted from 4-90 °C at 0.1 % strain (n = 3).

The Tg onset profile in Figure 4-2 was viewed with consideration to the 37 °C sintering temperature target. The profile was more clearly resolved with the mid-range molecular weight PEG blends performing better than PEG 200, 2000 and 5000. Similar results of blends with PEG 400 having a lower glass transition than those with PEG 200 have been previously described [291]. This may indicate that there is an optimum packing distribution based on the molecular weight distribution of the PEG or the presence of water.

The phase angle (delta (δ)) values show the viscoelastic properties in the Tg region, which indicates the adhesive properties of toughness and flexibility. The flexibility was due to the addition of PEG that increased the delta value, showing greater viscoelastic behaviour in comparison with the unmodified PLGA. To act as an adhesive, the PLGA/PEG blended material needs a degree of mobility to deform and spread. Viscoelastic behaviour in the Tg region dictates adhesive properties and the lower the delta value the higher the elastic modulus and adhesive strength as bonding involves low deformation rates.

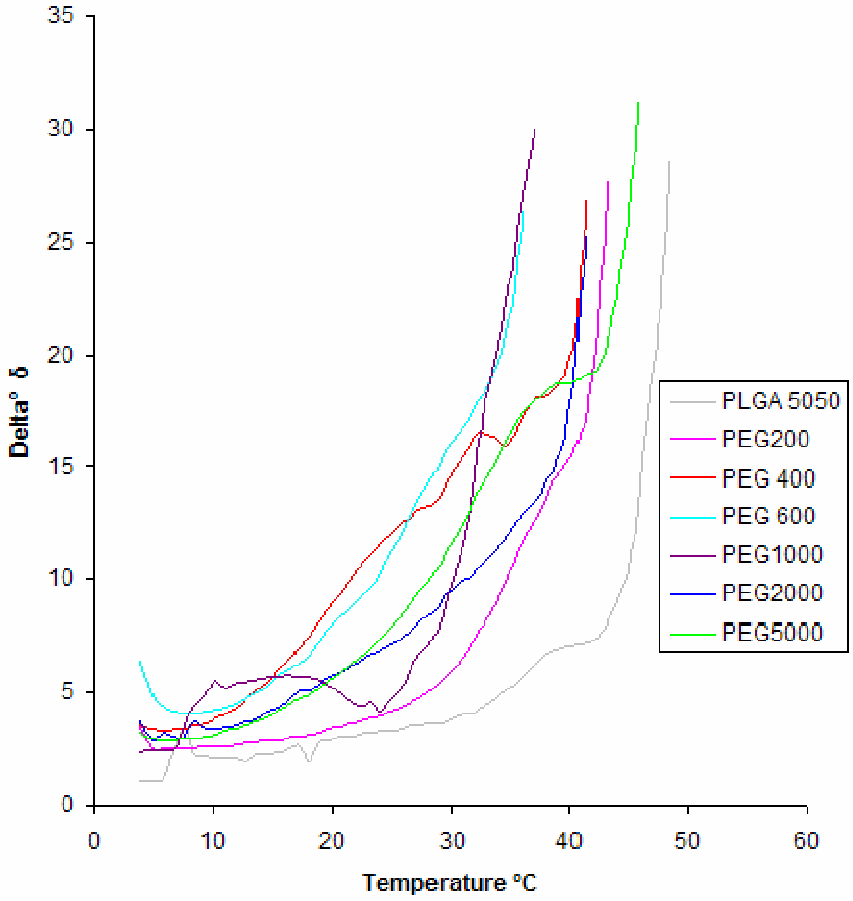

Figure 4-2 Oscillation temperature ramp profile comparing PLGA 50:50 and 5% weight blends with PEG of varying molecular weight from 4-60 °C at 0.1% strain (n = 3). This plot shows the activation region for Tg onset and viscoelastic mobility.

4.3.2 Effect of Sintering Temperature and Composition on Compressive Strength

The summary graph of cylindrical scaffold compressive strength in Figure 4-3 was compiled from materials dry sintered for 24 hours, then compression tested at 25 °C. There was an inverse relationship between PEG molecular weight and sintering temperature below 60 °C. The highest scaffold strength below 60 °C was achieved with low molecular weight blends. The sintered compressive strength of each PEG blend series decreased with temperature. The graph shows a very significant ($p < 0.001$) decrease in the PEG 200 blend compressive strength with sintering at 37 °C and 35 °C.

As the sintering temperature was raised incrementally for each condition there was an increase in the lateral mobility of particle surfaces then an increase in bulk diffusion [292]. Sintering at 60 °C exceeded the Tg of all materials and scaffolds were reduced in size to solid pellets. Sintering above the TG temperature results in Newtonian viscous flow [167]. The plasticising influence of PEG was not apparent at 60 °C and the statistical variation in the p-value was not significantly greater than would be expected by chance. The plasticizing influence of PEG was seen at sintering temperatures below the Tg for the unmodified PLGA such as 45 °C.

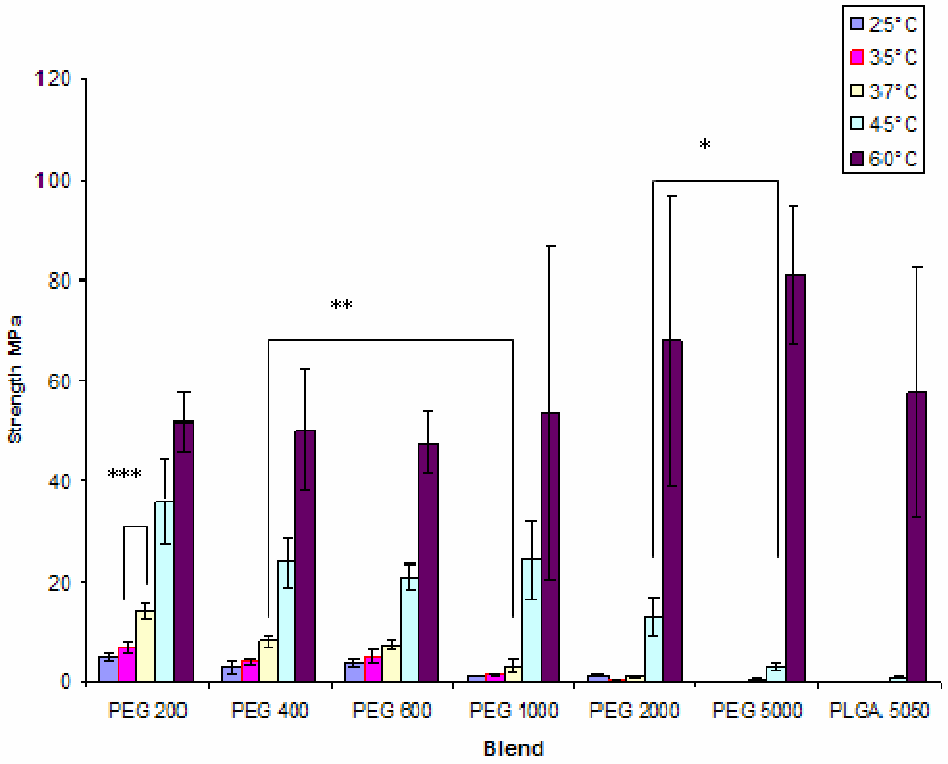

Figure 4-3 Comparison of unconstrained uniaxial compression strength of 95% PLGA cylindrical scaffolds sintered at a range of temperatures for 24 hours with PEGs of different molecular weight. Scaffolds (n = 4) were subjected to uniaxial compression at 0.01 mm/sec strain at 25 °C. Statistical significance denoted as * ($p < 0.05$), ** ($p < 0.01$) and *** ($p < 0.001$).

The unmodified PLGA particle formed a scaffold of lower strength than the PEG 5000 blend at 45 °C, but was not significantly different. Scaffolds formed by the PEG 5000 blend were significantly ($p< 0.05$) weaker in compressive strength than PEG 2000. The blend rheology profile in Figure 4-1 showed PEG 5000 to have the least influence on TG and was confirmed by low sintering strength below 45 °C. Figure 4-3 shows that low temperature sintering was best with low molecular weight PEG blends. Weak scaffolds were produced by PEG 2000 and 5000 blends, sintered at 37 °C. The strongest scaffolds were produced by low molecular weight PEG blends. Scaffold blends made from 5% PEG 2000 and 5000 in Figure 4-3 were very significantly lower in strength ($p< 0.001$) than the other PEG blends. From these results, blends with PEG 200-600 appear to be the most appropriate choices for low temperature sintering at and below 37 °C. For sintering at temperatures higher than 45 °C the choice of PEG 2000 and 5000 blends offer the added advantage of stable non-sintering products at room temperature in contrast to the low molecular weight PEGs that require cold storage for stability.

Figure 4-4 shows representative raw stress-strain compression profiles obtained for 95% PLGA blends with PEG scaffold series sintered at 37 °C. Compressive resistance to stress was inversely related to PEG molecular weight. The results in Figure 4-4 also show the ability of low molecular weight PEG to plasticize PLGA at low sintering temperatures to improve ductility [214].

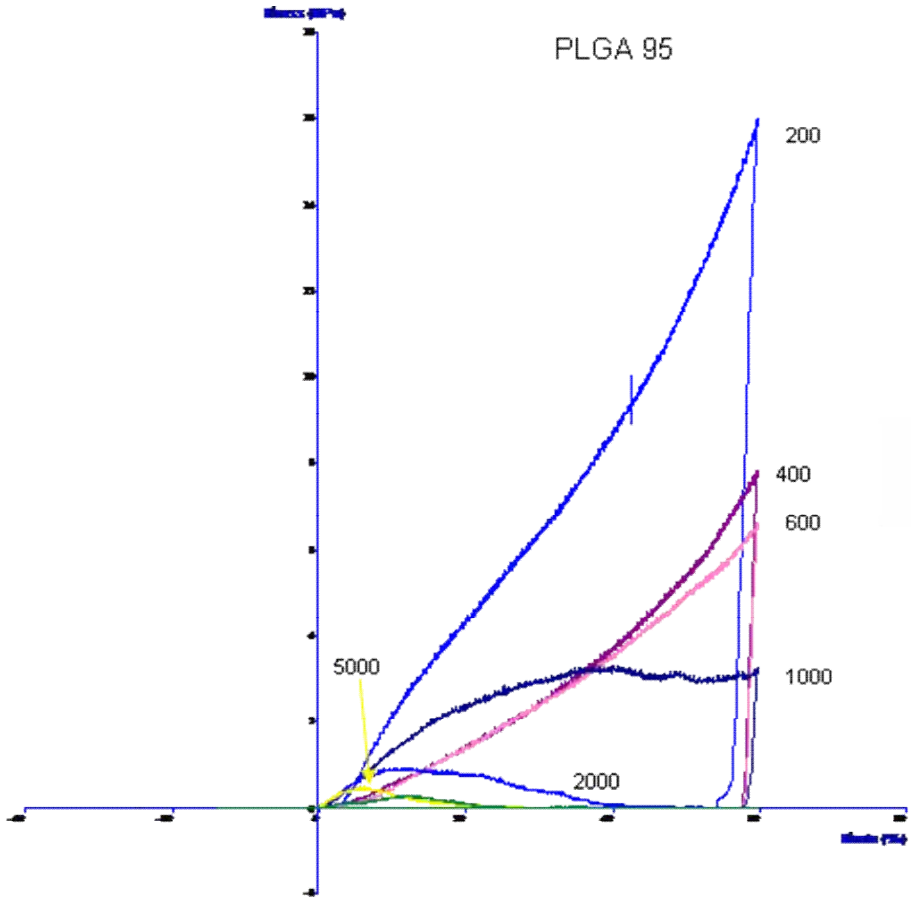

Figure 4-4 Representative stress/strain compression profiles (n = 4) of 95% PLGA blends with PEG of varying molecular weight sintered at 37 °C and compression tested at 0.01 mm/sec and 25 °C.

4.3.3 Sintered 98% PLGA 85:15 with PEG Varying in Molecular Weight

For comparison with the 95% PLGA series, 98% PLGA 85:15 blends with the same PEG profile as previous, were sintered and compression tested under the same experimental conditions and shown in Figure 4-5. The graph shows that the highest values of strength were obtained for the 60 °C sintering condition. At the 45 °C sintering condition, the unmodified PLGA and PEG 5000 blend failed to form viable scaffolds. The strongest scaffolds formed at 45 °C were blended with PEG 400. The ability of low molecular weight PEG to form scaffolds at 37 °C and below was lost in 98% PLGA blend compositions, showing the level of PEG inclusion to be vital to scaffold formation. Comparison of 95% and 98% PLGA 85:15 PEG blend series showed a very significant reduction in sintered strength for equivalent scaffolds.

4.3.4 Impact of Varying PEG400 Content on Sintered 85:15 PLGA

PLGA 85:15 and blends with PEG 400 at 45 °C were dry sintered for two and a half hours; equilibrated for an hour at room temperature and subjected to unconstrained compression test at 25 °C. The results (Figure 4-6) show the compressive strength to increase with PEG 400 addition reaching a maximum at 15% that was significantly ($p < 0.05$) higher in comparison to 5% PEG 400. Unmodified PLGA 85:15 polymer did not sinter under these conditions.

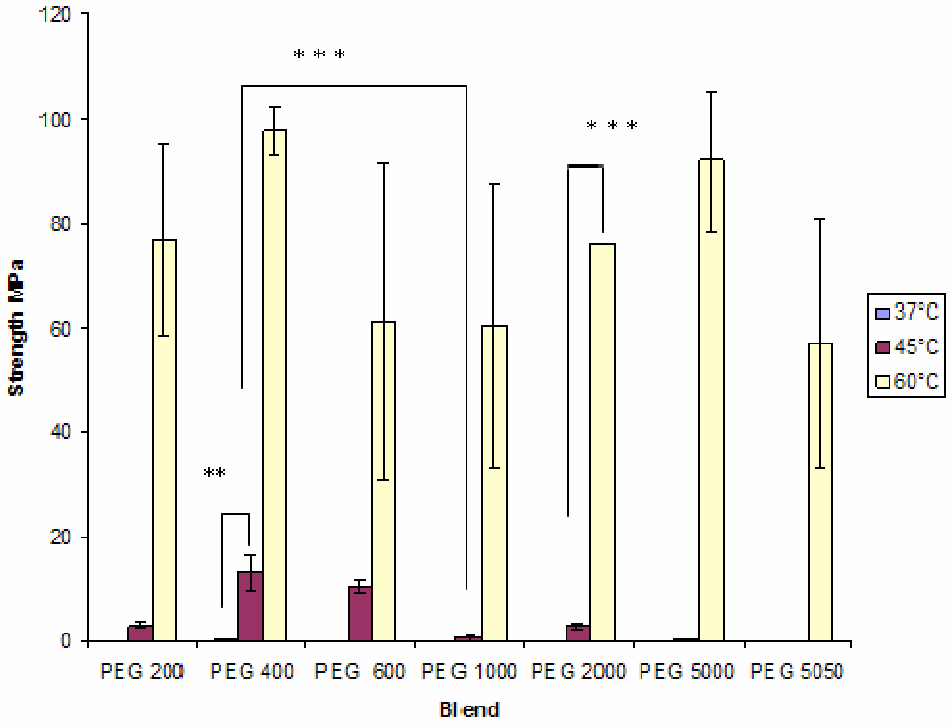

Figure 4-5 Comparison of compressive strength for 98% PLGA blended with varying PEG molecular weight after sintering for 24 hours at 45 °C. Compression profiles were obtained at 0.01 mm/sec and 25 °C (n = 4). Statistical significance denoted as ** ($p < 0.01$) and *** ($p < 0.001$).

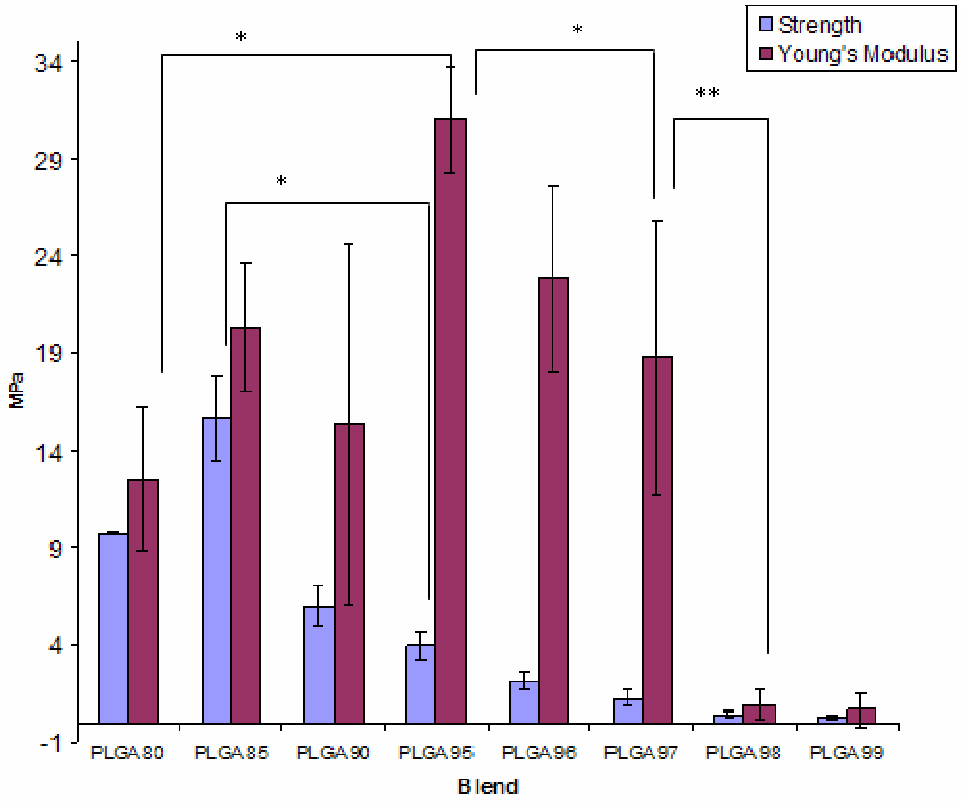

Figure 4-6 Effect of PEG 400 blends with PLGA 85:15 on compressive strength and Young's modulus of scaffolds, dry sintered at 45 °C for 2.5 hours. Compression profiles were obtained at 0.01 mm/sec strain and 25 °C (n = 4). Statistical significance denoted as * ($p < 0.05$) and ** ($p < 0.01$).

Unconstrained scaffold strength was increased by material flow at sintering temperatures and neck formation between particles. Therefore scaffold strength increased until material flow continued at the 25 °C test condition. The results in chapter 3 showed 15% PEG addition to reduce Tg within test conditions. The highest value for Young's modulus was obtained for the PLGA 95% blend and was within the range needed for cancellous bone. In the PLGA 95% blend Young's modulus shows neck formation to have occurred during sintering but the rigidity of the weld and Tg remained high and were unaffected by the 25 °C test condition. The effects of PEG were shown to become dominant at 10% addition in chapter 3 with Tg below 30 °C (Figure 3-12). Similar results of increased structure disruption at 10% plasticizer addition have been recorded [200, 202]. The significant ($p<0.01$) increase in Young's modulus with PEG 400 addition from 2 to 5% was due greater neck formation during sintering and Tg being unaffected by the compression test temperature. Scaffolds require stiffness for transmission of strain.

4.3.5 Comparison of 24 hour Dry and Wet Sintering

The image in Figure 4-7 shows wet sintering to alter the appearance of 85:15 PLGA with PEG 400 blends in comparison to unmodified PLGA. The appearance of the PLGA 85:15 control particles was unchanged and all particles were similar in appearance to the control before immersion.

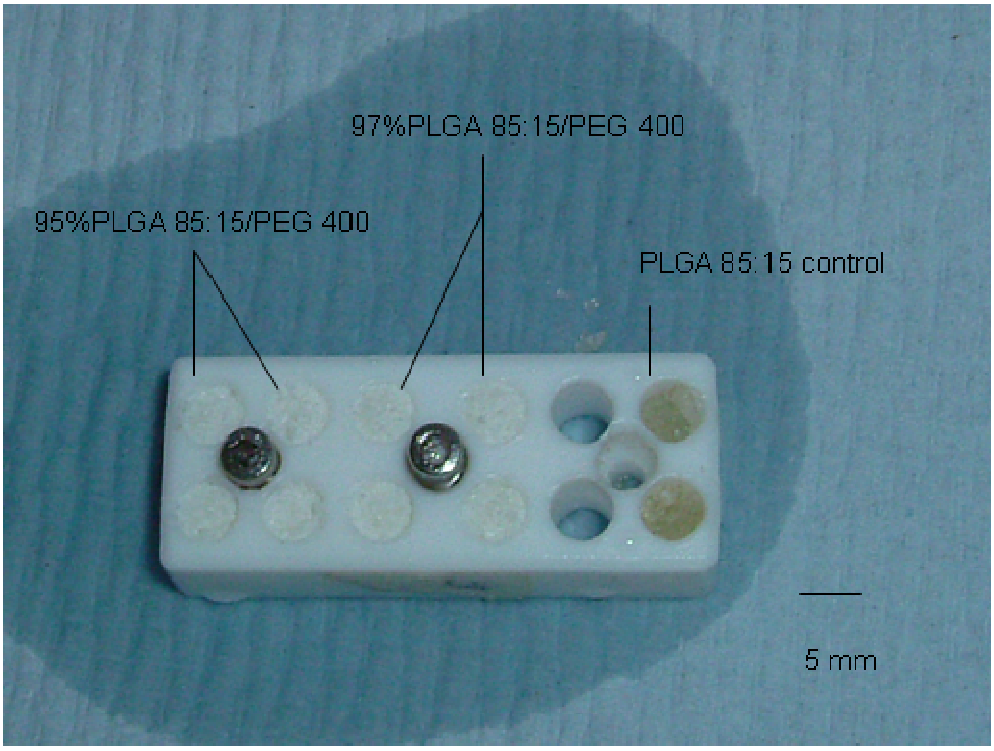

Figure 4-7 Teflon mould with scaffolds wet sintered in distilled water. The un modified PLGA 85:15 control particles were unchanged in appearance and did not sinter after 24 hours at 45 °C to form cylindrical scaffolds. Particles containing PEG 400 turned white in appearance from the colour of the PLGA 85:15 control.

The change in appearance may have been due to the creation of submicron pores that scatter light. Plasticizers have been postulated to occupy pores that disrupt polymer packing and lower Tg. When plasticizers are leached from polymers they leave subsurface voids of the order 0.2- 0.5 μm that scatter impinging light that pass through media with different refractive indices [293]. Similar results have been recorded by others with PEG migration [133, 294].

The particulate scaffold was intended for use as an injectable material, which would sinter *in situ* in a physiologically wet environment. Blended PLGA with PEG was evaluated under conditions that were clinically relevant. Blends were sintered at temperatures up to 45 °C and compression strength tested at 37 °C wet and dry for comparisons. In this study, wet sintering did not decrease scaffold compressive strength. The graph (Figure 4-8), confirmed earlier observation that sintering at 45 °C produces scaffolds with higher strength than at 37 °C for both dry and wet conditions. Sintering at both 37 and 45 °C in distilled water (DW) produced scaffolds significantly ($p < 0.001$) stronger than the dry condition. The result for dry compressive strength at 37 °C was similar to that 3.2 MPa obtained for foamed PLGA (Thomson et al 1995). Previous work with PLGA 75:25 films immersed in buffer has recorded increased strength and modulus [220]. Wet strength and modulus was demonstrated to increase with lactide content of PLGA [204].

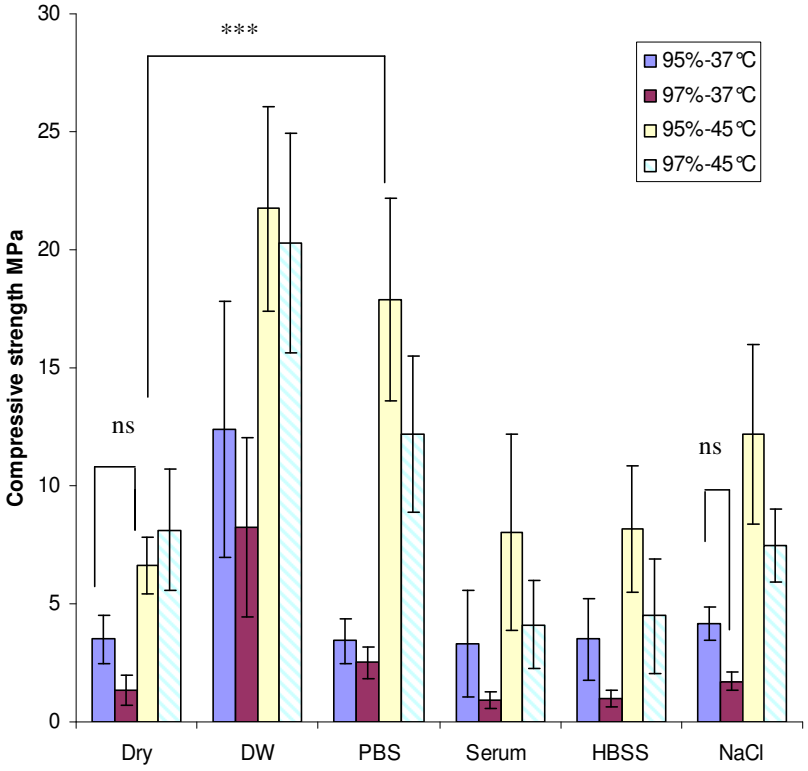

Figure 4-8 Comparison of wet and dry compressive strength of cylindrical scaffolds after 24 hours sintering at 37 and 45 °C. Particulate 95 and 97% PLGA 85:15 blends with PEG 400 were sintered dry, in DW (distilled water), PBS, Serum (10% serum containing media), HBSS and NaCl (0.9% sodium chloride solution). Compression test was conducted at 0.01 mm/sec strain and 37 °C ($n = 3$). Statistical significance denoted as ns (not significant) and *** ($p < 0.001$).

The data also show that PBS, serum, HBSS and sodium chloride at body temperature retard the development of scaffold strength in comparison to distilled water. With the exception of the dry sintered scaffolds at 45 °C, PLGA 97% produced weaker scaffolds than the corresponding PLGA 95% blend but was not significantly different. PBS sintering of the PLGA 95% PEG 400 blend at 45 °C produced scaffolds significantly ($p < 0.001$) stronger than the dry condition. Serum sintered scaffolds at 45 °C were of lower strength in comparison to 0.9% sodium chloride, water and HBSS. Serum proteins have been recorded to reduce the strength of calcium phosphate bone cement [128]. In contrast to these results increasing the temperature from 25 °C to simulated physiological environment at 37 °C for PBS incubated PLA and PLGA scaffolds reduced compressive strength and was attributed to water uptake [204, 241].

In Figure 4-9, the graph of Young's modulus for the PLGA 95% blends show that very significantly ($p < 0.001$) stiffer scaffolds were produced in distilled water (wet) sintering at both 45 and 37 °C in all combinations except for the 97% PLGA blends. At elevated temperatures of 45 °C significantly stiffer scaffolds ($p <0.001$) were produced under wet sintering conditions compared to dry. Sintering at 45 °C produced stronger scaffolds than at 37 °C and appears to offer a method to circumvent issues of interference with phosphates (PBS) and serum proteins.

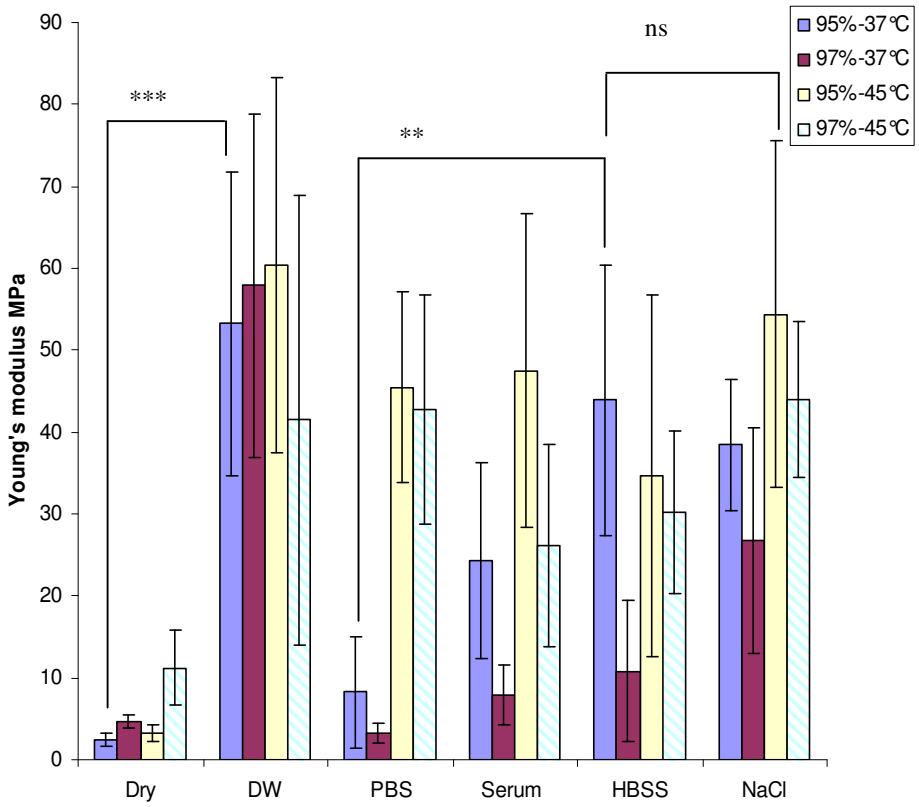

Figure 4-9 Comparison of dry and wet 24 hour sintering at 37 and 45 ° C to show Young's modulus developed under the experimental conditions with PEG 400 loading at 3% and 5%. The conditions were dry, DW (distilled water), PBS, Serum (10% serum containing media), HBSS and NaCl (0.9% sodium chloride solution). Compression profiles (n = 3) were obtained at 0.01 mm/sec and 37 °C conditions. Statistical significance denoted as ns (not significant), ** ($p < 0.01$) and *** ($p < 0.001$).

4.3.6 Sintering Strength Comparison at Short Timescales

This comparison was conducted at reduced time scales to determine the integrity of structures formed at clinically relevant timescales of 15 minutes and 1 hour in Figure 4-10. The scaffold structures formed were ~20% of the strength of 24 hour sintered scaffolds. 97% PLGA with PEG 400 blended particles formed a scaffold suitable for handling and test only in sodium chloride after one hour. After 15 minutes dry sintering 95% PLGA scaffolds were very significantly ($p < 0.001$) stronger than 97% PLGA. The scaffold structures formed in HBSS buffer by the 95% PLGA blend were comparable to those formed in sodium chloride and PBS.

The 95%PLGA blend in serum containing media was significantly weaker ($p < 0.05$) than HBSS and other sintering conditions except for PBS where there was no significant difference. The Young's modulus developed in these wet sintered scaffolds (Figure 4-11) was greater than those values developed by dry sintering with the exception of serum containing media. The 95% PLGA scaffolds sintered at 37 °C for 24 hours in both HBSS and sodium chloride solution were stiffer than those produced in PBS but not significantly so. These results indicate that the 95% PLGA 85:15 PEG 400 blend formed stronger scaffolds, faster than 97% PLGA. Both PBS and serum containing media appeared to retard the formation of scaffolds at 37 °C after 24 hours. Dried scaffolds formed at the reduced timescale were less stiff than wet sintered scaffolds.

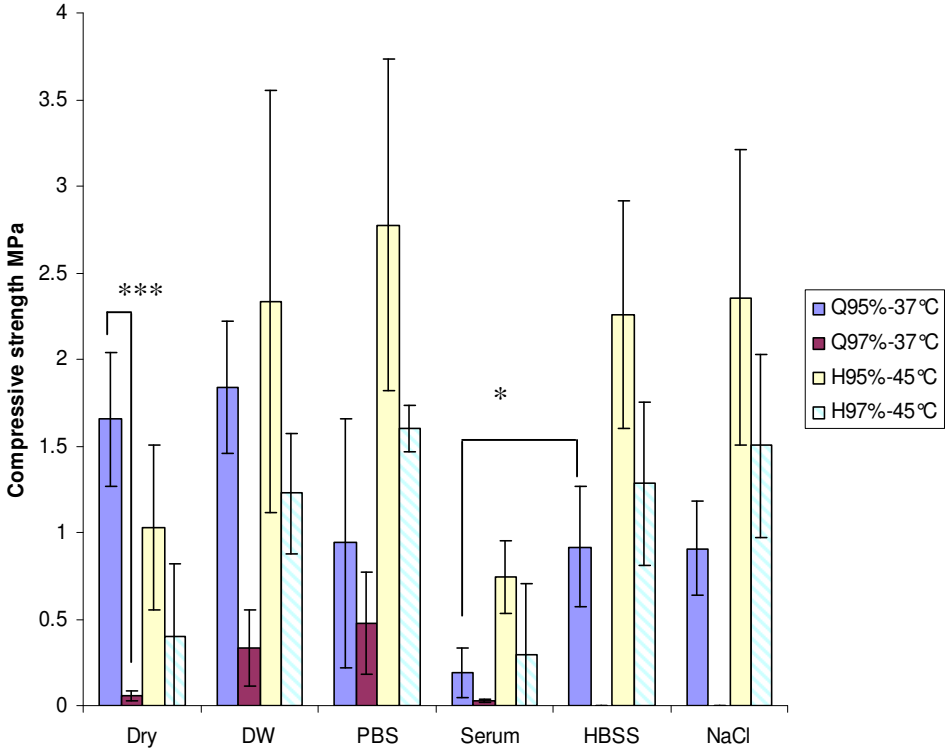

Figure 4-10 Comparison of scaffold compressive strengths after sintering at 15 minutes (Q) and one hour (H) with PEG 400 compositions at 5% (95%) and 3% (97%). The sintering conditions were dry, wet DW (distilled water), PBS, 10% serum containing media (Serum), HBSS and 0.9% sodium chloride solution (NaCl). Compression profiles were obtained for n = 3 at 0.01 mm/sec strain and 37 °C. Statistical significance denoted as * ($p < 0.05$) and *** ($p < 0.001$).

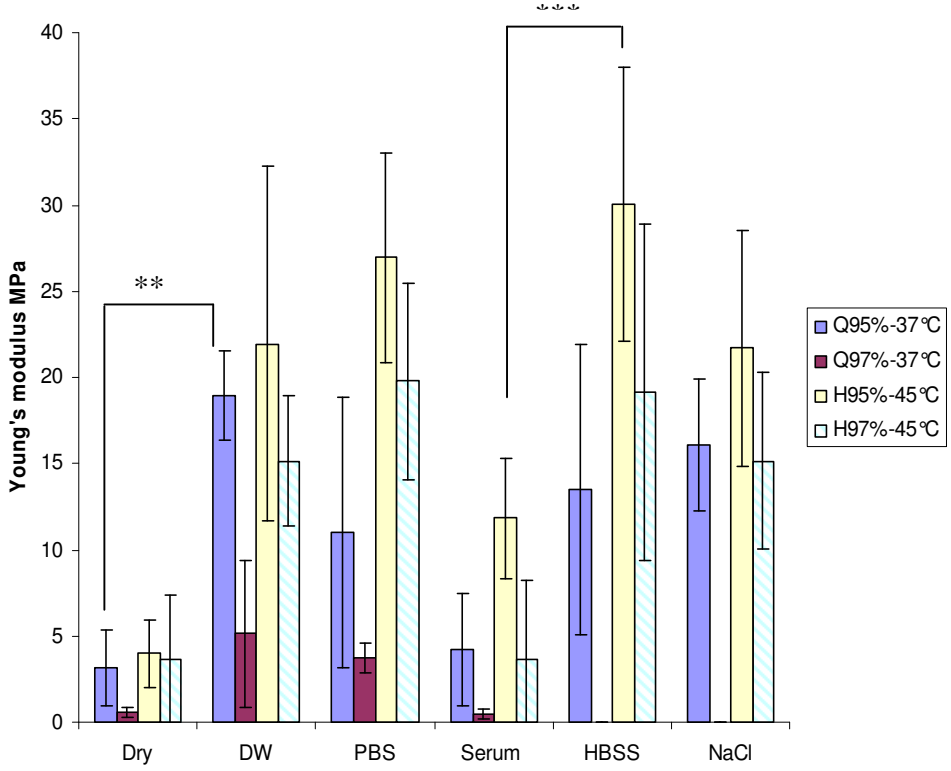

Figure 4-11 Graph comparing Young's modulus developed by scaffolds sintered at the reduced timescales of 15 minutes (Q) and one hour (H) with PEG 400 compositions at 5% (95%) and 3% (97%) loadings. The conditions were dry, wet DW (distilled water), PBS, 10% serum containing media (Serum), HBSS and 0.9% sodium chloride solution (NaCl). Compression profiles were obtained for n = 3 at 0.01 mm/sec strain and 37 °C. Statistical significance denoted as ** ($p < 0.01$) and *** ($p < 0.001$).

Dissolution of PEG is exothermic and its diffusion in water shows molecular weight dependence dominated by hydrogen bonding [274]. Water forms a hydration shell around surfaces to influence diffusion kinetics and thermodynamics. Water alone does not stop PEG migration or miscibility, which is influenced by the concentration and type of ion present in solution [295, 296]. The development of two or more immiscible phases in an aqueous system is commonplace with water soluble polymer and low molecular weight solute above a critical concentration. PEG is one of the most common components of these systems and is hydrated strongly with several water molecules accounting for its high solubility [297].

The electrostatic interaction of ions with surfaces affects the hydration layer and interaction of absorbed molecules such as proteins [298]. Phosphate anions have a greater electrostatic potential and interaction than chlorides in the Hofmeister series [296]. Ion induced hydration crowding of the surface may impede PEG desorption and interrupt surface sintering. PEG interaction with phosphate anion results in decreased solubility and increased hydrophobicity [295, 299]. The precise mechanism is uncertain and may involve direct ion-molecule interaction or electrostatic screening that result in charge shielding [300].

4.3.7 Comparison of Constrained and Unconstrained Strength Testing of 95%PLGA 85:15 with PEG 400

Comparison of unconstrained compression strength (Figure 4-12) shows the serum containing media to have the lowest strength 0.8 ± 0.19 MPa. The Young's modulus values for unconstrained saline (NaCl) solution was higher (12.29 ± 4 MPa) than PBS (5.3 ± 1 MPa). HBSS scaffolds produced very significantly ($p < 0.001$) higher values for Young's modulus than PBS. The constrained samples had higher strength values that were extremely significant ($p < 0.001$) in comparison to unconstrained scaffolds. The Young's modulus was also increased for the constrained sample. Injectable scaffolds were designed to be placed in a constrained tissue environment. The unconstrained material was of lower strength for all conditions and particularly affected by serum containing media.

Saline solution does not appear to hinder the formation of high strength scaffolds under the sintering conditions. Differences with PBS and serum containing media may be due to the presence of multivalent salts and the formation of a two phase aqueous system at elevated temperature with low levels of leached PEG 400 [300]. Monovalent salts form two phase systems at high concentrations of PEG ensuring that PEG 400 diffusion is unimpeded.

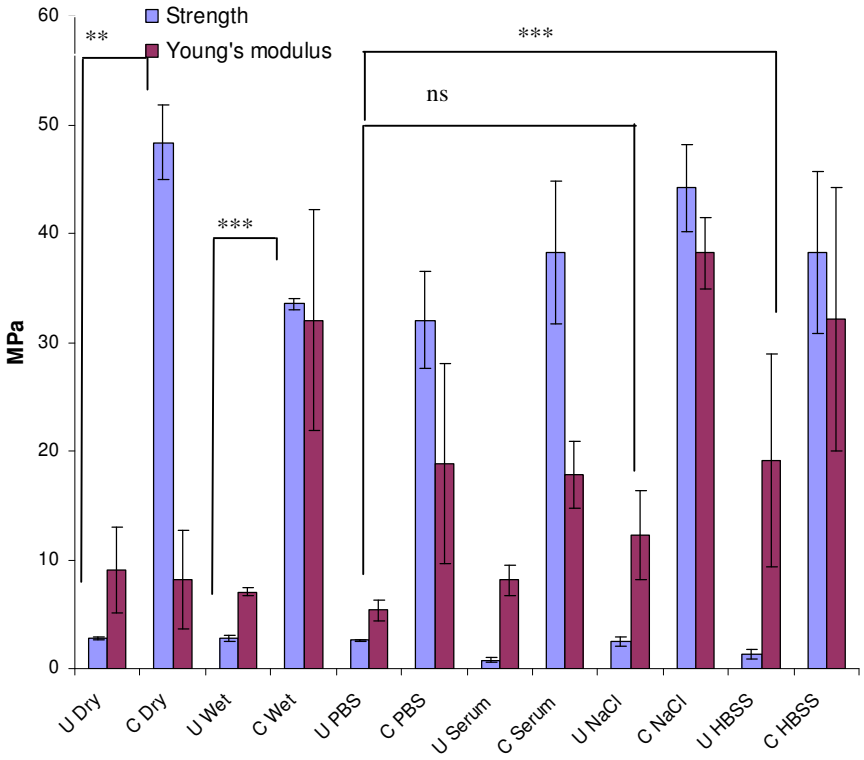

Figure 4-12 Comparison of constrained and unconstrained compression strength and Young's modulus was conducted on 95% PLA 85:15 with PEG 400 samples sintered wet and dry at 45 °C for an hour and tested at 37 °C. The unconstrained samples were prefixed (u) and constrained (c). Samples were sintered dry, wet (distilled water), PBS, serum (10% serum supplemented media), (NaCl) 0.9% sodium chloride solution and HBSS. Compression profiles were obtained at 0.01 mm/sec strain (n = 3). Statistical significance denoted as ns (not significant), ** ($p < 0.01$) and *** ($p < 0.001$).

4.3.8 Comparison of Un-sintered and Sintered Sized Particles

The constrained compressive test on un-sintered restricted size particles in Figure 4-13 shows the particles <100 µm to be significantly ($p < 0.01$) lower in strength than particles > 100 µm. Particles > 400 µm in size were significantly ($p > 0.01$) stronger than particles > 200 µm. The lower strength shown by particles < 100 µm may have been attributable to settling caused by compaction during compression. The Young's modulus was also reduced in comparison to compressive strength. The relationship may be due to the fact that the particles are connected by physical interlocking rather than a deformable bond.

Comparison of the un-sintered constrained strength in Figure 4-13 with dry and wet sintered scaffolds in Figure 4-12 shows the unconstrained scaffolds to have higher Young's modulus than strength. The relationship between strength and Young's modulus for sintered constrained scaffolds was generally similar with modulus not significantly greater than strength. The comparison of sintered scaffold strength in comparison to loose dry powder shows liquid sintering not to have softened the particles or made the scaffold susceptible to compaction under reduced force. This result was similar to other plasticizer leached systems [301].

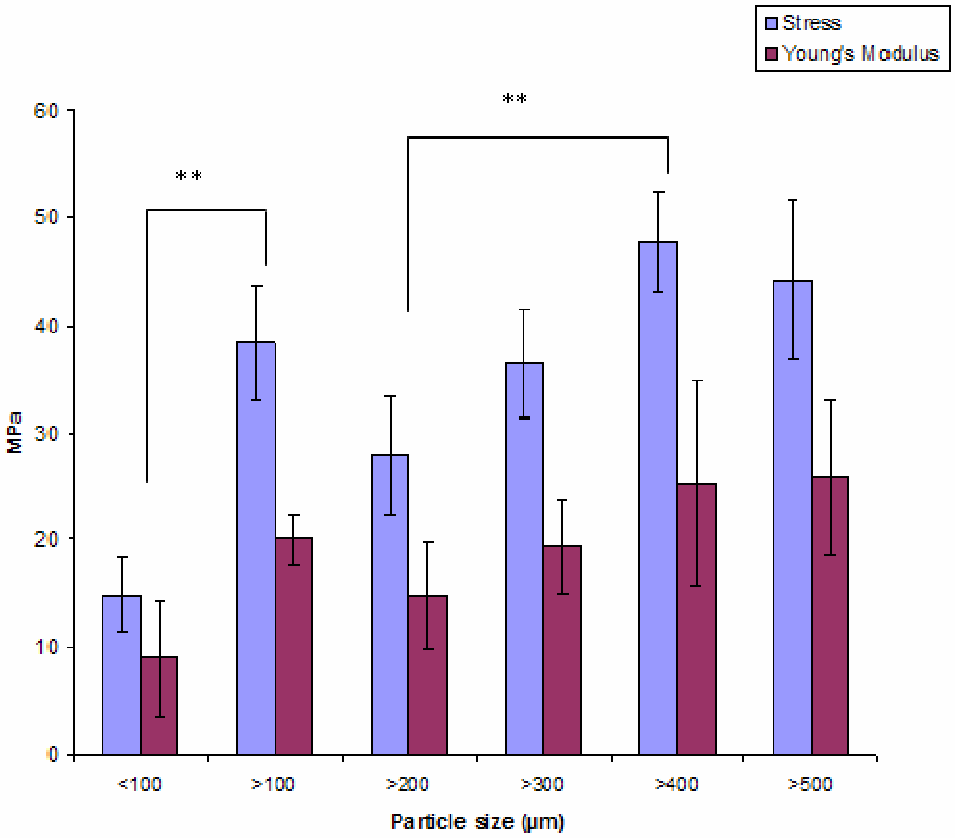

Figure 4-13 Comparisons of un-sintered size restricted 95% PLGA 85:15 with PEG 400 particulates, by constrained compression test (n = 3). The test was conducted dry at 25 °C and 0.01 mm/sec compression rate. Statistical significance denoted as ** ($p < 0.01$) and *** ($p < 0.001$).

4.3.9 Investigation of Liquid Sintering

To investigate liquid sintering at 37 °C, particles were rheologically compared before and after water immersion for 24 hours. Figure 4-14a of unmodified PLGA showed a 3 °C shift in the post sintered curve to lower temperatures in the Tg onset region with no other significant change noted in the oscillation profiles. The 97% PLGA blend, Figure 4-14b shows a slight shift to lower temperatures in the Tg onset zone with little separation in the remaining profile. A greater shift of 6 °C in the end TG region to higher temperatures was noted for (Figure 4-14c) 95% PLGA with PEG 400 blend. Figure 4-14d showed a 22 °C peak shift to higher temperatures for the 85% PLGA with PEG 400 blend. This peak shift represents a loss of 65% of the PEG 400 content. Plasticizer leaching has been previously observed with increased modulus [301].

Onset Tg reduction for the PLGA 85:15 control, may be due to retained water that also obscured the peak shift in the 97% PLGA sample; as the change in appearance of Figure 4-7 was substantial. The 95% PLGA with PEG 400 curve shift indicates a loss of > 20% of the initial PEG loading. This loss of PEG 400 and peak shift has simultaneously raised Tg and increased the stiffness modulus of the sintered material seen in earlier wet compression test results. These observations may explain differences in results for 95 and 97% PLGA material after sintering. This liquid based process may provide a mechanism to limit sintering at physiologically isostatic temperatures.

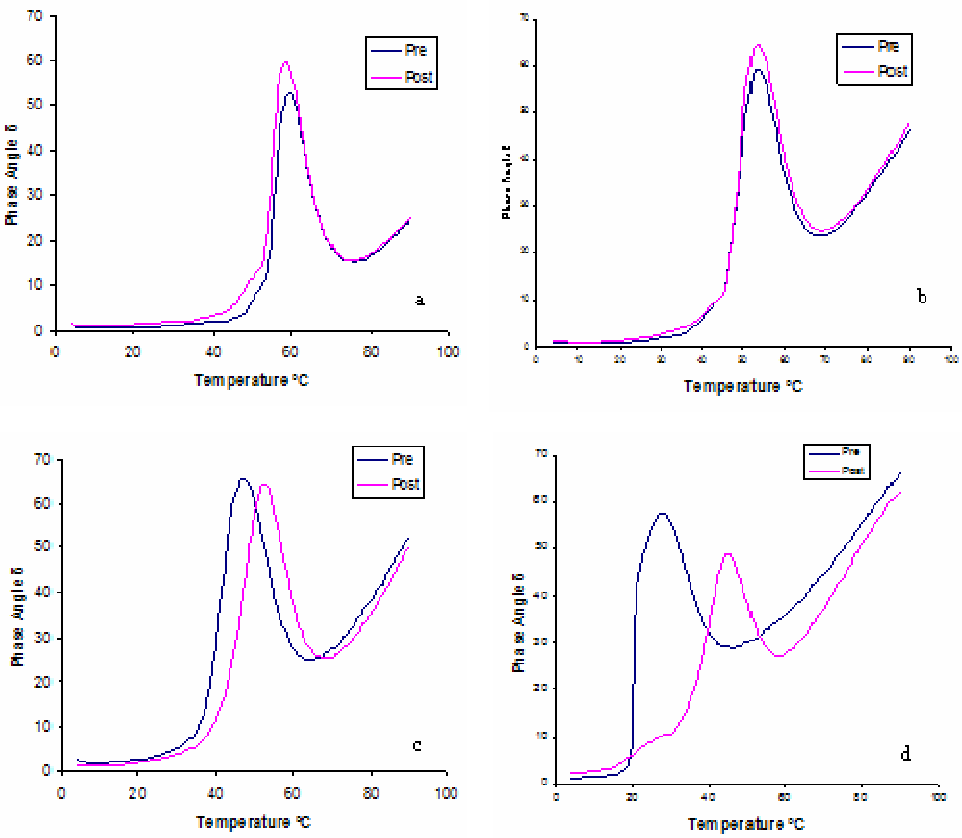

Figure 4-14 Representative wet sintering results showing oscillation temperature ramp comparisons with and without PEG 400. Particulates not sintered were designated pre and those sintered for 24 hours in distilled water at 37 °C then dried post. Graph (a) unmodified PLGA, (b) 97% PLGA (c) 95% PLGA and (d) 85% PLGA. Oscillation temperature ramp profiles were conducted from 4-90 °C at 0.1% strain.

4.3.10 MDSC Investigation of Liquid Sintering

MDSC investigation of thermal transitions was conducted on 85:15 PLGA with PEG 400 blends pre and post sintering for 24 hours in distilled water. In Figure 4-15(a), the unmodified 85:15 PLGA as the control material showed little variation in the comparison of 2nd cycle Tg profiles for pre and post sintered materials. The profiles overlay closely. In Figure 4-15(b), the comparison of pre and post sintered 97% PLGA with PEG 400 shows that there was a reduction in the heat flow profile with the Tg for the pre sintered sample of 40 °C and 34 °C for the post sintered material.

In Figure 4-16(a) comparison of the 95% PLGA blend pre and post sintering, shows the post sintered material with a a higher Tg transitions. A similar result was obtained for the comparison of pre and post sintered 85% PLGA with PEG 400 in Figure 4-16(b). The Tg profile for the 85% PLGA post sintered sample was narrower and more distinct than for the pre sintered material. These observations suggest a reduction in the PEG content for the 95% and 85% PLGA blend compositions. Similar results by others suggest the plasticizer was not completely leached out [282, 301]. Water bound to PLGA is not discernible by DSC and does not freeze [302]. An exchange of PEG for water in the 97% PLGA post sintered material, would depress Tg.

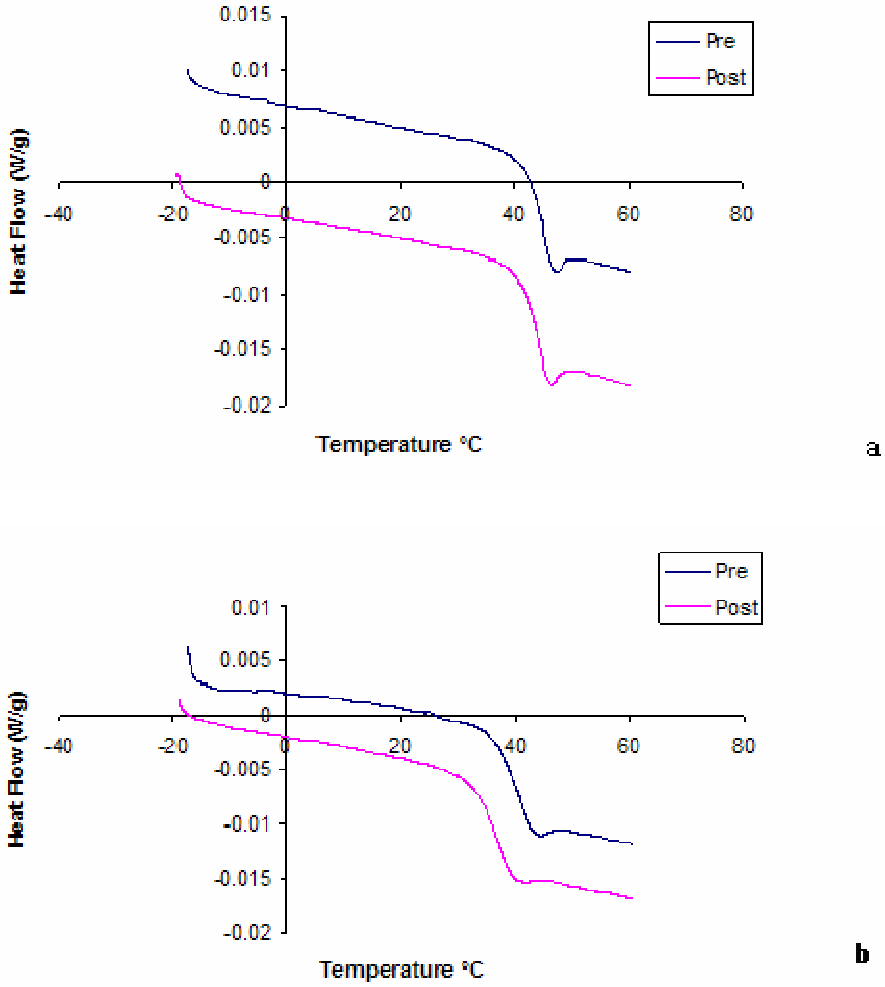

Figure 4-15 Modulated DSC second cycle Tg profile comparison of particulates not sintered was designated pre and those sintered for 24 hours in distilled water at 37 °C then dried post. Graphs (a) unmodified PLGA 85:15 and (b) 97% PLGA with PEG 400 blend. Modulated DCS was conducted at 1 °C/minute from -20 to 120 °C, modulated ± 0.16 °C for 60 seconds (n = 3).

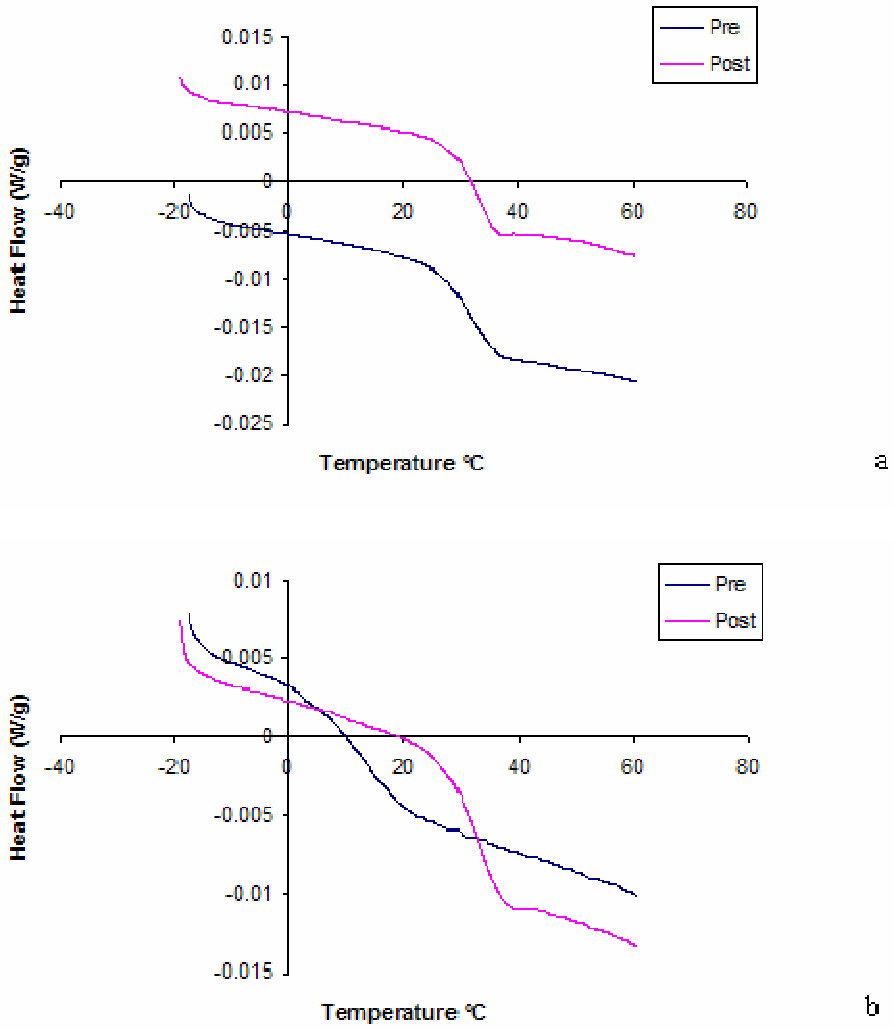

Figure 4-16 Modulated DSC second cycle Tg profile comparison of particulates not sintered designated pre and those sintered for 24 hours in distilled water at 37 °C then dried post. Graph (a) 95% PLGA 85:15 with PEG 400 blend and (b) 85% PLGA with PEG 400 blend. Modulated DCS was conducted at 1 °C/minute from -20 to 120 °C, modulated ± 0.16 °C for 60 seconds (n = 3).

The result summary of the 2nd cycle run Tg values for blends in Figure 4-17, compares the whole curve (onset, inflection and end) Tg values. Figure 4-17 shows the post sintered unmodified control and blends to 97% PLGA post sintered, having a lower Tg than the pre sintered blends. The Tg for post sintered materials at 5% PEG 400 addition and greater were higher than the pre sintered materials. These values plateau at 95% PLGA post sinter, indicating the loss of PEG 400 to a minimal value or a proportional uptake of bound water. This possible conclusion was reached by examination of the unmodified PLGA and 97% PLGA post sintering result in Figure 4-15 a,b.

Comparison of Figure 4-17 with Figure 3-12 show the pre blended PLGA 85:15 series to have a similar profile to earlier batches of the same polymer and the post sintered material to have a similar profile to PLGA 50:50. This comparison indicates that the loss of PEG during wet sintering may be proportional to the initial content as the lactide content of the polymers was different. If the Tg post sintered remains lower than the starting blend it may also indicate mass or strength loss [220].

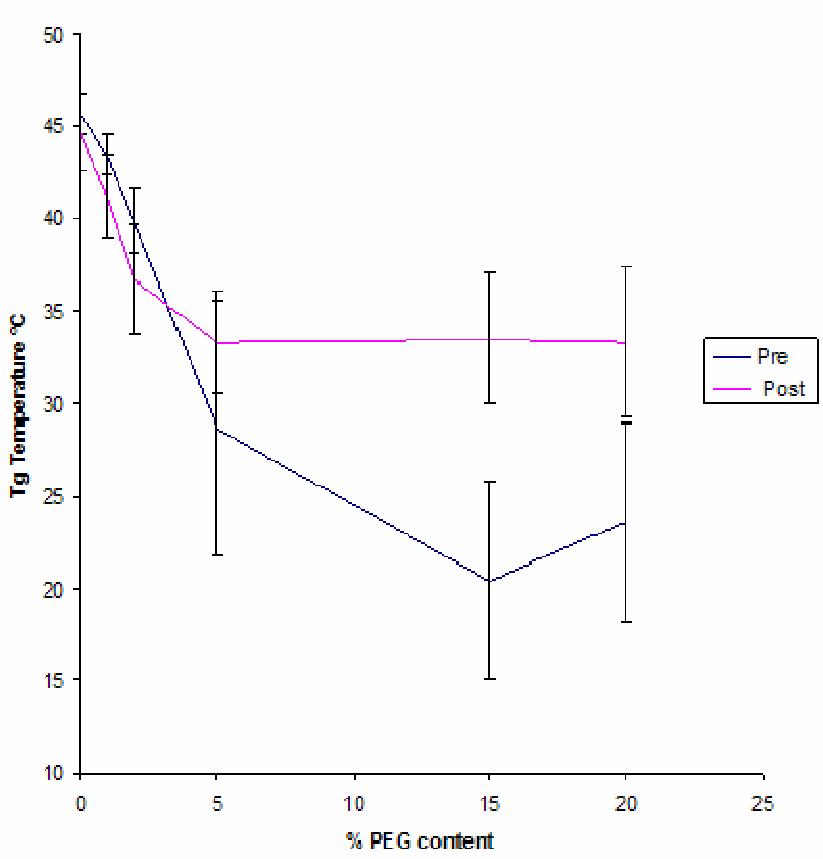

Figure 4-17 Modulated DSC summary plot of the second run Tg values for 85:15 PLGA with PEG 400 blends pre and post wet sintering (n = 3). Modulated DCS was conducted at 1°C/minute from -20 to 120 °C, modulated ± 0.16 °C for 60 seconds.

In Figure 4-18, the heat capacity values for Tg profiles of the blend pre and post sintering were compared. Increasing the content of PEG 400 in blends with 85:15 PLGA decreased the heat capacity of the Tg transition. The heat capacity for the post sintered control was reduced, when compared to the pre sintered control material. The heat capacities for the post sintered 99% and 97% PLGA with PEG 400 blends were lower than the pre sintered blends. Absorption of small quantities of bound water can reduce Tg as in the case of the untreated control and is similar rot results obtained elsewhere [303]. Residual PEG would also be present with residual water and depress further the Tg as previously observed for salt leached polymers [133].

The heat capacity for the 95% PLGA with PEG 400 blends was higher than its pre sintered blend. Post sintered blends above 5% PEG 400 addition had higher heat capacity values than pre sintered equivalents. The plateau of the values for heat capacity may indicate that a residual amount of PEG and bound water to be present. Similar conclusions have been reached by others [204].

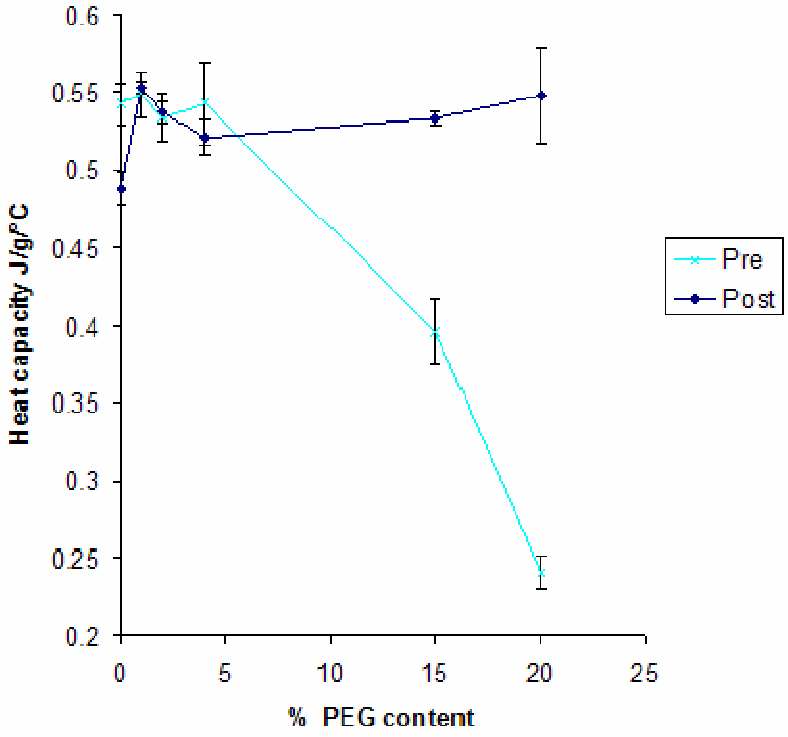

Figure 4-18 Modulated DSC summary plot of the second cycle Tg heat capacity values for 85:15 PLGA with PEG 400 blends pre and post wet sintering (n = 3). Pre sintered blends showed a decrease in heat capacity with Tg decreasing with PEG 400 content. The heat capacity for the post sintered unmodified 85:15 PLGA was reduced in comparison to the pre sintered material but post sintered blends above 5% PEG 400 had higher heat capacity values. Modulated DCS was conducted at 1 °C/minute from -20 to 120 °C, modulated ± 0.16 °C for 60 seconds.

Figure 4-19 compares the modulated DSC profiles of the first and second heat flow transition profiles for the post sintered 85% PLGA with PEG 400. The graph shows the first run cycle to have two glass transition regions. In the second cycle run, only one thermal transition was present. The presence of two transition regions may have been due to an uneven distribution of PEG remaining within particles after being leached out. Enthalpic relaxation would have been superimposed onto the glass transition region if it had occurred [304]. By heating to 120 °C the sample history was eliminated along with regional differences in the sample resulting in a single transition in the second run.

The SEM image in Figure 4-20(a) shows the results of wet sintering with adhesive particles sintered to each other and to (b) porous microspheres. The welded contact between the adhesive and porous particle shows that the microsphere has retained its morphology and the adhesive component has flowed to achieve sintering. The sintering between adhesive components appears virtually seamless and the distinction between particles was unclear.

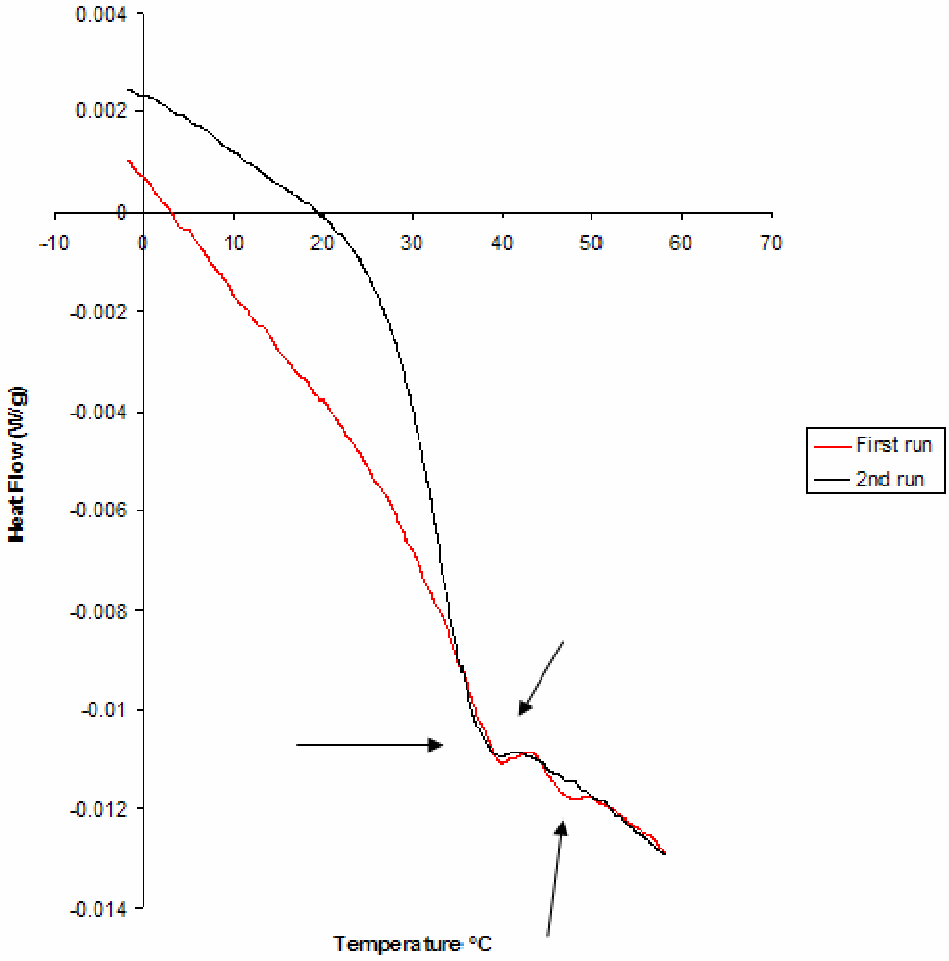

Figure 4-19 Modulated DSC comparison of the first and second heat flow transition profiles for post sintered 85% PLGA 85:15 blended with PEG 400. The graph shows the first run to have two glass transition regions and the second run to have one transition. Modulated DCS was conducted at 1 °C/minute from -20 to 120 °C, modulated ± 0.16 °C for 60 seconds.

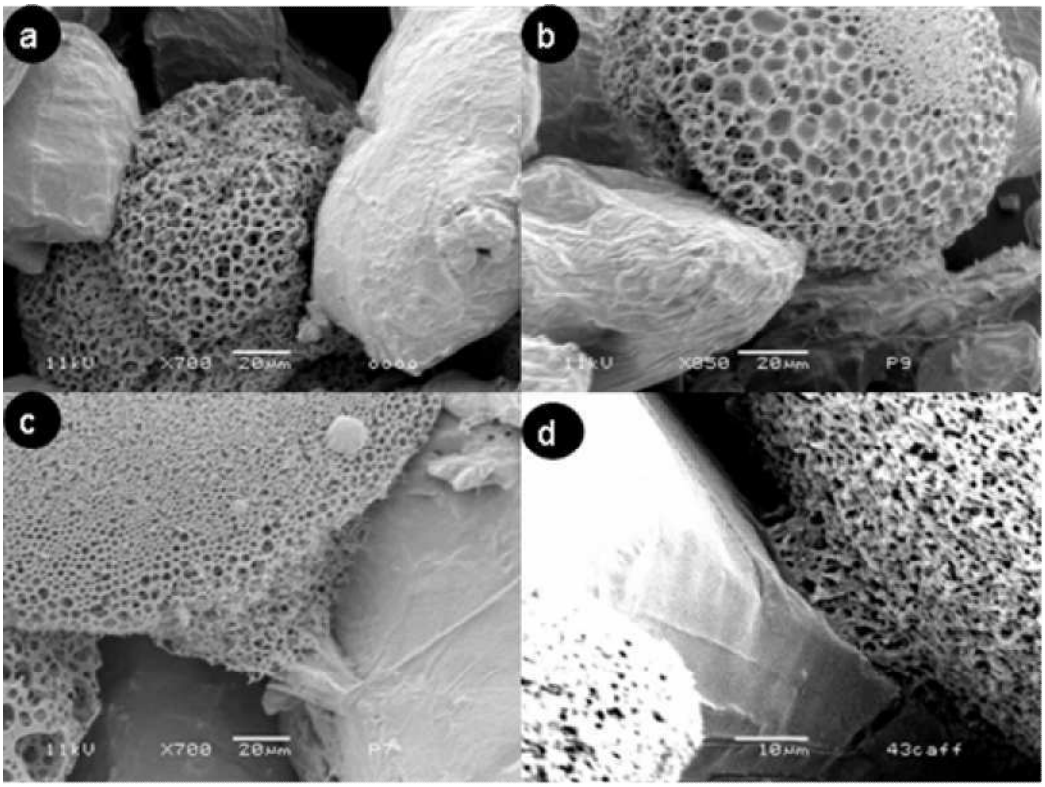

Figure 4-20 Representative SEM images of sintered PLGA 85:15 scaffold with porous type 1 sphere blended with type 2 adhesive particles in a 1:3 ratio and (a) dry pressed at 25 °C for two hours; (b) sintered in distilled water at 37 °C for 15 minutes, (c) one hour and (d) 24 hours. Scaffolds were gold coated and captured at 15 kV.

4.3.11 Proposed Sintering Mechanism

For sintering to occur, molecules at the surface must have sufficient mobility and plastic deformation to increase the contact area between particles [292]. Activation energy is required for surface diffusion which leads to a temperature dependence of an Arrhenius kind i.e. reaction rate depends on temperature; and has been experimentally confirmed by the increase in scaffold strength with sintering temperature.

Particles are packed to maximize exposed surface area whilst, encouraging flow to occur through pores. Desorption, requires reduced external pressure or increased temperature. In this sintering system a pre-warmed liquid is added to particles that sinter, to form a porous structure. The rate of exchange with the solid surface depends on the concentration of material in the solid, the surrounding bulk liquid phase and the temperature [168]. PEG interrupts PLGA inter-chain packing, promoting segmental mobility that increases thermal conductivity [168, 171]. Below Tg, thermal conductivity increases with temperature, reaching a maximum at Tg then decreases above it. PEG dissolution in water is rapid, due to hydrogen bonding interactions and high mobility [274]. As desorption proceeds, diffusing PEG molecules leave behind a void as the polymer reorders itself by condensing and decreasing chain mobility (Figure 4-21).

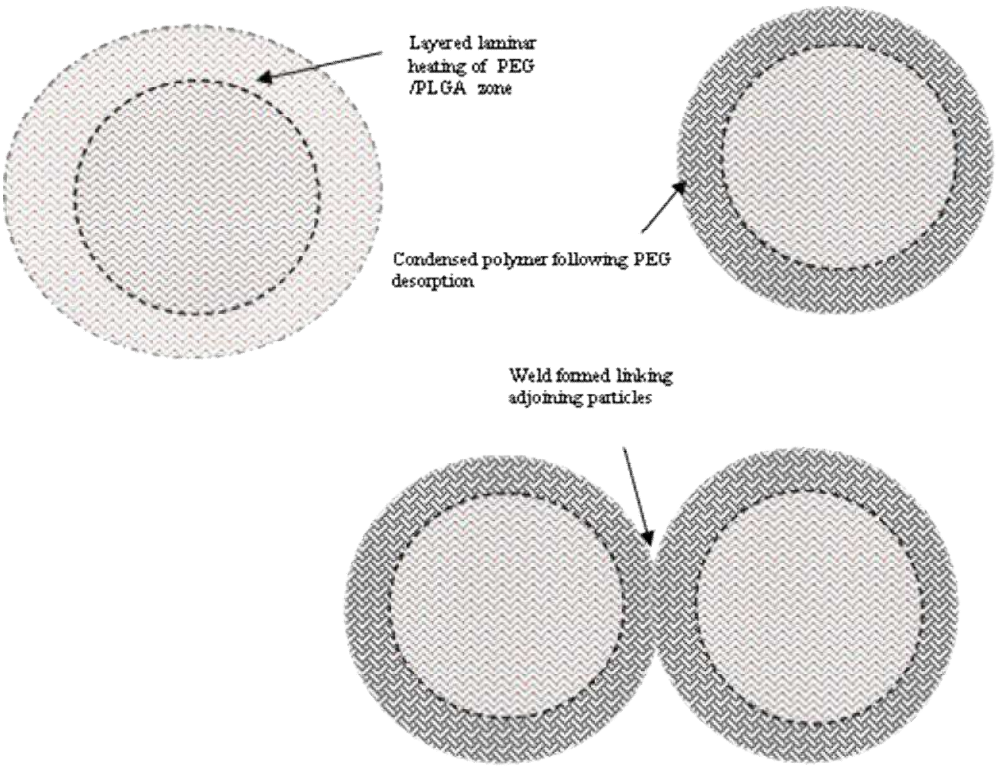

Figure 4-21 Schematic representation of the liquid welding process believed to be occurring during wet particulate sintering. It proposes that the particles encounter layered laminar heating that result in a zone of condensed polymer that participates in the sintering of touching particles.

The void created by PEG migration may be responsible for light scattering and the change in adhesive component appearance. As PEG is leached out thermal conductivity drops and the localized Tg increase PLGA hardening by phase separation. At the junction of point contact where polymer flow and chain entanglement has occurred an inter-particle neck is formed (Figure 4-21). The temperature gain from the bulk fluid to the particle is confined to a narrow boundary-layer at the surface. There is likely to be a significant Tg difference between the inner particle bulk and surface shell resulting in a PEG depleted PLGA zone. The peripherally increased Tg will slow further PEG diffusion from the inner bulk and the predominantly hydrophobic polymer surface loses its ability to soften when wet [204, 273, 301]; hence, a solid structure is formed between adjacent particles that are mechanically strong to withstand vibration and bulk movement

Low molecular weight PEG (< 1500 Da) diffuses into the continuous liquid volume and do not accumulate at the surface of PLGA [305]. However, PEG, though stable to a range of pH, can interact with ions to separate into polymer-rich and polymer-poor phases that are similar to temperature induced phase segregation and can retard diffusion [306, 307]. Inorganic salts can have a strong electrostatic effect on macromolecule to influence solubility and precipitation in water that follows the trend of the Hofmeister series of anions [296, 299]. The Hofmeister series ranks the effectiveness of salts in precipitating macromolecules and was thought to be due to the making and breaking of bulk water structure.

Water has a high dielectric constant and tends to shield ionic charge and reduce the energy of interaction by forming a hydration shell. Water near an isolated interface was conceptually divided into three single layers, each being one water molecule thick [308]. The solute determines the behaviour of the first, inner interfacial water layer and bulk water the third, with the intermediate second layer influenced by both. Recent time and thermodynamic studies with salt solutions have resolved that bulk water structure is not central to the Hofmeister series. Ions don't affect hydrogen-bonding networks beyond the first hydration shell [309] and consequently bulk water does not show structural variation consistent with the Hofmeister series [310].

Inorganic salts are divided into two groups based on the behavior of aqueous-macromolecules in the presence of salts and work by different mechanisms. Direct interactions of ions and macromolecules are key to understanding the Hofmeister series and may involve dispersion forces that depend on ion size and polarizability, ion binding to macromolecules and modulation of surface tension by the ions. There is a partitioning of ions from bulk solution to the aqueous interface of hydrophilic polymers [311] and water mobility at the surface is reduced by electrostatic interactions. Large anions bind more easily to hydrophilic groups due to binding site accessibility. Kosmotropes are responsible for salting out effects on macromolecules and order water molecules around themselves to lower entropy of the aqueous solution. Kosmotropic anions therefore polarize interfacial water attracting the protons in the first hydration shell. This polarizing effect weakens

the hydrogen-bonding to macromolecules. This effect may explain the reduction in strength observed in the wet sintering comparisons between distilled water and solutions with inorganic salts.

Chaotropic ions are water structure breakers with hydrophobic interactions dominated by the entropy of salvation that show salting in behaviour due to saturation binding of anions with macromolecules [312]. Chaotropes don't polarize polymer-associated water, instead they destabilise hydrophobic hydration. At high salt concentration surface tension is increased at the salt-polymer interface. Phosphate ions are more structure making than chloride ions. Chloride ions are anomalous in the Hofmeister series and show intermediate behaviour that may be a function of concentration. Chloride ions are weakly hydrated and sufficiently small not to induce polarization but can bind to weakly hydrated surfaces [313] and behave like chaotropes.

Charged amino acid groups present on protein surfaces at the protein-water interface can react electrostatically with surfaces and may be strongly hydrated. This hydration at the polymer surface may have retarded the diffusion and interaction of PEG with water, resulting in the lower strength values recorded for scaffolds wet sintered in media containing serum. There is increased screening and reduced mobility with ion concentration and packing around a charged molecule. In a vacuum the free energy of interaction between charged groups is entirely enthalpic and independent of temperature [312]. In water it is dominated by

entropy that reflects the ways ions can reconfigure. The dielectric constant responsible for the polarization of water decreases steeply with increasing temperature and results in greater water disorder [312]. The increase in disorder allows polarized groups to approach each other more closely and result in interaction. This may explain the increased strength of scaffolds wet sintered at 45°C where PEG hydration and release from the surface of the PLGA polymer resulted in increased Young's modulus.

4.4 Conclusion

Dry sintering of the scaffold could be reproducibly initiated from 25 ± 3 °C maintaining mild conditions for the protection of functional proteins and cells. Sintered scaffold strength was demonstrated to be inversely correlated with lower PEG molecular weight. The increased viscoelastic behaviour also correlated positively with scaffold strength at low sintering temperatures. Trapped moisture and air are known to decrease compressive strength in bone cement. However, in these particulate scaffolds, water was found to increase compressive strength and stiffness. Optimization of the components was demonstrated to produce scaffold strengths and modulus comparable with cancellous bone. Strong porous structures can be produced and maintained under this new liquid weld sintering regime.

The speed of wet sintering was demonstrated to require less than 15 minutes, at 37 °C to begin producing scaffolds with strengths in the region of cancellous bone.

The wet sintering process also provides a mechanism to control the degree of sintering that would otherwise leave the scaffold soft and deformable at body temperature with the potential of decreasing porosity. This environmentally responsive polymer composition was tuned to solidify at physiological temperature and pH within a clinically relevant time frame. A sintered porous network was achieved by wet sintering compacted particulates without gelation of the surrounding aqueous environment that can slow diffusion and stifle cell viability.

Injecttable scaffolds designed to sinter at body temperature need a mechanism to stop the sintering process after an appropriate time, with a reproducible structure of a defined strength and modulus to achieve required porosity and structural integrity. A sintering system with reverse temperature dependence has been developed that is tuned to undergo transition within physiological conditions and develop mechanical properties *in situ*.

5 Injectability and Scaffold Structure

5.1 Introduction

Alternative approaches to minimise the side effects of open craniofacial surgery have been demanded by surgeons [314]. Injectable porous biodegradable microspheres and particulates have been developed as low density cell carriers filling a gap with voids [315]. These materials have potential application in low density bone that resembles open-cell foam [316]. The reduced invasiveness of injectable procedures, allows the potential introduction of large volumes reducing the healing effort required to cope with surgical damage to soft tissue [317].

Biomaterial success depends on the outcome of a complex process requiring cell invasion and neovascularisation [115]. Bone induction does not occur on flat ceramic surfaces, instead, between particles, on profiled concavities and rough surfaces with microporosities for calcium nucleation [55, 102]. Porous synthetic organic surfaces in body fluids can precipitate a bone like carbonated hydroxyapatite surface layer in non-bone environments [10, 27, 109].

5.1.1 Injectable Scaffold Requirements

The ideal injectable material for use in bone repair must be non-migratory, non antigenic, encourage integration, be volume stabilizing and prevent adjacent tissue encroachment [118, 318]. Loose plasma sterilized PLGA 50:50 microspheres, injected from a 1ml syringe barrel into rabbit bone defect were demonstrated to enhance healing without inflammation and fully degraded after 12 weeks [129]. However, bone-grafts must also provide mechanical stabilisation [9]. Several injectable drug delivery systems form scaffolds comprising of composite nano- and microparticles based on modified PLGA [319]. For these systems injectability was dependent on particle–matrix ratio and the injector system used. Calcium phosphate cements are used as injectable bone substitutes and wet setting involves the exothermic reaction of acidic and basic components that can last for hours and raise pH locally [320]. In a composite cement/ PLGA microparticle blend, reduction in the ratio of the continuous calcium phosphate matrix and size of the extrusion orifice increased the injection force and decreased the homogeneity of the material flow [321].

Minimum porosity results in less dimensional change upon compression [316]. In theory, powders containing particles with a wide range of sizes can approach 0% porosity as the finest grains are distributed in the interstices of larger packed particles. However, powder mixtures do not naturally pack to the closest configuration even if free movement was induced by vibration or shaking [322].

Differential gravitational settling of the mixture tends to segregate particles and some degree of aggregation/jamming occurs immediately upon formation of the powder compress generating internal friction that strongly impedes further compaction by 15–20% porosity [323]. Initial particle packing influences mechanical strength, density of the microstructure on sintering, shrinkage and pore properties of the final product.

Hard mono-diameter spheres packed like cannonballs into body-centred arrays theoretically have a porosity of 25%, significantly lower than the disordered packing minimum of 35-45% for vibrated collections of mono diameter spheres [323, 324]. Packing density is a function of the initial packing efficiency, particle size ratio and volume fraction variation of the system [136]. Calculation of ideal packing density assumes the size ratio of course to fine is infinitely large [322]. For particle size ratios greater than 10, the maximum ideal packing density of two component systems is more closely predicted by the Furnas theoretical model [325]. The model is not predictable for a particle size ratio lower than 10 [322]. Packing efficiency and density are lower when the ratio of coarse to fine particles decreases [324]. Conventionally heat sintered PLGA scaffolds typically have an interconnected porosity around 32% and newer solvent/non-solvent systems have a maximum interconnected porosity of 37% [166].

Patient specific fabrication of preformed polymers can be time consuming before and during surgery; requiring open cavities and potentially damaging blood vessels and surrounding soft tissue, stimulating further inflammation to achieve a tight fit [319]. Cell seeding of preformed constructs can also be inefficient [326]. Injectability allows filling of defects with limited accessibility as exemplified by the techniques of vertebroplasty and kyphoplasty that are now preferred options to open surgery where large volumes can be introduced through small incisions [317, 327]. The composition, particle size distribution and shape are critical features of particulate solids [134]. For injectable systems, the resistance to flow is dominated by the size and shape of free space between particles that are in contact with each other [322]. Fluid flow across stationary granules sees a pressure drop due to the resistance of solid particles. A decrease in the average particle size, increases net particle surface area; enhancing the contact aggregation effect and improve the "green strength" of relatively uncompressed powder.

5.1.2 Injectability

Injectable calcium phosphate cements acting like grout set *in situ* forming an implant conforming to the contours of the defect void surfaces [144]. Injectability is not a clearly defined term [328]. However, bad injectability involving phase separation of solid/liquid components, blocking and partial extrusion is clear. Injectability is assisted by having a short travel distance and small particles relative to the cannula diameter. The force applied (max ~200 N by hand)

measures the ease of injection but in surgery cements are applied using injection guns. Bohner defined injectability in a constant geometry as the capacity to stay homogeneous during injection independent of the force required [328].

In-use reaction times need to be slow enough for surgeons to implant and fast enough not to delay the operation. Cement injectability decreases with time and must be completed in 6-8 minutes in the viscosity range 100-1000 Pa s before it increases to become stringy, forming a damaging cement tail can be deposited in soft tissue [328]. The viscosity of the hardening phase must increase quickly as short setting times from 11-17 minutes assist geometrical integrity and fast postoperative recovery of function [326, 329, 330]. Poly(ethylene glycol fumarate) hydrogels can be formed in 10 minutes at 37 °C alone or with PLGA microparticles/ microspheres [225].

Phase separation occurs when the pressure to filter liquid through the agglomerated particles is lower than the pressure to inject the paste i.e. filter pressing occurs and liquid is pushed out of the cannula [328]. The plastic limit is the minimum amount of liquid required to form a paste. Below the plastic limit the powder is dry and viscosity high. If the extrusion force is high and the flow rate too fast shear thickening (dilatancy) occurs and a powder cake is formed. Having a multimodal particle size decreases the amount of liquid required to form a paste, but also reduced the final porosity. Decreasing the particle size in a fixed geometry system reduces the extrusion force required [288].

High water content in calcium phosphate cement lowers viscosity, the extrusion force required and particle interaction. The ability of the final cement structure to harden is reduced and it is more porous with lower mechanical strength [289]. An upper plastic limit was not described by Bohner and Baroud; however, this might define it [328]. In addition transplant of autogenous cancellous grafts were determined to be most effective in low aspiration volumes [318].

5.2 Aims

The aim of the work in this chapter was to develop an injectable particulate scaffold that remains homogenous post injection. The injection force was measured to determine ease of injectability. In order to assess the morphology of the injected scaffold post hardening at physiological conditions, micro-computed tomography measurements were conducted to determine porosity and pore size. Scaffolds need flexibly to fill a fracture gap without settling, retaining the moulded defect shape then solidifying to a macroporous structure. The setting time was rheologically monitored to measure the injectability period before hardening began.

5.3 METHODOLOGY

5.3.1 Evaluation of Liquid Mixing Ratio for Injection

This experiment was devised to determine the appropriate ratio of liquid required to produce a self-levelling injectable paste. A 3:1 blend of 95% PLGA 85:15 with PEG 400 temperature sensitive particles to 85:15 PLGA sphere was prepared with HBSS buffer as the diluents added to the pre-weighed material in a Plastipak™ 1 mL syringe. The syringe nozzle was removed to leave a 4 mm diameter barrel. Particles 200-300 µm in diameter were ejected form the syringe. The ratio of solid to liquid evaluated was varied from 4:1 to 1:2. Mixing was achieved using the plunger to pull liquid through the loaded particulate. A second plunger was used to achieve compaction (Section 2.4.3) before the material was extruded from the syringe onto a six-well plate and incubated at 37 °C and 5% carbon dioxide for 30 minutes. Samples were also ejected into a 0.75 ml Eppendorf ™ tube to evaluate injectability.

5.3.2 Ease of Injectability

Injection force measurements were conducted at ambient conditions with a syringe holder on the Texture Analyser TA HD Plus supplied from Stable Micro Systems. Injection force was determined at an extrusion rate of 2 $mm.s^{-1}$ through a 1 mL BD Plastipak™ syringe. This extrusion rate was previously used by Bohner for investigations on injectable calcium phosphate cements [328]. Scaffold compression strength (wet and dry) was determined at 0.01 mm/sec following sintering in a 4 mm diameter syringe barrel at 37 °C for 30 minutes.

5.3.3 Evaluation of Structure with Micro CT

Micro CT assessment was conducted with a Scanco 40 instrument on dry two component scaffolds with a 4:3 ratio of adhesive particle to porous cell carrier after wet sintering in moulds for dimensional consistency. Scaffolds were constructed from sieved components with a 100 μm size width range. Scaffolds were scanned at 55 kV and a current of 55 mA.

5.3.4 Rheological Monitoring of Liquid Sintering

The injectable material being measured by oscillation rheology was transformed from a suspension to a solid structure. During transition, particles conformed to the smooth measuring surface of the parallel plate geometry resulting in slippage. A serrated geometry and Peltier base was used to grip the sample allowing structural detail to be resolved using an oscillation time sweep protocol at 0.01% strain, 37 °C and 1 Hz.

5.4 Results and Discussion

5.4.1 Evaluation of Liquid Mixing Ratio for Injection

Scaffolds were formed in a 1 mL syringe barrel then extruded onto the surface of a 6 well plate. Cylindrical scaffolds conforming to the syringe barrel dimensions were formed at solid: liquid ratio above 2:1 as can be seen in Figure 5-1. These samples showed no tendency to self-level after incubation at 37 °C without external application of force. The 1:1 scaffold showed some levelling under gravitational force whilst retaining a high degree of cohesion. At higher fluid content, beginning with the solid: liquid ratio of 1:1.5; there was extensive self-levelling and spreading of the extrudate, with no retention of the original mould shape. The unconstrained constructs were demonstrated to be cohesive at ≥ 1:1 solid to liquid blend under the influence of gravity and sintering at 37 °C. The 1:1 ratio blend showed time dependent levelling as the cylindrical shape was distorted. Scaffolds formed from the 1:1 ratio and higher solids content were strong, easily handled structures. The higher the levels of liquid present the less compact the structure formed and the weaker the scaffold in line with observations of calcium phosphate cement and its plastic limit [328, 331]. Capillary action exerts strong forces on particulate solids, equivalent to external pressure in liquid phase sintering. Problems associated with liquid sintering include shape distortion with excess liquid [162].

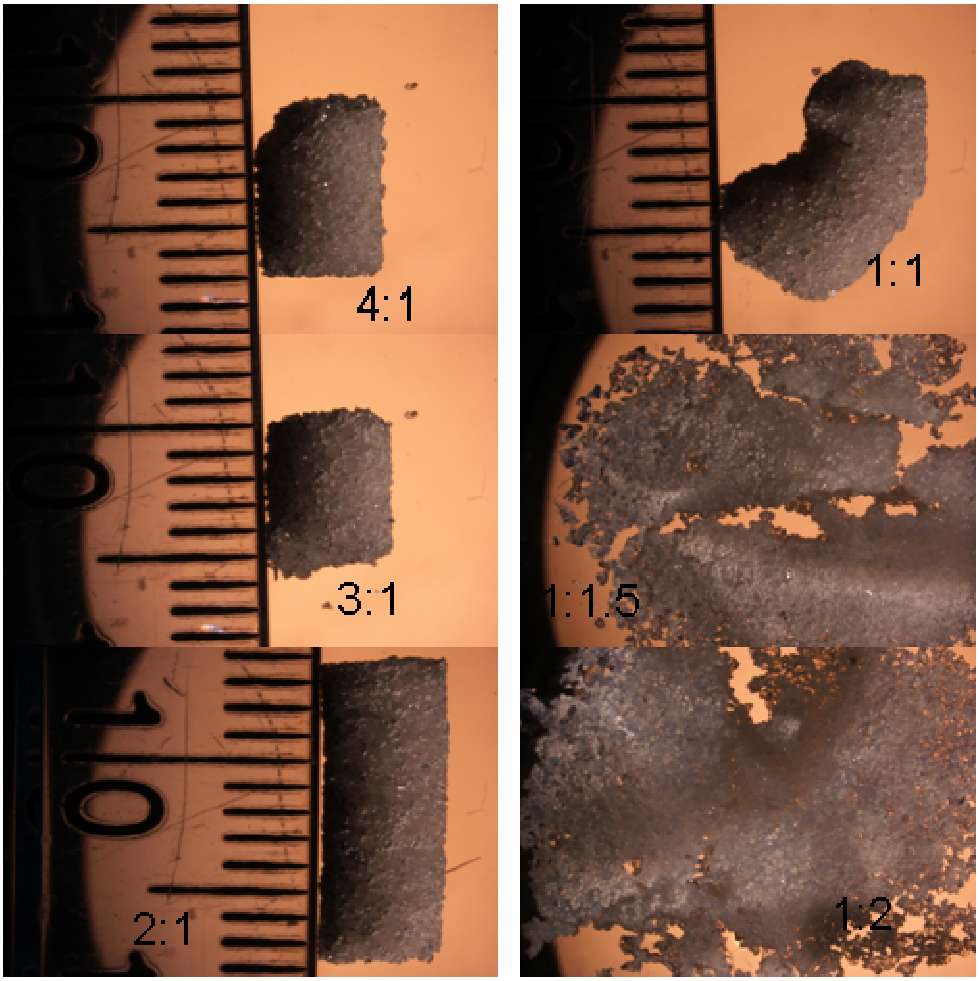

Figure 5-1 Comparison of wet scaffolds ejected from a 1ml syringe consisting of 95% PLGA 85:15 with PEG 400 adhesive particles and PLGA 85:15 spheres blended by weight at a 3:1 ratio. The solid to liquid wt: wt ratios of 4:1, 3:1, and 2:1 retained the cylindrical shape of the syringe barrel. Solid: liquid blends at higher liquid content leveled without retaining the shape of the syringe barrel. Compositions (n = 3) were sintered in a 37 °C humidified incubator at 5% carbon dioxide.

The 2:1 ratio had compressive strength of 88 ± 10 MPa compared to 5 ± 1.4 MPa for the 1:1.5 scaffolds (dry, ambient). Synerhesis was present in the 1:1 blend and higher liquid content and would not be clinically acceptable. Synerhesis does not provide the ideal situation for patients as wound sites need to be clean and free of excess liquid that may cause secondary issues of infection, inflammation and sepsis [40].

5.4.2 Injectability

Scaffold paste of various solid: liquid blends were injected into a 0.75 mL Epppendorf tube to simulate closed cavity defect filling Figure 5- 2. The results show that the 2:1 solid to liquid blend extruded into the closed cavity, conformed to the shape of the tube (defect) and retained it. The 1:1 blend failed to reach the end of the tube after three attempts. The 1:1 blend was observed to show a degree of compressibility and resistance, encountered pushing the scaffold backwards into the syringe after ejection. The 1:1.5 blends failed to fill the end of the tube, becoming fractured and showed some filtering of fluid. Some particulate material was lost from the high liquid content paste (1:1.5 blends) due to pooling of the excess liquid volume caused by synerhesis during ejection. These blends show that higher solids ratio may provide better controlled fill of a closed defect giving more intimate contact and precise fill. It may also be necessary to avoid tail formation encountered with cements in procedures such as vertebroplasty that cause soft tissue damage [144].

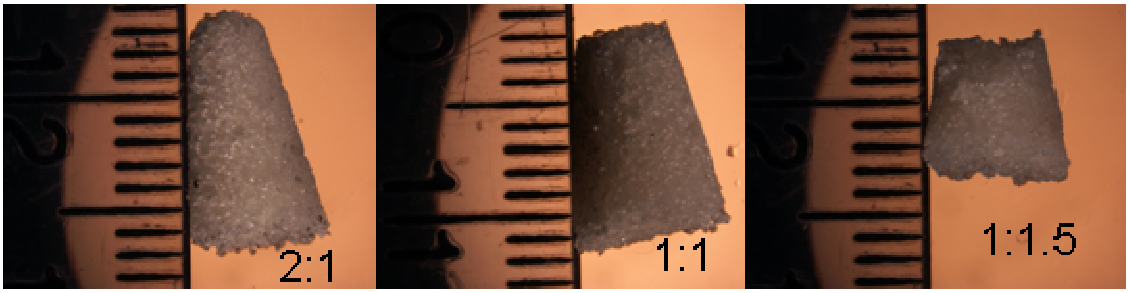

Figure 5-2 Comparison of scaffolds ejected from a 1 ml syringe barrel into a 0.75 mL Eppendorf tube to simulate filling of a small defect cavity (n = 3). This shows the degree of control possible with blends of solid: liquid ratios of 2:1, 1:1 and 1:1.5 being injected by hand into a tube. Scaffolds consisted of 95% PLGA 85:15 with PEG 400 adhesive particles and PLGA 85:15 spheres blended by dry weight at a 3:1 ratio.

5.4.3 Ease of Injection

The Plastipak 1 mL syringe used was tested to failure and the maximum injection force tolerated was 92.98 ± 2 N to distort the plunger piston. Figure 5-3 shows the force profile recorded to inject the dry material. It shows an initial peak followed by a plateau over the travel distance to extrude the syringe contents. The initial peak in force was in part due to the force needed to overcome the friction of the plunger in the barrel. The plot (Figure 5-3) shows the repeatability of the test procedure at a constant loading of powder at 0.64 ± 0.015 g/cm^3.

Figure 5-4 compares the initial and steady force needed to extrude varying volumes of dry particulate loads at a constant density of 0.64 ± 0.015 g/cm^3 loading from the 4 mm opening at 2 mm/sec. There was a very significant ($p < 0.001$) increase in the injection force on the initial volume loading of 0.1 cc compacted particulate in comparison to the empty syringe barrel. Figure 5-4 shows the initial injection force to be similar for loadings between 0.2-0.8 cc requiring 2.6 ± 0.11 N of force to initiate extrusion. Doubling the dry particulate load to 0.2 cc in the barrel very significantly ($p < 0.001$) increased the force to overcome inertia and friction in the syringe barrel. There was no further significant increase in force to initially extrude higher loadings from the syringe barrel from neither 0.2-0.4 cc nor 0.4 cc- 0.8 cc.

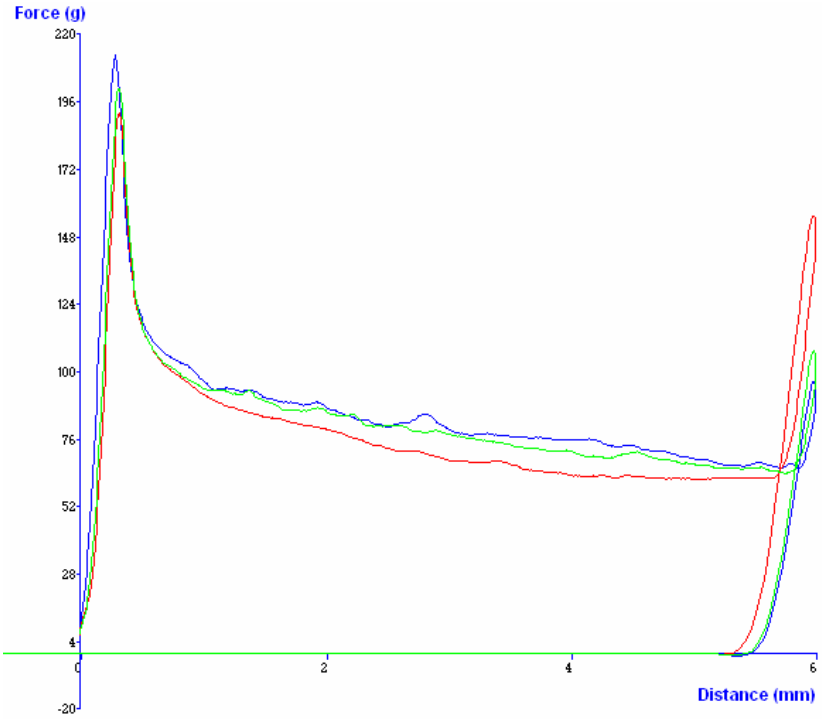

Figure 5-3 Repeat extrusion profiles of injection force used to deliver 0.1 cc loading volume of the dry scaffold from a 4 mm syringe opening (n = 3). The chart shows a profile of the initial force required to move the plunger in comparison to the force required to keep the bulk moving at a constant rate. Injection force was determined at an extrusion rate of 2 $mm.s^{-1}$.

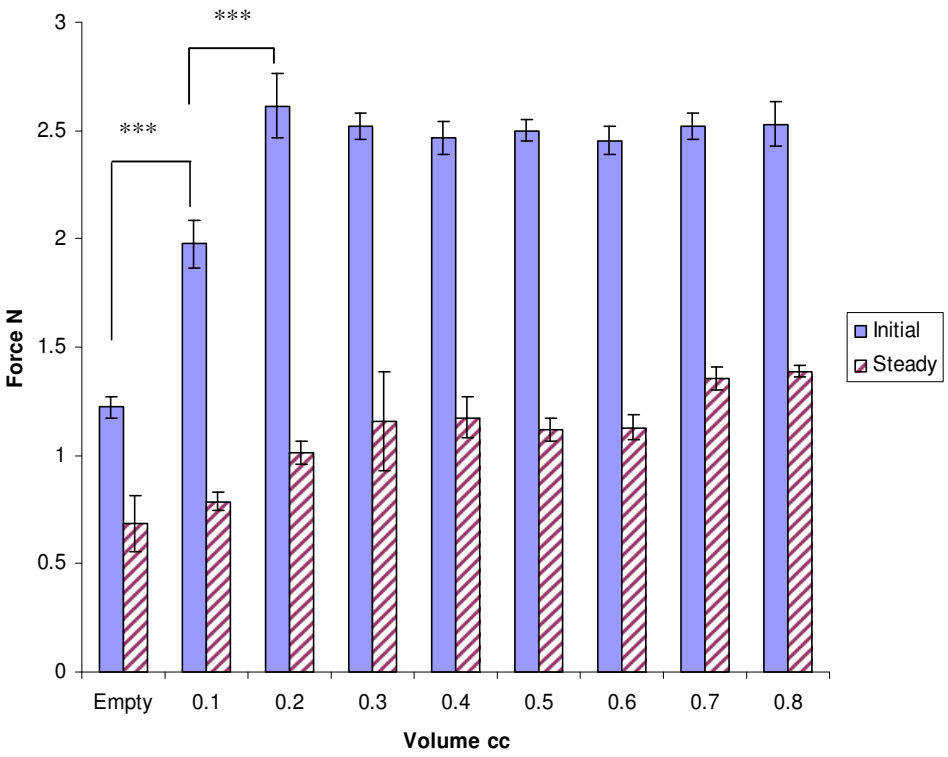

Figure 5-4 Comparison of initial and steady injection force required to move the plunger and deliver variable volumes of dry scaffold from a 4 mm syringe barrel (n = 3) at 0.64 g/ cm^3. Injection force was determined at an extrusion rate of 2 $mm.s^{-1}$. Statistical significance denoted as *** ($p < 0.001$).

When the packing density was raised to 0.74 g/cm^3 and above the force needed to eject the material from the barrel was increased 40 times across all loading volumes and shown in Figure 5-5. This deviation from homogeneous flow indicates that jamming and cake formation has occurred. This phenomenon was consistent for all volumes loaded $\geq$ 0.74 g/cm^3. In these circumstances extrusion is through fracture of the cake.

The plot in Figure 5-6 shows the force extrusion profile for the 60% wet sintered scaffold. The force required to overcome the initial inertia 4.6 ± 0.5 N was not exceeded by the force required to extrude the material at 2.7 ± 0.6 N. The jagged profile of the injection force required to extrude the wet formula was similar to the dry formula, but required less force. The profile variability may have been due to filtration and compaction of the material as force was transmitted through the bulk by the plunger.

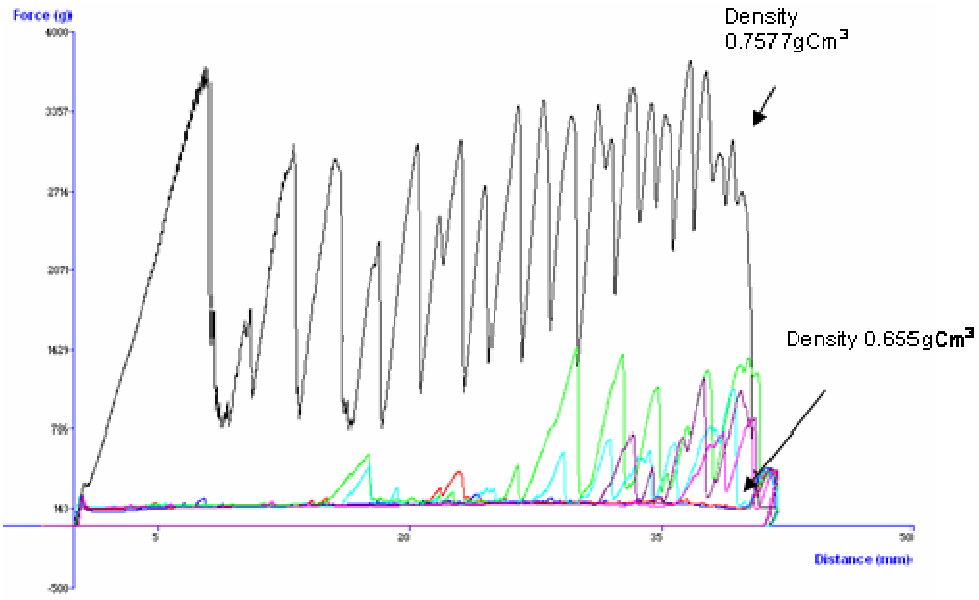

Figure 5-5 Injection force required to eject a dry scaffold blend, shows the effect of increased loading density at 0.65 and 0.74 g/cm^3 to result in a 40x increase in the force required to eject the sample (n = 4). Injection force was determined at an extrusion rate of 2 mm.s^{-1}.

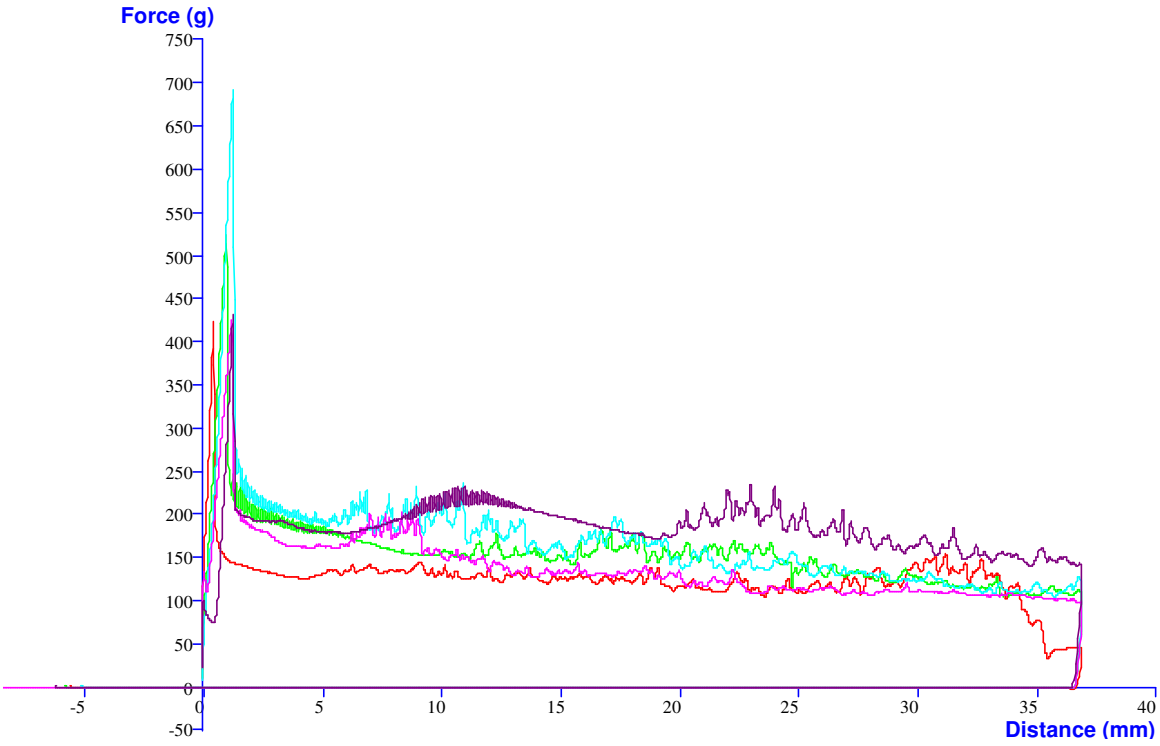

Figure 5-6 Extrusion force profile for a 60% wet scaffold composite (n = 5). Injection force was determined in a 1 mL syringe at an extrusion rate of 2 $mm.s^{-1}$.

5.4.4 Evaluation of Structure with Micro CT

Micro Ct imaging provides information on the internal structures formed by particulate scaffolds. Figure 5-7 shows a cross-section of wet sintered scaffolds and the internal structure created by use of restricted 100 µm particle size band to produce scaffolds. Scaffolds were made with 4:3 ratios of adhesive particles to microspheres in cylindrical moulds 9x5 mm (height x diameter). The decrease in the number of particles involved with increased particle size was most apparent when comparing >500 µm scaffold with other compositions. The apparent size of pores was also increased with particle size.

Figure 5-8 compares the porosity distribution across the particle size bands and shows that there was a plateau at 45% porosity for the > 100 to > 300 µm diameter size bands. This was very significantly higher ($p < 0.001$) than the < 100 µm particle size. Porosity was increased for the > 400 and > 500 µm particulate size band scaffolds with a significant ($p < 0.01$) difference between them. The difference between the >200 and >400 µm was very significant ($p < 0.01$). The difference between < 100 and > 100 µm particle sizes were extremely significant ($p < 0.001$) and attributable to a higher ratio of particle sizes present in the <100 µm blend. Within this band, particles < 10 µm would exceed the size ratio of 10:1 and pack more efficiently [322]. The measured porosity for the < 100 µm scaffold was < 35% indicating very efficient packing of the particles.

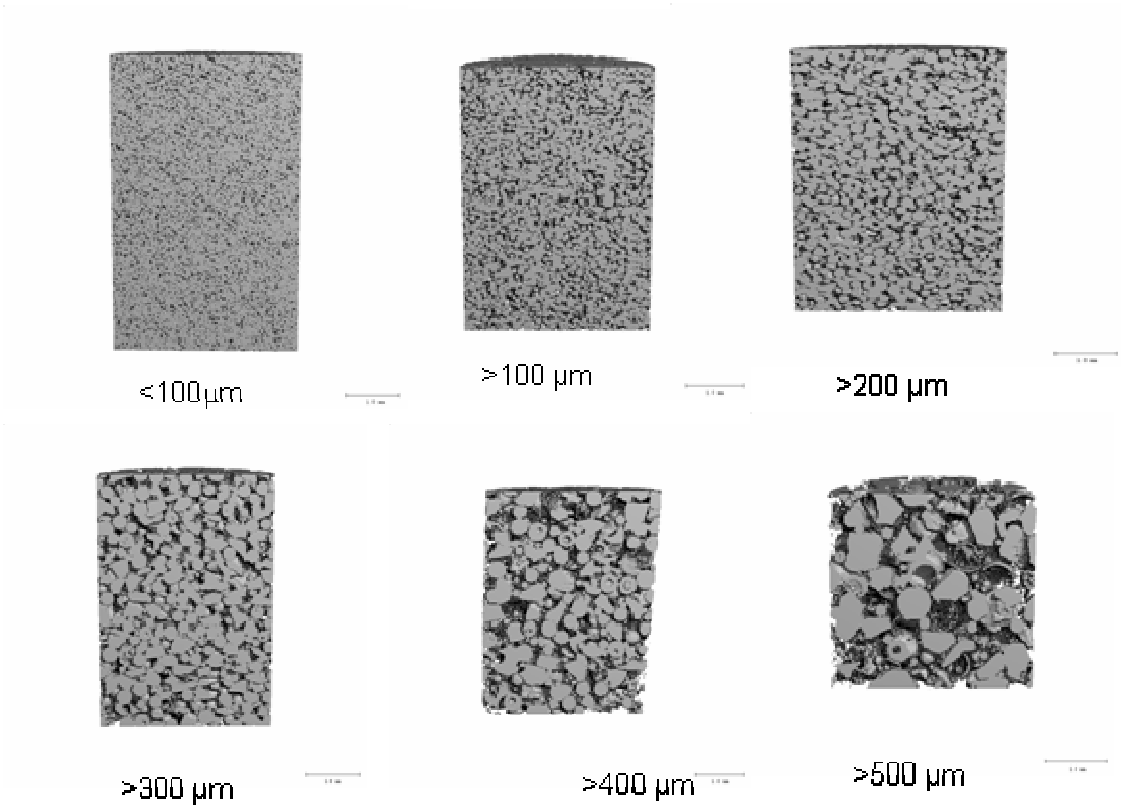

Figure 5-7 Micro Ct 40 µm resolution X-ray reconstructed images of 9x5 mm molded and wet sintered scaffolds with, 4:3 ratio of adhesive particles to spheres. Scaffolds were scanned at 55 kV.

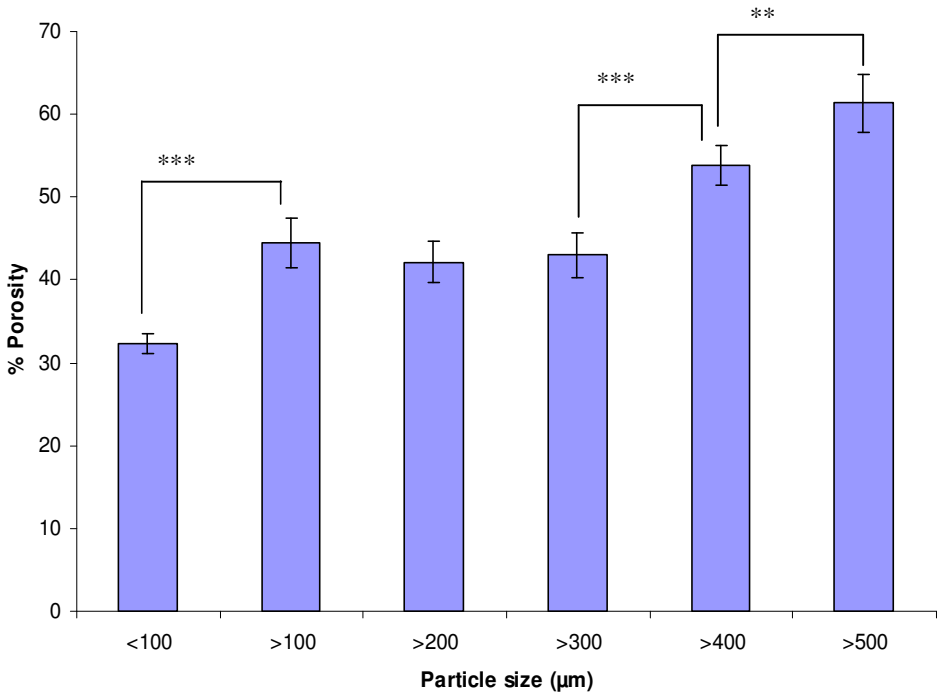

Figure 5-8 Porosity profile for the 9x5 mm diameter scaffolds with 100 µm restricted particle size distribution created from micro Ct evaluation of wet sintered two component scaffold with 4:3 ratio of adhesive type II to type I particles scanned at 55kV. Statistical significance denoted as ** ($p < 0.01$) and *** ($p < 0.001$).

The successive particle size rages have lower size ratios in the order 1:2 for the > 100 µm band, 1:1.5 for > 200 µm band, 1:1.3 for > 300 µm band, 1:1.25 for > 400 µm and 1:1.43 for the >500 µm band size as a 712 µm upper limit was used. The mid-range porosity did not significantly change however the size of the pores did as can be seen from the images in Figure 5-7. The graph in Figure 5-9 shows the scaffold pore size distribution to widen with the size of the particles. The two smallest particle size range at < 100 and >100 µm had very narrow pore size distribution with the smaller (< 100 µm) having no pores greater than 100 µm in diameter. For particles >100µm there were no pores greater than 150 µm in diameter.

Figure 5-10 shows more clearly the impact of restricted particle size change on the distribution of pore sizes present. As particle size was increased across the range of scaffolds the number of small pores diminished, becoming larger in size and more frequent distribution. The scaffold with > 400 µm particle size contained less than 25% of pores below 100 µm. The altered distribution of pore size may have significant impact on cell seeding and penetration into the scaffold. The consensus minimum average pore size required for bone growth is 100 µm [132, 242]. The percentage of pores required to achieve and exceed this minimum pore size has not been addressed. Figure 5-10 shows the percentage of pores greater than the critical 100 µm diameter generally agreed for *in vivo* cell growth and colonization of cells.

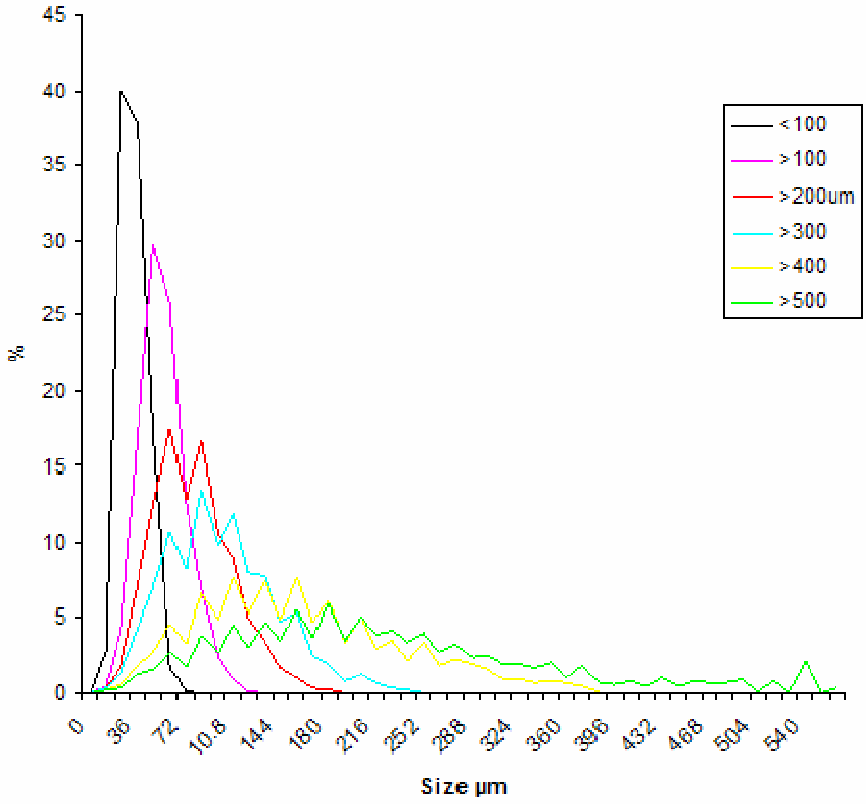

Figure 5-9 Effect of increased particle size on changes in scaffold pore size distribution with increased particle size. The graph was created from micro Ct evaluation of wet sintered two component scaffold with 4:3 ratio of adhesive type II to type I particles at 55 kV.

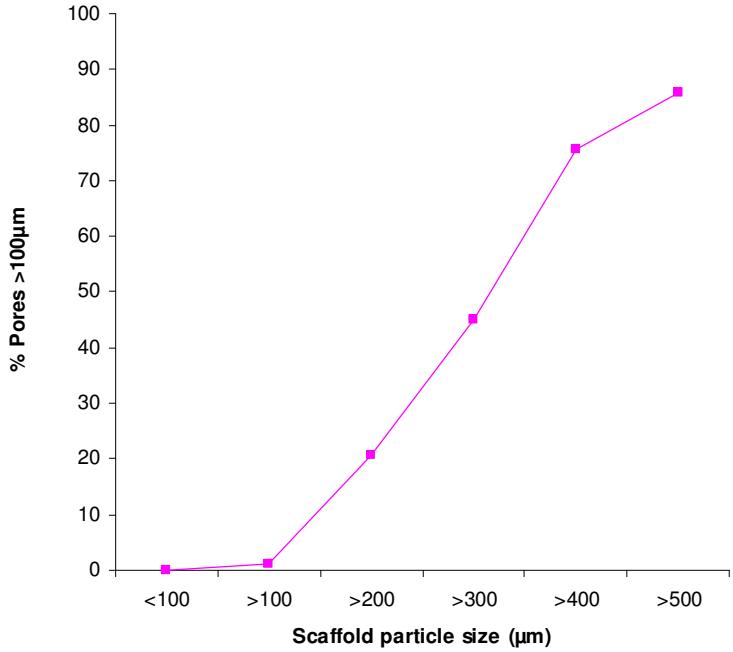

Figure 5-10 Percentage of pores greater than 100 µm in diameter with an increase in the average band width of particles used to form the scaffold. The graph was created from micro Ct evaluation of wet sintered two component scaffold with 4:3 ratio of adhesive type II to type I particles.

From Figure 5-10, scaffolds in the restricted particle size range > 300 µm have 45% of pores greater than 100 µm. What is not clear however is the amount of porosity required to achieve the goal of full colonization [245]. There are strategies to improve the supply of nutrients into the centre of the scaffold by drilling wide channels to boost the survivability of the construct [332]. These channels can lead to fibrous growth within the centre of constructs. In addition multi channelled pores can compromise the mechanical integrity of the scaffold. It may not be necessary to have all the pores within the scaffold to be greater than 100 µm diameter in order to achieve full colonisation and integration from initial implantation [132]. Pore interconnectivity was considered to be more important than pore diameter. The significance of this can only be determined by evaluation of cell growth and distribution in scaffolds.

5.4.5 Rheological Evaluation of Liquid-scaffold Interaction

Rheologically the wet sintering process was monitored on the rheometer by measuring the increase in structure build up as complex modulus (G*) at 37 °C. The oscillation time sweep profile in Figure 5-11 shows that significant structural build occurs sharply after 10-15 minutes exposure to fluid at body temperature. The initial increase in structure as measured by the complex modulus G* was followed by a gradual increase over time. Similar profiles of structure gain have been reported [204].

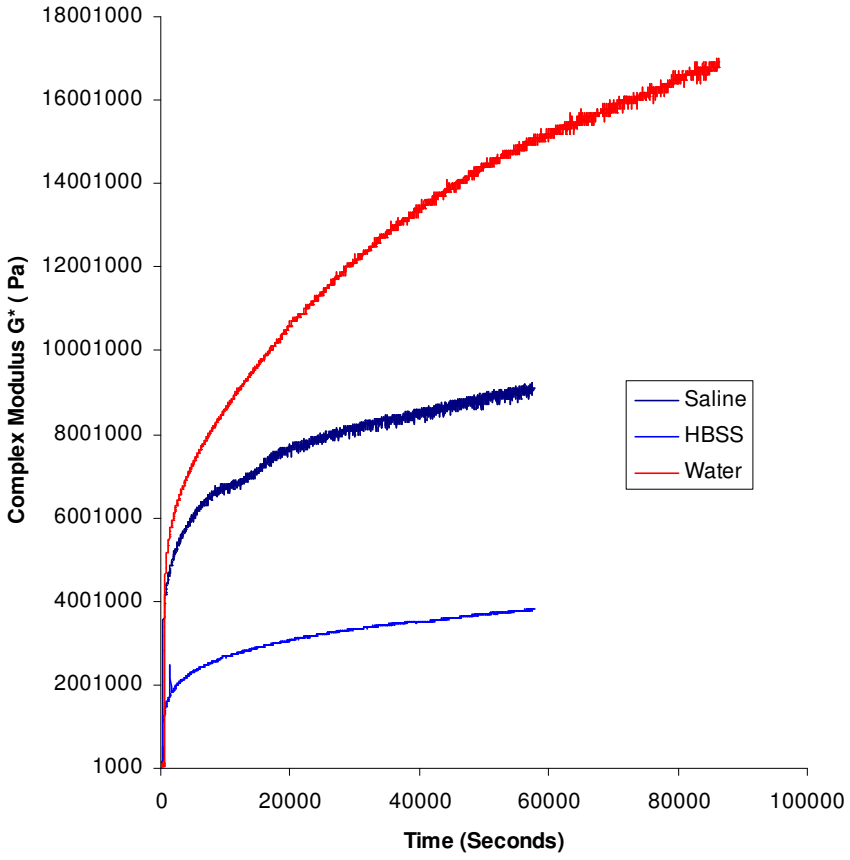

Figure 5-11 Representative oscillation time sweep profile of 95% PLGA with PEG 400 composite, conducted at 0.01% strain and 1.6 Hz. Samples were wet paste as would be prepared for injection to deliver cells and held at 37 °C. Oscillatory measurements were conducted in distilled water, Hanks balanced salts solution (HBSS) and 0.9% sodium chloride (saline) solution. The profile shows the change in complex modulus with time at a constant temperature.

5.5 Conclusion

The work here has demonstrated that the ratio of liquid to particulate component of the scaffold can potentially influence defect filling and self-levelling behaviour. The proposed injectable scaffold may be introduced as either a liquid suspension or semisolid paste that can self-level within a defect or be pushed into place, intimately interfacing with boundary walls without injury and restricting its distribution whilst allowing reshaping to fit.

The compaction and packing of the structure formed affects scaffold strength, retention and precision placement in void filling. Scaffold injectability ultimately depends upon the design of the injecting device and the relationship between exit orifice diameters with particle size. However, attention to solid packing density may help to assist in the reduction of force needed to extrude the material. This will be dependent on particle size ratio that crucially influences the porosity of the final scaffold structure. The lower the ratio of component particle sizes, the higher the likelihood that the void volume will approach 50%. Spherical particle shape and narrow particle size distribution are desirable when the end product is to be porous. The use of irregularly shaped particles increases the porosity of packed powders.

Porosity greater than 60% has been achieved by these scaffolds and more crucially high distributions of pores greater than 100 µm in diameter are present within the structures. It is not known what proportion of pores > 100 µm are crucial for full scaffold colonization; however, the larger the particle size the greater the distribution of pore diameters > 100 µm present in the scaffold that may positively impact on nutrient permeability, cell survival and cell penetration. Particle size may be used to match the required morphology of the defect site. The controlled sintering process was essential to preventing porosity loss following compaction and injection. These scaffolds may find use as cellular or acellular constructs. Polymer based scaffolds have been manipulated to perform increasingly complex and independent tasks such as cell and peptide delivery. The control of porosity with mild sintering may facilitate the development of facile, one shot solutions to achieve tissue regeneration and repair.

6 Cell Interaction with Injectable Scaffold

6.1 Introduction

The work in chapter 5 demonstrated the injectability of the scaffold material and its ability to solidify with controlled porosity. The field of regenerative medicine and cell therapy demands macroporous injectable systems that can deliver both growth factors and cells with maximal viability directly at the injury site by minimally invasive surgery. These systems should develop adequate mechanical integrity comparable to host tissue and have potential use in both elective and trauma surgery to promote engraftment [333].

In vitro cell proliferation for human transplantation is slow and expensive with risk of contamination from bacteria and virus. Cell expansion also risks depletion of proliferative capacity and selection of mutagenic cells [318]. Bone marrow aspirate contains progenitor cells with high proliferative capacity that enhances intramembranous bone formation [334, 335]. Aspiration is a relatively common, inexpensive procedure, with low morbidity, providing a cell suspension that can be processed intraoperatively, for immediate implantation [333]. An injectable scaffold able to utilise aspirated cells and deliver them into a defect by minimally invasive surgery could provide a cheap, quick procedure to prevent soft tissue collapse whilst assisting repair.

Most primary organ cells are anchorage dependent [99] and the injection of cells alone into a tissue site results mainly in death, with minor incorporation (3%) into the host without organ regeneration [336]. Cell carriers can dramatically improve survival and localisation *in vivo* acting as temporary architectural templates, for new tissue formation that provide a stable interface for host-cell integration [337]. Cell transplantation relies on attachment substrates having good performance and reproducibility hence the interest in poly(α-hydroxy ester). Cationic polyelectrolyte modification of polymer surfaces has been demonstrated to enhance cell adhesion, spreading and proliferation [338].

6.1.1 Biomimetic Activity

PLGA has been demonstrated to support and maintain the osteoblastic cell phenotype [148]. Organic substrates in human and simulated body fluids can precipitate an apatite-like surface layer through negatively charged carboxyl group induced heterogeneous nucleation [339]. The apatite layer formed is tightly attached to the polymer and correlated to the quantity of carboxyl groups. During cell delivery, physiologically compatible fluids are in contact with the scaffold components during and after surgery.

Carboxyl anions are responsible for strong electrostatic and repulsive forces among polymer chains that contribute to swelling [340]. Polymer swelling occurs gradually and is accelerated by low pH and reaction between carboxylic end groups with sodium cations. When constrained by the bone defect surface,

polymer swelling is restricted. The pressure generated creates a press fitting effect providing intimate contact and adhesion to the host tissue and is regarded as advantageous with respect to implant loosening and fracture stability by compression [341, 342].

6.1.2 Cell Carrier Size Limitations

In cell transplantation, access to nutrients and metabolite clearance is vital and dependent upon cell density and diffusivity distance [343]. Analyses of cell viability *in vitro* poorly translate *in vivo* [15], and scaffold support improves outcome if parameters have been optimised [185, 243, 336]. Few cells can tolerate diffusion distances in excess of 200 µm; hence, cartilage cells have been the most successful to date [318]. Typically on constructs, an outer 100-200 µm thick radius of live cells is formed around a central necrotic zone of [344]. Work by Holy *et al* [111] proposed the *in vitro* seeding level of $1x10^6$ osteoblast cells per cm^3 of scaffold as optimal, but Skuk *et al* [344] showed cell survival to diminish in primates when more than $0.3x10^6$ cells were transplanted. It is therefore crucial to select cells that contribute to tissue repair as in a graft of 5 mm radius; oxygen diffusion will support a limited number of transplanted cells [343]. In bone repair, initial cell colonization of scaffolds has been restricted to the superficial pore layers resulting in limited regenerated tissue depth [111, 345].

6.1.3 Poly(ethylenimine) Modified Cell Support

To enable use as cell carrier devices, scaffolds must support cell adhesion [346]. Adhesion to scaffolds is vital to control spatial distribution; cell survival and migration in the scaffold. Surface modification by plasma polymerized allyl amine has been demonstrated to enhance cell adhesion [255, 347, 348]. Chitosan as a cationic polyelectrolyte biopolymer supports cell adhesion and proliferation [349, 350]. The cationic polyelectrolyte poly(ethylenimine) (PEI) shows dose dependent cytotoxicity in freeform that was reduced by adsorption to solid (silica) nanoparticles and in complexes used to enhance transfection [351, 352]. PEI has been used to coat rigid porous supports for the ionic adsorption protein [353]. Fibronectin and vitronectin mediate osteoblast adhesion and have been demonstrated to adsorb to cationic surfaces [354, 355]. The adhesion, spreading and proliferation of fibroblasts and osteoblasts was enhanced on cationic surfaces in comparison to neutral and negatively charged surfaces[338, 356, 357]. In addition, the incorporation of PEI into polyester microspheres can increase porosity [358].

6.1.4 Growth Factor Delivery

Humans differ significantly from one another with respect to the cellularity of bone marrow and the prevalence of osteoblastic progenitor cells. Bone marrow cells from the ilium exhibiting osteoblastic phenotype decrease sharply with age after 20 years [359] with the number of alkaline phosphatase positive cells decreasing stronger in women than men [360]. In addition, the proliferation

potential of osteogenic progenitors decreased with age [361]. Low bone density, compromised repair potential and ageing conspire to reduce the rate at which fractures heal [64]. Stem cells derived from bone, muscle, cartilage, fat and vascular pericytes all require growth factor stimulation to direct differentiation into bone forming tissue [318, 362]. Delivery of osteogenic and angiogenic factors are key to the success of large diameter tissue engineered constructs [363]. Large doses are cost prohibitive and dangerous with tissue exposure being broader than necessary and in acute wounds BMP turnover is rapid, requiring protection [56, 76]. Microsphere based scaffolds act as growth factor depot delivery systems that can mimic natural signal events in a spatiotemporal manner, to regulate timing and the extent of tissue regeneration [257, 258]. Polymer immobilised sequential growth factor release is metered through the carrier degradation rate that dictates the concentration profile and has potential to dramatically improve effectiveness [333, 364]. Physiological levels of BMP-2 delivery were determined to have greater efficacy than pharmacological doses [365]. Sustained delivery of BMP-2 was demonstrated to enhance differentiation and bone formation [366]. Therefore, microspheres as an example of a solid delivery system can reduce administered dose with defined gradients and minimise unwanted collateral damage through low systemic exposure [318]. Reduced burst phase protein release from PLGA microspheres was achieved by incorporation of the growth factor onto a BSA carrier [258, 364]. There was no significant difference in the total BSA release from loose microspheres and 3D constructs; hence, the spatial release of growth factors from microspheres could be predicted. BSA has been shown to protect

growth factor integrity when used as an adjuvant during the loading process and slow PLGA polymer degradation[367].

The aims of the work in this chapter are to determine the habitability of the scaffold for cell attachment and proliferation in the presence of PEG; evaluate the interconnectivity of the particulate architecture through cell migration study; determine the compatibility of cells *in situ* with the hardening process; demonstrate sustained release of pharmacologically relevant dose of an active growth factor to control cell differentiation.

6.2 Methods

6.2.1 Viability and Proliferation Assay

Cells were cultured in supplemented Dulbecco's Modified Eagle's Medium (42430-025) as described in section 2.4. Briefly cells on tissue culture plates and scaffolds were washed in PBS prior to incubation with Alamar Blue solution (Serotec) diluted to 10% in HBSS, for a maximum period of 90 minutes as described in section 2.4.1. Cell number was correlated to metabolic activity for each cell type. Plates were read on a MFX Microplate reader with Dynex Revelation 4.21 software (Dynex Technologies Ltd., UK) at excitation 530 nm and emission 590 nm.

6.2.2 Toluidine Blue Staining

A 1% filtered (0.45 µm) toluidine blue solution in 25% IMS was added to cells/scaffolds rinsed in PBS, for 5-10 minutes then washed in distilled water to remove the excess before visualization.

6.2.3 Calcium Deposition

Scaffold samples were prepared as detailed in section 2.4.5 and stained with alizarin red to detect calcium deposition.

6.2.4 Alkaline Phosphatase Detection

Alkaline phosphatase enzyme activity was used as a marker of osteoblastic differentiation and conducted as detailed in section 2.4.6.

6.2.5 Comparison of Cell Growth on Scaffold Materials

Microspheres and particles used to make the two component scaffold were evaluated in culture using mouse 3T3 cells. The components examined were 95% PLGA 85:15 with 5% PEG 400 particles, PLGA 85:15 spheres and PEI/PLGA 85:15 spheres (200 mg). The components were UV irradiated on a plate shaker for 2 hrs then soaked in antibiotic/ antimycotic (5x) solution overnight at 4 °C. Spheres were washed three times in distilled water then soaked in media for 45 minutes in the incubator. Cells were seeded at $4x10^5$ in standard supplemented media with ascorbic acid (50 µg/mL) and cultured for eight days.

6.2.6 Impact of Cell Surface Area on Metabolic Activity

To determine which growing condition would best approximate those on the scaffold, cell metabolic activity was determined on tissue culture plastic of different surface areas. Human dermal fibroblasts were seeded in duplicates into six and 24 well plates over 24 hours and compared by Alamar Blue reduction.

6.2.7 Carrier Fluid Impact on Primary Cells

Human dermal neonatal fibroblast passage 4 cells ($5x10^5$) were suspended in both HBSS and 0.9% sodium chloride solutions and seeded onto 6 well tissue culture plates to determine the impact of carrier fluid on cells seeded onto tissue culture plastic. In addition, cells suspended in 1 mL volumes of HBSS and sodium chloride ($5x10^5$) was seeded into six well plates containing 1 mL of media. All samples were placed in the incubator for thirty minutes before an additional volume of media (3 mL) was added to each well. After 24 hours incubation, metabolic activity was assessed. The control consisted of cells seeded in standard supplemented media.

6.2.8 Growth of Cells on Preformed Scaffolds

Sieved scaffold components were separated into 100 µm bands, UV irradiated for 2 hours; and combined in a 4:3 ratio of 95% PLGA 85:15 with PEG 400 adhesive particles to PLGA 85:15/PEI spheres, loaded into a mould and sintered for 2.5 hours in distilled water at 37 °C in the incubator. The cylindrical (9x5 mm) scaffolds, four replicates for each particle size were treated with 5 x antibiotics

solution overnight as previously described then rinsed 3x in PBS and placed in the incubator for 45minutes in universal tubes in standard media. Human dermal neonatal fibroblasts (TCS cell works, UK), passage 4, were seeded at $4x10^5$onto preformed scaffolds in universal tubes with supplemented media containing ascorbic acid (50 µg/mL). The scaffolds were cultured for a month with regular changes of media every 2-3 days on an orbital shaker (88 rpm).

6.2.9 *In Situ* Cell Seeding of Scaffold

Sieved scaffold components were separated into 100 µm bands, UV irradiated for 2 hours and combined in a 3:1 ratio of 95% PLGA 85:15 with PEG 400 adhesive particles to PLGA 85:15/PEI spheres. The scaffold sizes examined were > 200 µm, > 300 µm, and > 400 µm. The scaffold loading procedure described in section 2.4.3. was used with human dermal neonatal fibroblasts ($5x10^5$) suspended in 200 µL of either HBSS or 0.9% sodium chloride solution to a 1:1 $^{wt}/_{wt}$ mix. The syringes were placed in a humidified incubator (37 °C, 5% carbon dioxide in air) for thirty minutes to sinter, then ejected into a non-tissue culture treated plastic 24 well plate with media. Alamar Blue assays were carried out at 24 and 72 hours post seeding.

6.2.10 In *Situ* Growth of Primary Human Osteoblasts on Scaffolds

Sieved and sterilized scaffold components were prepared as in section 6.2.9. The range of scaffolds examined were reduced to three with the following sizes > 200 µm, > 300 µm, and > 400 µm. The loading of scaffold components into syringes

and seeding were as previously detailed. Passage 4 human osteoblasts (TCS cell works, UK) were seeded at $5x10^5$ per scaffold.

The effects of supplementation without L-glutamine (Diff. media) and with various levels of ascorbic acid 2- phosphate (Diff Asc) were investigated. Cells were seeded at $2x10^4$ per well in duplicates and grown for eight days.

6.2.11 Effect of Supplementation on C2C12 Growth

C2C12 cells were maintained in a pre-confluent state in standard DMEM supplemented media and passage 19 cells seeded at $5x10^4$ per well in six well plates overnight. Cells were treated with varying levels of dexamethasone in media supplemented with and without L-glutamine for eight days.

6.2.12 Controlled Differentiation of C2C12 Cells

The effects of varying rhBMP-2 concentration 0-500 ng/mL were evaluated on P19 C2C12 cells seeded at $2x10^5$ per well (6 well plates) in media supplemented with and without L-glutamine for eight days. The stock solution of rhBMP-2 was 1 mg/mL with 0.01% BSA carrier.

6.2.13 Evaluation of Dye Encapsulation in Spheres

An evaluation of dye encapsulation in spheres was conducted by comparing aqueous and oil phase addition using a Eosin-y (Sigma E4382) 1% solution in

PVA 0.3% added as the primary emulsion and oil red-O (Sigma O-0652) 1% dissolved with the polymer in DCM as described in section 2.1.1.

6.2.14 Preparation of rhBMP-2 Loaded PLGA Spheres

Protein loaded spheres were manufactured using a method adapted from Morita *et al* [368-370]. In this study, 300 µL rhBMP-2 (1mg/mL) in 0.01% BSA was lyophilized with 1mL PEG 6000 (60 mg/mL). Microspheres were made as previously described in section 2.1.1 in a hardening bath of 800 mL 0.3% PVA. The lyophilized PEG 6000/rhBMP-2 blend was dispersed in DCM (500 µL) and transferred to the dissolved polymer PLGA 50:50 (Low IV 0.5-0.65 dL/g) 1 g in DCM 3 mL. The scintillation vial that contained the lyophilized protein was rinsed with a further 500 µL of DCM and added to the dissolved polymer. The polymer-protein mixture was vortex mixed for a minimum 60 seconds at maximum speed. To this was added 4 mL of PVA 0.3% solution and vortex mixed at 2000 rpm for 30 seconds. The primary emulsion was pipette transferred under the surface of the hardening bath and stirred for 8 hours to allow evaporation of DCM. The protocol was repeated to produce blank and FITC-BSA loaded spheres. The spheres were recovered by filtration, washed and vacuum dried for a minimum 48 hours. The spheres were sieved for 10 minutes on a Retsch 200 (Retsch., Germany), at amplitude 1.4 interval 40 seconds into 100 µm size bands protected from light and stored cold in vacuum sealed packs.

6.2.15 Evaluation of rhBMP-2 Loaded Spheres

A 3:1 scaffold blend was prepared using 95% PLGA85:15 with PEG 400 and the rhBMP-2 loaded PLGA 50:50 spheres from the > 300 µm fraction. The control contained blank > 300 µm PLGA 50:50 spheres. The scaffolds were prepared as previous by UV irradiation and dry loading into a 1 mL syringe barrel. Passage 18 C2C12 cells were seeded at $5x10^5$ per scaffold in HBSS (200 µL) and mixed using a plunger as previously described. The syringes were placed in a 37 °C incubator for 30 minutes then ejected into media contained within centrifuge tubes. There were three experimental conditions of scaffolds and cells (a) placed in media alone with PLGA 50:50 spheres without protein, (b) media supplemented with rhBMP-2 (100 ng/mL) up to day 18 and (c) scaffold containing rhBMP-2 loaded spheres in media. Scaffolds were examined at day 5, 18 and 28 time points for metabolic and alkaline phosphatase activity.

6.3 Results and Discussion

6.3.1 Comparison of 3T3 Cell Growth on Scaffold Materials

Scaffold components were shown by SEM (Figure 6-1) to have variation in surface morphology due to composition and the method of fabrication.

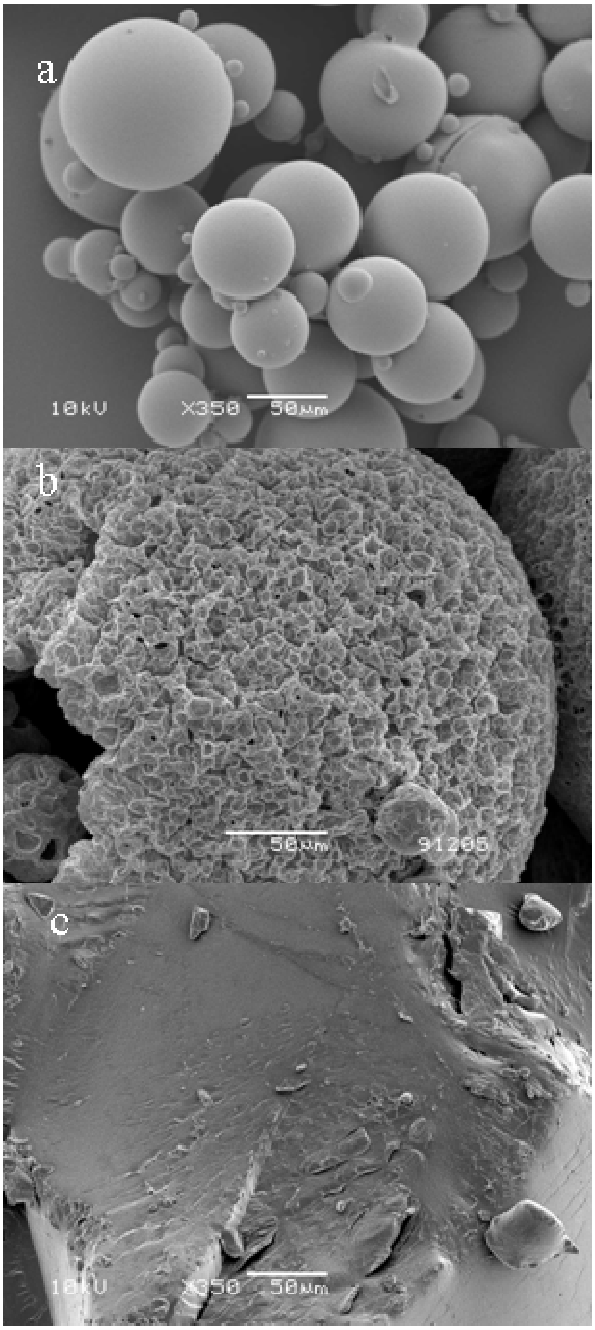

Figure 6-1 SEM images of 85:15 PLGA scaffold components showing spheres made by emulsion and solvent evaporation (a) by standard protocol, (b) with PEI in the polymer phase and (c) the adhesive component made by brittle fracture.

All particles supported cell attachment and proliferation (Figure 6-2). In media, standard PLGA spheres with smooth surfaces (Figure 6-2a,b) were submerged, with cells growing in sheaths. Spheres were not linked prior to seeding, but became encapsulated by cells and matrix. Similar observations have been reported for a variety of microspheres [257, 371]. PEI as a surfactant stabilized the air-polymer interface, forming foamed spheres that scattered light to appear white, with textured surfaces and tended to float [372]. Cells have spanned pores becoming anchored onto the spheres instead of forming encapsulating sheaths. Material was lost during media change making direct quantitative comparison of metabolic activity difficult. PEI has been used previously to produce porous particles [358].

Figures 6-2e,f show cell growth patterns on adhesive particles to align with surface contours and have a spindle like appearance. It was thought that PEG might reduce cell adhesion to the scaffold surface, but this was contrary to observations. Surface entrapment of PEG is known prevents polymer-protein interaction and hinder subsequent cell attachment [373, 374]. Low molecular weight PEG 600 and below were demonstrated to have poor surface entrapment and adsorption [305, 375]. Brittle fracture of the adhesive component produced a surface containing crevices and tracks. The subsequent alignment and growth pattern of cells (Figure 6-2e) show topography to influence cell morphology as reported in previous studies at nano and micron scale [112, 376, 377].

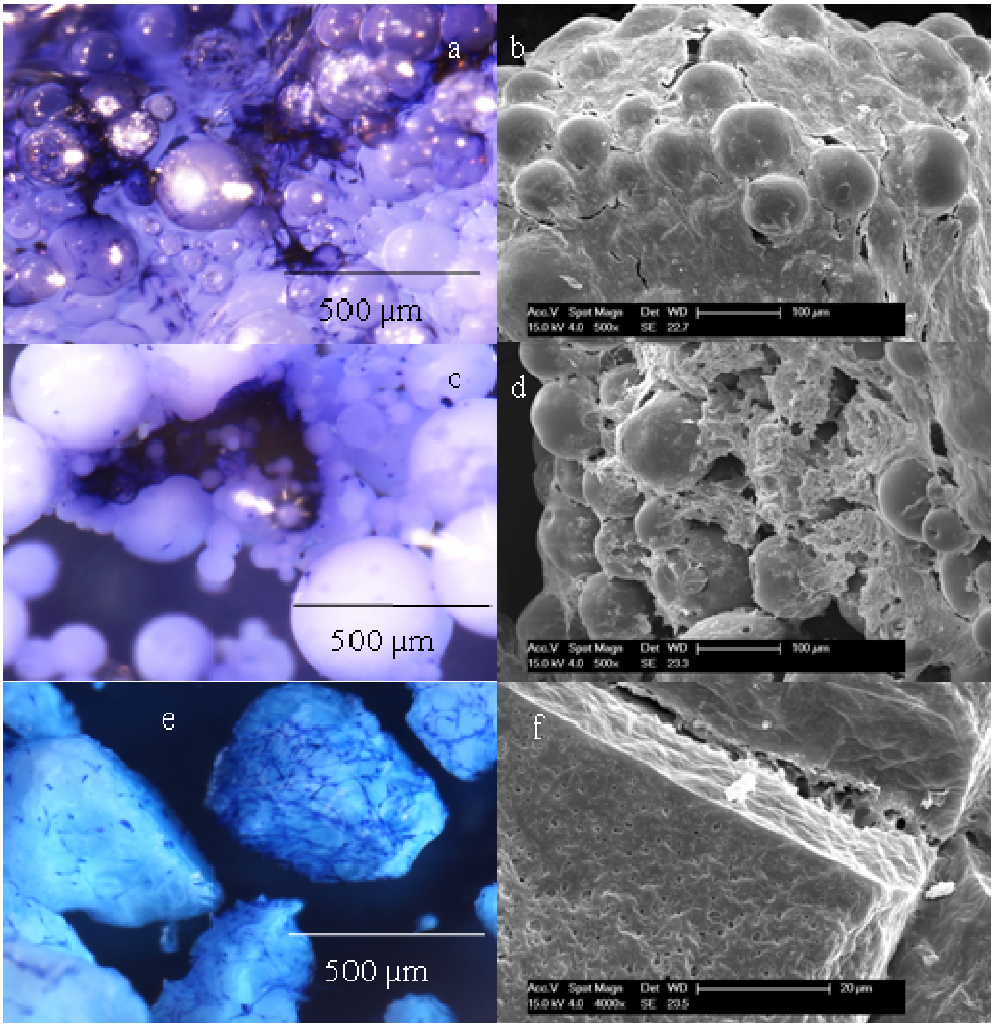

Figure 6-2 Light microscopy and SEM images of 3T3 cell growth on scaffold components. Cells grown on standard PLGA spheres (a, b), PEI in PLGA spheres (c,d) and 95% PLGA/PEG400 adhesive particles (e,f). Cells were seeded at $4x10^5$ in standard supplemented media with 50 µg/mL ascorbic acid and cultured for eight days. The cells were stained with toluidine blue for light microscopy.

The components examined were significantly different in surface chemistry and produced different patterns of growth, but indicate that cells can attach and spread across both components of the scaffold system. PEI has been utilized to enhance cell adhesion to spheres [356]. Toluidine Blue stains sulfated glycosaminoglycans and β pleated proteins [378]. Adhesive particles were also noted to undergo significant swelling in comparison to spheres.

6.3.2 Growth of Cells on Preformed Scaffolds

Human dermal fibroblast cells were seeded onto preformed scaffolds varying in particle size and grown for a month. In Figure 6-3a, b cell sheaths were observed on the surface of scaffolds with particles < 100 µm and >100 µm in size. Progressively less surface growth was present on scaffolds with increased particle size. Comparison of the initial sintered structure with the final cell colonized scaffolds show swelling to have occurred. The swelling appeared to increase with particle size; being most pronounced in the > 400 and > 500 µm scaffolds that have nearly doubled in size. Swelling was shown to be time dependent and progressive with degradation on diffusion [373, 375]. The loss of peripheral particles during growth and subsequent handling of scaffolds with >500 µm and to a lesser extent > 400 µm was probably due to the reduced number of sintering points with increased particle size. The >400 and >500 µm scaffolds therefore appear to be covered in cell growth due to the loss of peripheral particles.

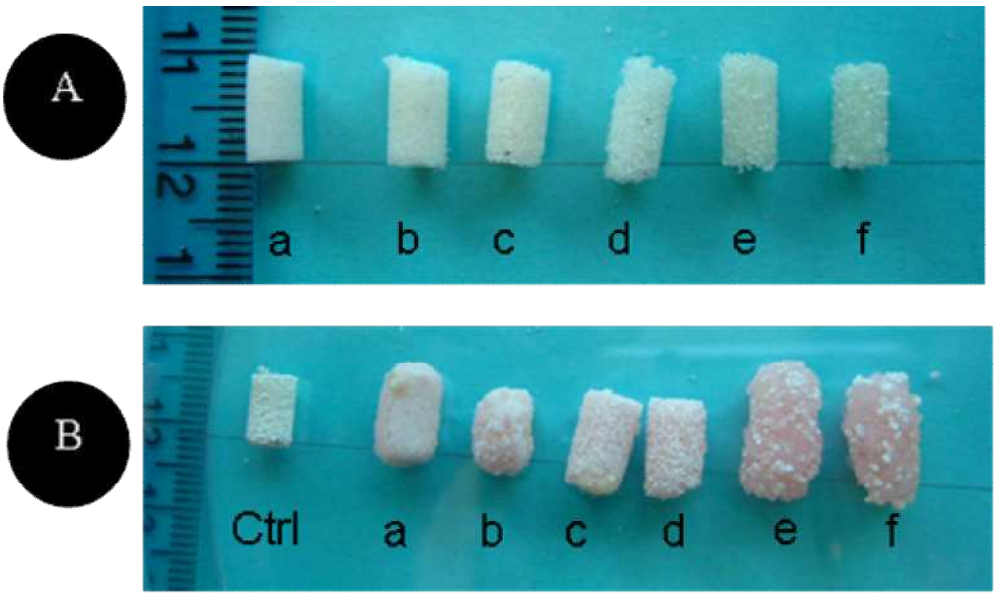

Figure 6-3 Preformed scaffolds (A) before and (B) after 3T3 growth for one month. The control (ctrl) shown was a >200 µm particle sized scaffold cell free as a comparison. The scaffolds seeded with $4x10^5$cells were (a) < 100 µm, (b) > 100 µm, (c) > 200 µm, (d) > 300 µm, (e) > 400 µm, and (f) > 500 µm. Sieved scaffold components were separated into 100µm bands, UV irradiated for 2 hours and combined in a 4:3 ratio of 95% PLGA 85:15 with PEG 400 adhesive particles to PLGA 85:15/PEI spheres. The blended particles were packed into a mould and heat sintered for 2.5 hours at 37 °C then soaked in a 5X antimicrobial solution overnight before use.

Metabolic activity was determined by Alamar Blue conversion assay in Figure 6-4 and shows a positive trend with increased particle size. There was a significant ($p < 0.05$) increase in detected activity with each step change in particle size with the comparison between <100 and > 300 µm being extremely significant ($p < 0.001$). The results from the > 500 µm scaffolds were not included as fragments with cells were lost during handling. Previous micro Ct measurements (Section 5.4.4) showed increased pore size and broadening distribution with incremental particle size blends of scaffold components. This may have facilitated an increase in the available surface area for cell growth and access to the Alamar Blue solution resulting in the observed trend. Similar trends for increased viability with pore size have been reported [379].

Cell distribution was shown through sulfated glycosaminoglycans and β-pleated protein staining with toluidine blue in Figure 6-5). This shows the surface aggregation of cells on the < 100 and >100 µm scaffolds. There was diminished surface cell aggregation with increased particle size in Figures 6-5 and 6-6 to > 200 and > 300 µm particle sized scaffolds. Cell growth on scaffolds with > 400 and > 500 µm particle size was different with concentrated clumps of cells growing around particles and through the large pores in Figure 6-6. The increased access to nutrients provided by the larger pores appeared to have facilitated growth on the inside of these scaffolds.

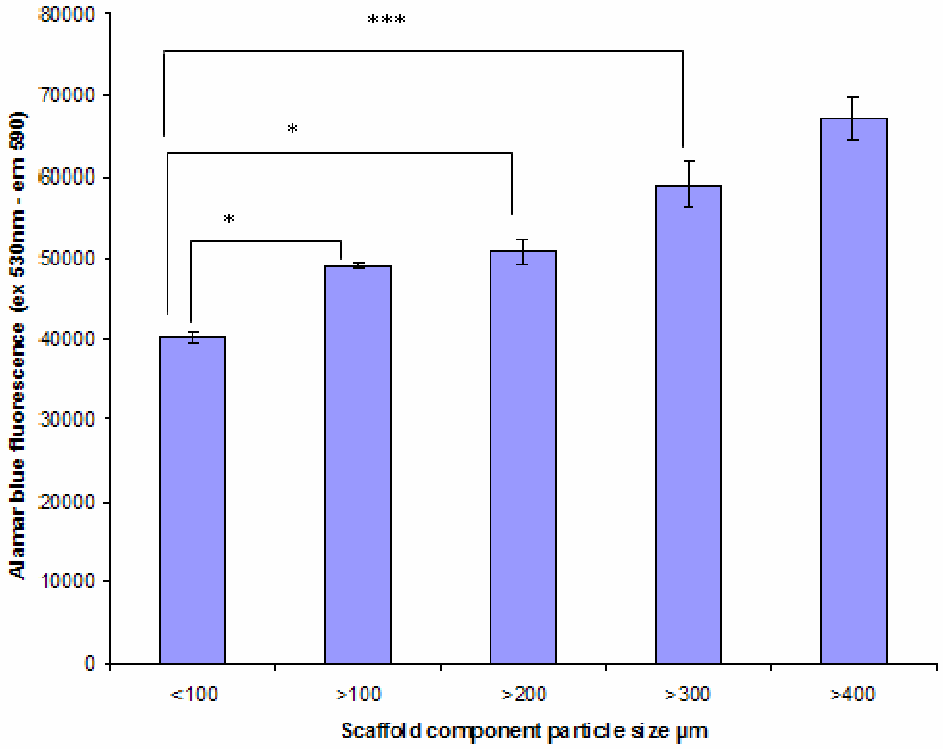

Figure 6-4 Alamar Blue reduction by 3T3 cells grown on preformed PLGA 85:15 scaffolds for one month. Scaffolds (n = 4) were seeded with cells on the outer surface. Statistical significance denoted as * ($p < 0.05$) and *** ($p < 0.001$).

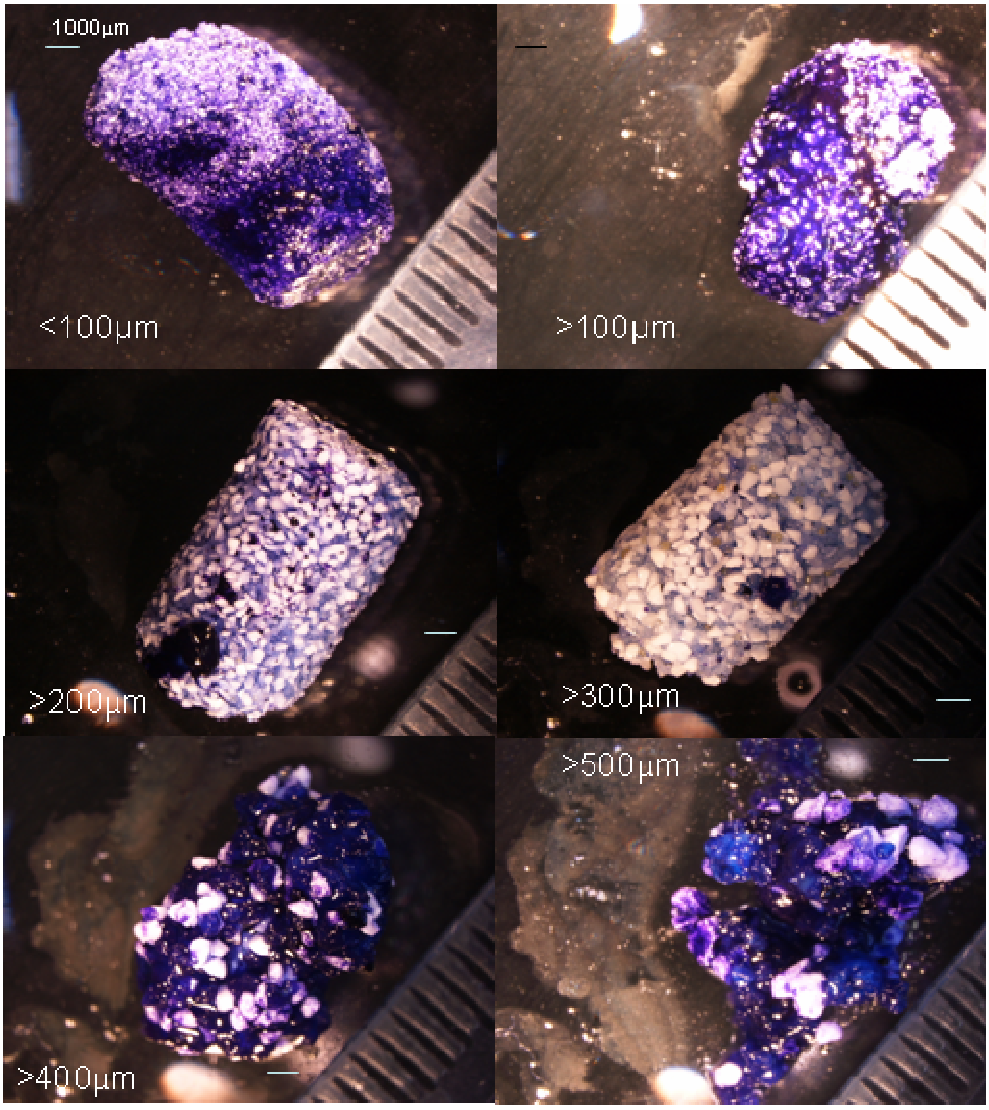

Figure 6-5 Representative photomicrographs showing toluidine blue stained 3T3 cell growth on PLGA 85:15 scaffolds. 3T3s were cultured for a month on the scaffolds and show the encapsulation of the outer surface of < 100 and > 100 µm component particle sized scaffolds in cells. The samples of component particle size > 400 and >500 µm were fragile and the peripheral scaffold components were lost showing the cell mass to have grown through the structure filling the pores.

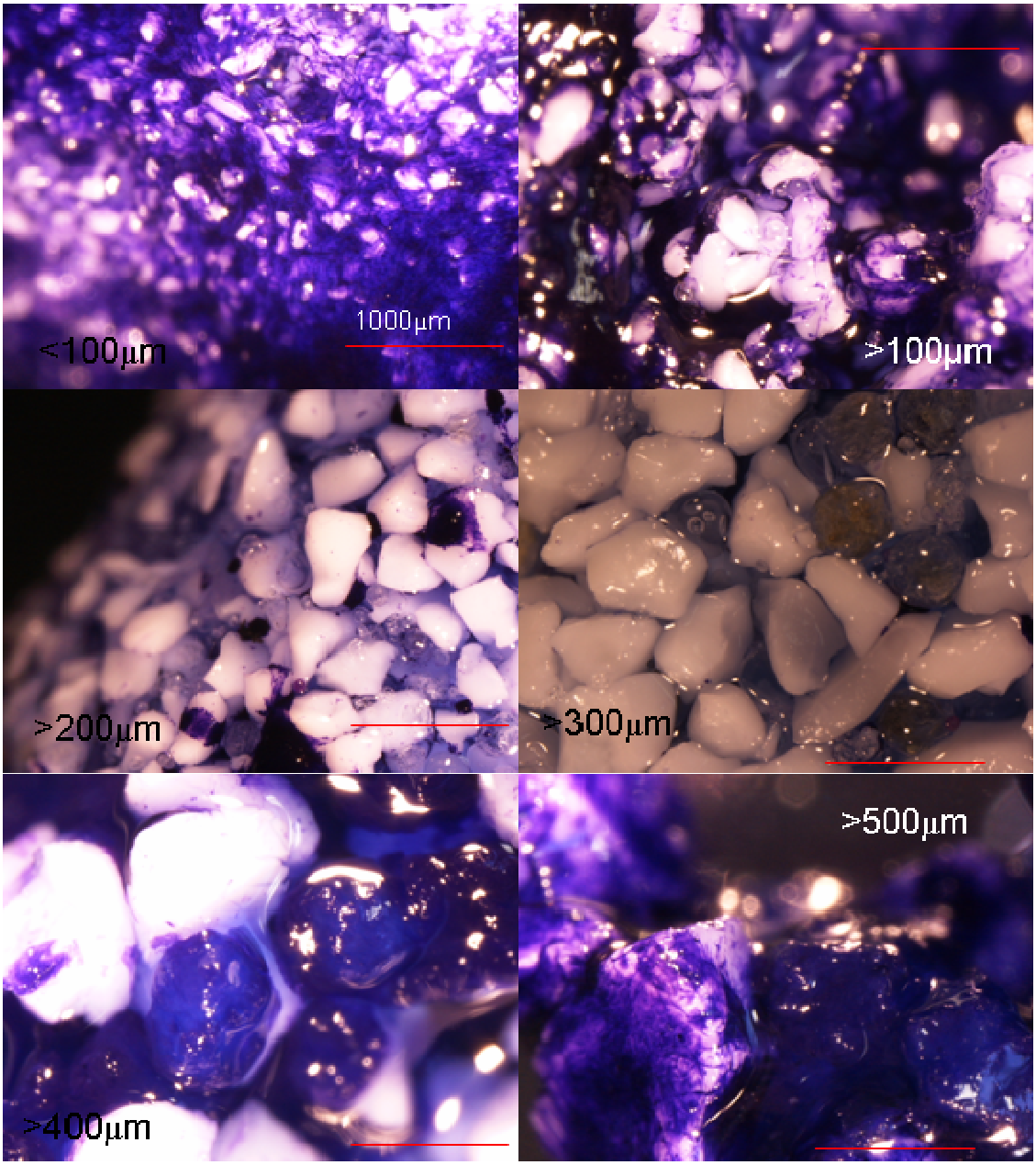

Figure 6-6 Representative photomicrograph at x5 magnification of toluidine blue staining, showing aggregated 3T3 cell growth after 1 month on scaffold surfaces. These images show the pattern of cell growth on restricted particle sized scaffold components.

The secondary staining with Sirius red to detect collagen in Figure 6-7 shows it to be pervasive across the scaffold structure, being produced on both particles present in the scaffold. The cells have spread across the scaffold components to colonize it. The pattern of cell growth across the adhesive component was similar to that seen earlier with 3T3 cells in Figure 6-2.

Micro Ct 3D reconstructed evaluation of these 3T3 colonized scaffolds with osmium tetroxide densification shows the pattern of cell ingrowth to vary with particle size (Figure 6-8). Scaffolds with particle < 100 µm in size and > 100 µm were similar in appearance and show high cell densities to occupy the periphery of the scaffold. Cells have penetrated into the centre of the structure by migration and indicate the interconnectivity of pores. There was reduced cell aggregation at the periphery of scaffolds with particles > 200 µm. Scaffolds with particles > 300 µm had cell growth throughout the structure. The size of cell aggregate clusters in the centre of the constructs (Figure 6-8) increased with particle size. Previous micro Ct results for scaffolds of varying pore size have reported tissue growth to be concentrated at the periphery [244]. Improved ingrowth was observed in pores > 100 µm [236]. Pores < 80 µm in diameter were shown to induce hypoxia and reduced bone growth [235, 244, 245]. Pore size and interconnectivity determine cellularity, cell migration and infiltration into the scaffold [132, 258, 380].

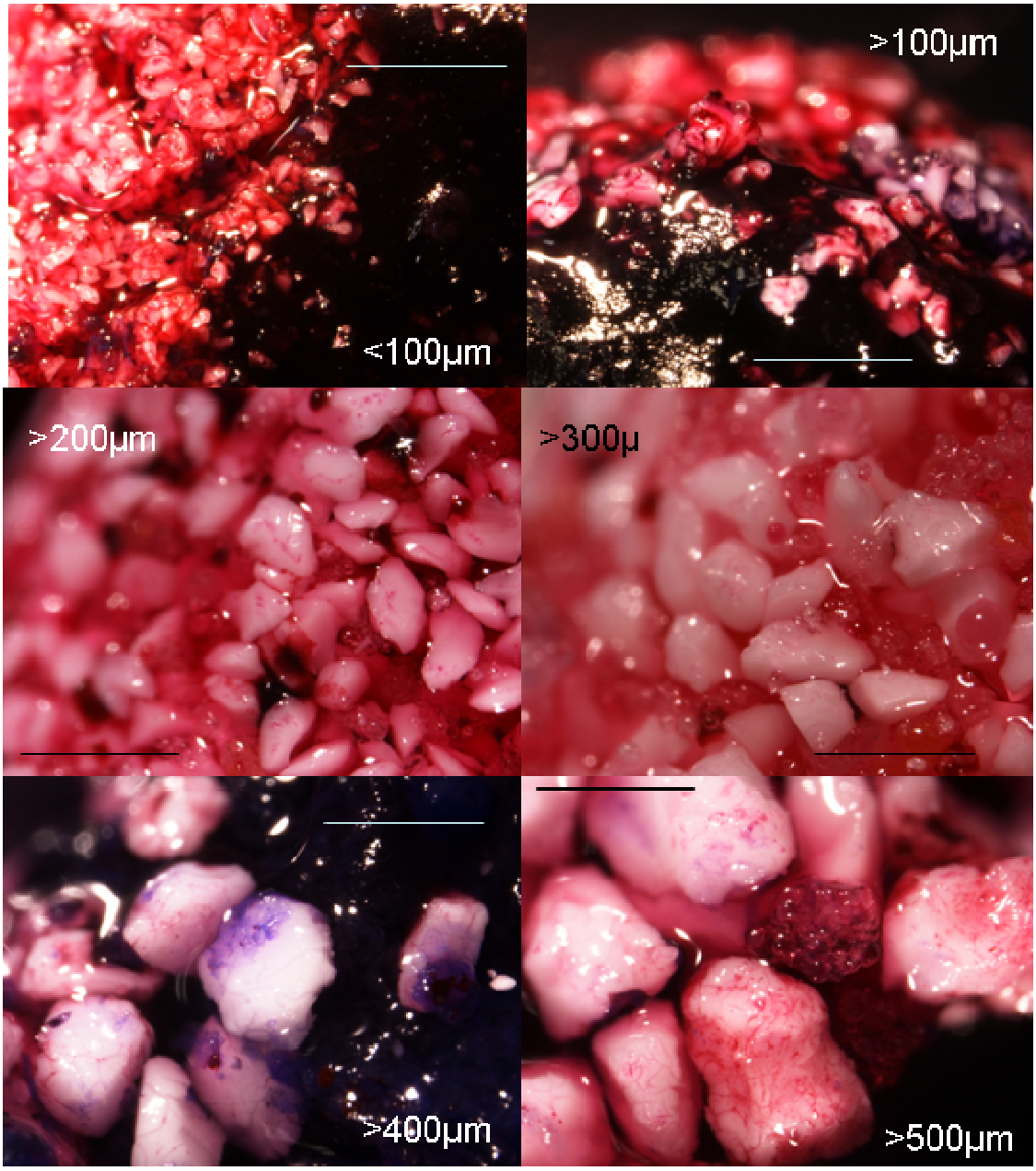

Figure 6-7 Representative photomicrograph at x5 magnification of scaffolds with sirius red stain for collagen on scaffolds with 3T3 cell growth after one month. Preformed scaffolds were seeded with cells on the surface and show wide coverage of all scaffolds with collagen based matrix. The scale bar represents 1 mm.

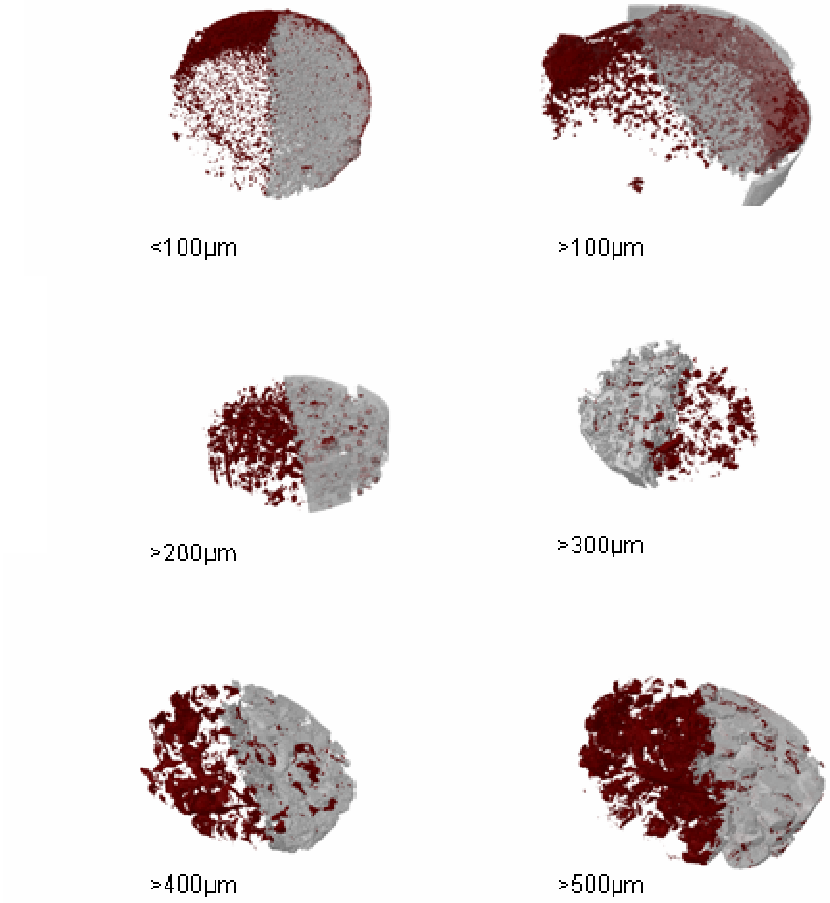

Figure 6-8 Representative micro Ct 3D reconstructed segments of 200 slices at a scan resolution of 14 µm with the PLGA 85:15 polymer in grey and osmium tetroxide stained 3T3 cells in red. These slices show the distribution pattern of cell growth to vary with particle size.

6.3.3 Comparison of Cell Seeding on Different Surface Areas

The effect of tissue culture plastic surface area on metabolic activity was assessed to determine the condition to best approximate the scaffold seeding condition. An Alamar Blue comparison of equivalent cell activity incubated for 12 hours post seeding on 6 and 24 well plates with surface areas of 9.6 cm^2 and 2 cm^2 respectively produced very significantly different ($p < 0.001$) values in Figure 6-9. The larger surface area of the 6 well plates produced a greater reduction of Alamar Blue throughout the cell seeding range. Six well plates provided better correlation with fibroblasts seeded onto scaffolds at 80 ± 10%. Alamar Blue penetrates the cell membrane and is reduced to resorufin that is released from within the cell and detected [265, 266].

6.3.4 Carrier Fluid Impact on Primary Fibroblasts

The effect of carrier fluids on primary human dermal fibroblasts were assessed 24 hours post seeding by Alamar Blue reduction. Cells were seeded on tissue culture plastic in a 1ml volume of carrier fluid for thirty minutes before the addition of serum supplemented media to simulate scaffold implantation *in vivo*.

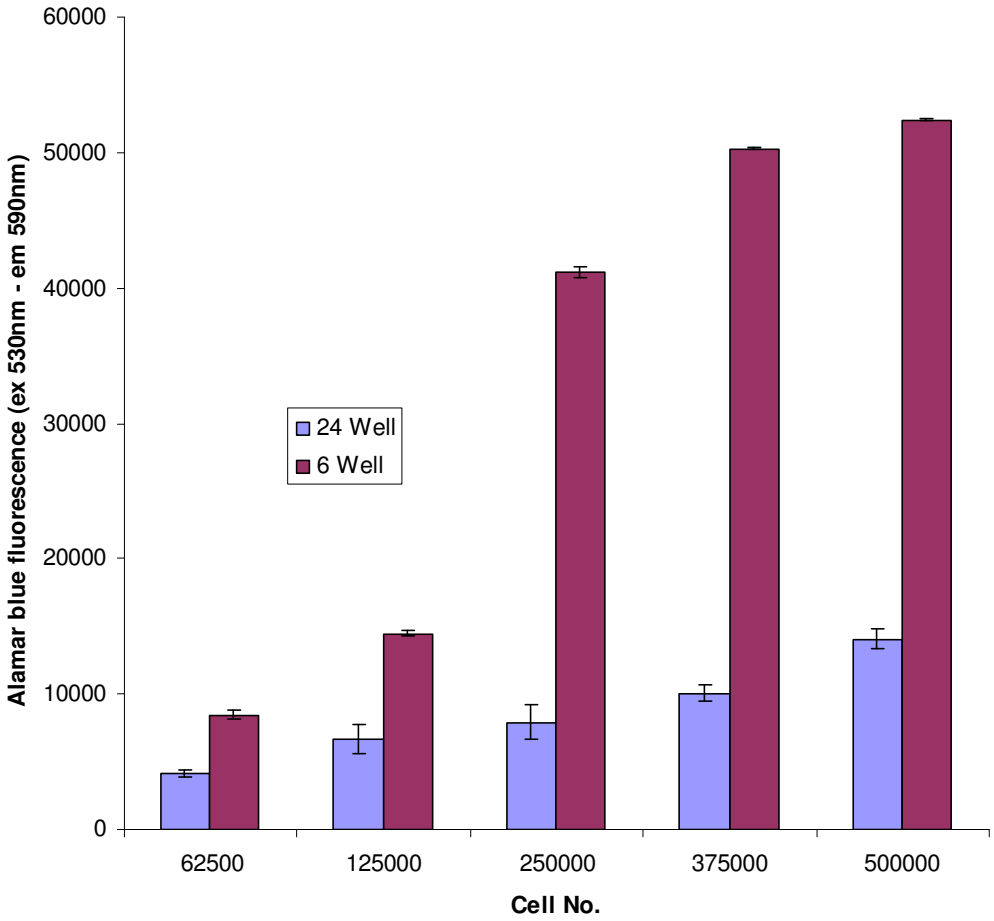

Figure 6-9 Primary human fibroblast cell activity following cell number seeding onto tissue culture plastic (n = 3) in 6 and 24 well plates. The cells were evaluated 12 hours after seeding with a 90 minute alamar blue assay.

The results in Figure 6-10 were conducted over three time points and show a significant difference ($p < 0.001$) between cells seeded in HBSS and 0.9% sodium chloride solutions at each time point recorded. The metabolic activity of fibroblast cells in 0.9% sodium chloride solution was higher than cells in HBSS buffer. The metabolic activity of cells in sodium chloride solution was not significantly different from the positive control at the 90 minutes end point. There was no significant difference between cells grown in mixed supplemented media conditions with HBSS or 0.9% sodium chloride solution. HBSS and mixed media with 0.9% sodium chloride solution were not significantly different in metabolic activity after 90 minutes.

The metabolic activity of fibroblast cells in 0.9% sodium chloride solution alone was significantly ($p < 0.001$) different to the mixed media with sodium chloride solution. This may be explained by metabolic stress induced by sodium chloride solution causing an up regulation of cell reduction / oxidation activity. The effect of HBSS on fibroblasts alone and in combination with media was similar, but less than that of the standard media. This induced metabolic stress may be due to sodium chloride solution containing no energy source to support cells actively trying to reattach to the substrate. The period of exposure was relatively short however its effect was significant. HBSS contains glucose as an energy source and has been found to sustain cells through the Alamar Blue evaluation for 90 minutes with minimal impact on cell activity.

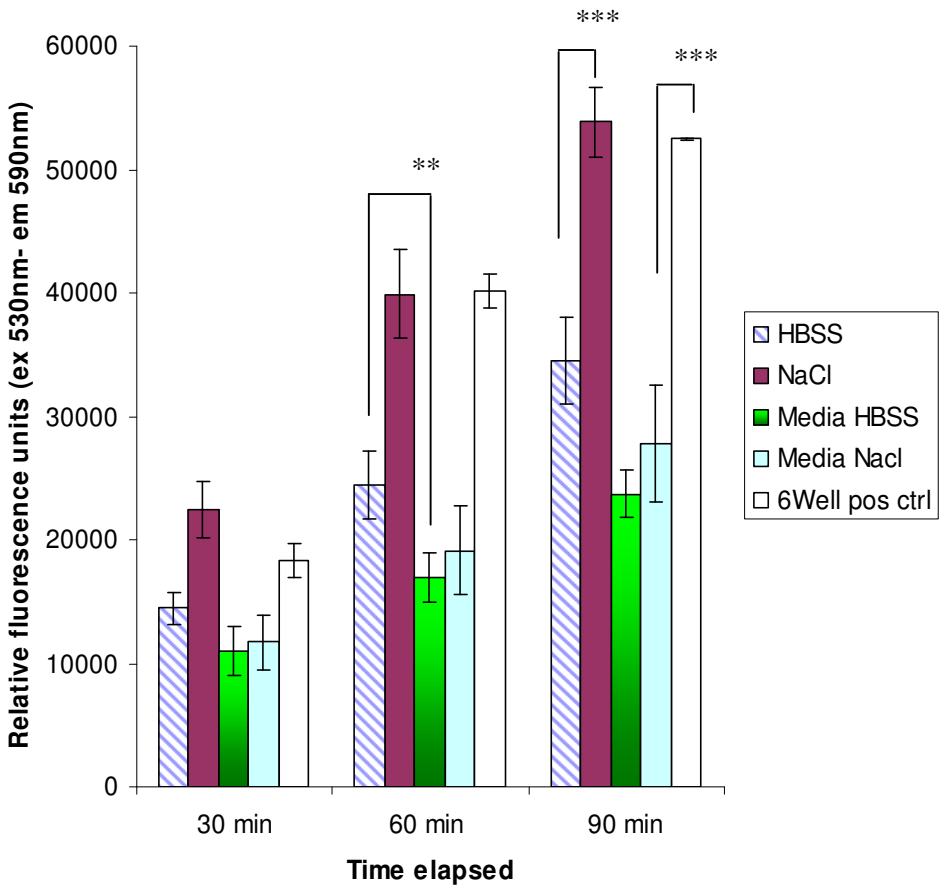

Figure 6-10 Primary human fibroblasts cell activity 24 hours after seeding $5x10^5$ cells in different fluids using 6 well tissue culture plastic and the Alamar Blue assay (n = 3). It shows the impact of an initial 30 minutes cell seeding period in test fluids on the ability of cells to convert alamar blue. Media was added to all cells prior to the 24 hours incubation. Statistical significance denoted as ** ($p < 0.01$) and *** ($p < 0.001$).

The results of DNA titration of human dermal fibroblast cells seeded on tissue culture plastic 6 well plates in Figure 6-11 shows that there was no significant difference in cell number between HBSS buffer and 0.9% sodium chloride solution. There was a significant ($p < 0.01$) reduction in cell number between 0.9% sodium chloride solution alone and the mixed media with HBSS or NaCl carrier. In mixed media, cell number was very significantly ($p < 0.001$) lower than the media treated control.

The lack of a statistically significant difference in cell number by DNA titration between HBSS and 0.9% sodium chloride as carrier fluids in Figure 6-11 was contrary to the metabolic activity measured in the Alamar Blue assay of Figure 6-10. This may indicate that difference in metabolic activity between cells exposed to HBSS and 0.9% sodium chloride measured in the Alamar Blue assay of Figure 6-10 was due to induced metabolic stress [381]. This explanation was consistent with the observation of no significant difference in cell number between media with HBSS and media with 0.9% sodium chloride solution. The differences in cell number for this experiment may have been caused by cell detachment during the addition of media 30 minutes post incubation to the restricted cell seeding volume.

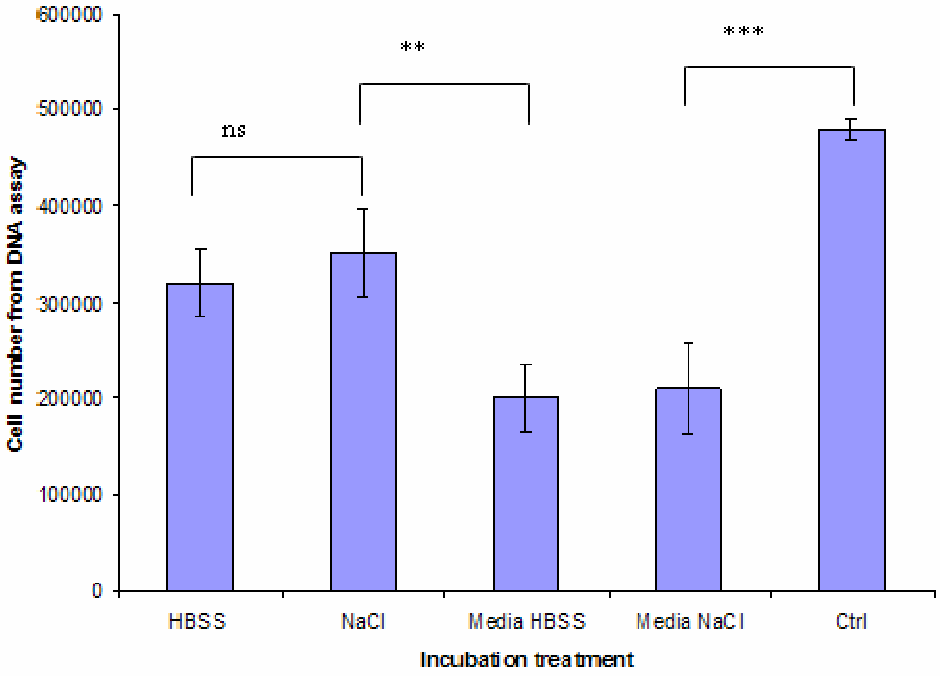

Figure 6-11 Effect of carrier fluid on human dermal fibroblasts cell number (n= 3), determined by DNA assay with Hoechst 33258 at excitation/ emission wavelength of 355/ 460nm. Well plates were seeded with 1mL of carrier fluid for 30 minutes in an incubator then topped up with 3mLs media and left for 24 hours. Statistical significance denoted as ns (not significant), ** ($p < 0.01$) and *** ($p < 0.001$).

6.3.5 Viability of Osteoblasts in Carrier Fluids After *in situ* Seeding

For HBSS seeded scaffolds of increasing particle size (> 200 µm, > 300 µm and > 400 µm), there was no statistically significant increase in cell metabolic activity detected at 24 and 72 hours (Figure 6-12). The level of cell activity detected after 24 hours with the 0.9% sodium chloride carrier was more variable and reduced in comparison to HBSS. Exposure to sodium chloride solution reduced the measured cell activity on scaffolds > 200 µm and >300 µm, in comparison to the > 400 µm construct which was comparable to HBSS seeded scaffolds at 24 hours. Cell activity was reduced further at 72 hours on all 0.9% sodium chloride treated constructs. There was no significant difference between 0.9% sodium chloride solution and HBSS buffer in the > 400 µM scaffold. This may indicate that increased pore size may positively influence cell survival in sodium chloride solution. The differences in cell activity detected with the > 200 µm and > 300 µm particle sized scaffolds may have been due to higher cell density in these scaffold pores.

The relatively large pores formed by the restricted particle size of the scaffolds' have enabled the Alamar Blue method to detect 80 ± 10% of the cell activity seen on tissue culture plastic with HBSS treatment after 24 hours. This indicates good cell survival through the handling processes of mixing with particulates, compression through delivery and wet scaffold sintering.

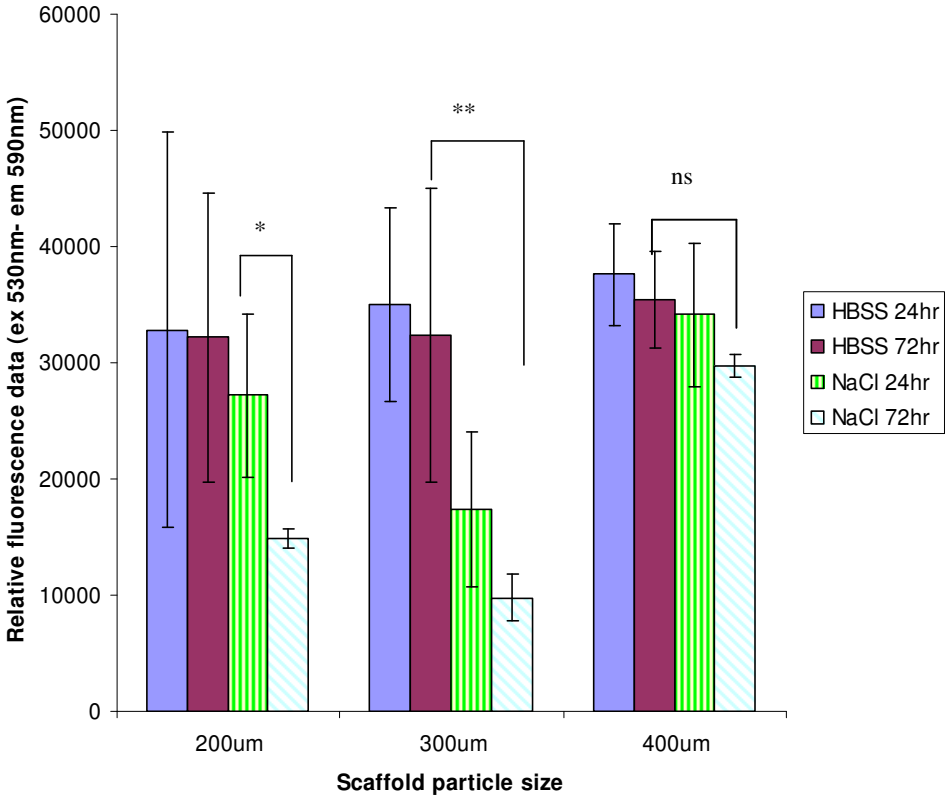

Figure 6-12 Human primary osteoblast cell survival and metabolic activity at 24 and 72 hr time points following *in situ* seeding and wet sintering with scaffolds of differing component particle size ranges. Cells ($5x10^5$) in 200 µL of carrier fluid were mixed at a 1:1 weight ratio with dry scaffold components, compressed by injection and extruded into a well plate. Scaffolds were incubated at 37 °C for 30 minutes before the addition of media. The Alamar Blue assay was conducted for 90 minutes in HBSS. Statistical significance denoted as * ($p < 0.05$), ** ($p < 0.01$) and ns (not significant).

HBSS was used as the material of choice for *in situ* seeding of further scaffolds in this work. It is envisaged that an intraoperatively conducted procedure to recover and seed bone stem cells might utilize this combination of materials.

6.3.6 Human Osteoblasts Response to Supplements

This investigation was conducted on tissue culture plastic and scaffolds to determine the effects of supplementation on the proliferation of primary osteoblast cells and measure the effect on alkaline phosphatase activity. Human primary osteoblasts were cultured for eight days in six well plates at $2x10^4$ cells per well in standard supplemented media; media without supplementary L-glutamine (Diff. media) and media without L-glutamine but added ascorbyl phosphate (Diff Asc).

The photomicrographs in Figure 6-13a, b, and c were representative of cell coverage after 8 days. Cells grown in standard media experienced the slowest rates of proliferation over 8 days. Cell numbers in standard media ($1x10^5 \pm 9500$) were significantly ($p < 0.001$) lower than cells grown without L-glutamine supplementation ($1.5x10^5 \pm 8800$). The addition of ascorbyl-2 phosphate further enhanced osteoblast proliferation in a dose dependant manner with $3x10^5 \pm 10500$ cells at 200 µg/mL.

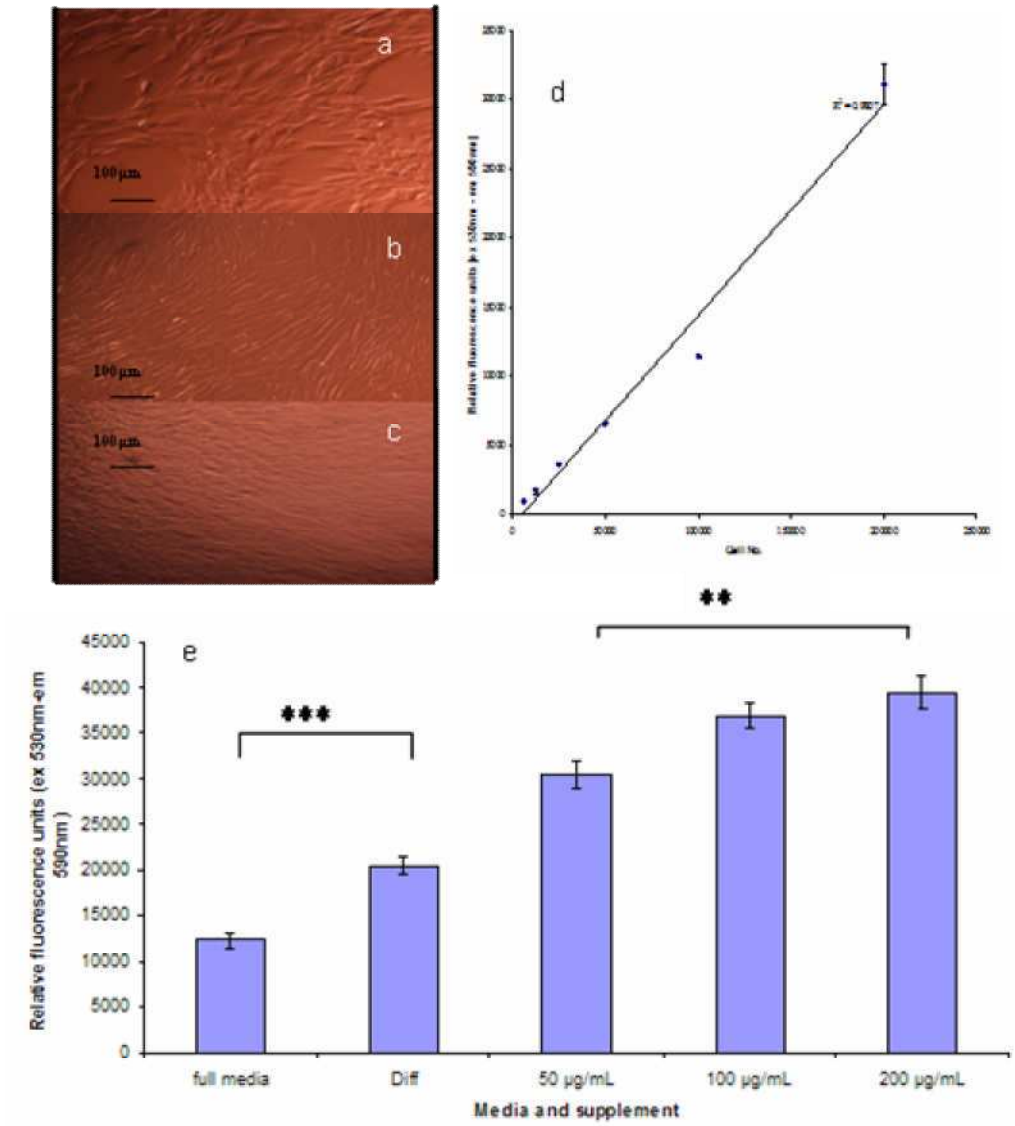

Figure 6-13 Osteoblasts after 8 days cell growth on tissue culture plastic in (a) standard supplemented media, (b) without added L-glutamine (c) with 200 µg/mL ascorbic acid 2- phosphate and without added L-glutamine. (d) Alamar Blue calibration 12 hours after seeding (R^2= 0.9807); (e) cell proliferation on tissue culture plastic after eight days (n = 3). Statistical significance denoted as ** ($p < 0.01$) and *** ($p < 0.001$).

As an essential amino acid, L-glutamine is added to media as an alternative energy source for cells with high metabolic activity. In addition, L-glutamine has been shown to be an antagonist of dexamethasone [382]. Here, addition of L-glutamine to serum supplemented media was shown to retard proliferation of primary osteoblasts. Serum alone can stimulate collagen synthesis and alkaline phosphatase activity; however, batch to batch variation necessitates the addition of ascorbate. The addition of long acting ascorbic acid 2-phosphate was shown to stimulate osteoblast proliferation and was similar to reported results [383].

Dimethyl sulfoxide is used as a carrier for dexamethasone and the compatibility of the material was evaluated on primary osteoblast cell activity after 8 days in differentiated media without L-glutamine (Figure 6-14). Dimethyl sulfoxide at 10 µL/mL did not significantly reduce cell proliferation in media without supplementary L-glutamine and was not significantly different to the control differentiated media. At levels > 10 µL/mL dimethyl sulfoxide was inhibitory to cell proliferation. Alkaline phosphatase activity in the presence of dimethyl sulfoxide at and above 100 µL/mL (Figure 6-15) was significantly ($p < 0.01$) reduced. The level of alkaline phosphatase produced without additional L-glutamine supplement was very significantly higher than that produced in media with supplementary L-glutamine. The results for alkaline phosphatase activity were of similar profile to that obtained for cell activity in Figure 6-14, 15.

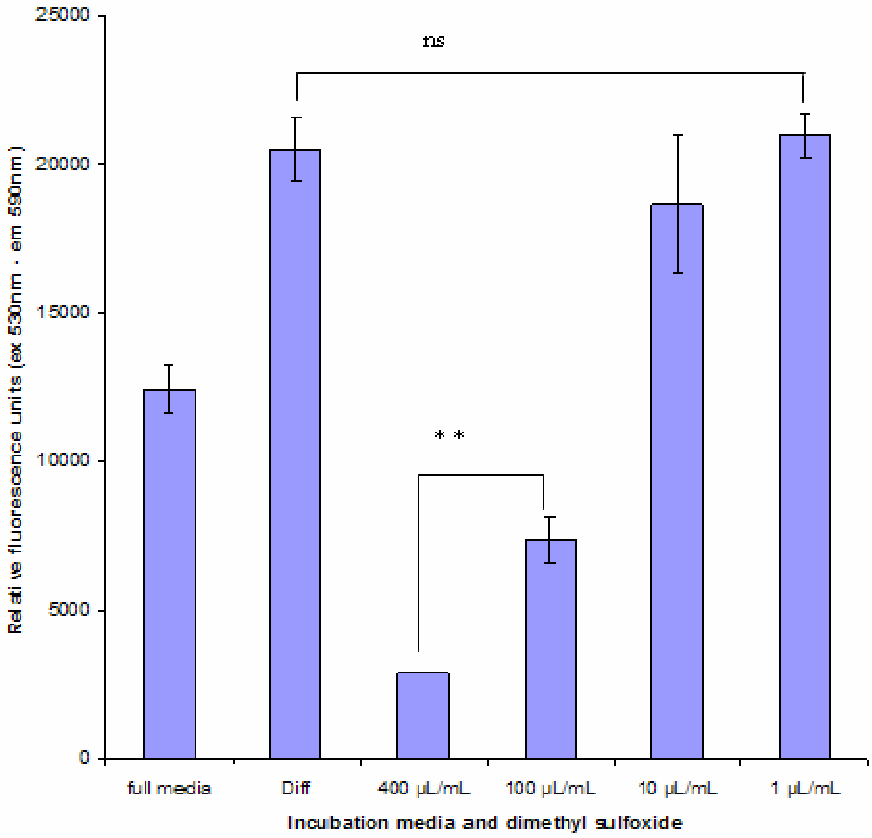

Figure 6-14 Effect of dimethyl sulfoxide on the reduction of Alamar Blue by primary osteoblasts after eight days growth on tissue culture plastic (n = 3). Statistical significance denoted as ns (not significant) and ** ($p < 0.01$).

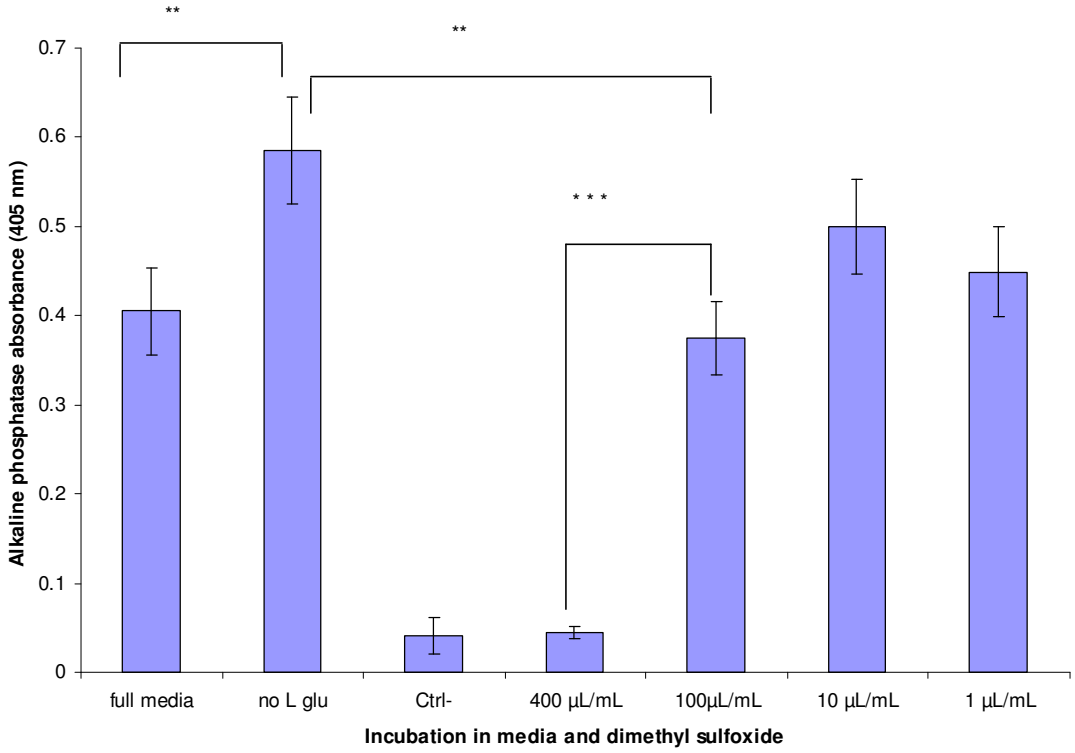

Figure 6-15 Effect of dimethyl sulfoxide (0-400 µL/ mL) on alkaline phosphatase activity in human osteoblasts after eight days growth in media. Statistical significance denoted as ** ($p < 0.01$) and *** ($p < 0.001$).

6.3.7 Impact of Dexamethasone on Human Primary Osteoblasts

In Figure 6-16, comparison of dexamethasone impact on cell activity shows that it is inhibitory at all concentrations above 0.01µM when compared to cell activity in full media. Supplementary addition of ascorbic acid 2-phosphate (50 µg/mL) significantly diminished the negative impact of dexamethasone on osteoblast cells throughout the range of concentrations used. The degree of protection and enhanced proliferation was significant ($p < 0.01$) with 100 µM dexamethasone having higher metabolic activity than cells in full media.

Alkaline phosphatase production (Figure 6-17) mirrored the results for cell activity determined with Alamar Blue in Figure 6-16. The inhibitory effect of dexamethasone was concentration dependant and effective throughout the range evaluated. The impact of ascorbic acid 2- phosphate supplementation (50 µg/mL) became significant at 300 µM dexamethasone addition when compared to the 400 µM dose on cells. The increase in alkaline phosphatase activity in osteoblasts was inversely related to the concentration of dexamethasone added. Ascorbic acid 2-phosphate increased cell proliferation and detected alkaline phosphatase activity in a dose dependent manner (Figure 6-16 and 6-17). The positive impact of ascorbic acid 2-phosphate addition was observed in the extremely significant ($p < 0.001$) difference between dexamethasone concentrations at 400 and 100 µM Figure 6-16. Alkaline phosphatase activity in Figure 6-17, showed a similar trend and was therefore linked to cell number.

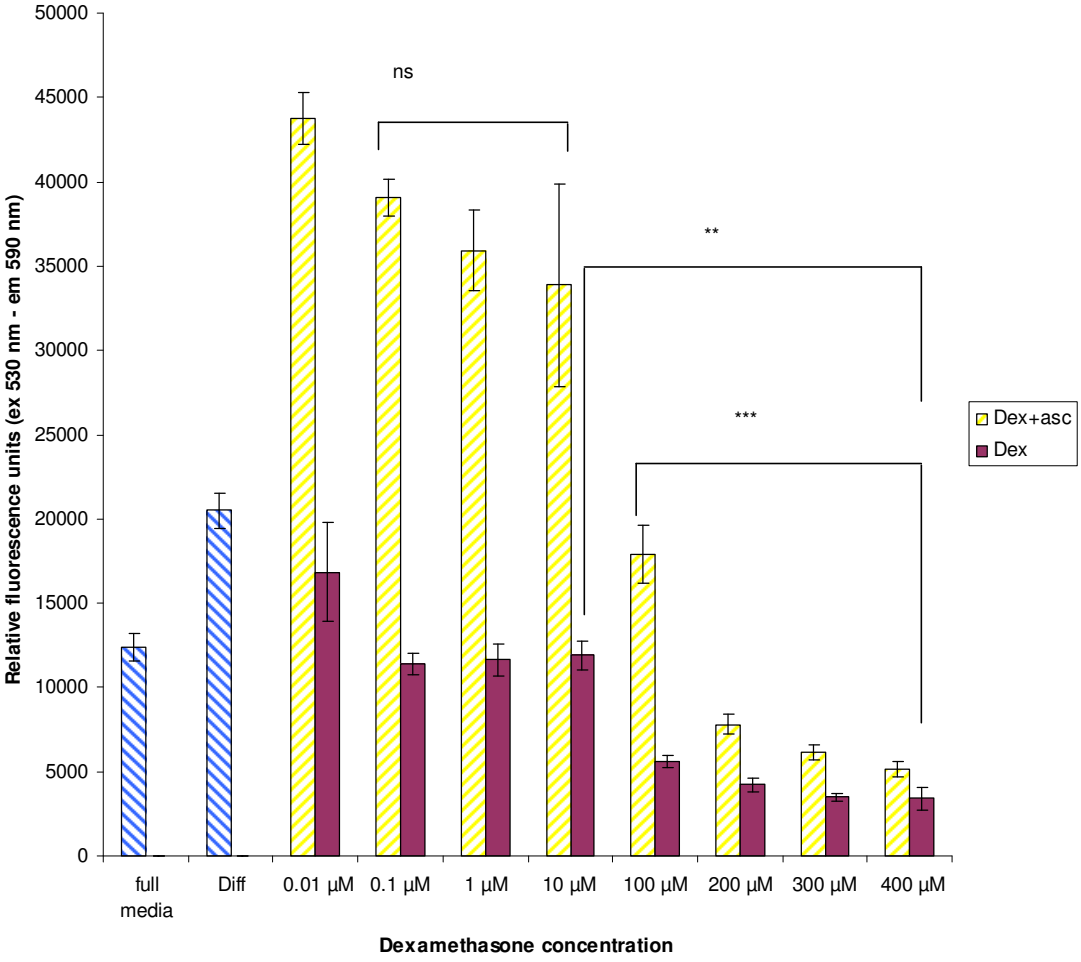

Figure 6-16 Effect of ascorbic acid 2-phosphate supplementation at 50 µg/mL on osteoblasts cell growth in media with dexamethasone after 8 days. Osteoblasts metabolic activity was determined by an end point Alamar Blue conversion after 90 minutes. Statistical significance denoted as ns (not significant), ** ($p < 0.01$) and *** ($p < 0.001$).

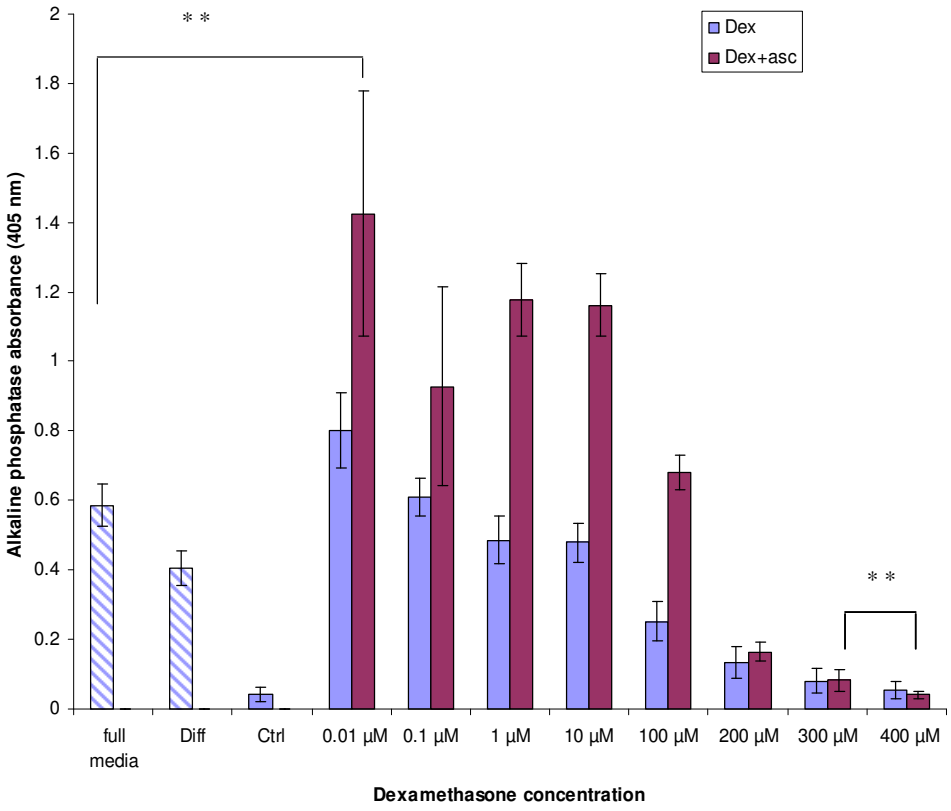

Figure 6-17 Comparison of dexamethasone and 50 µg/mL ascorbic acid 2-phosphate supplementation on alkaline phosphatase activity of primary human osteoblasts. Statistical significance denoted as ** ($p < 0.01$).

Ascorbic acid 2-phosphate addition was extremely significant ($p < 0.001$) to increasing osteoblast alkaline phosphatase activity in the comparison made in Figure 6-18 between media with and without it. Differences observed in alkaline phosphatase activity with cell number indicated that dexamethasone inhibited primary cell proliferation.

At the highest levels dexamethasone inhibited cell proliferation. Time dependent effects of dexamethasone have been recorded after 4 hours with depression of protein synthesis and reduced proliferation of cells [384]. In addition, dexamethasone can disturb the homeostatic balance within cells through suppression of the genes encoding antioxidant enzymes leading to impaired viability and reduced proliferation attributable to increased hydrogen peroxide within cells [385]. The antioxidant effect of ascorbic acid 2-phosphate abrogated dexamethasone induced cell death [385]. Dexamethasone is a differentiation factor for osteoprogenitor cells that can induce bone nodule formation in culture and increase the size of bone nodules formed [386].

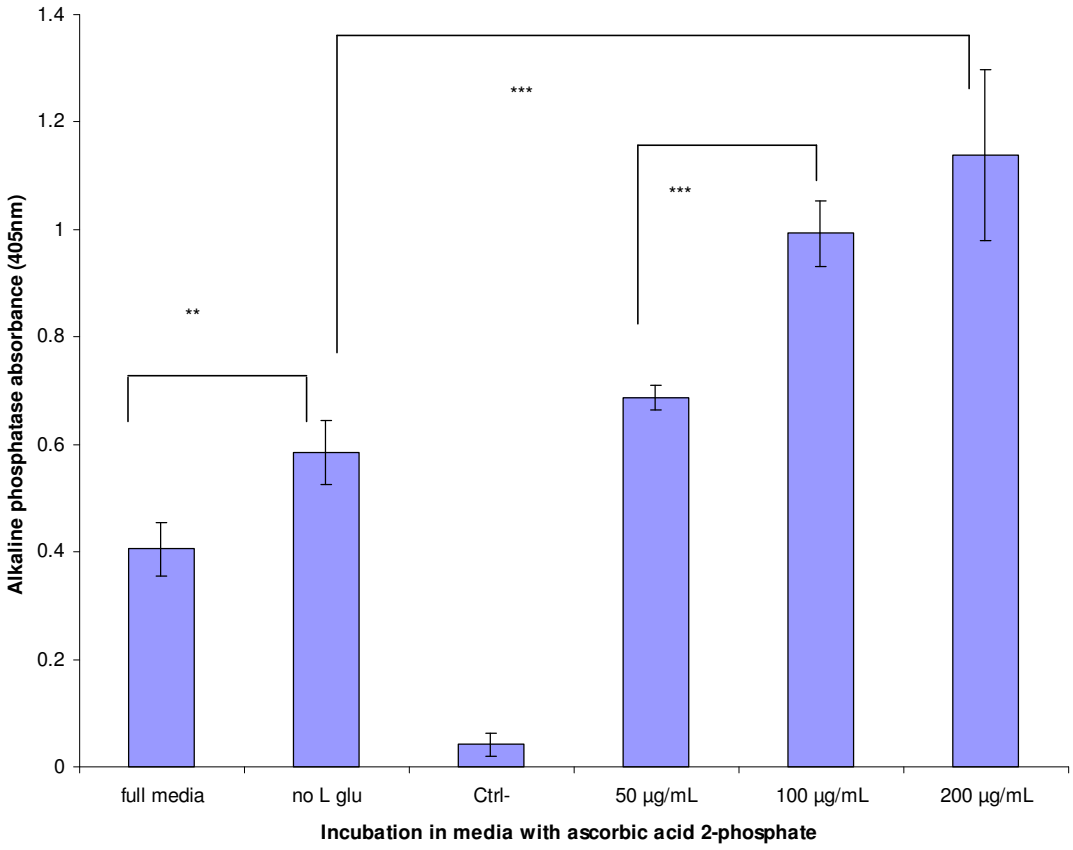

Figure 6-18 Alkaline phosphatase activity in primary human osteoblasts after eight days growth in media supplemented by ascorbic acid 2-phosphate (n=3). Statistical significance denoted as ** ($p < 0.01$) and *** ($p < 0.001$).

6.3.8 *In Situ* Osteoblast Seeding in Scaffolds

Osteoblasts were *in situ* seeded with a 3:1 $^{wt}/_{wt}$ adhesive particle to PEI sphere at three particle size ranges of; > 200 µm, > 300 µm and > 400 µm, for eight days in triplicate. Standard supplemented media was used with 50 µg/mL ascorbic acid 2-phosphate. Cell attachment was observed on both scaffold components and varied in distribution with pore size in Figure 6-19. Cells on the > 200 µm scaffold were visually, more densely distributed on the surface and ends of the scaffold. Progressively fewer cells were apparent on the outside of structures as pore size increased in accordance with earlier observations (section 6.3.2). Transversely fractured dried scaffold specimens examined by SEM show cells were distributed across the scaffold components and in addition crystalline deposits were present on the scaffold Figure 6-20. The crystals were most prominent on adhesive components, but were also observed on the carrier component of the scaffold.

These scaffolds were positively stained for calcium deposition with alizarin red indicating that the primary osteoblasts were attached and producing calcified deposits after eight days. Mineralization *in vitro* has typically been reported to be initiated from day 14-21 on both tissue culture plastic and polyester scaffold in the presence of β-glycerophosphate [148, 182, 387-390]. There is no *in vivo* equivalent of β-glycerophosphate [391].

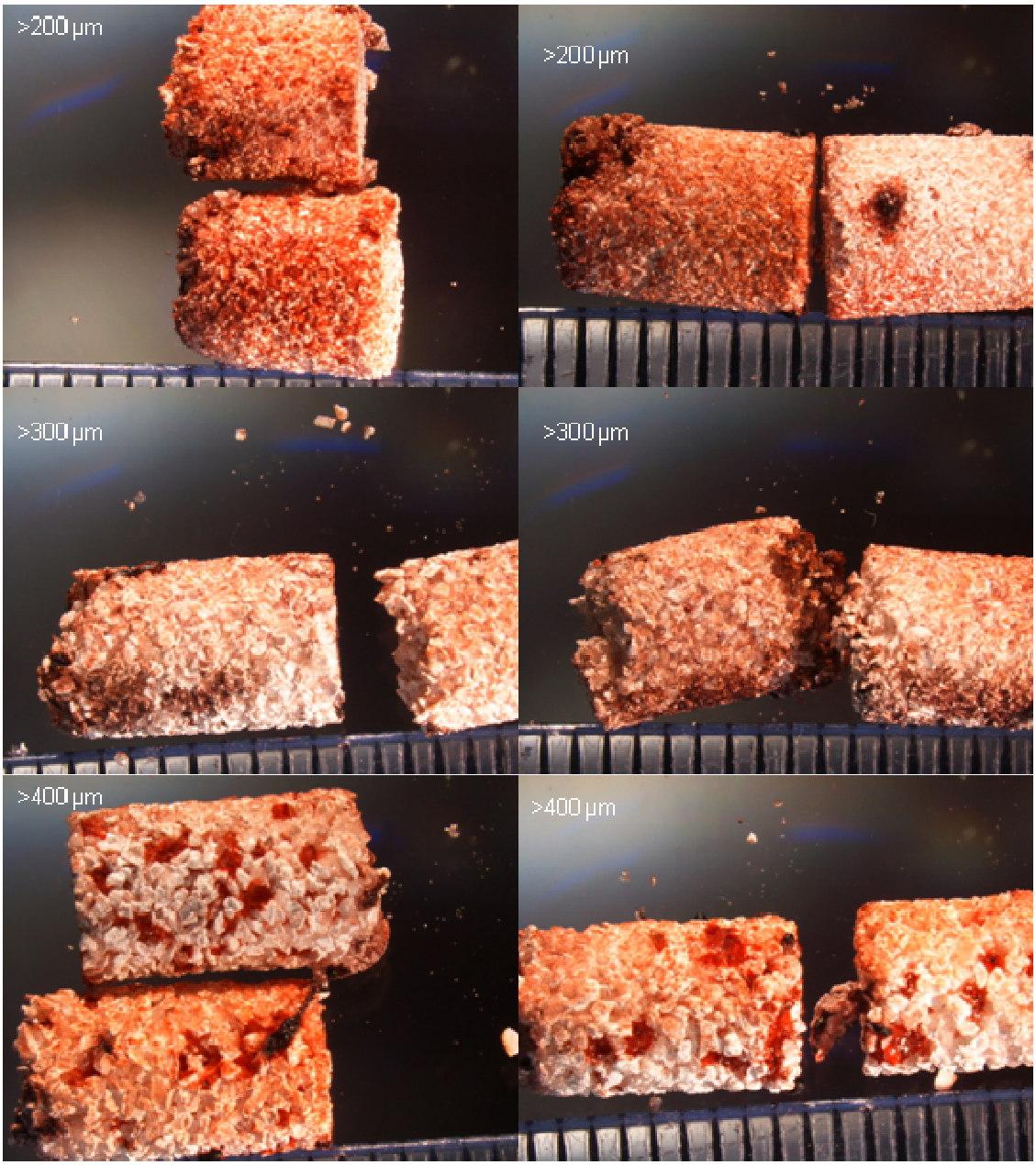

Figure 6-19 Scaffolds varying in particle size were stained with alizarin red to detect calcium deposition following *in situ* osteoblasts seeding and growth in wet sintered scaffold for eight days in standard media supplemented with 50 µg/mL ascorbic acid 2- phosphate (n = 3).

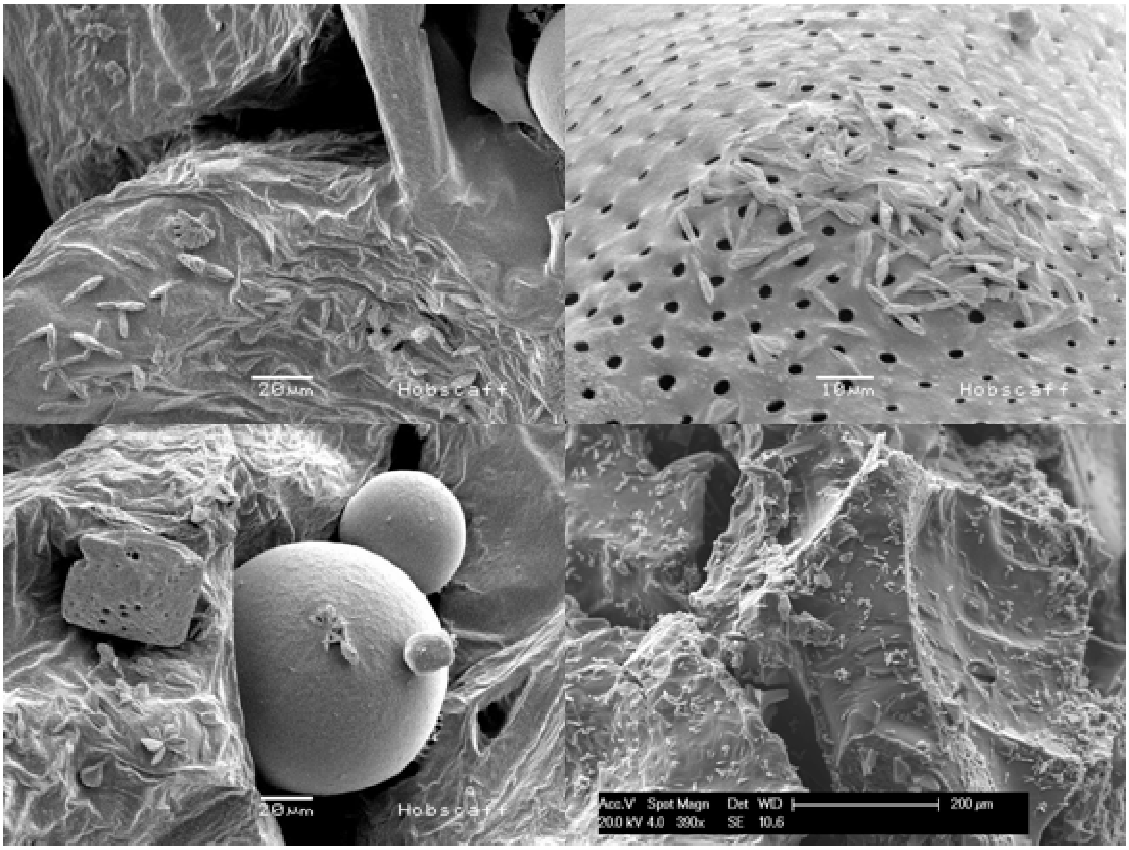

Figure 6-20 SEM images of freeze fractured two component wet sintered scaffolds, following 8 days of osteoblasts growth in standard media supplemented with 50 µg/mL ascorbic acid 2- phosphate. Scaffolds were fractured transversely to show cell distribution.

Analysis of the crystals by energy dispersive x-ray, Figure 6-21 confirmed calcium to be present. Areas of the scaffold without the crystals produced a carbon and oxygen rich component indicative of the polymer itself. Mineralization has been reported to be dependent on the presence of ascorbic acid, dexamethasone and β-glycerophosphate [388]. However, previous work has demonstrated that in the presence of long acting ascorbyl-2-phosphate mineralization can occur in the absence of beta-glycerophosphate [387]. The crystalline materials were not present after 3T3 growth in the same media Figure 6-2 and therefore specific to osteoblasts.

The type of polymorph crystal formed is dependent on calcium concentration in the media and mechanism of crystallization. Aragonite (sheaf-bundle) crystals were demonstrated to be formed from anionic polymer induced heterogenous nucleation and growth by an ion-by-ion addition at low calcium concentration (1-25 mM) over six days [392]. The crystals formed on these scaffold surfaces were of high uniformity and narrow size distribution that indicate controlled growth. Mineralization was not observed with fibroblast or 3T3 growth over 28 days in DMEM. Colonization by osteogenic cells is an essential prerequisite of *de novo* bone formation on scaffold surfaces. Osteogenic cells stimulate matrix initiation by producing non-collagenous proteins that adsorb to solid surfaces [27]. Mature osteoblasts are not expected to achieve end points representative of relatively young precursor cells *in vitro* [386].

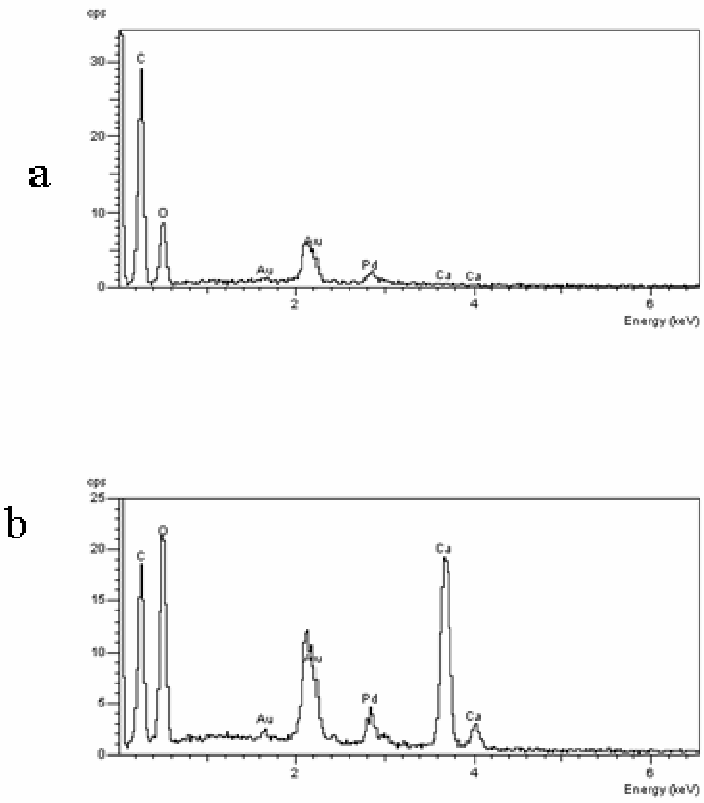

Figure 6-21 Elemental abundance distribution X-ray analysis plots obtained during SEM examination of wet sintered scaffolds following eight days of osteoblasts cell growth with (a) representative of clear polymer surface without crystals and (b) of crystals with high levels of calcium detected.

In new bone growth, mineralization requires bone sialoprotein and osteocalcin [393, 394]. Ascorbate is a cofactor in osteocalcin binding of calcium ions that controls mineral maturation [16, 395]. In the absence of adhesion peptides, cells interact with scaffolds *via* adsorbed proteins with hydrophilicity and topography being critical features. Hydrophilic polymers adsorb proteins in a hydrated interfacial phase where the proteins are likely to retain functionality [396, 397]. In addition, hydrophilic surfaces induce more homogeneous cell growth and mineral deposition in comparison to hydrophobic surfaces [398].

The surface charge of functional groups can alter the conformation of bound fibronectin to up regulate alkaline phosphatase activity and mineralization to produce a carbonate-containing hydroxyapatite similar to the mineral phase of bone. The influence of surface chemistry on osteoblastic matrix mineralization was demonstrated to be independent of cell proliferation [399]. Hydrophilic surface chemistry of hydroxyl and amino groups were shown to modify adsorbed fibronectin structure and positively influence the binding of $\alpha_5\beta_1$ integrin. Surfaces enriched with hydroxyl and amino groups up regulate osteoblast- specific gene expression for alkaline phosphatase activity and mineralization in comparison to carboxylic acid and hydrophobic methyl groups. PEI modified PLGA surface with amino presenting groups, increase hydrophilicity and control the conformational presentation of adsorbed bioactive moieties to influence cell-biomaterial interaction [356].

The texture of biomaterial substrates at nano and micron scale have been known to influence cell morphology, adhesion and gene expression [376, 400]. Cell response to surface topography varies, with stem cells more responsive to concave pits than fibroblasts [102, 401]. PLGA surfaces modified with concave pits had improved cell coverage and osteoinductive properties [55, 102]. Textured orthopaedic devices have been demonstrated to have the potential to initiate osteoinduction and osteogenesis by topography [402, 403]. The dimensions of surface features vary, but Biggs *et al* have shown grooves 330 nm deep to increase osteoblast-specific function and skeletal development in primary human osteoblasts [377]. Primary human osteoblasts, here in non optimized DMEM media show up regulation of calcium deposition. In addition, the wet sintering mechanism involving the migration of PEG produced a change in particle appearance attributed to the formation of light scattering voids of the order 200-400 nm [133, 293]. The effectiveness of a scaffold in bone repair is dependent on its bone-bonding ability. Achieving a strong bond between native tissue and synthetic material is a major challenge in regenerative medicine that can be overcome by matrix accumulation that facilitates integration by transition. Contact osteogenesis results in direct matrix deposition onto a solid surface to establish anchorage and mechanical stability [404].

6.3.9 Controlled Differentiation of C2C12 Cells

C2C12 cells were subjected to growth in media with a range of dexamethasone concentrations without supplementary L-glutamine (Diff. media) for 8 days. Dexamethasone levels up to 10 µM had the highest plateau cell activity observed in Figure 6-22. Incremental dexamethasone levels greater than 10 µM were inhibitory ($p < 0.01$), progressively retarding cell activity. The decrease in metabolic activity detected in control wells without dexamethasone may have been due to C2C12 cell confluence that can result in the formation of myotubes that contract and are easily detached from plastic surfaces.

Many cells are alkaline phosphatase positive, but do not produce the abundant quantities of osteoblast-like cells. At dexamethasone concentrations of 100 nM myotube formation was evident. At ≥ 300 µM there appeared to be some evidence of cell blebbing that was reflected in the metabolic activity determined by Alamar Blue profile of. There was no evidence of enhanced alkaline phosphatase activity present in any of the wells screened and indicates serum to have minimal impact. Neither the presence nor absence of dexamethasone stimulated C2C12 cells to produce alkaline phosphatase.

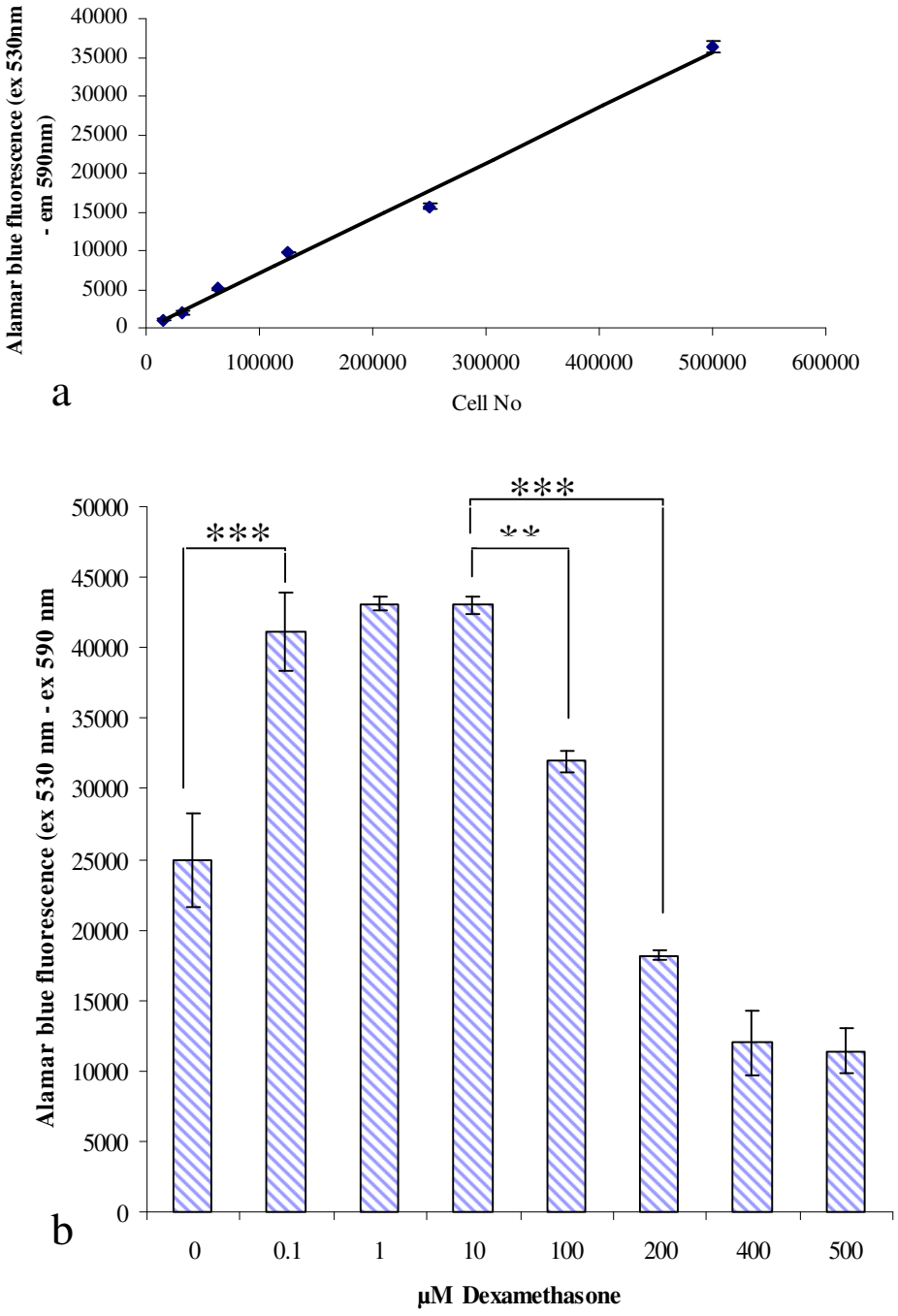

Figure 6-22 (a) Alamar Blue calibration of C2C12 cell activity 12 hours post seeding ($R^2 = 0.9929$) and (b) effect of dexamethasone supplementation on C2C12 cell activity after eight days in culture. Statistical significance denoted as ** ($p < 0.01$) and *** ($p < 0.001$).

C2C12 cells ($2x10^4$) were incubated with rhBMP-2 (0-50 ng/mL) in standard supplemented media with and without supplementary L-glutamine for five days. From Figure 6-23, media without supplementary L-glutamine addition again stimulated an increase in cell number. Alamar Blue determination of cell numbers in standard media was $1x10^5$ and $1.5x10^5$ in media without supplementary L-glutamine. Variation in rhBMP-2 concentration did not affect cell number and was apparently non-toxic to cells throughout the administered range of concentrations used.

There was positive correlation ($R^2 = 0.949$) of alkaline phosphatase stimulation, with rhBMP-2 up to 200 ng/mL followed by saturation in Figure 6-24. Similar results have been previously reported [257]. The lowest concentration of rhBMP-2 used increased alkaline phosphatase production to an extremely significant level ($p < 0.001$), above the baseline detected. The step change from 50-100 ng/mL rhBMP-2 was very significant ($p < 0.01$) doubling the level alkaline phosphatase detected without an increase in cell number. The confluence of these factors of stimulation without toxicity was considered ideal for selection of C2C12 cells to demonstrate controlled growth factor delivery in a scaffold.

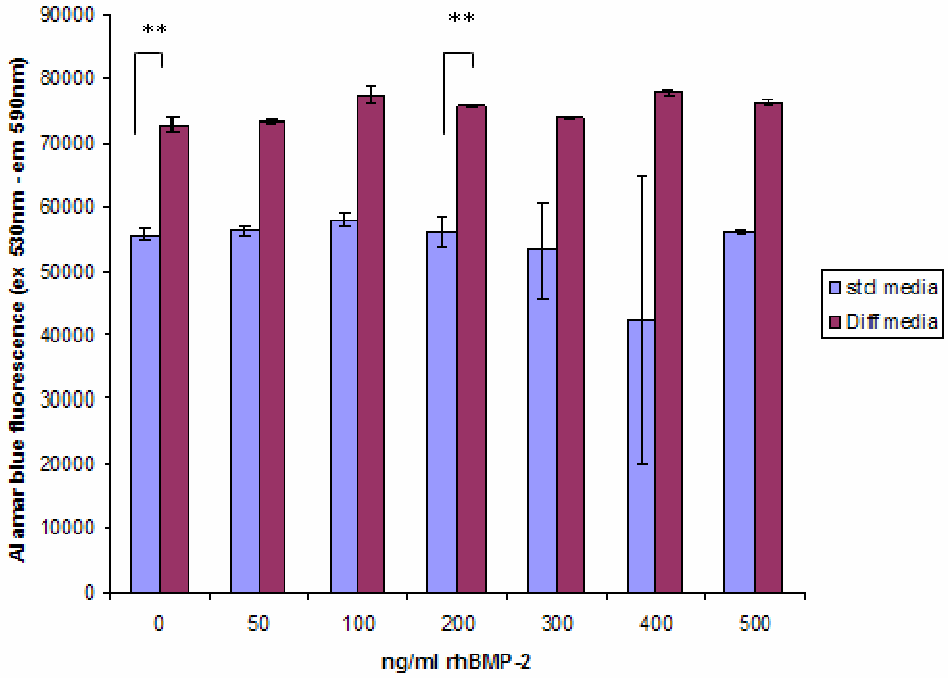

Figure 6-23 Effect of varying rhBMP-2 levels (0-500 ng/mL) on C2C12 cells after 8 days of growth in standard and differentiated media without L-glutamine (Diff media). Statistical significance denoted as ** ($p < 0.01$) for n = 3.

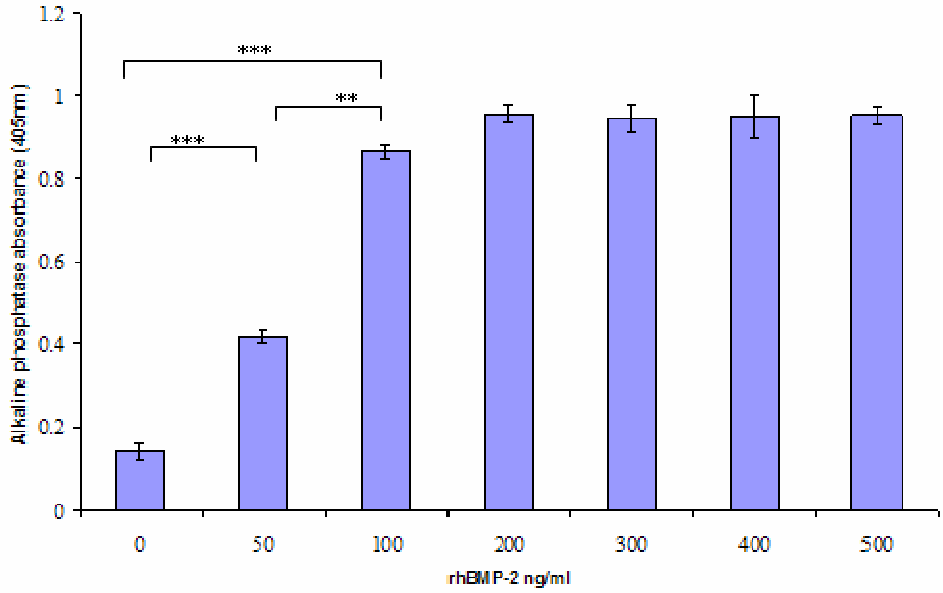

Figure 6-24 Effect of varying rhBMP-2 levels (0-500 ng/mL) on the induction of alkaline phosphatase activity in C2C12 cells in standard media. Statistical significance denoted as ** ($p < 0.01$) and *** ($p < 0.001$) for n= 3.

6.3.10 Dye Encapsulation in Spheres

On addition of the hydrophilic dye formulation to the hardening bath there was a significant amount of colour leaching observed as polymer spheres were formed. The light microscopy images in Figure 6-25 a, c show the distribution of the remaining dye to be patchy with few particles retaining any colour. The extent of colour leaching can be ascertained from bulk comparison of spheres in Figure 6-25e. During production aqueous channels were believed to be formed within the microsphere during polymer solidification and solvent removal [358, 405]. There was no colour leaching observed from dye addition to the oil phase Figure 6-25 b,d.

6.3.11 Manufacture of Spheres for rhBMP-2 Delivery

FITC-BSA had a 75% yield by weight for spheres > 200 µm in size compared to 85% for BSA microspheres Figure 6-26c. FITC addition to BSA alters protein size and charge; hence its use to estimate behaviour [406]. Lyophilized BSA entrapment in microspheres without loss of function has been demonstrated. FITC-BSA was used to model rhBMP-2-BSA distribution and release from PLGA spheres [368, 407-409]. As a transport protein, BSA is negatively charged at neutral pH and interacts with positively charged rhBMP-2 [53, 410]. BSA was shown to protect BMP-2 when used as an adjuvant during the loading process [81, 411].

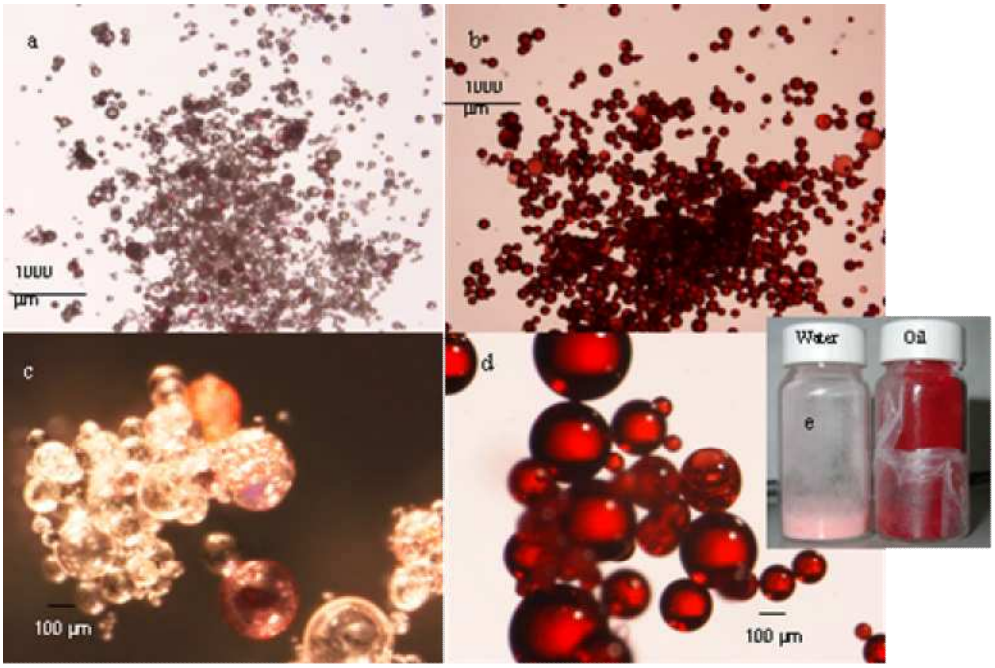

Figure 6-25 Comparison of dye retention and distribution within spheres following inclusion of 1% eosin-y into the primary emulsion water phase (a & c) with (b,d) oil red-O addition to the polymer phase. Image (e) shows the bulk appearance of the spheres.

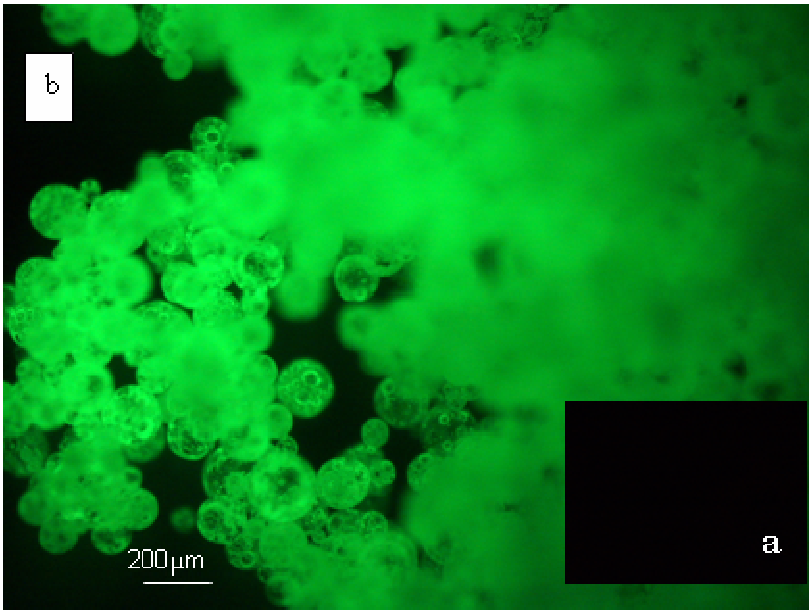

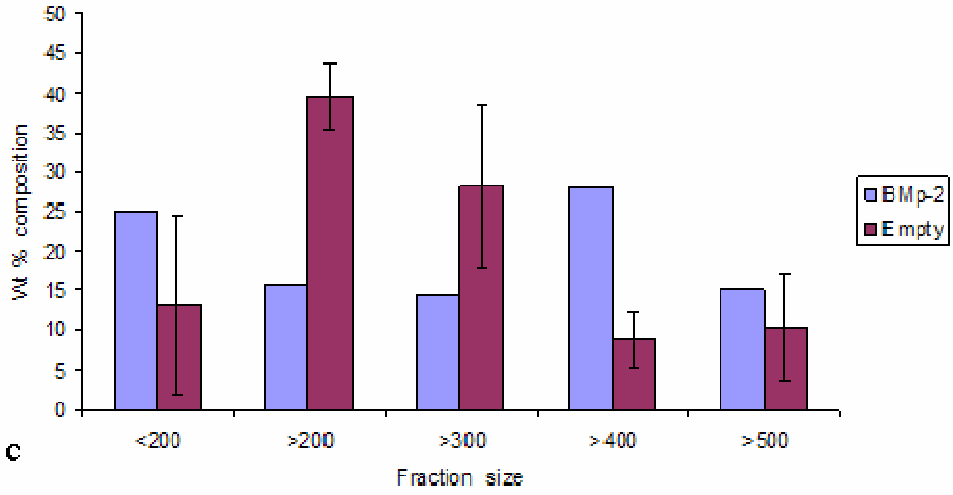

Figure 6-26 Photomicrograph of (a) blank PLGA 50:50 microsphere without fluorescent protein (b) microsphere loaded with FITC-BSA and (c) graph showing the distribution of sphere sizes obtained from the batches.

6.3.12 Controlled rhBMP-2 Release in Scaffolds

Scaffolds > 300 µm size in a 3:1 ratio of adhesive particles to BSA/rhBMP-2 loaded spheres were produced *in situ* with C2C12 cells seeded in HBSS for 30 minutes prior to being ejected in standard media. The controls were both *in situ* C2C12 seeded scaffolds with blank spheres ejected into standard media with and without 100 ng/mL rhBMP-2 supplement. Cells on the particulate scaffolds at the first time point of 5 days were demonstrated to be metabolically active (Figure 6-27a), showing survival of the wet *in situ* sintering process. Variation in the levels of cells detected on the scaffolds at day 5 was not significant. There was significant proliferation ($p < 0.001$) demonstrated over the two successive time points at 15 and 28 days.

Very significant alkaline phosphatase activity was detected at day 5 and was demonstrated to increase significantly ($p < 0.01$) at the second time point of day 18 in the scaffolds where rhBMP-2 was present (Figure 6-26b). The images in Figure 6-28 at day 5 show cells to be present on all scaffolds, but alkaline phosphatase activity was detected only in conditions where rhBMP-2 was present. Alkaline phosphatase activity on scaffolds sintered with loaded rhBMP-2 spheres was 80% of that detected in the 100 ng/mL supplemented media.

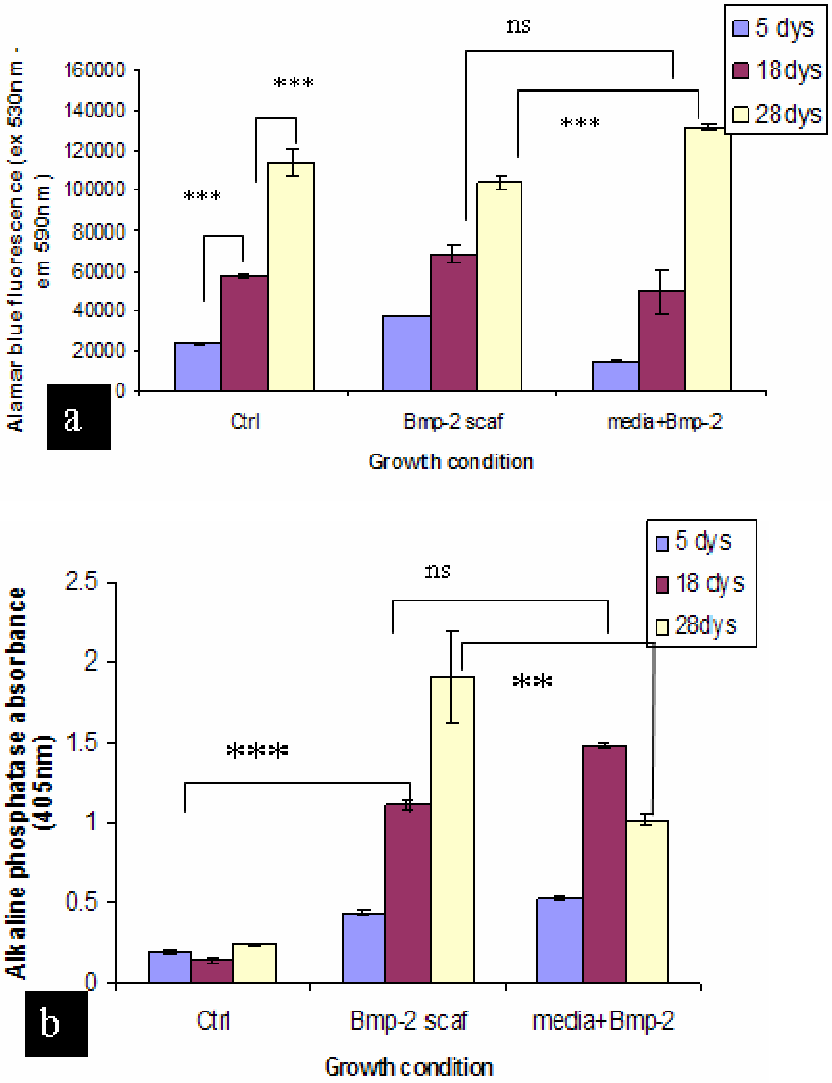

Figure 6-27 Response of *in situ* seeded C2C12 cells on scaffold over 28 days with control (Ctrl) without rhBMP-2, a 100 ng/mL Bmp-2 supplement in media and *in situ* BMP-2 loaded microspheres (Bmp-2 scaf). Graph (a) shows cell activity determined by Alamar Blue and (b) alkaline phosphatase production at 5,18 and 28 day time points. The rhBMP-2 was withdrawn from the media supplement after day 18 (media+ BMP-2). Statistical significance denoted as ns (not significant), ** ($p < 0.01$) and *** ($p < 0.001$).

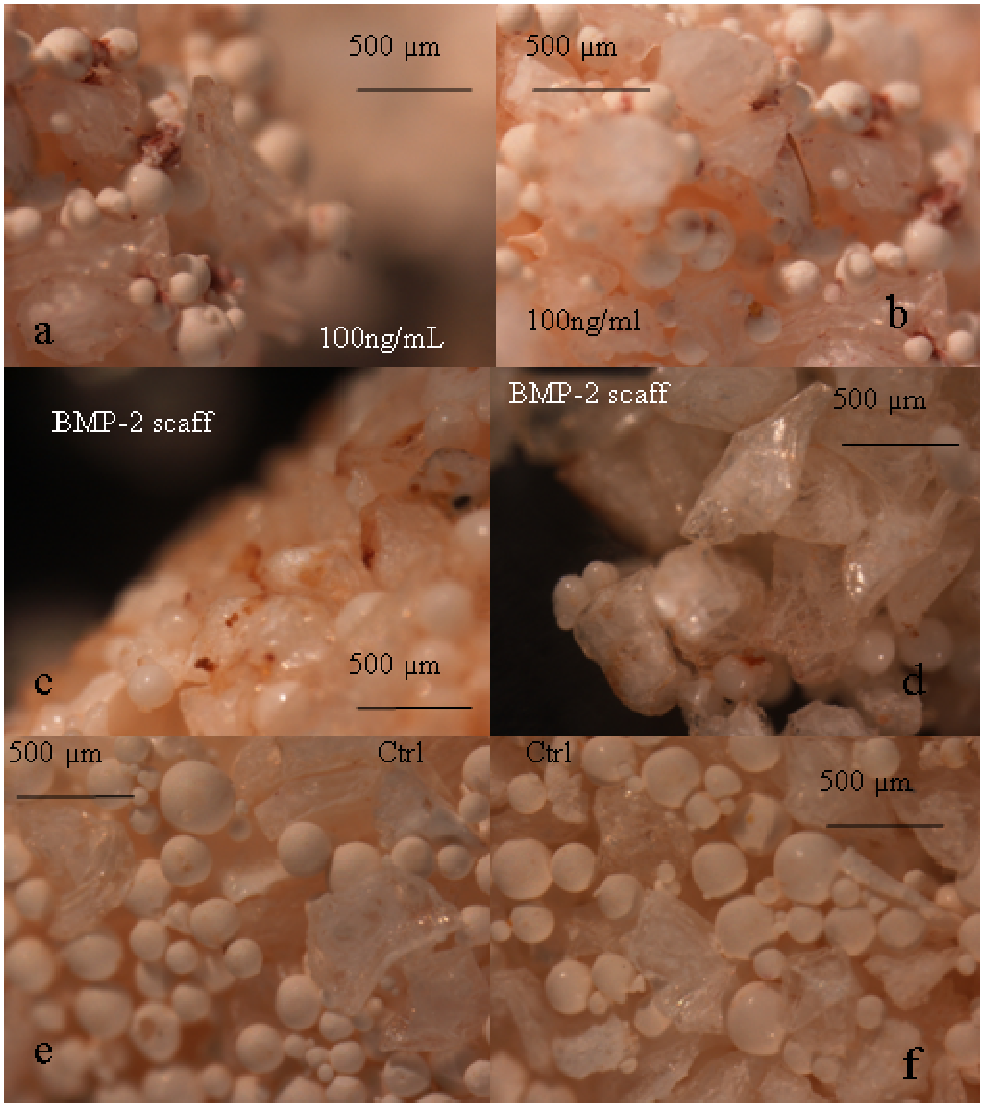

Figure 6-28 Alkaline phosphatase activity of C2C12 cells at day 5 on scaffolds in media supplemented with (a, b)100 ng/mL rhBMP-2, (c, d) BMP-2 scaff with growth factor loaded microspheres and (e, f) blank microspheres without growth factor (Ctrl).

Increased alkaline phosphatase activity was detected at day 18 in Figure 6-29 indicating sustained release of rhBMP-2 from the loaded microspheres. The images of alkaline phosphatase positive cells showed attachment and spreading on both the spheres and the adhesive component. At day 18 the difference in alkaline phosphatase activity between rhBMP-2 supplemented media and that released from scaffold components was not significant (Figure 6-27b).

For the final stage of the incubation between days 18 to 28, rhBMP-2 was withdrawn from the supplemented media. The effect seen in Figure 6-27b was a reduction in the level of alkaline phosphatase detected in this treatment in comparison to the day 18 result with a significant ($p < 0.001$) increase in cell number in Figure 6-27a. The rhBMP-2 loaded microspheres continued to release active protein resulting in further stimulation of the proliferating C2C12 cells and detection of significantly ($p< 0.01$) higher levels of alkaline phosphatase activity at day 28 Figure 6-27b. The detected increase in alkaline phosphatase levels may be linked with cell proliferation throughout the experimental period.

Figure 6-30 shows the scaffolds at day 28 with alkaline phosphatase negative control scaffolds. The media in which supplementation was withdrawn, shows patchy alkaline phosphatase staining with areas of new cell growth that were negative for alkaline phosphatase activity. BMP-2 loaded scaffolds, maintained differentiation of C2C12 cells and were intensely stained.

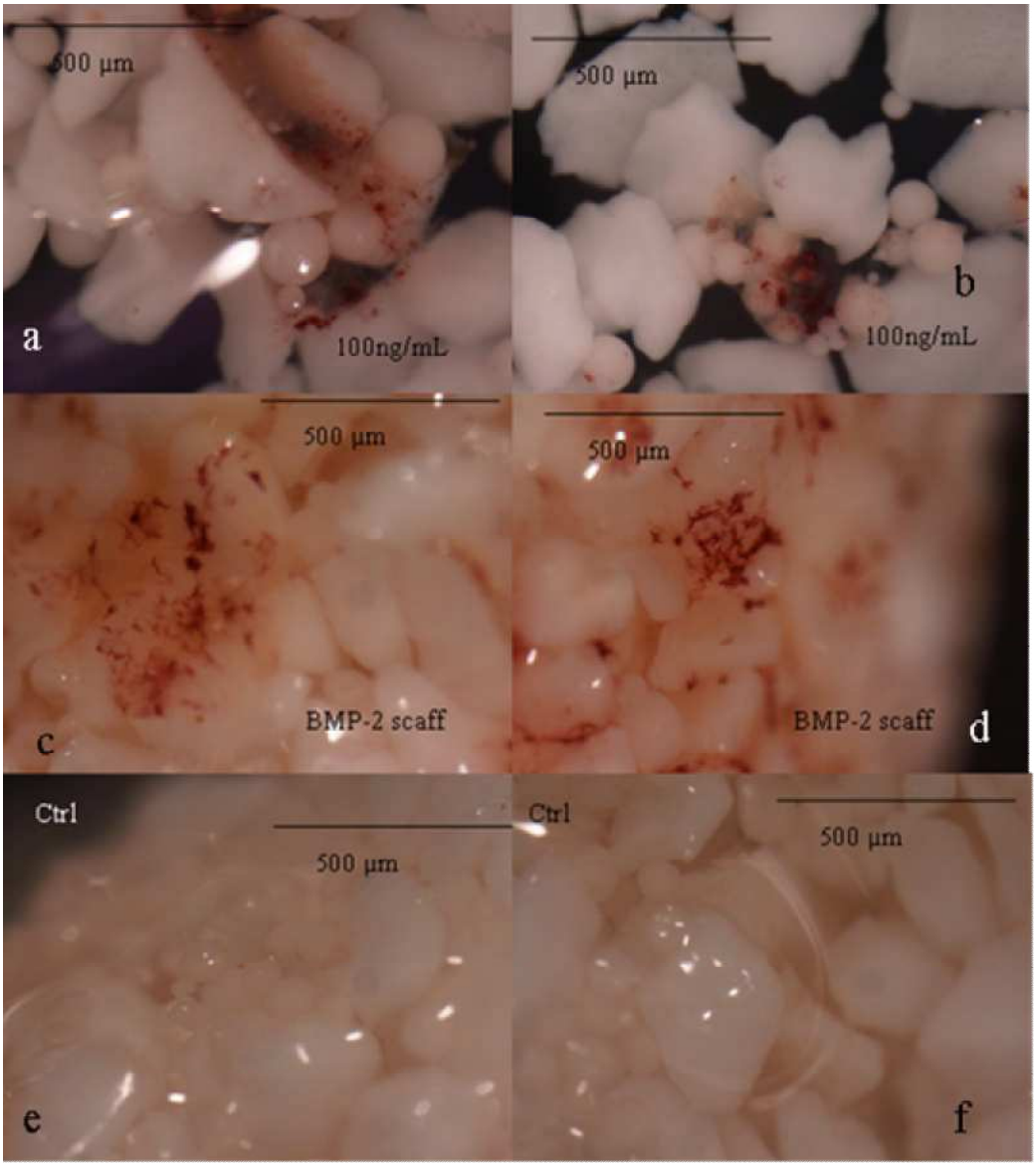

Figure 6-29 Alkaline phosphatase activity of C2C12 cells at day 18 on scaffolds in (a, b) media supplemented with 100 ng/mL rhBMP-2, (c, d) BMP-2 scaff growth factor loaded microspheres and (e, f) blank microspheres without growth factor (Ctrl).

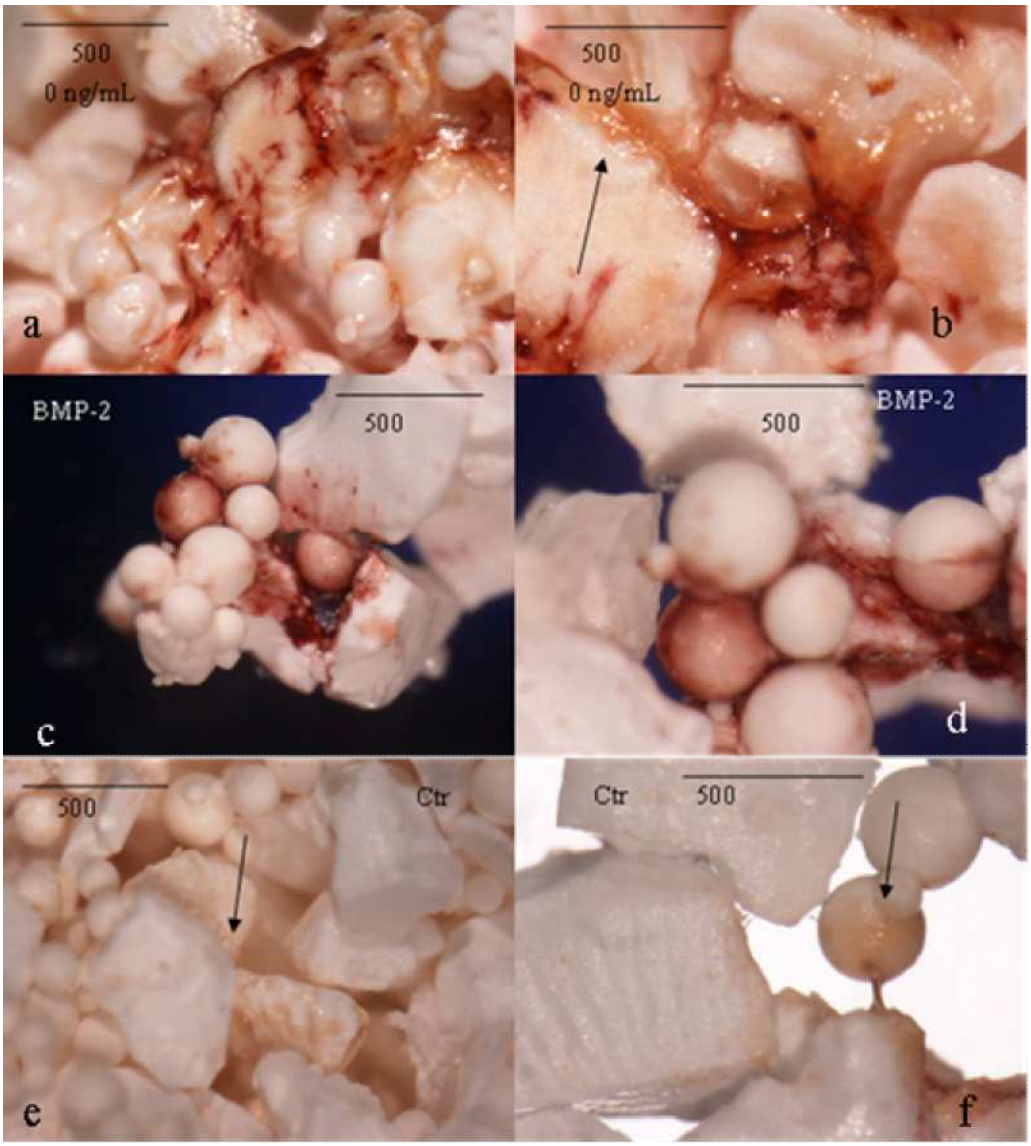

Figure 6-30 Alkaline phosphatase activity of C2C12 cells at day 28 on scaffolds (a, b) in standard media after rhBMP-2 supplement was withdrawn at day 18 (0 ng/mL), (c, d) BMP-2 loaded microspheres and (e, f) without growth factor (Ctrl). The arrows indicate areas of cell and matrix production where there were no alkaline phosphatase positive cells on the withdrawn supplemented scaffold and on the control.

Growth factors *in vivo* are bound to extracellular matrix and therefore function in a localized manner as part of a membrane complex. Simple tethering of growth factors to biomaterial surfaces can elicit a more potent response than the soluble form of the protein. Incorporation of growth factors into polymeric matrices can stabilize the protein and retain activity at the point of release [81, 155, 156]. Localized growth factor release and concentration have been previously demonstrated and diffusion gradients in 3-d structures have been documented [233, 257, 262].

6.4 Conclusion

This two component scaffold system has demonstrated both components to be capable of supporting cell attachment, proliferation and migration. Pore size controls nutrient diffusion and influences cell migration. In this system, control of pore size was achieved by restriction of particulate size distribution. The interconnectivity of this particulate system was demonstrated by cell migration from the outside into the scaffold. Scaffolds with different porosities can be tailored to fit different site requirements as bone is produced by intramembranous and endochondral ossification. The duration of experiments and proliferation results demonstrates the mildness of the *in situ* sintering process with cell suspension to develop mechanically strong structures. The potential for osteointegration was demonstrated by the cultivation of osteoblasts cells that rapidly synthesized calcium based deposits throughout the scaffold following *in*

situ seeding. Dexamethasone did not significantly up regulate alkaline phosphatase activity in mature osteoblasts or C2C12 cells; however, rhBMP-2 did significantly up regulate alkaline phosphatase activity in C2C12 cells in a dose dependent manner. Prolonged release of rhBMP-2 was demonstrated to induce and maintain differentiation of C2C12, for a sustained period of time from an *in situ* sintered scaffold without affecting proliferation. The scaffold has been demonstrated to have the potential to function as an injectable device with the ability to support *in situ* cell survival and invasion.

7 Final Conclusions

The strategy of tissue engineering utilises space filling scaffold materials that can support cells and deliver therapeutic agents. The ideal material needs to meet a range of requirements that include being biodegradable, osteoconductive, integrative, mechanically compatible with native bone and ideally osteoinductive. Injectable delivery systems are placed at the target site and interaction with the surrounding tissue is determined by surface area, diffusion, porosity and pore size. Injectable scaffolds have potential to deliver therapy cheaper, faster and arguably safer given the developing methods of minimally invasive surgery. The objective of this work was to develop an injectable scaffold system capable of cell and growth factor delivery. The strategy used a two component scaffold system that sintered at body temperature. Component I was multifunctional as a porous cell carrier and spacer that facilitated the hierarchical design of a macroporous system with additional functionality for controlled release.

In Chapter 3 the adhesive component II was refined using a combination of techniques to monitor thermal, physical and mechanical changes in polymer behaviour that defined the sintering regime needed to make three- dimensional structures. In Chapter 4 formulations were evaluated to determine the uniaxial compressive strengths, temperatures and rates at which structures were

formed. The prominent discovery here was the significant compressive strength developed by the wet sintered scaffold with Young's modulus within the range desired for applications in cancellous bone. Investigation of the wet sintering systems was fundamental in enabling the survival of suspended cells in a formulation that was shown to be injectable in Chapter 5. The solidification mechanism was demonstrated to occur over a clinically relevant timescale comparable with currently used bone cement. The process of bonding and densification is commonly used to make solid structures with changes in physical properties after sintering that include porosity loss after aggregation. The injectable scaffold proposed does not form a viscous gel, but a particulate skeleton system surrounded by low viscosity media without restricting diffusion. The proposed mechanism of wet sintering was by desorption using surface mobilisation of non-toxic PEG. Wet scaffold strength increased with sintering temperature.

In Chapter 5, the injectability through a simple syringe system showed the material to remain cohesive at constant loading and low carrier content. When the syringe was loaded to higher densities heterogeneous extrusion occurred. The two component system with restricted particle size distribution demonstrated that the control of porosity was positively correlated to particle size of the system. It showed that pore size distribution increased with particle size and a high content of pores > 100 μm was achieved in the scaffold with sieved particles > 300 μm in diameter.

The priority of preserving cell viability restricts the use of many materials to those compatible with living tissue. In Chapter 6 the interaction of scaffolds 5 mm in diameter with cells were examined. Both scaffold components were shown to support cell growth and migration. Cell additions to preformed scaffold surfaces were observed to spread and migrate to the centre of the structure with increased particle and pore size. *In situ* seeding and sintering showed cells to survive processing proliferate and colonise the structure. The survival of primary osteoblasts and their deposition of calcium based crystals onto the scaffold after 8 days in culture showed the surface to be osteoconductive. Cell growth and spreading on the solid PLGA adhesive particles was probably due to a combination of factors including surface topography created during particle size reduction by fracturing and PEG migration.

Surgery utilizes compression and immobilization for alignment between fracture surfaces to stimulate repair. Here swelling of the polymer may be utilized to tightly fit the interface to avoid issues of implant shrinkage and loosening. Press fitting also allows transmission of strain that directionally stimulates metabolism and growth, reflecting the native mechanical environment. The encapsulation and delivery of the differentiation factor rhBMP-2 over 28 days confirmed the scaffold to have potential as a cell carrier, template for tissue growth and therapeutic protein delivery.

The overall conclusions from the work presented here suggest that the two component scaffold design has significant potential to be developed into a therapeutic tissue engineered control delivery system with and without cells. Under the sintering conditions used, cell delivery and prolonged growth factor release were demonstrated. The materials used were of low toxic potential in the *in vitro* studies conducted. PEI was used as a modifier of the cell carrier component and could be replaced by alternative treatments. The materials can be manufactured on an industrial scale by well established procedures with known controllable process parameters. All reactions can occur within the normal range of body temperatures in the presence of cells without significant viability loss in dimensions that approach critical sized defects. The sintering process manipulates the response of the materials to temperature and time producing strong porous open celled scaffolds.

The biodegradable injectable scaffold system as presented has potential to be utilised as a therapeutic cell and protein delivery device to provide environmental cues to direct differentiation, template tissue growth and develop mechanical properties compatible with cancellous bone.

7.1 Future Work

The work presented in this thesis has looked at aspects of design, characterisation and simulation of use for this injectable scaffold system. This two component system has potential for multi-component release at different rates. The particulate scaffold system forms a predictably porous interconnected structure that may deliver cells, growth factors and other materials such as antibiotics and therapeutic actives. Substitution of component I with hydroxyapatite or bisphosphonates should be investigated to determine the localised impact on stem cell differentiation.

The ideal material needs to meet a range of requirements that change with time and the swelling behaviour may increase porosity and pore size in a temporal manner to satisfy the diffusion requirements of proliferating cells. In addition the influence of polymer swelling on attached cells should be investigated as it is a source of further mechanical stimulation. Evaluation of sintering conditions showed the strength of the scaffold to increase with temperature. The localised wound temperature due to inflammation can exceed 40°C and cell viability in these environments should be studied in mono and co-culture. The evaluation of endothelial with osteoblast cells may prove beneficial in aiding repair.

8 References

1. Vacanti, C.A., *History of tissue engineering and a glimpse into its future.* Tissue Eng, 2006. **12**(5): p. 1137-42.
2. Silva, G.A., et al., *Materials in particulate form for tissue engineering. 2. Applications in bone.* J Tissue Eng Regen Med, 2007. **1**(2): p. 97-109.
3. Vacanti, J.P., *Beyond transplantation. Third annual Samuel Jason Mixter lecture.* Arch Surg, 1988. **123**(5): p. 545-9.
4. Langer, R. and J.P. Vacanti, *Tissue engineering.* Science, 1993. **260**(5110): p. 920-6.
5. Green, H., J.G. Rheinwald, and T.T. Sun, *Properties of an epithelial cell type in culture: the epidermal keratinocyte and its dependence on products of the fibroblast.* Prog Clin Biol Res, 1977. **17**: p. 493-500.
6. Folkman, J. and C. Haudenschild, *Angiogenesis in vitro.* Nature, 1980. **288**(5791): p. 551-6.
7. Bonfield, W., *From concept to patient--biomaterials solutions to medical problems.* Med J Malaysia, 2004. **59 Suppl B**: p. 1.
8. Hubbell, J., *Biomaterials in tissue engineering.* Biotechnology (N Y), 1995. **13**(6): p. 565-76.
9. Hing, K.A., *Bone repair in the twenty-first century: biology, chemistry or engineering?* Philos Transact A Math Phys Eng Sci, 2004. **362**(1825): p. 2821-50.
10. Habibovic, P. and K. de Groot, *Osteoinductive biomaterials--properties and relevance in bone repair.* J Tissue Eng Regen Med, 2007. **1**(1): p. 25-32.
11. Furth, M.E., A. Atala, and M.E. Van Dyke, *Smart biomaterials design for tissue engineering and regenerative medicine.* Biomaterials, 2007. **28**(34): p. 5068-73.
12. Evans, C.H., et al., *Facilitated endogenous repair: making tissue engineering simple, practical, and economical.* Tissue Eng, 2007. **13**(8): p. 1987-93.
13. Spector, M., *Biomaterials-based tissue engineering and regenerative medicine solutions to musculoskeletal problems.* Swiss Med Wkly, 2007. **137 Suppl 155**: p. 157S-165S.
14. Currey, J., *Bone architecture and fracture.* Current osteoporosis Reports, 2005. **3**: p. 52-56.
15. Hilborn, J. and L.M. Bjursten, *A new and evolving paradigm for biocompatibility.* J Tissue Eng Regen Med, 2007. **1**(2): p. 110-9.
16. Davies, J.E., *Bone Engineering*, ed. J.E. Davies. 2000: Rainbow Graphic and Printing Ltd. .

17. Currey, J., *Bones Structure and mechancs*. Second edition ed. 2002, New Jersey: Princeton University Press.
18. Cen, L., et al., *Collagen tissue engineering: development of novel biomaterials and applications.* Pediatr Res, 2008. **63**(5): p. 492-6.
19. Li, X.J., Jee, W.S.S., *Current Topics in Bone Biology*, in *Integrated Bone Tissue Anatomy and Physiology* H. Deng, Liu, Y., Guo, C.,chen, D., Editor. 2005, World scientific publishing company: New Jersey.
20. Liebschner, M.A.K.W., M.A., *Optimization of bone engineering for load bearing applications*, in *Topics in Tissue engineering*, N.F. Ashammakhi, P., Editor. 2003, University of oulu.
21. Davies, J.E., *Understanding peri-implant endosseous healing.* J Dent Educ, 2003. **67**(8): p. 932-49.
22. Currey, J.D., *Bone strength: what are we trying to measure?* Calcif Tissue Int, 2001. **68**(4): p. 205-10.
23. Hench, L.L., Wilson, J. , *Introduction to bioceramics*. World scientific 1993: University of Florida.
24. Winwood, K., et al., *Strain patterns during tensile, compressive, and shear fatigue of human cortical bone and implications for bone biomechanics.* J Biomed Mater Res A, 2006. **79**(2): p. 289-97.
25. Robling, A.G., A.B. Castillo, and C.H. Turner, *Biomechanical and molecular regulation of bone remodeling.* Annu Rev Biomed Eng, 2006. **8**: p. 455-98.
26. Cowin, S.C., *Tissue growth and remodeling.* Annu Rev Biomed Eng, 2004. **6**: p. 77-107.
27. Davies, J.E., Hosseini, M.M., *Histodynamics of endosseous wound healing*, in *Bone engineering*, J.E. Davies, Editor. 2000, em squared incorporated: Toronto. p. 3-14.
28. Miller, S.C., Jee, W.S.,, *The bone lining cell: A distinct phenotype.* Calcified Tissue int., 1986. **41**.
29. Miller, S.C., et al., *Bone lining cells: structure and function.* Scanning Microsc, 1989. **3**(3): p. 953-60; discussion 960-1.
30. Burger, E.H., Lein Nulend, J., in *Principles of bone biology*, R.L.G. Bilezikian J.P, Editor. 2002. p. 101.
31. Schmid-Schonbein, G.W., *Analysis of inflammation.* Annu Rev Biomed Eng, 2006. **8**: p. 93-131.
32. Roth, J., et al., *Molecular aspects of fever and hyperthermia.* Neurol Clin, 2006. **24**(3): p. 421-39, v.
33. Gemmell, C.H., *Activation of platelets by in vitro whole blood contact with materials: increases in microparticle, procoagulant activity, and soluble P-selectin blood levels.* J Biomater Sci Polym Ed, 2001. **12**(8): p. 933-43.
34. Carano, R.A. and E.H. Filvaroff, *Angiogenesis and bone repair.* Drug Discov Today, 2003. **8**(21): p. 980-9.
35. Shapiro, F., *Bone development and its relation to fracture repair. The role of mesenchymal osteoblasts and surface osteoblasts.* Eur Cell Mater, 2008. **15**: p. 53-76.
36. Ross, F.P., *Cytokine regulation of osteoclast formation and function.* J Musculoskelet Neuronal Interact, 2003. **3**(4): p. 282-6; discussion 292-4.

37. Lee, S.H. and H. Shin, *Matrices and scaffolds for delivery of bioactive molecules in bone and cartilage tissue engineering.* Adv Drug Deliv Rev, 2007. **59**(4-5): p. 339-59.
38. Forriol, F. and F. Shapiro, *Bone development: interaction of molecular components and biophysical forces.* Clin Orthop Relat Res, 2005(432): p. 14-33.
39. Gautschi, O.P., S.P. Frey, and R. Zellweger, *Bone morphogenetic proteins in clinical applications.* ANZ J Surg, 2007. **77**(8): p. 626-31.
40. Bohner, M. *The gap between research and clinical application of bone substitutes*. in *European cells and materials*. 2007.
41. Agrawal, C.M. and K.A. Athanasiou, *Technique to control pH in vicinity of biodegrading PLA-PGA implants.* J Biomed Mater Res, 1997. **38**(2): p. 105-14.
42. Perren, S.M. *State of the art and future of bone repair*. in *European cells and materials* 2007.
43. Jacobs, C.R., *Primary cilia.* J Musculoskelet Neuronal Interact, 2007. **7**(4): p. 297-8.
44. Jacobs, C.R., et al., *Differential effect of steady versus oscillating flow on bone cells.* J Biomech, 1998. **31**(11): p. 969-76.
45. Tormala, P., T. Pohjonen, and P. Rokkanen, *Bioabsorbable polymers: materials technology and surgical applications.* Proc Inst Mech Eng [H], 1998. **212**(2): p. 101-11.
46. Chu, T.M., et al., *Segmental bone regeneration using a load-bearing biodegradable carrier of bone morphogenetic protein-2.* Biomaterials, 2007. **28**(3): p. 459-67.
47. Burwell, R.G., *Studies in the transplantation of bone VII. The Fresh Composite Homograft-Autograft of Cancellous Bone.* J Bone Joint Surg Br, 1964. **46-B**: p. 110-40.
48. Urist, M.R., *Bone: formation by autoinduction.* Science, 1965. **150**(698): p. 893-9.
49. Shin, M., et al., *Development of a biodegradable scaffold with interconnected pores by heat fusion and its application to bone tissue engineering.* J Biomed Mater Res A, 2008. **84**(3): p. 702-9.
50. Anderson, J.M., A. Rodriguez, and D.T. Chang, *Foreign body reaction to biomaterials.* Semin Immunol, 2008. **20**(2): p. 86-100.
51. Leung, V.Y., D. Chan, and K.M. Cheung, *Regeneration of intervertebral disc by mesenchymal stem cells: potentials, limitations, and future direction.* Eur Spine J, 2006. **15 Suppl 3**: p. S406-13.
52. Peter, S.J., et al., *Polymer concepts in tissue engineering.* J Biomed Mater Res, 1998. **43**(4): p. 422-7.
53. Geiger, M., R.H. Li, and W. Friess, *Collagen sponges for bone regeneration with rhBMP-2.* Adv Drug Deliv Rev, 2003. **55**(12): p. 1613-29.
54. Bodde, E.W., et al., *No Increased Bone Formation Around Alendronate or Omeprazole Loaded Bioactive Bone Cements in a Femoral Defect.* Tissue Eng, 2007.

55. Lickorish, D., L. Guan, and J.E. Davies, *A three-phase, fully resorbable, polyester/calcium phosphate scaffold for bone tissue engineering: Evolution of scaffold design.* Biomaterials, 2007. **28**(8): p. 1495-502.
56. Corsi, K.A., et al., *Regenerative medicine in orthopaedic surgery.* J Orthop Res, 2007. **25**(10): p. 1261-8.
57. Cancedda, R., P. Giannoni, and M. Mastrogiacomo, *A tissue engineering approach to bone repair in large animal models and in clinical practice.* Biomaterials, 2007. **28**(29): p. 4240-50.
58. Oest, M.E., et al., *Quantitative assessment of scaffold and growth factor-mediated repair of critically sized bone defects.* J Orthop Res, 2007. **25**(7): p. 941-50.
59. Athanasiou, K.A., G.G. Niederauer, and C.M. Agrawal, *Sterilization, toxicity, biocompatibility and clinical applications of polylactic acid/polyglycolic acid copolymers.* Biomaterials, 1996. **17**(2): p. 93-102.
60. Bonfield, W., *Designing porous scaffolds for tissue engineering.* Philos Transact A Math Phys Eng Sci, 2006. **364**(1838): p. 227-32.
61. Ripamonti, U. and L. Renton, *Bone morphogenetic proteins and the induction of periodontal tissue regeneration.* Periodontol 2000, 2006. **41**: p. 73-87.
62. McCarthy, T.L., Ji, C., and Centrella, M. , *Links among growth factors, hormones, and nuclear factors with essential roles in bone formation* Crit Rev Oral Biol Med 2000. **11**(4): p. 409-422.
63. Street, J., et al., *Vascular endothelial growth factor stimulates bone repair by promoting angiogenesis and bone turnover.* Proc Natl Acad Sci U S A, 2002. **99**(15): p. 9656-61.
64. Hollinger, J.O., et al., *Accelerated fracture healing in the geriatric, osteoporotic rat with recombinant human platelet-derived growth factor-BB and an injectable beta-tricalcium phosphate/collagen matrix.* J Orthop Res, 2008. **26**(1): p. 83-90.
65. Bilezikian, J.P., Raisz L.G, , *Principles of Bone biology*. 2000: Academic Press.
66. Jiang, T., W.I. Abdel-Fattah, and C.T. Laurencin, *In vitro evaluation of chitosan/poly(lactic acid-glycolic acid) sintered microsphere scaffolds for bone tissue engineering.* Biomaterials, 2006. **27**(28): p. 4894-903.
67. Hosseini, M.M., Sodek, J., Franke, R., Davies, J.E. , *The Bone-implant interface*, in *Bone Engineering*, J.E. Davies, Editor. 2000, Rainbow Graphics: Hong Kong. p. 295-304.
68. Ripamonti, U., C. Ferretti, and M. Heliotis, *Soluble and insoluble signals and the induction of bone formation: molecular therapeutics recapitulating development.* J Anat, 2006. **209**(4): p. 447-68.
69. Kloen, P., et al., *BMP signaling components are expressed in human fracture callus.* Bone, 2003. **33**(3): p. 362-71.
70. Mussano, F., et al., *Bone morphogenetic proteins and bone defects: a systematic review.* Spine, 2007. **32**(7): p. 824-30.
71. De Long, W.G., Jr., et al., *Bone grafts and bone graft substitutes in orthopaedic trauma surgery. A critical analysis.* J Bone Joint Surg Am, 2007. **89**(3): p. 649-58.

72. Gupta, M.C. and S.N. Khan, *Application of bone morphogenetic proteins in spinal fusion.* Cytokine Growth Factor Rev, 2005. **16**(3): p. 347-55.
73. Cheng, H., et al., *Osteogenic activity of the fourteen types of human bone morphogenetic proteins (BMPs).* J Bone Joint Surg Am, 2003. **85-A**(8): p. 1544-52.
74. Chen, D., M. Zhao, and G.R. Mundy, *Bone morphogenetic proteins.* Growth Factors, 2004. **22**(4): p. 233-41.
75. Partridge, K., et al., *Adenoviral BMP-2 gene transfer in mesenchymal stem cells: in vitro and in vivo bone formation on biodegradable polymer scaffolds.* Biochem Biophys Res Commun, 2002. **292**(1): p. 144-52.
76. Zhao, B., et al., *Heparin potentiates the in vivo ectopic bone formation induced by bone morphogenetic protein-2.* J Biol Chem, 2006. **281**(32): p. 23246-53.
77. Sodek, J., Cheifetz, S.,, *Molecular regulation of osteogenesis*, in *Bone Engineering*, D. JE, Editor. 2000, em Squared Inc.: Toronto. p. 31-43.
78. Siebers, M.C., et al., *Integrins as linker proteins between osteoblasts and bone replacing materials. A critical review.* Biomaterials, 2005. **26**(2): p. 137-46.
79. Hynes, R.O., *The emergence of integrins: a personal and historical perspective.* Matrix Biology, 2004. **23**(6): p. 333-340.
80. van Grunsven, L.A., et al., *Smads and chromatin modulation.* Cytokine Growth Factor Rev, 2005. **16**(4-5): p. 495-512.
81. Schmidmaier, G., et al., *Carrier systems and application of growth factors in orthopaedics.* Injury, 2008. **39 Suppl 2**: p. S37-43.
82. Han, D., et al., *Optimal delivery systems for bone morphogenetic proteins in orthopedic applications should model initial tissue repair structures by using a heparin-incorporated fibrin-fibronectin matrix.* Med Hypotheses, 2008. **71**(3): p. 374-8.
83. Gupta, M.C. and S. Maitra, *Bone grafts and bone morphogenetic proteins in spine fusion.* Cell Tissue Bank, 2002. **3**(4): p. 255-67.
84. Luginbuehl, V., et al., *Localized delivery of growth factors for bone repair.* Eur J Pharm Biopharm, 2004. **58**(2): p. 197-208.
85. Csiszar, A., et al., *Bone morphogenetic protein-2 induces proinflammatory endothelial phenotype.* Am J Pathol, 2006. **168**(2): p. 629-38.
86. Rose, F.R., Q. Hou, and R.O. Oreffo, *Delivery systems for bone growth factors - the new players in skeletal regeneration.* J Pharm Pharmacol, 2004. **56**(4): p. 415-27.
87. Alanay, A., et al., *The adjunctive effect of a binding peptide on bone morphogenetic protein enhanced bone healing in a rodent model of spinal fusion.* Spine, 2008. **33**(16): p. 1709-13.
88. Huang, Y.C., et al., *Combined angiogenic and osteogenic factor delivery enhances bone marrow stromal cell-driven bone regeneration.* J Bone Miner Res, 2005. **20**(5): p. 848-57.
89. Giannoudis, P.V., et al., *The diamond concept--open questions.* Injury, 2008. **39 Suppl 2**: p. S5-8.

90. Starr, A.J., *Fracture repair: successful advances, persistent problems, and the psychological burden of trauma.* J Bone Joint Surg Am, 2008. **90 Suppl 1**: p. 132-7.
91. Dahabreh, Z., et al., *A cost analysis of treatment of tibial fracture nonunion by bone grafting or bone morphogenetic protein-7.* Int Orthop, 2008.
92. Moss, M.L., *Extraction of an osteogenic inductor factor from bone.* Science, 1958. **127**(3301): p. 755-6.
93. Ripamonti, U., *Soluble osteogenic molecular signals and the induction of bone formation.* Biomaterials, 2006. **27**(6): p. 807-22.
94. Ripamonti, U., et al., *Bone induction by BMPs/OPs and related family members in primates.* J Bone Joint Surg Am, 2001. **83-A Suppl 1**(Pt 2): p. S116-27.
95. Agarwal, C.M., *Reconstructing the human body using biomaterials* Journal of the Minerals, Metals and Materials Society, 1998. **50**(1): p. 31-35
96. Quatela, V.C. and J. Chow, *Synthetic facial implants.* Facial Plast Surg Clin North Am, 2008. **16**(1): p. 1-10, v.
97. Sheridan, M.H., et al., *Bioabsorbable polymer scaffolds for tissue engineering capable of sustained growth factor delivery.* J Control Release, 2000. **64**(1-3): p. 91-102.
98. Cao, L. and D.J. Mooney, *Spatiotemporal control over growth factor signaling for therapeutic neovascularization.* Adv Drug Deliv Rev, 2007. **59**(13): p. 1340-50.
99. Yang, S., et al., *The design of scaffolds for use in tissue engineering. Part I. Traditional factors.* Tissue Eng, 2001. **7**(6): p. 679-89.
100. Whang, K., et al., *Engineering bone regeneration with bioabsorbable scaffolds with novel microarchitecture.* Tissue Eng, 1999. **5**(1): p. 35-51.
101. Williams, D.F., *To engineer is to create: the link between engineering and regeneration.* Trends Biotechnol, 2006. **24**(1): p. 4-8.
102. Graziano, A., et al., *Concave pit-containing scaffold surfaces improve stem cell-derived osteoblast performance and lead to significant bone tissue formation.* PLoS ONE, 2007. **2**(6): p. e496.
103. Warnke, P.H., et al., *Growth and transplantation of a custom vascularised bone graft in a man.* Lancet, 2004. **364**(9436): p. 766-70.
104. Chung, H.J. and T.G. Park, *Surface engineered and drug releasing pre-fabricated scaffolds for tissue engineering.* Adv Drug Deliv Rev, 2007. **59**(4-5): p. 249-62.
105. Davies, J.E., *Bone bonding at natural and biomaterial surfaces.* Biomaterials, 2007. **28**(34): p. 5058-67.
106. Kadow-Romacker, A., et al., *Effect of Mechanical Stimulation on Osteoblast- and Osteoclast-Like Cells in vitro.* Cells Tissues Organs, 2008.
107. Angele, P., et al., *Cyclic, mechanical compression enhances chondrogenesis of mesenchymal progenitor cells in tissue engineering scaffolds.* Biorheology, 2004. **41**(3-4): p. 335-46.
108. Diab, T. and D. Vashishth, *Effects of damage morphology on cortical bone fragility.* Bone, 2005. **37**(1): p. 96-102.

109. Mendes, V.C., R. Moineddin, and J.E. Davies, *The effect of discrete calcium phosphate nanocrystals on bone-bonding to titanium surfaces.* Biomaterials, 2007. **28**(32): p. 4748-55.
110. Holy, C.E., et al., *In vitro degradation of a novel poly(lactide-co-glycolide) 75/25 foam.* Biomaterials, 1999. **20**(13): p. 1177-85.
111. Holy, C.E., M.S. Shoichet, and J.E. Davies, *Engineering three-dimensional bone tissue in vitro using biodegradable scaffolds: investigating initial cell-seeding density and culture period.* J Biomed Mater Res, 2000. **51**(3): p. 376-82.
112. Kuboki, Y., et al., *BMP-induced osteogenesis on the surface of hydroxyapatite with geometrically feasible and nonfeasible structures: topology of osteogenesis.* J Biomed Mater Res, 1998. **39**(2): p. 190-9.
113. Karp, J.M., M.S. Shoichet, and J.E. Davies, *Bone formation on two-dimensional poly(DL-lactide-co-glycolide) (PLGA) films and three-dimensional PLGA tissue engineering scaffolds in vitro.* J Biomed Mater Res A, 2003. **64**(2): p. 388-96.
114. Rezwan, K., et al., *Biodegradable and bioactive porous polymer/inorganic composite scaffolds for bone tissue engineering.* Biomaterials, 2006. **27**(18): p. 3413-31.
115. Unger, R.E., et al., *Tissue-like self-assembly in cocultures of endothelial cells and osteoblasts and the formation of microcapillary-like structures on three-dimensional porous biomaterials.* Biomaterials, 2007. **28**(27): p. 3965-76.
116. Kaigler, D., et al., *Endothelial cell modulation of bone marrow stromal cell osteogenic potential.* Faseb J, 2005. **19**(6): p. 665-7.
117. Csiszar, A., et al., *Regulation of bone morphogenetic protein-2 expression in endothelial cells: role of nuclear factor-kappaB activation by tumor necrosis factor-alpha, H2O2, and high intravascular pressure.* Circulation, 2005. **111**(18): p. 2364-72.
118. Atala, A., *Engineering tissues, organs and cells.* Journal of Tissue Engineering and Regenerative Medicine, 2007. **1**(2): p. 83-96.
119. Hutmacher, D.W., et al., *State of the art and future directions of scaffold-based bone engineering from a biomaterials perspective.* J Tissue Eng Regen Med, 2007. **1**(4): p. 245-60.
120. Bensaid, W., et al., *A biodegradable fibrin scaffold for mesenchymal stem cell transplantation.* Biomaterials, 2003. **24**(14): p. 2497-502.
121. Patel, V.V., et al., *An in vitro and in vivo analysis of fibrin glue use to control bone morphogenetic protein diffusion and bone morphogenetic protein-stimulated bone growth.* Spine J, 2006. **6**(4): p. 397-403; discussion 404.
122. Le Nihouannen, D., Le Guehennec, L., Rouillon, T., Pilet, P., Bilban, M., Layrolle, P., Daculsi, G., *Micro-architecture of calcium phosphate granules and fibrin glue composites for bone tissue engineering* Biomaterials, 2006. **27**(13): p. 2716-2722.
123. Kong, H.J. and D.J. Mooney, *The effects of poly(ethyleneimine) (PEI) molecular weight on reinforcement of alginate hydrogels.* Cell Transplant, 2003. **12**(7): p. 779-85.

124. Yannas, I.V., *Similarities and differences between induced organ regeneration in adults and early foetal regeneration.* J R Soc Interface, 2005. **2**(5): p. 403-17.
125. Yu, X., et al., *Bioreactor-based bone tissue engineering: the influence of dynamic flow on osteoblast phenotypic expression and matrix mineralization.* Proc Natl Acad Sci U S A, 2004. **101**(31): p. 11203-8.
126. Kim, M., et al., *Muscle regeneration by adipose tissue-derived adult stem cells attached to injectable PLGA spheres.* Biochem Biophys Res Commun, 2006. **348**(2): p. 386-92.
127. Silva, G.A., P. Ducheyne, and R.L. Reis, *Materials in particulate form for tissue engineering. 1. Basic concepts.* J Tissue Eng Regen Med, 2007. **1**(1): p. 4-24.
128. Welkerling, H., et al., *Painful soft-tissue reaction to injectable Norian SRS calcium phosphate cement after curettage of enchondromas.* J Bone Joint Surg Br, 2003. **85**(2): p. 238-9.
129. Bodde, E.W., et al., *Bone regeneration of porous beta-tricalcium phosphate (Conduit TCP) and of biphasic calcium phosphate ceramic (Biosel) in trabecular defects in sheep.* J Biomed Mater Res A, 2007. **82**(3): p. 711-22.
130. Mastrogiacomo, M., et al., *Tissue engineering of bone: search for a better scaffold.* Orthod Craniofac Res, 2005. **8**(4): p. 277-84.
131. Kirkpatrick, C.J., et al., *Visions for regenerative medicine: interface between scientific fact and science fiction.* Artif Organs, 2006. **30**(10): p. 822-7.
132. Jones, J.R., P.D. Lee, and L.L. Hench, *Hierarchical porous materials for tissue engineering.* Philos Transact A Math Phys Eng Sci, 2006. **364**(1838): p. 263-81.
133. Wake, M.C., P.K. Gupta, and A.G. Mikos, *Fabrication of pliable biodegradable polymer foams to engineer soft tissues.* Cell Transplant, 1996. **5**(4): p. 465-73.
134. Conway, J.H., Sloan, N.J.H., *Sphere packings, lattice and groups* Third ed. 1998.
135. Aste, T., Weaire, D. , *The persuit of perfect packing*. 2000: Institute of Physics.
136. Okii, N., et al., *In vivo histological changes occurring in hydroxyapatite cranial reconstruction--case report.* Neurol Med Chir (Tokyo), 2001. **41**(2): p. 100-4.
137. Yuan, H., et al., *Use of an osteoinductive biomaterial as a bone morphogenetic protein carrier.* J Mater Sci Mater Med, 2001. **12**(9): p. 761-6.
138. Royce, S.M., M. Askari, and K.G. Marra, *Incorporation of polymer microspheres within fibrin scaffolds for the controlled delivery of FGF-1.* J Biomater Sci Polym Ed, 2004. **15**(10): p. 1327-36.
139. DeFail, A.J., et al., *Controlled release of bioactive TGF-beta 1 from microspheres embedded within biodegradable hydrogels.* Biomaterials, 2006. **27**(8): p. 1579-85.
140. Keshaw, H., A. Forbes, and R.M. Day, *Release of angiogenic growth factors from cells encapsulated in alginate beads with bioactive glass.* Biomaterials, 2005. **26**(19): p. 4171-9.

141. Hall, H., *Modified fibrin hydrogel matrices: both, 3D-scaffolds and local and controlled release systems to stimulate angiogenesis.* Curr Pharm Des, 2007. **13**(35): p. 3597-607.
142. Fischer, E.M., et al., *Bone formation by mesenchymal progenitor cells cultured on dense and microporous hydroxyapatite particles.* Tissue Eng, 2003. **9**(6): p. 1179-88.
143. Kofron, M.D. and C.T. Laurencin, *Bone tissue engineering by gene delivery.* Adv Drug Deliv Rev, 2006. **58**(4): p. 555-76.
144. Bodde, E.W., et al., *Investigation as to the osteoinductivity of macroporous calcium phosphate cement in goats.* J Biomed Mater Res B Appl Biomater, 2007. **83**(1): p. 161-8.
145. del Real, R.P., E. Ooms, J. G. C. Wolke 2, M. Vallet-Regí 1, J. A. Jansen *In vivo bone response to porous calcium phosphate cement* J Biomed Mater Res 2003. **65A**: p. 30-36.
146. Day, R.M., et al., *In vivo characterisation of a novel bioresorbable poly(lactide-co-glycolide) tubular foam scaffold for tissue engineering applications.* J Mater Sci Mater Med, 2004. **15**(6): p. 729-34.
147. Martins, A.M. *Natural origin scaffolds with with in situ gradual pore forming ability: development and characterisation*. in *7th World biomaterial congress*. 2004. Sidney Australia.
148. El-Amin, S.F., et al., *Integrin expression by human osteoblasts cultured on degradable polymeric materials applicable for tissue engineered bone.* J Orthop Res, 2002. **20**(1): p. 20-8.
149. Behravesh, E., K. Zygourakis, and A.G. Mikos, *Adhesion and migration of marrow-derived osteoblasts on injectable in situ crosslinkable poly(propylene fumarate-co-ethylene glycol)-based hydrogels with a covalently linked RGDS peptide.* J Biomed Mater Res A, 2003. **65**(2): p. 260-70.
150. Solchaga, L.A., et al., *Repair of osteochondral defects with hyaluronan- and polyester-based scaffolds.* Osteoarthritis Cartilage, 2005. **13**(4): p. 297-309.
151. Kleinschmidt, J.C., et al., *A multiphase system bone implant for regenerating the calvaria.* Plast Reconstr Surg, 1993. **91**(4): p. 581-8.
152. Liu, Y., et al., *Accelerated repair of cortical bone defects using a synthetic extracellular matrix to deliver human demineralized bone matrix.* J Orthop Res, 2006. **24**(7): p. 1454-62.
153. Borden, M., et al., *Tissue-engineered bone formation in vivo using a novel sintered polymeric microsphere matrix.* J Bone Joint Surg Br, 2004. **86**(8): p. 1200-8.
154. Hedberg, E.L., et al., *Controlled release of an osteogenic peptide from injectable biodegradable polymeric composites.* J Control Release, 2002. **84**(3): p. 137-50.
155. Taluja, A., Youn, Yu Seok., and Bae, You Han, *Novel approaches in microparticulate PLGA delivery systems encapsulating proteins.* J. Mater. Chem., 2007. **17**(38): p. 4002 - 4014.
156. Giteau, A., et al., *Reversible protein precipitation to ensure stability during encapsulation within PLGA microspheres.* Eur J Pharm Biopharm, 2008. **70**(1): p. 127-36.

157. Gibson, I.R., et al., *Effect of powder characteristics on the sinterability of hydroxyapatite powders.* J Mater Sci Mater Med, 2001. **12**(2): p. 163-71.
158. Jenkin, C.F., *Principle of dilatancy.* Proc. R. Soc.Lon A, 1931. **131**(816): p. 53-89.
159. Diego, R.B., et al., *Polymer scaffolds with interconnected spherical pores and controlled architecture for tissue engineering: fabrication, mechanical properties, and finite element modeling.* J Biomed Mater Res B Appl Biomater, 2007. **81**(2): p. 448-55.
160. Brophy, J.H., Rose, R.M., Wulff, J., *The Structure and properties of Materials :Thermodynamics of Structure*. Vol. II. 1964: Wiley.
161. German, R.M., *Theory of in situ strength evaluation during sintering.* Science of sintering, 2000. **32 Special issue**: p. 17-31.
162. German, R.M., *Liquid Phase Sintering*. 1985, New York: Plenum Press. 240.
163. Antonov, E.N., et al., *Three-Dimensional Bioactive and Biodegradable Scaffolds Fabricated by Surface-Selective Laser Sintering.* Adv Mater Deerfield, 2004. **17**(3): p. 327-330.
164. German, R.M., *Sintering Theory and Practice*. 1996, Toronto: John Wiley & son inc. 550.
165. Hollister, S.J., *Porous scaffold design for tissue engineering.* Nat Mater, 2005. **4**(7): p. 518-24.
166. Brown, J.L., L.S. Nair, and C.T. Laurencin, *Solvent/non-solvent sintering: A novel route to create porous microsphere scaffolds for tissue regeneration.* J Biomed Mater Res B Appl Biomater, 2007.
167. Rosenzweig, N., Narkis, M., *Sintering rheology of amorphous polymers.* Polymer Engineering And Science, 1981. **21**(17): p. 1167-72.
168. Coulson, J.M., Richardson, J.R., Backhurst J.R., Harker, J.H., *Chemical engineering Particle technology and separation* 4th Edition ed. Vol. Volume II 1991.
169. Fakhraai, Z. and J.A. Forrest, *Measuring the surface dynamics of glassy polymers.* Science, 2008. **319**(5863): p. 600-4.
170. German, R.M., *Rheological model for viscous flow densification during supersolidus liquid phase sintering.* Science of sintering, 2006. **38**(1): p. 27-40.
171. Zhang, J., Roberts, C.J., Shakesheff, K.M., Davies, M.C.,Tendler, S.J.B., *Micro- and macrothemal analysis of bioactive surface-engineered polymer formed by physical entrapment of poly(ethylene glycol) into poly(lactic acid).* Macromolecules., 2003. **36**: p. 1215-1221.
172. Gilding, D.K., Reed, A.M. , *Biodegradable polymers for use in surgery - polyglycolic/poly (lactic acid) homo and copoymers:1.* Polymer, 1979. **20**: p. 1459-1464.
173. Tormala, P., *Biodegradable self-reinforced composite materials; manufacturing structure and mechanical properties.* Clin Mater, 1992. **10**(1-2): p. 29-34.
174. Cutright, D.E. and E.E. Hunsuck, *The repair of fractures of the orbital floor using biodegradable polylactic acid.* Oral Surg Oral Med Oral Pathol, 1972. **33**(1): p. 28-34.

175. Ratner, B.D., Hoffman, A.S., Schoen, F.J., Lemons, J.E., , *Biomaterials Science : an introduction to materials in medicine*. 2nd ed., ed. 2004: Elsevier Academic press.
176. Coombes, A.G. and J.D. Heckman, *Gel casting of resorbable polymers. 1. Processing and applications.* Biomaterials, 1992. **13**(4): p. 217-24.
177. Hu, Y., et al., *Fabrication of poly(alpha-hydroxy acid) foam scaffolds using multiple solvent systems.* J Biomed Mater Res, 2002. **59**(3): p. 563-72.
178. Freiberg, S. and X.X. Zhu, *Polymer microspheres for controlled drug release.* Int J Pharm, 2004. **282**(1-2): p. 1-18.
179. Hollinger, J.O., *Preliminary report on the osteogenic potential of a biodegradable copolymer of polyactide (PLA) and polyglycolide (PGA).* J Biomed Mater Res, 1983. **17**(1): p. 71-82.
180. El-Amin, S.F., et al., *Human osteoblast cells: isolation, characterization, and growth on polymers for musculoskeletal tissue engineering.* J Biomed Mater Res A, 2006. **76**(3): p. 439-49.
181. Borden, M., Attawia, M., Laurencin, C.T. , *The sintered microsphere matrix for bone tissue engineering: In vitro osteoconductivity studies* Journal of Biomedical Materials Research Part B: Applied Biomaterials, 2002. **61**(3): p. 421 - 429.
182. El-Amin, S.F., et al., *Extracellular matrix production by human osteoblasts cultured on biodegradable polymers applicable for tissue engineering.* Biomaterials, 2003. **24**(7): p. 1213-21.
183. Borden, M., et al., *Structural and human cellular assessment of a novel microsphere-based tissue engineered scaffold for bone repair.* Biomaterials, 2003. **24**(4): p. 597-609.
184. Kang, S.W., O. Jeon, and B.S. Kim, *Poly(lactic-co-glycolic acid) microspheres as an injectable scaffold for cartilage tissue engineering.* Tissue Eng, 2005. **11**(3-4): p. 438-47.
185. Kang, S.W., et al., *The use of poly(lactic-co-glycolic acid) microspheres as injectable cell carriers for cartilage regeneration in rabbit knees.* J Biomater Sci Polym Ed, 2006. **17**(8): p. 925-39.
186. Ren, J., et al., *Repair of mandibular defects using MSCs-seeded biodegradable polyester porous scaffolds.* J Biomater Sci Polym Ed, 2007. **18**(5): p. 505-17.
187. Athanasiou, K.A., et al., *Orthopaedic applications for PLA-PGA biodegradable polymers.* Arthroscopy, 1998. **14**(7): p. 726-37.
188. Tracy, M.A., et al., *Factors affecting the degradation rate of poly(lactide-co-glycolide) microspheres in vivo and in vitro.* Biomaterials, 1999. **20**(11): p. 1057-62.
189. Hedberg, E.L., et al., *In vitro degradation of porous poly(propylene fumarate)/poly(DL-lactic-co-glycolic acid) composite scaffolds.* Biomaterials, 2005. **26**(16): p. 3215-25.
190. De Jong, S.J., ARIAS, E. R., RIJKERS, D. T. S., VAN NOSTRUM, C. F., KETTENES-VAN DEN BOSCH, J. J., HENNINK W. E. ; , *New insights into the hydrolytic degradation of poly(lactic acid): participation of the alcohol terminus.* Polymer, 2001. **42**: p. 2795-2802.

191. Lu, L., C.A. Garcia, and A.G. Mikos, *In vitro degradation of thin poly(DL-lactic-co-glycolic acid) films.* J Biomed Mater Res, 1999. **46**(2): p. 236-44.
192. Siepmann, J., et al., *How autocatalysis accelerates drug release from PLGA-based microparticles: a quantitative treatment.* Biomacromolecules, 2005. **6**(4): p. 2312-9.
193. Nair, P., P. R. and J. Schug, *Observations on healing of human tooth extraction sockets implanted with bioabsorbable polylactic-polyglycolic acids (PLGA) copolymer root replicas: a clinical, radiographic, and histologic follow-up report of 8 cases.* Oral Surg Oral Med Oral Pathol Oral Radiol Endod, 2004. **97**(5): p. 559-69.
194. Zhang, Y., et al., *Effects of metal salts on poly(DL-lactide-co-glycolide) polymer hydrolysis.* J Biomed Mater Res, 1997. **34**(4): p. 531-8.
195. Ceonzo, K., et al., *Polyglycolic acid-induced inflammation: role of hydrolysis and resulting complement activation.* Tissue Eng, 2006. **12**(2): p. 301-8.
196. Mercier, N.R., et al., *A novel injectable approach for cartilage formation in vivo using PLG microspheres.* Ann Biomed Eng, 2004. **32**(3): p. 418-29.
197. Ding, A.G. and S.P. Schwendeman, *Determination of water-soluble acid distribution in poly(lactide-co-glycolide).* J Pharm Sci, 2004. **93**(2): p. 322-31.
198. Arnett, T.R., *Extracellular pH regulates bone cell function.* J Nutr, 2008. **138**(2): p. 415S-418S.
199. Palade, L., Lehermeier, H. J., ; Dorgan, John R. , *Melt rheology of high L-content poly(lactic acid).* Macromolecules 2001. **34**(5): p. 1384-90.
200. Jacobsen, S.F., H. G. , *Plasticizing polylactide - The effect of different plasticizers on the mechanical properties.* Polymer Engineering And Science 1999. **39**: p. 1303-1310.
201. Martin, O., Averous, L, *Poly(lactic acid):plasticization and properties of biodegradable muliphase system.* Polymer, 2001. **42**: p. 6209.
202. Ren, T., et al., *The bone formation in vitro and mandibular defect repair using PLGA porous scaffolds.* J Biomed Mater Res A, 2005. **74**(4): p. 562-9.
203. Hancock, B.C., S.L. Shamblin, and G. Zografi, *Molecular mobility of amorphous pharmaceutical solids below their glass transition temperatures.* Pharm Res, 1995. **12**(6): p. 799-806.
204. Wu, L., Zhang, J., Jing, D. and Ding, J, *"Wet-state" mechanical properties of three-dimensional polyester porous scaffolds.* J. Biomed. Mater. Res A 2006. **76**(2): p. 264-71.
205. Woodle, M.C., M.S. Newman, and J.A. Cohen, *Sterically stabilized liposomes: physical and biological properties.* J Drug Target, 1994. **2**(5): p. 397-403.
206. Deng, M. and K.E. Uhrich, *Effects of in vitro degradation on properties of poly(DL-lactide-co-glycolide) pertinent to its biological performance.* J Mater Sci Mater Med, 2002. **13**(11): p. 1091-6.
207. An, J.H., KIM, H. S., CHUNG, D. J., LEE, D. S. & KIM, S. , *Thermal behaviour of poly(epsilon-caprolactone)-poly(ethylene glycol)-poly(epsilon-caprolactone) tri-block copolymers.* 2001. **36**: p. 715-722.
208. Loret, S., et al., *Analysis of PEG 400 and 4000 in urine for gut permeability assessment using solid phase extraction and gel permeation chromatography*

with refractometric detection. J Chromatogr B Analyt Technol Biomed Life Sci, 2004. **805**(2): p. 195-202.
209. Lockard, J.S. and R.H. Levy, *Polyethylene glycol 400: solvent and anticonvulsant?* Life Sci, 1978. **23**(25): p. 2499-502.
210. Lahooti, S. and M.V. Sefton, *Microencapsulation of normal and transfected L929 fibroblasts in a HEMA-MMA copolymer.* Tissue Eng, 2000. **6**(2): p. 139-49.
211. Pillin, I., Nicolas, A., Montrelaya, and Grohensa, Y., *Thermo-mechanical characterization of plasticized PLA: Is the miscibility the only significant factor?* . Polymer, 2006. **47**(13): p. 4676-4682
212. Harris, J.M., Zalipsky S., , *Poly(ethylene glycol): chemistry and biological applications*. 1997: American Chemical Society.
213. Herold, D.A., K. Keil, and D.E. Bruns, *Oxidation of polyethylene glycols by alcohol dehydrogenase.* Biochem Pharmacol, 1989. **38**(1): p. 73-6.
214. kulinski, Z., Piorkowska, E., *Crystallization, structure and properies of plasticized poly (l-lactide)* Polymer, 2005. **46**: p. 10290-10300.
215. Gines, J.M., Arias, M. J., Rabasco, A. M., Novak, C., RUIZCONDE, A. & SANCHEZSOTO, P. J. , *Thermal characterization of polyethylene glycols applied in the pharmaceutical technology using differential scanning calorimetry and hot stage microscopy.* Journal Of Thermal Analysis 1996. **46**: p. 291-304.
216. Hu, Y., Rogunova, M., Topolkaraev, V., Hiltner,A., Baer, E., *Aging of poly(lactide)/poly(ethylene glycol) blends. Part 1. Poly(lactide) with low stereoregularity.* Polymer, 2003. **44**: p. 5701-5710.
217. Hatakeyama, T., *Applications of Thermal Analysis.*, in *Thermal Analysis: Fundamentals and Applications to Polymer Science* F.X. Quinn, Editor. 1994, John Wiley & Sons. p. 168.
218. Hunt, B.J., James, M.I.,, *Polymer characterisation.* , ed. B.J. Hunt, James, M.I., . 1993, Glasgow,: Blackie (Chapman & Hall) Academic and Professional. 362.
219. Garcia, J.T., Fariña JB, Munguía O, Llabrés M., *Comparative degradation study of biodegradable microspheres of poly(DL-lactide-co-glycolide) with poly(ethyleneglycol) derivates.* J Microencapsul., 1999. **16**((1)): p. 83-94.
220. Santovena, A., et al., *Structural properties of biodegradable polyesters and rheological behaviour of their dispersions and films.* J Biomater Sci Polym Ed, 2005. **16**(5): p. 629-41.
221. Woodle, M.C., C.M. Engbers, and S. Zalipsky, *New amphipatic polymer-lipid conjugates forming long-circulating reticuloendothelial system-evading liposomes.* Bioconjug Chem, 1994. **5**(6): p. 493-6.
222. Benoit, J.P., Vonarbourg, A., Passirani, C., Saulnier, P. , *Parameters influencing the stealthiness of colloidal drug delivery systems.* Biomaterials, 2006. **27**: p. 4356-4373.
223. Anseth, K.S., V.R. Shastri, and R. Langer, *Photopolymerizable degradable polyanhydrides with osteocompatibility.* Nat Biotechnol, 1999. **17**(2): p. 156-9.

224. Stanczyk, M. and B. van Rietbergen, *Thermal analysis of bone cement polymerisation at the cement-bone interface.* J Biomech, 2004. **37**(12): p. 1803-10.
225. Temenoff, J.S. and A.G. Mikos, *Injectable biodegradable materials for orthopedic tissue engineering.* Biomaterials, 2000. **21**(23): p. 2405-12.
226. Temenoff, J.S., et al., *In vitro cytotoxicity of redox radical initiators for cross-linking of oligo(poly(ethylene glycol) fumarate) macromers.* Biomacromolecules, 2003. **4**(6): p. 1605-13.
227. Payne, R.G., et al., *Development of an injectable, in situ crosslinkable, degradable polymeric carrier for osteogenic cell populations. Part 3. Proliferation and differentiation of encapsulated marrow stromal osteoblasts cultured on crosslinking poly(propylene fumarate).* Biomaterials, 2002. **23**(22): p. 4381-7.
228. Hou, Q.P., De Bank, P. A. & Shakesheff, K. M. , *Injectable scaffolds for tissue regeneration.* Journal of Materials Chemistry 2004. **14**: p. 1915-1923.
229. Vernon, B., Gutowska, S.W., Kim, Y., Bae, Y.H. , Macromolecular Symp., 1996. **109**: p. 155-167.
230. Lin, H.H., and Cheng, Y.L. , *In-Situ Thermoreversible Gelation of Block and Star Copolymers of Poly(ethylene glycol) and Poly(N-isopropylacrylamide) of Varying Architectures.* Macromolecules, 2001. **34**: p. 3710-3715.
231. Alexander, C.a.S., KM *Responsive Polymers at the Biology/Materials Science Interface.* Adv. Mat., 2006. **18**(24): p. 3321-3328.
232. Saito, N., et al., *New synthetic absorbable polymers as BMP carriers: plastic properties of poly-D,L-lactic acid-polyethylene glycol block copolymers.* J Biomed Mater Res, 1999. **47**(1): p. 104-10.
233. Saito, N. and K. Takaoka, *New synthetic biodegradable polymers as BMP carriers for bone tissue engineering.* Biomaterials, 2003. **24**(13): p. 2287-93.
234. Salem, A.K., Rose, F.R.A.J., Oreffo, R.O.C., Yang,X., Davies, M.C., Mitchell,J.R., Roberts,C.J., Stolnik-Trenkic, S., Tendler, S.J.B., Williams,P.M., Shakesheff, K.M. , *Porous Polymer and Cell Composites That Self-Assemble In Situ.* advanced materials, 2003. **15**(3): p. 210-213.
235. Lin, C.Y., Kikuchi, N. & Hollister, S. J. , *A novel method for biomaterial scaffold internal architecture design to match bone elastic properties with desired porosity.* Journal Of Biomechanics 2004. **37**: p. 37, 623-636.
236. Karageorgiou, V. and D. Kaplan, *Porosity of 3D biomaterial scaffolds and osteogenesis.* Biomaterials, 2005. **26**(27): p. 5474-91.
237. Mikos, A.G., et al., *Preparation of poly(glycolic acid) bonded fiber structures for cell attachment and transplantation.* J Biomed Mater Res, 1993. **27**(2): p. 183-9.
238. Kuboki, Y., et al., *Two distinctive BMP-carriers induce zonal chondrogenesis and membranous ossification, respectively; geometrical factors of matrices for cell-differentiation.* Connect Tissue Res, 1995. **32**(1-4): p. 219-26.
239. Otsuki, B., et al., *Pore throat size and connectivity determine bone and tissue ingrowth into porous implants: three-dimensional micro-CT based structural analyses of porous bioactive titanium implants.* Biomaterials, 2006. **27**(35): p. 5892-900.

240. Goldstein, A.S., et al., *Effect of osteoblastic culture conditions on the structure of poly(DL-lactic-co-glycolic acid) foam scaffolds.* Tissue Eng, 1999. **5**(5): p. 421-34.
241. Guan, L. and J.E. Davies, *Preparation and characterization of a highly macroporous biodegradable composite tissue engineering scaffold.* J Biomed Mater Res A, 2004. **71**(3): p. 480-7.
242. Hulbert, S.F., et al., *Potential of ceramic materials as permanently implantable skeletal prostheses.* J Biomed Mater Res, 1970. **4**(3): p. 433-56.
243. Ikada, Y., *Challenges in tissue engineering.* J R Soc Interface, 2006. **3**(10): p. 589-601.
244. Jones, A.C., et al., *Assessment of bone ingrowth into porous biomaterials using MICRO-CT.* Biomaterials, 2007. **28**(15): p. 2491-504.
245. Rose, F.R., et al., *In vitro assessment of cell penetration into porous hydroxyapatite scaffolds with a central aligned channel.* Biomaterials, 2004. **25**(24): p. 5507-14.
246. Kuboki, Y., Q. Jin, and H. Takita, *Geometry of carriers controlling phenotypic expression in BMP-induced osteogenesis and chondrogenesis.* J Bone Joint Surg Am, 2001. **83-A Suppl 1**(Pt 2): p. S105-15.
247. Roosa, S.M., et al., *The pore size of polycaprolactone scaffolds has limited influence on bone regeneration in an in vivo model.* J Biomed Mater Res A, 2009.
248. Klawitter, J., Hulbert, S., *Application of porous ceramics for the attachment of load bearing internal orthopedic applicatins* J. Biomed. Mater. Res A, 1971. **2**: p. 161-229.
249. Dunne, N.J., et al., *The relationship between porosity and fatigue characteristics of bone cements.* Biomaterials, 2003. **24**(2): p. 239-45.
250. Currey, J., *Whole-bone mechanics: 'The best is the enemy of the good'.* Vet J, 2007.
251. Discher, D.E., P. Janmey, and Y.L. Wang, *Tissue cells feel and respond to the stiffness of their substrate.* Science, 2005. **310**(5751): p. 1139-43.
252. Cancedda, R., et al., *Bulk and interface investigations of scaffolds and tissue-engineered bones by X-ray microtomography and X-ray microdiffraction.* Biomaterials, 2007. **28**(15): p. 2505-24.
253. Colnot, C., et al., *Molecular analysis of healing at a bone-implant interface.* J Dent Res, 2007. **86**(9): p. 862-7.
254. Waters, S.L., et al., *Tissue growth in a rotating bioreactor. Part I: mechanical stability.* Math Med Biol, 2006. **23**(4): p. 311-37.
255. Barry, J., Howard, D., Shakesheff, K.M., Howdle,S., Alexander, M.R.,, *Using a Core-Sheath Distribution of Surface Chemistry through 3D Tissue Engineering Scaffolds to Control Cell Ingress.* Advanced Materials, 2006. **18**(11): p. 1406-10.
256. Stevens, M.M., et al., *In vivo engineering of organs: the bone bioreactor.* Proc Natl Acad Sci U S A, 2005. **102**(32): p. 11450-5.
257. Suciati, T., et al., *Zonal release of proteins within tissue engineering scaffolds.* J Mater Sci Mater Med, 2006. **17**(11): p. 1049-56.

258. Jaklenec, A., et al., *Novel scaffolds fabricated from protein-loaded microspheres for tissue engineering.* Biomaterials, 2008. **29**(2): p. 185-92.
259. Kreuter, J., *Evaluation of nanoparticles as drug-delivery systems. III: materials, stability, toxicity, possibilities of targeting, and use.* Pharm Acta Helv, 1983. **58**(9-10): p. 242-50.
260. Beck, L.R., Pope, V.Z., Tice, T.R., Gilley, RM., *Long-acting injectable microsphere formulation for the parenteral administration of levonorgestrel.* Adv Contracept, 1985. **1**(2): p. 119-29.
261. Langer, R. and M. Moses, *Biocompatible controlled release polymers for delivery of polypeptides and growth factors.* J Cell Biochem, 1991. **45**(4): p. 340-5.
262. Schmidmaier, G., et al., *Bone morphogenetic protein-2 coating of titanium implants increases biomechanical strength and accelerates bone remodeling in fracture treatment: a biomechanical and histological study in rats.* Bone, 2002. **30**(6): p. 816-22.
263. Strahm, B., Plattner, B., Huber, G., Rokey, G., *Application of Food Polymer Science and Capillary Rheometry in Evaluating Complex Extruded Products.* . Cereal Foods World. , 2000. **45**(7).
264. Strahm, B., *Fundamentals of polymer science as an applied extrusion tool.* Cereal Foods World, 1998. **43**(8): p. 621-25.
265. O'Brien, J., et al., *Investigation of the Alamar Blue (resazurin) fluorescent dye for the assessment of mammalian cell cytotoxicity.* Eur J Biochem, 2000. **267**(17): p. 5421-6.
266. Gonzalez, R.J. and J.B. Tarloff, *Evaluation of hepatic subcellular fractions for Alamar blue and MTT reductase activity.* Toxicol In Vitro, 2001. **15**(3): p. 257-9.
267. Petrenko, Y.A., et al., *The reduction of Alamar Blue by peripheral blood lymphocytes and isolated mitochondria.* Ukr Biokhim Zh, 2005. **77**(5): p. 100-5.
268. Ritman, E.L., *Micro-computed tomography—current status and developments.* Annual Review of Biomedical Engineering, 2004. **6**: p. 185-208.
269. Stock, S.R., *Recent advances in X-ray microtomography applied to materials* International Materials Reviews 2008. **53**(3): p. 129-181.
270. Boyd, L.M. and A.J. Carter, *Injectable biomaterials and vertebral endplate treatment for repair and regeneration of the intervertebral disc.* Eur Spine J, 2006. **15 Suppl 3**: p. S414-21.
271. Bonzani, I.C., et al., *Synthesis of two-component injectable polyurethanes for bone tissue engineering.* Biomaterials, 2007. **28**(3): p. 423-33.
272. Niemela, T., et al., *Self-reinforced composites of bioabsorbable polymer and bioactive glass with different bioactive glass contents. Part I: Initial mechanical properties and bioactivity.* Acta Biomater, 2005. **1**(2): p. 235-42.
273. Hu, Y., Rogunova, M., Topolkaraev, V., Hiltner, A., Bare, E., *Ageing of poly (lactide)/ poly (ethylene glycol) blends.Part 1. Poly (lactide) with low stereoregularity.* Polymer, 2003. **44**: p. 5701-5710.

274. Shimada, K., Kato, H., Saito,T., *Precise measurement of the self-diffusion coefficient for poly(ethylene glycol) in aqueous solution using uniform oligomers.* J. Chem. Phys. , 2005. **122**(24): p. 244914.
275. Hu, Y., Hu, Y. S., Topolkaraev, V., Hiltner, A., Baer, E., *Aging of poly(lactide)/poly(ethylene glycol) blends. Part 2. Poly(lactide) with high stereoregularity.* Polymer, 2003. **44**(19): p. 5711-20.
276. Kulinski, Z., et al., *Plasticization of poly(L-lactide) with poly(propylene glycol).* Biomacromolecules, 2006. **7**(7): p. 2128-35.
277. Chen, H.Y., Chum, S.P., Hiltner, A., Baer, E.,, *Phase Behavior of Partially Miscible Ethylene−Styrene Copolymer Blends.* Macromolecules, 2001. **34**(12): p. 4033–4042.
278. Plattner, B., Strahm, B., Rausch, K, *The Phase Transition Analyzer and its impact on extrusion processing of Food stuffs*, in *American Society of Agricultural Engineers*. 2001, ASAE: California, USA.
279. Wetton, R.E., *Thermomechanical methods*, in *Handbook of Thermal Analysis and Calorimetry,*, M.E. Brown, Editor. 1998. p. 363-399.
280. Murphy, W.L. and D.J. Mooney, *Bioinspired growth of crystalline carbonate apatite on biodegradable polymer substrata.* J Am Chem Soc, 2002. **124**(9): p. 1910-7.
281. Thomson, R.C., et al., *Fabrication of biodegradable polymer scaffolds to engineer trabecular bone.* J Biomater Sci Polym Ed, 1995. **7**(1): p. 23-38.
282. Wu, L., et al., *Fabrication of three-dimensional porous scaffolds of complicated shape for tissue engineering. I. Compression molding based on flexible-rigid combined mold.* Tissue Eng, 2005. **11**(7-8): p. 1105-14.
283. Jones, J.R., et al., *Extracellular matrix formation and mineralization on a phosphate-free porous bioactive glass scaffold using primary human osteoblast (HOB) cells.* Biomaterials, 2007. **28**(9): p. 1653-63.
284. Cowin, S.C., *Bone Mechanics Handbok*. 2nd ed. 2001: CRC Press.
285. Liebschner, M.A. and T.S. Keller, *Hydraulic strengthening affects the stiffness and strength of cortical bone.* Ann Biomed Eng, 2005. **33**(1): p. 26-38.
286. Knight, M.M., et al., *Mechanical compression and hydrostatic pressure induce reversible changes in actin cytoskeletal organisation in chondrocytes in agarose.* J Biomech, 2006. **39**(8): p. 1547-51.
287. Ghosh, K. and D.E. Ingber, *Micromechanical control of cell and tissue development: implications for tissue engineering.* Adv Drug Deliv Rev, 2007. **59**(13): p. 1306-18.
288. Bohner, M., U. Gbureck, and J.E. Barralet, *Technological issues for the development of more efficient calcium phosphate bone cements: a critical assessment.* Biomaterials, 2005. **26**(33): p. 6423-9.
289. Bohner, M., *Reactivity of calcium phosphate cements.* J. Mater. Chem.,, 2007. **17**(38): p. 3980 - 3986.
290. Lestel, L., Guegan, P., Boileau, S., Cheradame,H., Laupretre, F., *Influence of the chemical nature of cross-links on the local dynamics of bulk poly(ethylene oxide) networks as studied by carbon-13 NMR at temperatures*

well above the glass-transition temperature. Macromolecules, 1992. **25**(22): p. 6024-28.
291. Berkowicz, B.D., Peppas, N.A. , *Characterization of surgical adhesives from UV-polymerized poly(PEG dimethacrylate-co-2-hydroxyethyl methacrylate) copolymers* Journal of Applied Polymer Science 2003. **56**(6): p. 715-20.
292. Jaycock, M.J., *Properties of the solid-liquid interface of relevance to dispersion*, in *Dispersion of Powders in Liquid*, G.D. Parfitt, Editor. 1981, Applied science London.
293. Tiberg, F., Daici, J., Froberg, J., *Surface Chemistry of Paper* in *Handbook of Aplied Surface and Colloid chemistry*, K. Holmberg, Editor. 2001, John Wiley & Sons. p. 121-173.
294. Younes, H., et al., *Biodegradable PELA block copolymers: in vitro degradation and tissue reaction.* Biomater Artif Cells Artif Organs, 1988. **16**(4): p. 705-19.
295. Willauer, H.D., Huddleston, J.G., Rogers, R.D.,, *Solvent Properties of Aqueous Biphasic Systems Composed of Polyethylene Glycol and Salt Characterized by the Free Energy of Transfer of a Methylene Group between the Phases and by a Linear Solvation Energy Relationship.* Ind.Eng. Chem. Res., 2002. **41**(11): p. 2591-2601.
296. Willauer, H.D., Huddleston, J.G., Rogers, R.D.,, *Solute Partitioning in Aqueous Biphasic Systems Composed of Polyethylene Glycol and Salt: The Partitioning of Small Neutral Organic Species.* Ind.Eng. Chem. Res., 2002. **41**: p. 1892-1904.
297. Sadeghi, R., Ziamajidi, F., *Thermodynamic properties of aqueous polypropylene oxide 400 solutions from isopiestic measurements over a range of temperatures.* Fluid Phase Equilibra, 2006. **249**(1-2): p. 169-72.
298. Kasemo, B., *Biological surface science.* Surface Science, 2002. **500**: p. 656-677.
299. Zhang, Y. and P.S. Cremer, *Interactions between macromolecules and ions: The Hofmeister series.* Curr Opin Chem Biol, 2006. **10**(6): p. 658-63.
300. Stellwagen, E., E. Olivieri, and P.G. Righetti, *Salt-promoted protein folding, preferential binding, or electrostatic screening?* Proteins, 2002. **49**(2): p. 147-53.
301. Kranz, H., et al., *Physicomechanical properties of biodegradable poly(D,L-lactide) and poly(D,L-lactide-co-glycolide) films in the dry and wet states.* J Pharm Sci, 2000. **89**(12): p. 1558-66.
302. Blasi, P., et al., *Plasticizing effect of water on poly(lactide-co-glycolide).* J Control Release, 2005. **108**(1): p. 1-9.
303. Hancock, B.C. and G. Zografi, *The relationship between the glass transition temperature and the water content of amorphous pharmaceutical solids.* Pharm Res, 1994. **11**(4): p. 471-7.
304. Bailey, N.A., Sandor,M., Kreitz,M., Mathiowitz, E. , *Comparison of the enthalpic relaxation of poly(lactide-co-glycolide) 50:50 nanospheres and raw polymer.* Journal of Applied Polymer Science, 2002. **86**(8): p. 1868-72.

305. Quirk, R.A., Davies, M.C., Tendler, S.J.B., and . Shakesheff, K.M., *Surface Engineering of Poly(lactic acid) by Entrapment of Modifying Species.* macromolecules, 2000. **33**(2): p. 258-60.
306. Guo, Z., Li, m., Willauer,H.D., Huddleston, J.G., April,G.C., Rogers, R.D., , *Evaluation of Polymer-Based Aqueous Biphasic Systems As Improvement for the Hardwood Alkaline Pulping Process.* Ind.Eng. Chem. Res., 2002. **41**(10): p. 2535-2542.
307. Chen, J., Spear, S.K., Huddleston, J.G., Rogers, R.D., , *Polyethylene glycol and solutions of polyethylene glycol as green reaction media.* Green Chem., , 2005. **7**: p. 64-82.
308. Collins, K.D. and M.W. Washabaugh, *The Hofmeister effect and the behaviour of water at interfaces.* Q Rev Biophys, 1985. **18**(4): p. 323-422.
309. Omta, A.W., et al., *Negligible effect of ions on the hydrogen-bond structure in liquid water.* Science, 2003. **301**(5631): p. 347-9.
310. Gurau, M.C., et al., *On the mechanism of the hofmeister effect.* J Am Chem Soc, 2004. **126**(34): p. 10522-3.
311. Leunissen, M.E., et al., *Electrostatics at the oil-water interface, stability, and order in emulsions and colloids.* Proc Natl Acad Sci U S A, 2007. **104**(8): p. 2585-90.
312. Gitlin, I., J.D. Carbeck, and G.M. Whitesides, *Why are proteins charged? Networks of charge-charge interactions in proteins measured by charge ladders and capillary electrophoresis.* Angew Chem Int Ed Engl, 2006. **45**(19): p. 3022-60.
313. Collins, K.D., *Sticky ions in biological systems.* Proc Natl Acad Sci U S A, 1995. **92**(12): p. 5553-7.
314. Zuk, P.A., *Tissue engineering craniofacial defects with adult stem cells? Are we ready yet?* Pediatr Res, 2008.
315. Senuma, Y., et al., *Bioresorbable microspheres by spinning disk atomization as injectable cell carrier: from preparation to in vitro evaluation.* Biomaterials, 2000. **21**(11): p. 1135-44.
316. Gibson, L.J., *Biomechanics of cellular solids.* J Biomech, 2005. **38**(3): p. 377-99.
317. Lavelle, W., et al., *Vertebroplasty and kyphoplasty.* Anesthesiol Clin, 2007. **25**(4): p. 913-28.
318. Patterson, T.E., et al., *Cellular strategies for enhancement of fracture repair.* J Bone Joint Surg Am, 2008. **90 Suppl 1**: p. 111-9.
319. Kertlow, J.D., Klouda, L., Mikos, A.G., *Injectable matrices and scaffolds for drug delivery in tissue engineering.* Advanced Drug Delivery, 2007. **59**: p. 263-273
320. Brunner, T.J., Robert N. Grass, Marc Bohner and Wendelin J. Stark, *Effect of particle size, crystal phase and crystallinity on the reactivity of tricalcium phosphate cements for bone reconstruction.* J. Mater. Chem., , 2007. **17**(38): p. 4072 - 4078.
321. Habraken, W.J., et al., *Injectable PLGA microsphere/calcium phosphate cements: physical properties and degradation characteristics.* J Biomater Sci Polym Ed, 2006. **17**(9): p. 1057-74.

322. Zheng, J., Carlson, W.B., Reed, J.S., *The packing density of binary powder mixtures.* J. of the European ceramic society 1995. **15**(5): p. 479-83.
323. Dexter, A.R., Tanner, D.w., *Packing densities of mixtures of sphees with Log-normal size distributions.* Nature Physical science, 1972. **238**(80): p. 31-32.
324. Brown, R.L., Hawsley, P.G.W., *Packing of regular (spherical) and irregular particles*, in *Nature*. 1945. p. 421-22.
325. Furnas, C.C., *Grading aggregates, I-mathematical relations for beads of broken solids of maximum density.* Industrial and Engineering Chemistry, 1931. **23**(9): p. 1052-8.
326. Xu, H.H., et al., *Injectable and macroporous calcium phosphate cement scaffold.* Biomaterials, 2006. **27**(24): p. 4279-87.
327. Karp, J.M. and R. Langer, *Development and therapeutic applications of advanced biomaterials.* Curr Opin Biotechnol, 2007. **18**(5): p. 454-9.
328. Bohner, M. and G. Baroud, *Injectability of calcium phosphate pastes.* Biomaterials, 2005. **26**(13): p. 1553-63.
329. Burguera, E.F., H.H. Xu, and M.D. Weir, *Injectable and rapid-setting calcium phosphate bone cement with dicalcium phosphate dihydrate.* J Biomed Mater Res B Appl Biomater, 2006. **77**(1): p. 126-34.
330. Burguera, E.F., H.H. Xu, and L. Sun, *Injectable calcium phosphate cement: effects of powder-to-liquid ratio and needle size.* J Biomed Mater Res B Appl Biomater, 2008. **84**(2): p. 493-502.
331. Bohner, M., N. Doebelin, and G. Baroud, *Theoretical and experimental approach to test the cohesion of calcium phosphate pastes.* Eur Cell Mater, 2006. **12**: p. 26-35.
332. Silva, M.M., et al., *The effect of anisotropic architecture on cell and tissue infiltration into tissue engineering scaffolds.* Biomaterials, 2006. **27**(35): p. 5909-17.
333. Mooney, D.J., Vandenburgh H.. *Cell delivery mechanisms for tissue repair.* Cell stem cell 2008. **2(3)**: p. 205-13.
334. Friedenstein, A.J., *Precursor cells of mechanocytes.* Int Rev Cytol, 1976. **47**: p. 327-59.
335. Friedenstein, A.J., R.K. Chailakhyan, and U.V. Gerasimov, *Bone marrow osteogenic stem cells: in vitro cultivation and transplantation in diffusion chambers.* Cell Tissue Kinet, 1987. **20**(3): p. 263-72.
336. Hill, E., T. Boontheekul, and D.J. Mooney, *Regulating activation of transplanted cells controls tissue regeneration.* Proc Natl Acad Sci U S A, 2006. **103**(8): p. 2494-9.
337. Kohane, D.S. and R. Langer, *Polymeric biomaterials in tissue engineering.* Pediatr Res, 2008.
338. De Rosa, M., et al., *Cationic polyelectrolyte hydrogel fosters fibroblast spreading, proliferation, and extracellular matrix production: Implications for tissue engineering.* J Cell Physiol, 2004. **198**(1): p. 133-43.
339. Ohtsuki, C., M. Kamitakahara, and T. Miyazaki, *Coating bone-like apatite onto organic substrates using solutions mimicking body fluid.* J Tissue Eng Regen Med, 2007. **1**(1): p. 33-8.

340. Proikakis, C.S., Mamouzelos, N.J., Andreopoulos, A.G., *Stability of DL-poly(lactic acid) in aqueous Solutions.* J. Applied polymer Science, , 2003. **87**: p. 795-804.
341. Boesel, L.F. and R.L. Reis, *The effect of water uptake on the behaviour of hydrophilic cements in confined environments.* Biomaterials, 2006. **27**(33): p. 5627-33.
342. Rüedi, T.P., Buckley, R.E., Moran, C.G., *AO Principles of Fracture Management*. Second expanded edition ed. 2007. 635 & 467.
343. Dunn, J.C., *Analyses of cell growth in tissue-engineering scaffolds.* Regen Med, 2008. **3**(3): p. 421-4.
344. Skuk, D., et al., *Ischemic central necrosis in pockets of transplanted myoblasts in nonhuman primates: implications for cell-transplantation strategies.* Transplantation, 2007. **84**(10): p. 1307-15.
345. Holy, C.E., et al., *Use of a biomimetic strategy to engineer bone.* J Biomed Mater Res A, 2003. **65**(4): p. 447-53.
346. Howard, D., et al., *Tissue engineering: strategies, stem cells and scaffolds.* J Anat, 2008. **213**(1): p. 66-72.
347. Yang, J., Shi, G., Bei, J., Wang, S., Cao, Y., Shang, Q., Yang, G., Wenjing Wang, *Fabrication and surface modification of macroporous poly(L-lactic acid) and poly(L-lactic-co-glycolic acid) (70/30) cell scaffolds for human skin fibroblast cell culture.* Journal of Biomedical Materials Research Part A, 2002. **62**(3): p. 438-46.
348. Zelzer, M., et al., *Investigation of cell-surface interactions using chemical gradients formed from plasma polymers.* Biomaterials, 2008. **29**(2): p. 172-84.
349. Hamano, T., et al., *Effects of polyelectrolyte complex (PEC) on human periodontal ligament fibroblast (HPLF) function. I. Three-dimensional structure of HPLF cultured on PEC.* J Biomed Mater Res, 1998. **41**(2): p. 257-69.
350. Inui, H., M. Tsujikubo, and S. Hirano, *Low molecular weight chitosan stimulation of mitogenic response to platelet-derived growth factor in vascular smooth muscle cells.* Biosci Biotechnol Biochem, 1995. **59**(11): p. 2111-4.
351. Godbey, W.T., et al., *Poly(ethylenimine)-mediated transfection: a new paradigm for gene delivery.* J Biomed Mater Res, 2000. **51**(3): p. 321-8.
352. Lv, H., Zhang, S., Wang, b., Cui, S., Yan,J., *Toxicity of cationic lipids and cationic polymers in gene delivery.* J. Controlled Release, 2006. **114**: p. 100-9.
353. Mateo, C., et al., *Reversible enzyme immobilization via a very strong and nondistorting ionic adsorption on support-polyethylenimine composites.* Biotechnol Bioeng, 2000. **68**(1): p. 98-105.
354. Altankov, G., et al., *On the tissue compatibility of poly(ether imide) membranes: an in vitro study on their interaction with human dermal fibroblasts and keratinocytes.* J Biomater Sci Polym Ed, 2005. **16**(1): p. 23-42.
355. Khang, D., et al., *Selective adhesion and mineral deposition by osteoblasts on carbon nanofiber patterns.* Int J Nanomedicine, 2006. **1**(1): p. 65-72.

356. Vancha , A.R., Govindaraju , S., Parsa , K.V.L., Jasti , M., González-García, M., and Ballestero, R.P., *Use of polyethyleneimine polymer in cell culture as attachment factor and lipofection enhancer.* BMC Biotechnology, 2004. **4**(23): p. 1-12.
357. Kunzler, T.P., et al., *Systematic study of osteoblast response to nanotopography by means of nanoparticle-density gradients.* Biomaterials, 2007. **28**(33): p. 5000-6.
358. De Rosa, G., et al., *Poly(lactide-co-glycolide) microspheres for the controlled release of oligonucleotide/polyethylenimine complexes.* J Pharm Sci, 2002. **91**(3): p. 790-9.
359. Nishida, S., et al., *Number of osteoprogenitor cells in human bone marrow markedly decreases after skeletal maturation.* J Bone Miner Metab, 1999. **17**(3): p. 171-7.
360. Muschler, G.F., et al., *Age- and gender-related changes in the cellularity of human bone marrow and the prevalence of osteoblastic progenitors.* J Orthop Res, 2001. **19**(1): p. 117-25.
361. Oreffo, R.O., et al., *Patients with primary osteoarthritis show no change with ageing in the number of osteogenic precursors.* Scand J Rheumatol, 1998. **27**(6): p. 415-24.
362. Richardson, T.P., et al., *Polymeric system for dual growth factor delivery.* Nat Biotechnol, 2001. **19**(11): p. 1029-34.
363. Levenberg, S., et al., *Engineering vascularized skeletal muscle tissue.* Nat Biotechnol, 2005. **23**(7): p. 879-84.
364. Jaklenec, A., et al., *Sequential release of bioactive IGF-I and TGF-beta(1) from PLGA microsphere-based scaffolds.* Biomaterials, 2008. **29**(10): p. 1518-25.
365. Liu, Y., et al., *Delivery mode and efficacy of BMP-2 in association with implants.* J Dent Res, 2007. **86**(1): p. 84-9.
366. Jeon, O., et al., *Long-term delivery enhances in vivo osteogenic efficacy of bone morphogenetic protein-2 compared to short-term delivery.* Biochem Biophys Res Commun, 2008. **369**(2): p. 774-80.
367. Silva, E.A. and D.J. Mooney, *Spatiotemporal control of vascular endothelial growth factor delivery from injectable hydrogels enhances angiogenesis.* J Thromb Haemost, 2007. **5**(3): p. 590-8.
368. Morita, T., Horikiri, Y., Yamahara, H., Suzuki, T., Yoshino, H., *Formation and Isolation of Spherical Fine Protein Microparticles Through Lyophilization of Protein-Poly(ethylene Glycol) Aqueous Mixture.* Pharmaceutical Research, 2000. **17**(11): p. 1367-1373.
369. Morita, T., et al., *Evaluation of in vivo release characteristics of protein-loaded biodegradable microspheres in rats and severe combined immunodeficiency disease mice.* J Control Release, 2001. **73**(2-3): p. 213-21.
370. Morita, T., et al., *Protein encapsulation into biodegradable microspheres by a novel S/O/W emulsion method using poly(ethylene glycol) as a protein micronization adjuvant.* J Control Release, 2000. **69**(3): p. 435-44.
371. Borden, M., et al., *Tissue engineered microsphere-based matrices for bone repair: design and evaluation.* Biomaterials, 2002. **23**(2): p. 551-9.

372. Riggleman, R.A., J.F. Douglas, and J.J. de Pablo, *Tuning polymer melt fragility with antiplasticizer additives.* J Chem Phys, 2007. **126**(23): p. 234903.
373. Desai, N.P. and J.A. Hubbell, *Solution technique to incorporate polyethylene oxide and other water-soluble polymers into surfaces of polymeric biomaterials.* Biomaterials, 1991. **12**(2): p. 144-53.
374. Elbert, D.L., Hubbell, J, A,, *Surface Treatments of Polymers for Biocompatibility.* Annual Review of Materials Science, 1996. **26**: p. 365-394
375. Quirk, R.A., Davies, M.C., Tendler, S.J.B., Chan, W.C., and Shakesheff, K.M., *Controlling Biological Interactions with Poly(lactic acid) by Surface Entrapment Modification.* Langmuir, 2001. **17**(9): p. 2817–2820.
376. Curtis, A.S. and M. Varde, *Control of Cell Behavior: Topological Factors.* J Natl Cancer Inst, 1964. **33**: p. 15-26.
377. Biggs, M.J., et al., *Interactions with nanoscale topography: Adhesion quantification and signal transduction in cells of osteogenic and multipotent lineage.* J Biomed Mater Res A, 2008.
378. Shapiro, F., *Cortical bone repair. The relationship of the lacunar-canalicular system and intercellular gap junctions to the repair process.* J Bone Joint Surg Am, 1988. **70**(7): p. 1067-81.
379. El-Ayoubi, R., Eliopoulos, N., Diraddo, R., Galipeau, J., Yousefi, A., *Design and fabrication of 3D scaffolds to facilitate cell-based gene therapy.* Tissue Eng Part A, 2008. **14**(6): p. 1037-47.
380. Tabata, Y., *Biomaterial technology for tissue engineering applications.* J.R.Soc. Interface, 2009. **online march 4**.
381. Jelluma, N., Yang, X., Stokoe, D., Evan, G.I., Dansen, T.B., Haas-Kogan, D.A., *Glucose Withdrawal Induces Oxidative Stress followed by Apoptosis in Glioblastoma Cells but not in Normal Human Astrocytes.* Mol Cancer Res, 2006. **4**(5): p. 319-30.
382. Salehian, B., et al., *The effect of glutamine on prevention of glucocorticoid-induced skeletal muscle atrophy is associated with myostatin suppression.* Metabolism, 2006. **55**(9): p. 1239-47.
383. Takamizawaa, S., Maehataa, Y., Imaic, K., Senooc, H., Satob, S., and Hata, R *Effects of ascorbic acid and ascorbic acid 2-phosphate, a long-acting vitamin C derivative, on the proliferation and differentiation of human osteoblast-like cells* Cell Biology International, 2004. **28**(4): p. 255-265.
384. Te Pas, M.F., de Jong, P.R., Verburg, F.J., *Glucocorticoid inhibition of C2C12 proliferation rate and differentiation capacity in relation to mRNA levels of the MRF gene family.* Mol Biol Rep. , 2000. **27**(2): p. 87-98.
385. Orzechowski, A., et al., *Dexamethasone-mediated regulation of death and differentiation of muscle cells. Is hydrogen peroxide involved in the process?* Reprod Nutr Dev, 2002. **42**(3): p. 197-216.
386. Aubin, J.E., *Osteogenic cell differentiation* in *Bone engineering*, J.E. Davies, Editor. 2000, em squared Toronto p. 19-30.
387. Beresford, J.N., S.E. Graves, and C.A. Smoothy, *Formation of mineralized nodules by bone derived cells in vitro: a model of bone formation?* Am J Med Genet, 1993. **45**(2): p. 163-78.

388. Jaiswal, N., et al., *Osteogenic differentiation of purified, culture-expanded human mesenchymal stem cells in vitro.* J Cell Biochem, 1997. **64**(2): p. 295-312.
389. Coelho, M.J., Cabral, A., Fernandes, M.H., *Human bone cell cultures in biocompatibility testing. Part I: Osteoblastic differentiation of serially passaged human bone marrow cells cultured in alpha-MEM and in DMEM.* Biomaterials, 2000. **21**: p. 1087-94.
390. Coelho, M.J. and M.H. Fernandes, *Human bone cell cultures in biocompatibility testing. Part II: effect of ascorbic acid, beta-glycerophosphate and dexamethasone on osteoblastic differentiation.* Biomaterials, 2000. **21**(11): p. 1095-102.
391. Whitson, P.A., et al., *Dexamethasone effects on creatine kinase activity and insulin-like growth factor receptors in cultured muscle cells.* J Cell Physiol, 1989. **140**(1): p. 8-17.
392. Xu, A., Dong, W., Antonietti, M., Colfen, H., *Polymorph Switching of Calcium Carbonate Crystals by Polymer-Controlled Crystallization.* adv. Funct. Mat, 2008. **18**(8): p. 1307-1313.
393. Kasugai, S., et al., *Expression of bone matrix proteins associated with mineralized tissue formation by adult rat bone marrow cells in vitro: inductive effects of dexamethasone on the osteoblastic phenotype.* J Cell Physiol, 1991. **147**(1): p. 111-20.
394. Yao, K.L., R. Todescan, Jr., and J. Sodek, *Temporal changes in matrix protein synthesis and mRNA expression during mineralized tissue formation by adult rat bone marrow cells in culture.* J Bone Miner Res, 1994. **9**(2): p. 231-40.
395. Franceschi, R.T., J.X. Wilson, and S.J. Dixon, *Requirement for Na(+)-dependent ascorbic acid transport in osteoblast function.* Am J Physiol, 1995. **268**(6 Pt 1): p. C1430-9.
396. Liu, X., et al., *Influence of substratum surface chemistry/energy and topography on the human fetal osteoblastic cell line hFOB 1.19: Phenotypic and genotypic responses observed in vitro.* Biomaterials, 2007. **28**(31): p. 4535-50.
397. Vogler, E.A., *Structure and reactivity of water at biomaterial surfaces.* Adv Colloid Interface Sci, 1998. **74**: p. 69-117.
398. Lim, J.Y., et al., *Surface energy effects on osteoblast spatial growth and mineralization.* Biomaterials, 2008. **29**(12): p. 1776-84.
399. Keselowsky, B.G., D.M. Collard, and A.J. Garcia, *Integrin binding specificity regulates biomaterial surface chemistry effects on cell differentiation.* Proc Natl Acad Sci U S A, 2005. **102**(17): p. 5953-7.
400. Dalby, M.J., et al., *Increasing fibroblast response to materials using nanotopography: morphological and genetic measurements of cell response to 13-nm-high polymer demixed islands.* Exp Cell Res, 2002. **276**(1): p. 1-9.
401. Price, R.L., et al., *Nanometer surface roughness increases select osteoblast adhesion on carbon nanofiber compacts.* J Biomed Mater Res A, 2004. **70**(1): p. 129-38.

402. Dalby, M.J., et al., *Osteoprogenitor response to defined topographies with nanoscale depths.* Biomaterials, 2006. **27**(8): p. 1306-15.
403. Biggs, M.J., et al., *Adhesion formation of primary human osteoblasts and the functional response of mesenchymal stem cells to 330nm deep microgrooves.* J R Soc Interface, 2008. **5**(27): p. 1231-42.
404. Huitema, L.F. and A.B. Vaandrager, *What triggers cell-mediated mineralization?* Front Biosci, 2007. **12**: p. 2631-45.
405. Kim, H.K. and T.G. Park, *Comparative study on sustained release of human growth hormone from semi-crystalline poly(L-lactic acid) and amorphous poly(D,L-lactic-co-glycolic acid) microspheres: morphological effect on protein release.* J Control Release, 2004. **98**(1): p. 115-25.
406. Bingaman, S., V.H. Huxley, and R.E. Rumbaut, *Fluorescent dyes modify properties of proteins used in microvascular research.* Microcirculation, 2003. **10**(2): p. 221-31.
407. Rao, J.K., D.V. Ramesh, and K.P. Rao, *Controlled release systems for proteins based on gelatin microspheres.* J Biomater Sci Polym Ed, 1994. **6**(5): p. 391-8.
408. Morita, T., et al., *Applicability of various amphiphilic polymers to the modification of protein release kinetics from biodegradable reservoir-type microspheres.* Eur J Pharm Biopharm, 2001. **51**(1): p. 45-53.
409. Estey, T., et al., *BSA degradation under acidic conditions: a model for protein instability during release from PLGA delivery systems.* J Pharm Sci, 2006. **95**(7): p. 1626-39.
410. Yampolskaya, G. and D. Platikanov, *Proteins at fluid interfaces: adsorption layers and thin liquid films.* Adv Colloid Interface Sci, 2006. **128-130**: p. 159-83.
411. Kim, H.D. and R.F. Valentini, *Human osteoblast response in vitro to platelet-derived growth factor and transforming growth factor-beta delivered from controlled-release polymer rods.* Biomaterials, 1997. **18**(17): p. 1175-84.